Janete Antónia da Cunha Santos

DELAYING NEURODEGENERATION THROUGH CALORIC RESTRICTION APPROACHES: FROM MECHANISMS TO MOLECULAR THERAPY

· U · C ·

UNIVERSIDADE DE COIMBRA

Delaying neurodegeneration through caloric restriction approaches: From mechanisms to molecular therapy

Janete Antónia da Cunha Santos

Setembro 2016

· U C ·

UNIVERSIDADE DE COIMBRA

Delaying neurodegeneration through caloric restriction approaches: From mechanisms to molecular therapy

Janete Antónia da Cunha Santos

Thesis submitted to the Faculty of Pharmacy of the University of Coimbra for the attribution of the Doctor degree in Pharmaceutical Sciences, in the specialty field of Pharmacology and Pharmacotherapy.

Tese apresentada à Faculdade de Farmácia da Universidade de Coimbra para prestação de provas de doutoramento em Ciências Farmacêuticas, no ramo de Farmacologia e Farmacoterapia.

Setembro 2016

· U   C ·

UNIVERSIDADE DE COIMBRA

Delaying neurodegeneration through caloric restriction approaches: From mechanisms to molecular therapy

Front cover:

Microscope image of DAPI-staining of cerebellar sagittal sections of wild-type mice (**top images**) and transgenic MJD animals (**bottom images**), spanning from the lateral to the medial region of the left cerebellar hemisphere.

Ao meu pai.

Acknowledgments/Agradecimentos

À Professora Doutora Cláudia Cavadas gostaria de agradecer todo o apoio e toda a confiança depositada em mim, apoio esse que vai muito mais além destes quatro anos. Agradeço toda a amizade, alegria, boa disposição, disponibilidade e incentivo científico que sempre acompanharam todas as fases desta caminhada. Muito obrigada pelo demonstrar que é sempre possível alcançar o que pensamos inicialmente ser inatingível e pelo transmitir de uma constante motivação. Quero ainda agradecer ao Professor Doutor Luís Pereira de Almeida pela excelente oportunidade de fazer parte do seu excelente grupo de investigação, por ter sempre uma palavra de incentivo e ter sempre um tempo para me ouvir e aconselhar. Um grande muito obrigado pela enorme contribuição para o desenvolvimento da minha visão científica que muito contribuiu para a minha evolução ao longo destes últimos anos.

I also want to acknowledge to Professor Leonard Guarente. It was an honor to have you as my co-supervisor and advisor. Thank you for the time that you spend discussing my work and also for all the kindness and encouragement transmitted every time. For me it was a real pleasure to meet and work with the "sirtuin's father". I also want to thank to Professor David Sinclair for receiving me on his laboratory and to give me the great opportunity to belong to his wonderful group. A big thank you for all the encouragement, enthusiasm, and support, even with his busy schedule. A sincere thank you for both to give me the excellent opportunity to be with and where the work that I admire so much is done.

À Professora Doutora Catarina Resende de Oliveira e ao Professor Doutor João Ramalho gostaria de agradecer a excelente oportunidade de desenvolver este trabalho no Centro de Neurociências e Biologia Celular (CNC) da Universidade de Coimbra.

Gostaria ainda de agradecer à Fundação para a Ciência e Tecnologia (FCT) pelo suporte financeiro muito importante para a realização deste trabalho.

Obviamente agradeço também a todos os meus colegas e amigos do Grupo de Vetores e Terapia Génica e do Grupo de Neuroendocrinologia e Envelhecimento do Centro de Neurociências e Biologia Celular (CNC) pela boa disposição, amizade, companheirismo e pelo constante apoio científico e não só. Às "CC's" agradeço em particular à "Patrícia CC" que foi a primeira pessoa que me recebeu, ainda numa fase muito precoce do meu desenvolvimento científico, e que sempre me apoiou e me fez rir mesmo nos momentos em que a vontade para isso era pouca. Um muito obrigado ainda à Joana Salgado, Célia, Lígia, Ana Rita, Magda, Mariana Botelho, Sara Silva e Marisa. Um especial obrigado ao Pedro, pela partilha científica e amizade, e pelo finalmente ter mais um elemento na tão pequena "sirtuin's team". Aos "LA's" um grande, grande muito obrigado por tão bem me receberem e me acolhido num grupo que não era o meu "principal", mas que tão bem me fez sentir, e que sempre partilhou comigo todas as minhas "alegrias científicas e não científicas" (e tristezas também). Agradeço particularmente à minha Dina Maria, à Isabel, Mariana Conceição, Geetha, Ana Cristina, Ana Teresa e Nélio, "Patrícia LA", "Sara Lôpez", Filipa, Teresinha, Susana Paixão, Rui, Liliana, Clévio, Sónia e Catarina. Ao Marco, à Sandra e ao "Johnny" um obrigado por tornarem as curtas horas de almoço em divertidíssimos momentos.

Table of Contents

CHAPTER 1

CHAPTER 2

CALORIC RESTRICTION AMELIORATES NEUROPATHOLOGY AND MOTOR DEFICITS IN MACHADO-JOSEPH DISEASE MOUSE MODELS THROUGH THE ACTIVATION OF SIRT1 PATHWAY

CHAPTER 3

NAD$^+$ DECREASE INDUCES NUCLEAR-MITOCHONDRIAL COMMUNICATION DISRUPTION IN MACHADO-JOSEPH DISEASE MOUSE MODELS

CHAPTER 4

PHARMACOLOGICAL ACTIVATION OF SIRTUIN AMELIORATES NEUROPATHOLOGY AND IMPROVES MOTOR FUNCTION IN A TRANSGENIC MACHADO-JOSEPH DISEASE MOUSE MODEL

CHAPTER 5

Abbreviations

3-D	Three-Dimensional
Ab	Antibody
AceCS-1	Acetyl-CoA synthetase 1
AcFOXO1	Acetylated forkhead box 1
AD	Alzheimer's disease
ADP	Adenosine diphosphate
AIN-93G	American institute of nutrition 93 G recommendation
AL	*Ad libitum*
ALS	Amyotrophic lateral sclerosis
AMC	Aminomethylcoumarine
AMP	Adenosine monophosphate
AMPK	Adenosine monophosphate kinase
ANOVA	Analysis of variance
APP	Amyloid precursor protein
ART	Adenosine diphosphate (ADP)-ribose transferases
Atgs	Autophagy-related proteins
ATP	Adenosine triphosphate
ATP5a1	ATP synthase subunit 5 alpha 1
ATP6	ATP synthase F_0 subunit 6
Atx3 27Q	Wild-type ataxin-3
Atx3 72Q	Mutant ataxin-3
BCA	Bicinchoninic acid
BRASTO	Brain-specific transgenic overexpression of SIRT1
BSA	Bovine serum antigen
cADPR	Cyclic ADP-ribose
CAG	Citosine-Adenine-Guanine trinucleotide
CALERIE	Comprehensive assessment of long term effects of reducing intake of energy
CBP	CREB-binding protein
CD38	Cluster of differentiation 38

CD157	Cluster of differentiation 157
cDNA	Complementary DNA
CMV	Cytomegalovirus
CNS	Central nervous system
COX1	Cytochrome c oxidase subunit I
COX2	Cytochrome c oxidase subunit II
COX5b	Cytochrome c oxidase subunit 5b
CR	Caloric restriction
CREB	cAMP response element-binding protein
CRTC2	CREB-protein regulated transcriptional co-activators
Ct	Cycle threshold
Cytb	Cytochrome b
DAB	3,3'-diaminobenzidine
DAPI	4',6-diamino-2-phenylindole
DARPP-32	Dopamine- and cyclic AMP-regulated phosphoprotein of 32 kDa
DHEAS	Dehydroepiandrosterone sulfate
DMSO	Dimethyl sulfoxide
DNA	Deoxyribonucleic acid
DRPLA	Dentatorubral-pallidoluysian atrophy
DTT	1,4-Dithiothreitol
E230K	Mutagenesis Glutamate position 230 Lysine
ECF	Enhanced chemifluorescence
EGFP	Enhanced green fluorescent protein
ELISA	Enzyme-linked immunosorbent assay
eNOS	Endothelial nitric oxide synthase
ERC	Extrachromosomal rDNA circles
FCCP	Carbonyl cyanide p-(trifluoromethoxi)phenylhydrazone
FOXO1/3	Forkhead box O1/3
GAPDH	Glyceraldehyde 3-phosphate dehydrogenase
GFAP	Glial fibrillary acidic protein
H1/3/4	Histone 1/3/4
H363Y	Mutated sirtuin 1 without deacetylase activity
HA	Hemagglutinin

HD	Huntington's disease
HDAC	Histone deacetylase
HEK293T	Human embryonic kidney 293T cell line
HSP70	Heat shock protein 70
Iba-1	Ionized calcium binding adaptor molecule 1
IF	Intermittent fasting
IGF-1	Insulin growth factor 1
Iκ-Bα	Nuclear factor of kappa light polypeptide gene enhancer in B-cells inhibitor, alpha
IL-1β	Interleukin 1 beta
IL-6/10	Interleukin 6/10
INF-γ	Interferon gamma
KO	Knockout
LC3B	Microtubule-associated protein 1 light chain 3 B
LV	Lentivirus
MJD	Machado-Joseph disease
MPTP	1-methyl-4-phenyl-1,2,3,6-tetrahydropyridine
mRNA	Messenger ribonucleic acid
mtDNA	Mitochondrial DNA
mTOR	Mammalian target of rapamycin
mTORC1	Mammalian target of rapamycin complex 1
NAD$^+$	Oxidized nicotinamide adenine dinucleotide
NADH	Reduced nicotinamide adenine dinucleotide
NAM	Nicotinamide
NAMPT	Nicotinamide phosphorybosyltransferase
NCor	Nuclear receptor co-repressor 1
ND1	NADH-ubiquinone oxireductase core subunit 1
NDUFS8	NADH-ubiquinone oxireductase core subunit S8
Neuro2a	Mouse neuroblastoma cell line
NES	Nuclear export signal
NeuN	Neuronal nuclei
NF-κB	Nuclear factor kappa B
NIH	National Institute of Health

NLS	Nuclear localization signal
NMN	Nicotinamide mononucleotide
NMNAT	Nicotinamide mononucleotide adenylyltransferase
NP-40	Nonyl phenoxypolyethoxylethanol
NR	Nicotinamide riboside
NRF-1/2	Nuclear respiratory factor 1/2
NRK	Nicotinamide riboside kinase
n.s.	Not significant
OCR	Oxygen consumption rate
OXPHOS	Oxidative phosphorylation system
p300	Histone acetyltransferase
p53	Tumor protein p53
p62	Sequestosome 1
PARP1	Poly (ADP-ribose) polymerase 1
PBS	Phosphate buffered saline
PCAF	p300 and p300/CBP-associated factor
PCR	Polymerase chain reaction
PD	Parkinson's disease
PGC-1α	Peroxisome proliferator-activated receptor gamma coactivator 1-alpha
PGC-1β	Peroxisome proliferator-activated receptor gamma coactivator 1-beta
PGK	Phosphoglycerate kinase
PMSF	Phenylmethanesulfonyl fluoride
PolyQ	Polyglutamine
PPAR-α	Peroxisome proliferator-activated receptor alpha
PPAR-γ	Peroxisome proliferator-activated receptor beta
PS1/2	Presenilin 1/2
PVDF	Polyvinylidene fluoride
qRT-PCR	Quantitative real-time polymerase chain reaction
rDNA	Ribosomal DNA
RESV	Resveratrol
RIPA	Radio immuno precipitation assay
RNA	Ribonucleic acid
r.p.m.	Rotation per minute

Rsp18	Ribosomal protein s18
SBMA	Spinal and bulbar muscular atrophy
SCA	Spinocerebellar ataxia
SDHb	Succinate-dehydrogenase [ubiquinone] iron-sulfur subunit
SDS	Sodium dodecyl sulfate
SDS-PAGE	Sodium dodecyl sulfate polyacrylamide gel electrophoresis
SEM	Standard error of the mean
shRNA	Short hairpin RNA
shAtg5	shRNA targeting Atg5
shCNTL	Negative shRNA
shSIRT1	shRNA targeting SIRT1
Sir2	Silent information regulator 2
SIRT1-7	Sirtuin 1-7
SQSTM1	Sequestosome 1
STACs	Sirtuin activating compounds
TAMRA	Carboxitetramethylrhodamine
TBS-t	Tris-buffered saline with 0.01% Tween-20
TFAM	Mitochondrial transcription factor A
TH	Tyrosine hydroxylase
Tg	Transgenic
TNF-α	Tumor necrosis factor alpha
UIM	Ubiquitin interacting motif
UPS	Ubiquitin-proteasome system
UTR	Untranslated region
VMAT2	Vesicular monoamine transporter
WldS	*Wallerian* degeneration slow
WT	Wild-Type
YAC	Yeast artificial chromosome

Summary

Machado-Joseph disease (MJD), also known as spinocerebellar ataxia type 3 (SCA3), is a fatal autosomal dominant neurodegenerative disease. MJD is caused by the CAG trinucleotide expansion in the C-terminal coding region of the *ATXN3* gene, at chromosomal *locus* 14q32.1. The wild-type *ATXN3* gene presents from 12 to 44 CAG repeats and the mutant *ATXN3* gene presents from 55 to 86 CAG, in the 10th exon. The polyglutamine (polyQ)-expanded mutant ataxin-3 can interact with several proteins, and accumulates in the form of aggregates in the brain, particularly in the nucleus of neurons. The main affected brain areas are the cerebellum, brainstem, and basal ganglia, particularly *substantia nigra* and striatum. MJD is the most common dominantly inherited ataxia worldwide, and is a late-onset disease that manifests with cerebellar ataxia, rigidity, and distal muscle atrophies. Unfortunately, there is no therapy to cure or even to retard the progression of this disease.

Caloric restriction (CR) is the oldest and the most reliable experimental manipulation that is known to extend the lifespan in several species. Additionally, it has been shown that CR is neuroprotective. There are several mechanisms underlying CR beneficial effects. One of the more important mechanisms is the effect of CR on the levels and activity of sirtuins. Sirtuins are NAD$^+$-dependent deacetylases, existing seven sirtuins in mammals (SIRT1-7). SIRT1, the most studied sirtuin so far, mediates CR effects, since CR is able to increase SIRT1 activity and levels.

In this work we aimed at unravelling the potential beneficial effects of CR in MJD and the role of SIRT1 in these effects, and also to investigate the mechanisms underlying mitochondrial dysregulation associated with MJD pathogenesis. For this we used cellular and mouse models of MJD.

This thesis is organized in five chapters. In Chapter 1 is provided a review of the main literature regarding MJD, CR, and sirtuins, with a focus on SIRT1.

In Chapter 2 we evaluate the role of CR in two different and complementary mouse models of MJD, and we study the contribution of SIRT1 for these effects. We show that CR robustly ameliorates motor deficits and the associated neuropathology of MJD. Moreover, we also observe that SIRT1 is particularly involved in these outcomes, since its knockdown abolishes the beneficial effects of CR. In addition, the specific and localized SIRT1 overexpression ameliorates MJD neuropathology. We also provide data demonstrating that SIRT1 is able to activate autophagy, leading to the clearance of toxic species of mutant ataxin-3, and is also able to reduce neuroinflammation associated with MJD.

In Chapter 3 we investigate the crosstalk between the nucleus and mitochondria in MJD experimental models. Our data suggest that the alteration of the nuclear-mitochondrial communication, generated by a severe decrease in NAD^+, is connected to the mitochondrial dysfunction. Moreover, we elucidate that this decrease in NAD^+ probably results from the increase in the consumption of NAD^+, due to an increase in cluster of differentiation 38 (CD38), and a malfunction of the NAD^+-salvage pathway, associated with a decrease in nicotinamide mononucleotide adenylyltransferase 1 (NMNAT1). Likewise, our data also demonstrate that the lentiviral overexpression of NMNAT1 is able to reestablish nuclear-mitochondrial communication, and consequently mitochondrial respiration.

In Chapter 4 we evaluate the potential beneficial effects resulting from the pharmacological increase of NAD^+ (with nicotinamide mononucleotide - NMN) or the pharmacological activation of SIRT1 (with resveratrol). We show that the intraperitoneal administration of 500 mg/kg body weight/day of NMN during eight weeks induces a mild amelioration of the ataxic behavior of transgenic MJD mice, with no significant alterations in the neuropathology. Importantly, we observed that eight weeks of intraperitoneally-administered resveratrol at a dose of 10 mg/kg body weight/day in transgenic MJD mice, robustly alleviates motor incoordination and imbalance. Moreover, resveratrol treatment also ameliorates the accompanying neuropathology. Altogether, these results highlight the relevance of the use of resveratrol as a therapy to treat MJD.

At the end, in Chapter 5, we provide a final discussion, conclusion, and future perspectives about the results presented in Chapters 2, 3, and 4.

In conclusion, with this work we present evidence that SIRT1 activation with caloric restriction or resveratrol, is a promising therapeutic strategy to treat MJD or to delay MJD progression. Furthermore, we also unravel a new pathway related with the mitochondrial dysfunction patent in the disease, creating new potential targets to guide new therapeutic approaches for MJD.

Resumo

A doença de Machado-Joseph (DMJ), também conhecida por ataxia espinocerebelosa do tipo 3, é uma doença neurodegenerativa autossómica dominante fatal. A DMJ é causada pela expansão do trinucleótido CAG na região codificante carboxi-terminal do gene *ATXN3*, localizado no cromossoma 14q32.1. O gene *ATNX3* apresenta de 12 a 44 repetições CAG mas a mutação no gene *ATXN3* resulta em 55 a 86 repetições CAG, no exão 10. A ataxina-3 mutante resultante apresenta um aumento do número de repetições de glutamina, podendo interagir com outras proteínas, sendo acumulada na forma de agregados no cérebro, mais abundantemente nos núcleos dos neurónios. As principais regiões cerebrais afetadas na DMJ são o cerebelo, o tronco cerebral e os gânglios da base, incluindo a *substantia nigra* e o estriado. Esta doença é a ataxia dominante mais comum em todo o mundo, sendo uma doença de início tardio que se manifesta com ataxia cerebelosa, rigidez e atrofias musculares distais. Presentemente não existe nenhuma terapia para curar ou atrasar a progressão da DMJ.

A restrição calórica (RC) é uma abordagem experimental conhecida à mais de 80 anos que aumenta a longevidade de diferentes espécies animais usadas em laboratório. Para além disso, estudos demonstram que a RC poderá ter efeitos neuroprotetores. Os mecanismos que estão na base dos efeitos benéficos da RC são diversos. Um dos mais importantes mecanismos consiste no efeito da RC nos níveis e na atividade das sirtuínas. As sirtuínas são desacetilases dependentes de NAD^+, existindo sete sirtuínas nos mamíferos (SIRT1-7). A SIRT1, que é a sirtuína mais estudada até agora, medeia os efeitos da RC, dado que a RC tem a capacidade de aumentar os seus níveis e atividade.

Nesta tese os principais objetivos consistiram na avaliação do potencial efeito benéfico da RC na DMJ e do papel da SIRT1 nesses efeitos, e também na investigação dos mecanismos associados com a disfunção mitocondrial patente na patogénese da DMJ. Para isto recorremos a modelos celulares e de murganho da DMJ.

Esta tese está organizada em cinco capítulos. No Capítulo 1 apresenta-se uma revisão da literatura da DMJ, da RC e das sirtuínas, mais particularmente da SIRT1.

No Capítulo 2 avaliamos o papel da RC em dois modelos de murganho da DMJ, e estudamos a contribuição da SIRT1 para esses efeitos. Os resultados obtidos demonstram que a RC melhora os problemas motores e a neuropatologia associada à DMJ. Além disso, demonstramos que a SIRT1 está envolvida nesses efeitos visto que a sua redução bloqueia os efeitos benéficos da RC. A sobrexpressão específica e localizada da SIRT1 melhora significativamente a neuropatologia do modelo animal da

DMJ. Adicionalmente, os nossos resultados sugerem que a SIRT1 tem a capacidade de ativar a autofagia, contribuindo para a degradação das espécies tóxicas da ataxina-3 mutante e para a redução da neuroinflamação associada à DMJ.

No Capítulo 3 estudamos a relação existente entre o núcleo e a mitocôndria em modelos experimentais da DMJ. Os nossos resultados sugerem que a alteração da comunicação núcleo-mitocôndria, desencadeada pela redução do NAD^+, está associada à disfunção mitocondrial presente na DMJ. Para além disso, clarificamos que esta redução provavelmente está relacionada ao aumento do consumo de NAD^+, dado o aumento do *cluster* de diferenciação 38 (CD38), e o comprometimento da via de regeneração do NAD^+, pela redução da nicotinamida mononucleótido adenililtransferase 1 (NMNAT1). Além disso, os nossos resultados ainda sugerem que a sobrexpressão do NMNAT1 tem a capacidade de restabelecer a comunicação núcleo-mitocôndria e consequentemente a respiração mitocondrial.

No Capítulo 4 avaliamos os possíveis efeitos benéficos resultantes do aumento farmacológico do NAD^+, recorrendo à administração periférica de nicotinamida mononucleótido (NMN) ou resultantes da ativação da SIRT1 pela administração periférica de resveratrol. Neste capítulo observamos que o tratamento diário de murganhos transgénicos para a DMJ com NMN (500 mg/kg peso corporal/dia) administrado por via intraperitoneal durante oito semanas, induz uma ligeira melhoria da ataxia motora, sem alterações significativas da neuropatologia. Contudo, observamos que o tratamento diário dos murganhos transgénicos para a DMJ com resveratrol (10 mg/kg peso corporal/dia), administrado por via intraperitoneal durante oito semanas, melhora a descoordenação motora e o desequilíbrio característicos da doença. Para além disso, o resveratrol melhora a neuropatologia associada. Em conjunto, estes resultados salientam a relevância do uso do resveratrol como terapia para a DMJ.

No Capítulo 5 elaboramos uma discussão geral, conclusão final e perspetivas futuras, relativas aos resultados apresentados nos Capítulos 2, 3 e 4.

Em conclusão, nesta tese demonstramos que a ativação da SIRT1 através da restrição calórica ou da administração do resveratrol, são estratégias terapêuticas promissoras, para tratar e/ou atrasar a progressão da DMJ. Além disso, nesta tese sugerimos um novo mecanismo relacionado com a disfunção mitocondrial que ocorre na doença, criando novos potenciais alvos farmacológicos de modo a auxiliar o desenvolvimento de novas abordagens terapêuticas para a DMJ.

CHAPTER 1

General introduction

Science is simply the word we use to describe
a method for organizing our curiosity.
(Tim Michin)

1.1 <u>Neurodegenerative diseases involving repeat expansions</u>

Neuronal dysfunction and death can be caused by the expansion of unstable repetitive tracts that can occur in coding (exons), or non-coding (3' or 5'-untranslated regions – UTRs – or introns) sequences. These expansions lead to RNA alterations, such as in transcription, processing, nuclear exportation, and translation (reviewed in La Spada and Taylor, 2010). The mutations involved in these diseases are classified as dynamic mutations due to changes in the repeat size (trinucleotide, tetranucleotide, pentanucleotide, or hexanucleotide), generating a high genomic instability (Silveira et al., 2000; Matsuura et al., 2004).

There are several neuromuscular and neurological diseases caused by repeat expansions in coding regions, such as Huntington's disease (HD), spinocerebellar ataxias (SCAs), spinal and bulbar muscular atrophy (SBMA), among others (La Spada et al., 1991; Biancalana et al., 1992; Snell et al., 1993; La Spada et al., 1994; Bingham et al., 1995). In all of these diseases, trinucleotide expanded repeats have been identified (Figure 1.1). The resultant proteins exhibit an alteration of their function leading to cellular dysfunction and consequent neurodegeneration in specific brain areas. Cognitive, motor, and neuromuscular deficits are the main hallmarks of these diseases. Their onset is related with the repeat motif, length, and also the gene location (reviewed in La Spada and Taylor, 2010; Nelson et al., 2013). Mirkin and colleagues (2006) provided a theoretical molecular model of repeat instability that gave some clues about the origin of these triplet disorders. They hypothesized that DNA unwinding or complete strand separation processes trigger abnormal DNA structures generated by some repeats in genomic DNA (Mirkin, 2006). This suggests that all these disorders share a common genomic profile, leading to complications in DNA replication, but also in recombination and repair, contributing to the repeat instability characteristic of these diseases.

REPEAT EXPANSION DISEASES (in coding regions)

POLYALANINE DISEASES
OPMD $(GCN)_{11-17}$
XLMR $(GCG)_{20/23}$

| 5'UTR | EXON | 3'UTR |

POLYGLUTAMINE DISEASES
HD $(CAG)_{>36}$
SBMA $(CAG)_{>38}$
DRPLA $(CAG)_{>48}$
SCA1 $(CAG)_{>40}$
SCA2 $(CAG)_{>33}$
SCA3 $(CAG)_{>55}$
SCA6 $(CAG)_{>20}$
SCA7 $(CAG)_{>36}$
SCA17 $(CAG)_{>43}$
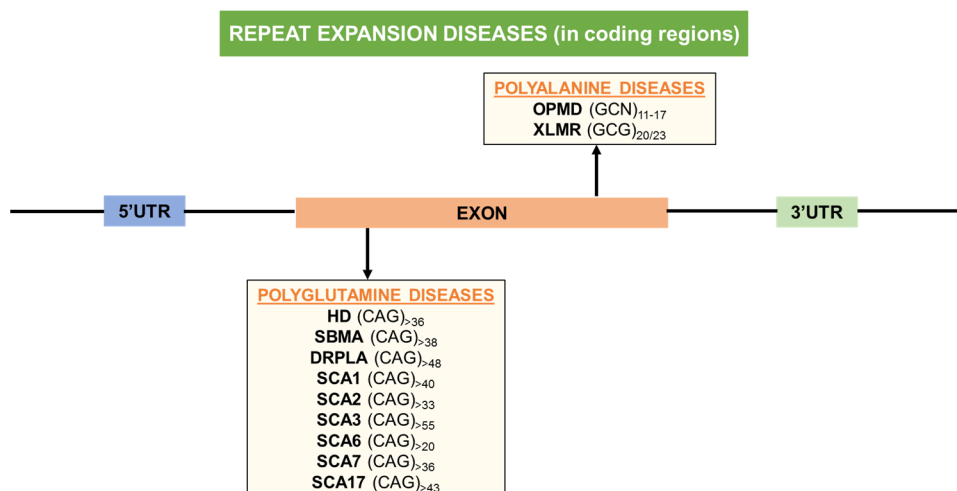
Figure 1.1 <u>Diseases involving trinucleotide repeat expansion in coding regions.</u> Until now it is known two different groups of neurodegenerative diseases that result from
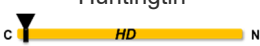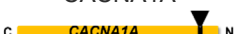
Figure 1.1 (cont.) mutations involving trinucleotide repeat expansions in coding regions: polyglutamine diseases, that involve CAG trinucleotide repetitions, leading to abnormal larger glutamine tracts within the respective proteins, and polyalanine diseases with GCN or GCG trinucleotide repetitions, leading to abnormal alanine tracts in the specific proteins. <u>CAG:</u> Citosine-Adenine-Guanine trinucleotide; <u>DRPLA:</u> Dentatorubral-pallidoluysian atrophy; <u>GCG:</u> Guanine-Citosine-Guanine trinucleotide; <u>GCN:</u> Guanine-Citosine-Any base trinucleotide; <u>HD:</u> Huntington's disease; <u>OPMD:</u> Oculopharyngeal muscular dystrophy; <u>SBMA:</u> Spinal and bulbar muscular atrophy; <u>SCA:</u> Spinocerebellar ataxia; <u>UTR:</u> Untranslated Region; <u>XLMR:</u> X-linked mental retardation.

1.1.1 Polyglutamine diseases

Polyglutamine (polyQ) diseases are the main group of hereditary neurodegenerative diseases caused by a trinucleotide repeat expansion (cytosine-adenine-guanine, CAG) in coding regions of the DNA. They are usually adult onset disorders with a progressive evolution of the clinical features. The respective resulting protein carries abnormal polyQ tracts in C or N-terminal regions of the proteins (see Table 1.1). Although, besides the presence of a common polyglutamine tract in all polyQ diseases, the specific protein of each disease share no homology outside the polyQ tract (reviewed in Zoghbi and Orr, 2000; Gatchel and Zoghbi, 2005). Disease severity, known as the onset of the symptoms and the extent of pathology, is closely related with the size of the polyQ tract, namely as long as the number of glutamines as severe is the disease, resulting in earlier ages of onset, and a worse neuropathology (Maciel et al., 1995; Ranum et al., 1995; Durr et al., 1996; reviewed in Riess et al., 2008). This relation results from an inherited instability in the number of glutamines in successive generations, contributing to a tendency to the expansion of the number of repeats – a phenomenon called anticipation (Myers et al., 1982; Myers et al., 1991; La Spada and Taylor, 2010).

There are nine polyQ diseases: HD, SBMA, dentatorubralpallidoluysian atrophy (DRPLA), and SCA 1, 2, 3, 6, 7, and 17 (reviewed in Zoghbi and Orr, 2000; Gatchel and Zoghbi, 2005; Shao and Diamond, 2007). All polyQ diseases are autosomal dominant, excluding SBMA that is an X-linked recessive disease (Zoghbi and Orr, 2000). Regardless of a widespread expression of the mutated proteins, all the polyQ diseases exhibit a selective neurotoxicity. Specific and well identified neuronal populations are affected in each polyQ disease resulting in characteristic clinical manifestations (see Table 1.1). The mechanisms underlying polyQ proteins neurotoxicity are not completely understood, but include: i) functional modifications of the host protein; ii) generation of toxic polyQ-containing fragments and inclusions; iii) transcriptional changes; iv) proteotoxic stress due to the disruption of the quality control systems of the cell; and v) mitochondrial dysfunction (reviewed in Shao and Diamond, 2007; Weber et al., 2014).

Table 1.1 The polyQ diseases.

PolyQ Disease	Causative protein Gene scheme	CAG repeat	Affected brain region	Inclusions location	Clinical features
HD	Huntingtin (HD)	36-121	Striatum, *globus pallidus*, cerebellar cortex	Nucleus and Cytoplasm	Chorea, dystonia, cognitive deficits, psychiatric problems
SBMA	Androgen Receptor (AR)	37-70	Motor neurons of the anterior horn and bulbar regions, dorsal root ganglia, skeletal muscle	Nucleus and Cytoplasm	Proximal and bulbar muscle weakness, muscle atrophy and fasciculation, mild androgen insensitivity
DRPLA	Atrophin-1 (ATN1)	49-88	Cerebellum (dentate nucleus), cerebral cortex, *globus pallidus*, basal ganglia	Nucleus	Ataxia, epilepsy/seizures, myoclonus, choreoathethosis, dementia
SCA1	Ataxin-1 (ATXN1)	39-91	Cerebellum (Purkinje cells and dentate nucleus), inferior olive, pons, anterior horn cells, pyramidal tracts	Nucleus	Ataxia, dysarthria, cognitive impairments, progressive motor deterioration
SCA2	Ataxin-2 (ATXN2)	32-200	Cerebellum (Purkinje cells), inferior olive, pons, *substantia nigra*, frontotemporal lobes	Nucleus	Ataxia, decreased reflexes, dysarthria, parkinsonian rigidity, sensory disturbance, mental deterioration
MJD/ SCA3	Ataxin-3 (ATXN3)	55-86	Cerebellum (mainly dentate nucleus), *globus pallidus*, pons, *substantia nigra*, striatum, cranial nerve nuclei, reticular formation, thalamus, spinal cord	Nucleus	Ataxia, neuromuscular complications, visual disorders, corticospinal and autonomic nervous system dysfunctions, neuropathy, weight loss
SCA6	CACNA1A (CACNA1A)	18-30	Cerebellum (Purkinje cells, dentate nucleus), inferior olive	Cytoplasm	Ataxia, dysarthria, oculomotor disorders, incontinence, peripheral neuropathy
SCA7	Ataxin-7 (ATXN7)	34-300	Cerebellum (Purkinje cells, molecular and granular layers), pons, inferior olive, visual cortex	Nucleus	Ataxia, retinal degeneration, dysphagia, dysarthria, changes in reflexes or sensation
SCA17	TATA-Binding Protein (TBP)	43-66	Cerebellum (Purkinje cells), inferior olive	Nucleus	Ataxia, cognitive decline/dementia, epilepsy/seizures, psychiatric problems

Until now, there are nine polyQ diseases described. For each disease is indicated the mutated protein, showing schematically the gene where the mutation occurred along with the glutamine expansion position (black rectangle and triangle). Affected brain region, main clinical features and main subcellular localization of inclusions are also showed. <u>CACNA1A:</u> Alpha 1A subunit of the voltage-gate Ca^{2+} channel; <u>DRPLA:</u> Dentatorubral-pallidoluysian atrophy; <u>HD:</u> Huntington's disease; <u>MJD:</u> Machado-Joseph disease; <u>SBMA:</u> Spinal and bulbar muscular atrophy; <u>SCA:</u> Spinocerebellar ataxia. Adapted from Todd and Lim, 2013; Cortes and La Spada, 2015.

1.1.1.1 Machado-Joseph disease

Machado-Joseph disease (MJD), also known as spinocerebellar ataxia type 3 (SCA3; Haberhausen et al., 1995), is a polyglutamine disease caused by a CAG repeat expansion, and is the most common autosomal dominant ataxia worldwide (reviewed in Ranum et al., 1995; Schols et al., 2004; Riess et al., 2008). It was originally described in people of Portuguese Azorean descent. Although, the disease has been identified in many other countries, including Australia, Brazil, Canada, China, Germany, Italy, Japan, United States of America, Spain, and Taiwan (reviewed in Bettencourt and Lima, 2011). MJD was initially identified in emigrant American families, namely Machado and Joseph families, from Azorean archipelago, to be exact São Miguel and Flores islands, respectively (Nakano et al., 1972; Rosenberg et al., 1976). The subsequent identification of families in Portugal led to the unification of the disease (Coutinho and Andrade, 1978).

ATXN3 gene is the gene causatively related with MJD, and is located on chromosome 14 (14q32.1; Takiyama et al., 1993; Kawaguchi et al., 1994). In normal conditions this gene has between 10 and 44 CAG repeats, but in pathological conditions the number is increased from 55 to 86 (Maciel et al., 2001). While intermediate size alleles are rare (45-54 CAG repeats), there are some reports of disease with this number of CAG repeats (Takiyama et al., 1995; van Alfen et al., 2001; Padiath et al., 2005). The mutation in the *ATXN3* gene leads to the expression of a mutated protein, namely mutant ataxin-3. Ataxin-3 is present in cytoplasm and nucleus (Paulson et al., 1997a; Schmidt et al., 1998; Tait et al., 1998; Trottier et al., 1998), and is also found in mitochondria (Pozzi et al., 2008). Mutant ataxin-3 contributes to neurodegeneration on specific cerebral regions, leading to specific symptoms that will be referred in the next sections.

1.1.1.1.1 Epidemiology

SCAs are globally considered rare diseases, with prevalence around 0.3 to 3.0 per 100,000 people (van de Warrenburg et al., 2002). MJD/SCA3 is considered the most common form of SCA worldwide (Schols et al., 2004). Initially it was considered a geographic distribution pattern of MJD related with the Portuguese discoveries. Although, since the molecular test, it is currently known that it is present in many ethnic backgrounds (Schols et al., 2004).

Regarding the prevalence of MJD in Portugal, in the mainland the prevalence is rare (1:100,000) (reviewed in Bettencourt and Lima, 2011), with some exceptions, such as a small area of the Tagus River Valley (1:1000) (Maciel et al., 2001). Though, it is highly prevalent in the Azores islands, where the highest worldwide prevalence occurs

in Flores island (1:239) (Bettencourt et al., 2008). Among SCAs, the relative frequency of MJD is higher in countries, such as Brazil (69-92%), Portugal (58-74%), Singapore (53%), China (48-49%), the Netherlands (44%), Germany (42%), and Japan (28-63%) (reviewed in van der Warrenburg et al., 2002; Bettencourt and Lima, 2011). Although, in countries as Canada, United States of America, Mexico, Australia, and India, the relative frequency is lower (reviewed in Bettencourt and Lima, 2011).

1.1.1.1.2 From *MJD1/ATXN3* gene to protein

The *MJD1/ATXN3* gene lengths ~48 kb and includes 11 exons, with the CAG repeat expansion residing in exon 10 (Ichikawa et al., 2001). Some years ago, in human brain and in non-nervous tissues, four different transcripts were described (Ichikawa et al., 2001). These multiple transcripts may result from an alternative splicing in exons 2, 10, and 11, in combination with different polyadenylation signals (Ichikawa et al., 2001). Three additional transcripts, that differ from the others, mainly at the C-terminal, were also previously reported (Goto et al., 1997). Later, several other new alternative splicing variants were discovered (Bettencourt et al., 2010; Harris et al., 2010; Bettencourt et al., 2013).

There is scarce information about the regulation of *MJD1/ATXN3* gene. The recent identification of two single nucleotide polymorphisms in the 3'UTR of ataxin-3 mRNA that are related with an earlier onset, indicated that this region is very important in the regulation of ataxin-3 (Long et al., 2015b). Moreover, the presence of different transcripts carrying different 3'UTRs suggests additional regulation at this level (Ichikawa et al., 2001). Recent publication also pointed to the potential regulation of ataxin-3 in this region by endogenous and non-endogenous microRNAs (Rodriguez-Lebron et al., 2013; Huang et al., 2014).

Since 1994, the year when *MJD1* gene was reported for the first time by Kawaguchi and colleagues, several studies were made in order to improve the knowledge about the characteristics and properties of ataxin-3 protein (Kawaguchi et al., 1994). It was demonstrated that ataxin-3 is widely expressed in different body tissues and cell types, including brain (with different patterns of expression in different brain regions), and neurons (Paulson et al., 1997a; Schmidt et al., 1998; Trottier et al., 1998; Ichikawa et al., 2001; Costa et al., 2004). Regarding its structure, ataxin-3 has a globular N-terminal domain followed by a flexible C-terminal tail (Masino et al., 2003). The N-terminal domain, also called Josephin domain, exhibits ubiquitin protease activity, whereas the flexible C-terminal tail presents two ubiquitin-interacting motifs (UIMs),

followed by the polyQ region of variable length (Burnett et al., 2003; Albrecht et al., 2004). As referred before, alternative splicing sites have been described, resulting different isoforms with the longest having an approximate molecular weight of 42 kDa (Goto et al., 1997; Trottier et al., 1998; Ichikawa et al., 2001). The most common isoform in the human brain has a third UIM localized in the C-terminal region, downstream of the polyQ sequence (Figure 1.2; Harris et al., 2010).

Figure 1.2 <u>Representation of the primary structure of ataxin-3.</u> Ataxin-3 contains an N-terminal deubiquituinase catalytic domain (Josephin domain, in blue) followed by 2 or 3 ubiquitin-interacting motifs (UIMs) (depending on the isoform, in orange), and a polyglutamine sequence of variable length (Q_n, in green). <u>Ub:</u> Ubiquitin. <u>UIM:</u> Ubiquitin Interacting Motif; <u>Q_n:</u> Polyglutamine tail.

Ataxin-3 function is not fully understood. The first *in vivo* clue about ataxin-3 function came from studies involving ataxin-3 knockout (Schmitt et al., 2007; Rodrigues et al., 2007). These studies indicated that ataxin-3 has a deubiquitinating activity, and is involved in the ubiquitin-proteosome pathway, due to an over accumulation of ubiquitinated proteins (Schmitt et al., 2007; Rodrigues et al., 2007). There are five families of deubiquitinases, and one of them is constituted by ataxin-3 and other Josephin domain-containing proteins (reviewed in Reyes-Turcu et al., 2009). Ataxin-3 is able to interact with poly-ubiquitin chains through the first two UIMs located at the C-terminal region, in an UIM-dependent manner, including in neural cells (Burnett et al., 2003; Berke et al., 2005). The third UIM is not relevant for the deubiquitinase activity (Donaldson et al., 2003; Chai et al., 2004; Harris et al., 2010). A different feature of ataxin-3 function includes its possible involvement in transcription regulation. In fact, it seems that ataxin-3 is able to regulate the expression of many genes (Evert et al., 2003). Ataxin-3 interacts with cAMP response element-binding protein (CREB)-binding protein (CBP), p300 and p300/CBP-associated factor (PCAF; Li et al., 2002), histone deacetylase 3 (HDAC3; Evert et al., 2006a), nuclear receptor co-repressor (NCor; Evert et al., 2006a), and histones (Li et al., 2002), interfering with gene expression.

1.1.1.1.3 Neuropathology and clinical symptoms

The expression of mutant ataxin-3 leads to neurodegeneration that affects several brain regions of the spinocerebellar tract and other areas of the central nervous system. Regarding the cerebellum, the cerebellar cortical neurons are preserved in most

cases and are not the focus of the neurodegeneration, although in some patients the loss of some Purkinje cells occurs (Kumada et al., 2000; Munoz et al., 2002). The cerebellar white matter atrophies and exhibits myelin pallor due to degeneration of pontocerebellar and spinocerebellar fibers. The dentate nucleus of the deep cerebellar nuclei shows a moderate to severe neuronal loss. Regarding basal ganglia, *substantia nigra* exhibits severe neuronal loss, while *globus pallidus* can be moderately affected (Rosenberg et al., 1976; Coutinho and Andrade, 1978; Coutinho et al., 1982; Yamada et al., 2008). Moreover, the striatum (caudate and putamen) shows progressive hypometabolism, such as reduced glucose uptake, and decreased dopaminergic metabolism (Taniwaki et al., 1997; Yen et al., 2000; Wullner et al., 2005). Additionally, in some non-human models, the striatum displays metabolic abnormalities and neuronal dysfunction (Goti et al., 2004; Bichelmeier et al., 2007; Alves et al., 2008b). Neuroimaging techniques (magnetic resonance imaging and quantitative volumetric 3-D analysis) demonstrated a severe atrophy in the whole brainstem (Schulz et al., 2010). Neurodegeneration is also found in the pontine nuclei (pons), cranial nerve nuclei, and reticular formation (Rosenberg et al., 1976; Coutinho and Andrade, 1978; Coutinho et al., 1982; Yamada et al., 2008). Thalamus, spinal cord, and cerebral cortex are also affected (Coutinho and Andrade, 1978; Kanda et al., 1989; Rosenberg, 1992; Sudarsky and Coutinho, 1995; Durr et al., 1996; Rub et al., 2008). Moreover, it was also reported a significant correlation of both brainstem and cerebellar atrophies with CAG repeat length, age, disease duration, and degree of disability (Camargos et al., 2011). Figure 1.3 summarizes the main brain regions affected in MJD.
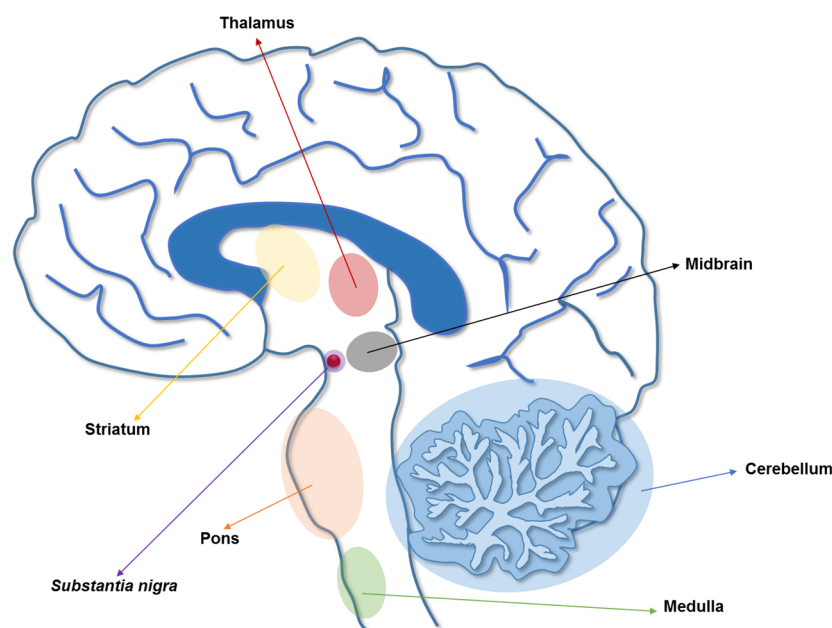
Figure 1.3 Main brain regions affected in MJD. The principal sites of neuronal dysfunction and death in MJD are: cerebellum, basal ganglia (striatum and *substantia nigra*), thalamus, midbrain, pons, and medulla.

MJD pathogenesis leads to a group of particular clinical symptoms. Most frequently in affected individuals a slowly progressive ataxia syndrome appears, typically beginning the ages of 20 to 50 years, with a survival after disease onset estimated in 21.18 years (Coutinho and Andrade, 1978; Paulson, 1993; Kieling et al., 2007). Other symptoms intrinsically-related appear, such as neuromuscular complications causing dystonia, dysarthria, spasticity, rigidity, postural instability and proprioceptive loss, visual disorders (nystagmus, eyelid retraction, ophtalmoparesis, and double vision), dysphagia, amyotrophy, corticospinal and autonomic nervous system dysfunctions, neuropathy, and loss of body weight (Rosenberg, 1992; Sudarsky and Coutinho, 1995; Riess et al., 2008).

1.1.1.1.4 Molecular mechanisms involved in neurodegeneration

Besides the clear description of the genetic basis of MJD, unfortunately the molecular understanding is still weak and sometimes controversial. Moreover, a part of the mechanistic underlying MJD is shared with other polyglutamine disorders (reviewed in Takahashi et al., 2010), and potentially not specific for MJD. Several pathogenic events contribute to MJD pathogenesis. One of them involves the toxicity of the expanded polyglutamine stretch that leads to the oligomerization and aggregation of mutant ataxin-3, generating toxic products (Figure 1.4). MJD is also linked with the dysregulation of quality control systems, such as autophagy, leading to the acceleration of disease progression (Figure 1.4). Mitochondrial impairments were also found, contributing to an increase of the oxidative stress (Figure 1.4). These are the mechanisms that will be focused on this thesis, on the next subsections. Besides that, other mechanisms can have an important role on MJD pathogenesis, such as transcriptional dysregulation, excitotoxicity and calcium homeostasis alterations, axonal transport disruption, abnormal protein-protein interactions, post-translational modifications, among others (reviewed in Costa Mdo and Paulson, 2012).
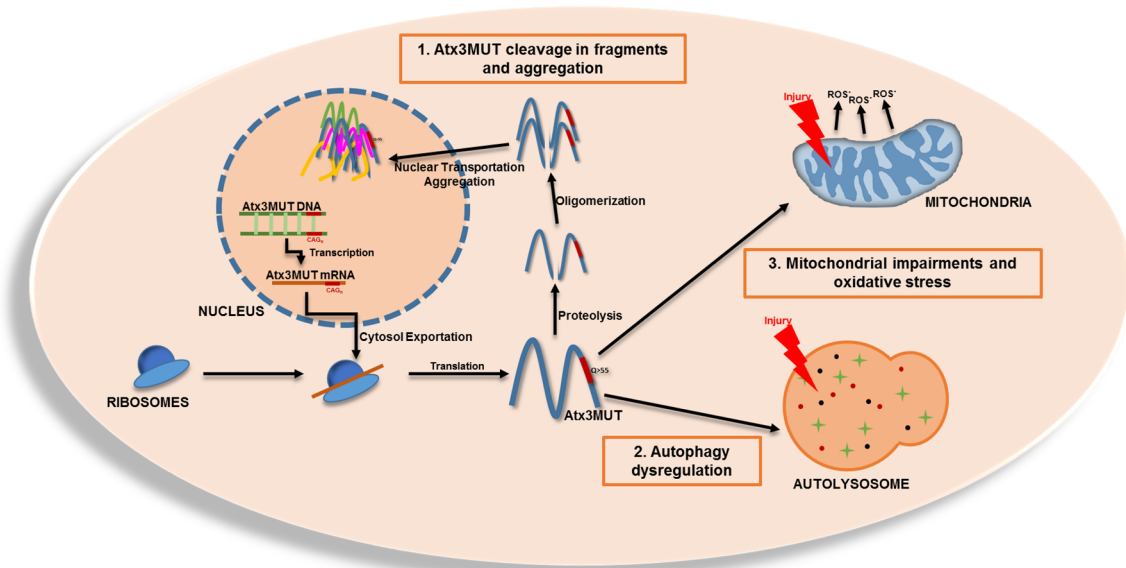
Figure 1.4 <u>Mechanisms behind Machado-Joseph disease pathogenesis.</u> Numerous mechanisms can contribute to the pathogenesis of MJD, such as: 1) the proteolytic cleavage of mutant ataxin-3 can generate toxic fragments, and the misfolded monomers, or toxic oligomers, can assemble into intranuclear inclusions; 2) the expression of the mutated ataxin-3 also contributes to the impairment of the quality-control system, as autophagy; 3) mutant ataxin-3 induces a dysfunction of the mitochondrial dynamics, contributing to the increase in oxidative stress. <u>Atx3MUT</u>: Mutant ataxin-3.

1.1.1.1.4.1 Mutant ataxin-3 aggregation and cleavage in fragments

In vitro and *in vivo* studies shed light about how the CAG repeat expansion in the *ATXN3* gene triggers the pathogenic mechanisms. In 2008, a study using a *Drosophila* model of MJD demonstrated that a RNA transcript with a hyper expanded CAG repeat is toxic, and leads to degeneration (Li et al., 2008a). While, several evidences suggest that mutant ataxin-3 protein is the most toxic specie. It is known that this expanded protein undergoes conformational changes and acquires toxic properties. These toxic properties are conferred either as a monomer, or as a part of an oligomeric/aggregate specie, causing an alteration of molecular interactions. Mutant ataxin-3 tends to aggregate in the nucleus (Paulson et al., 1997b; Evert et al., 1999; Fujigasaki et al., 2000), and thus the nucleus is considered an important subcellular localization for its pathogenesis (Bichelmeier et al., 2007). Mutant ataxin-3 can also interact with other proteins via exposed hydrophobic surfaces, negatively interfering with the normal function of these proteins, due to their trapping within aggregates. It was proposed that these large inclusions are the main cause of neurodegeneration (Paulson et al., 1997b). Nevertheless, recent studies have demonstrated that inclusions cannot be completely related with the pathogenic process, due to a not perfect match of such aggregates with neuronal loss (Trottier et al., 1998; Goti et al., 2004; Chou et al., 2008; Silva-Fernandes

et al., 2010). Moreover, accumulating evidences indicate that non-aggregated species, namely fragments that result from proteolysis mediated, for example by calpains, and oligomers, are more toxic than large insoluble aggregates (Figure 1.4; Ikeda et al., 1996; Hubener et al., 2011; Simoes et al., 2012; Simoes et al., 2014). In summary, there is not a consensual understanding about the main contributor (fragments, oligomers, or aggregates) for expanded ataxin-3 toxicity by the fact that different experimental paradigms using the full length or fragments of mutant ataxin-3 can lead to divergent results. Although, it is known that all these species are toxic. This is also controversial in other polyglutamine diseases, such as Huntington's disease.

1.1.1.1.4.2 Autophagy dysregulation

Cells are continuously producing a large amount of misfolded proteins and damaged organelles. Quality-control systems, such as ubiquitin-proteasome system (UPS) and autophagy are crucial in the maintenance of cellular function and viability. Ataxin-3 participates in the UPS system through the recruitment of poly-ubiquitinated substrates (Burnett et al., 2003; Mao et al., 2005; Schmitt et al., 2007; Rodrigues et al., 2007; Winborn et al., 2008). Thus, a loss of mutant ataxin-3 function could enhance neurodegeneration through the disruption of UPS pathway. Furthermore, mutant ataxin-3 nuclear inclusions are polyubiquitinated also suggesting a disruption of the UPS (Paulson et al., 1997b; Chai et al., 1999). Ataxin-3 can also be eliminated through autophagy and the induction of autophagy can rescue toxicity mediated by UPS malfunction (Pandey et al., 2007; Rubinsztein, 2007; Menzies et al., 2010; Nascimento-Ferreira et al., 2011; Nascimento-Ferreira et al., 2013).

There are three main different types of autophagy regarding the delivery of the cargo to lysosomes: chaperone-mediated autophagy, microautophagy, and macroautophagy. Henceforth, the focus will be macroautophagy, also simply called autophagy. Macroautophagy is the principal pathway of the degradation of long-lived proteins and also organelles. It is characterized by the formation of doubled-membrane autophagic vacuoles – autophagosomes – which then fuse with lysosomes to form autolysosomes (Figure 1.5). Once inside the lysosome, acidic lysosomal enzymes degrade the content and inner membrane of autophagosomes (reviewed in Levine and Klionsky, 2004; Mizushima et al., 2008). There are two important players on autophagy pathway, generally used to monitor autophagy: p62 or sequestosome 1 (SQSTM1) and light chain 3B (LC3B). The p62 is a polyubiquitin-binding protein that recognizes toxic cellular waste. It resides freely in the cytosol and in the nucleus, and can be scavenged

by sequestration in the autophagosomes and lysosomal structures (Bjorkoy et al., 2005; Rusten and Stenmark, 2010). The lack of autophagy leads to an increase in the size and number of p62 bodies and protein levels (Bjorkoy et al., 2005). It is degraded inside the autolysosomes. On the other hand, LC3B colocalizes with p62 bodies, indicating that these two proteins participate in the same complexes. Once autophagy is activated, the cytosolic form of LC3B (LCBI) is conjugated with phosphatidylethanolamine to form LC3-phosphatidylethanolamine conjugate (LC3BII), which is recruited to autophagosomal membranes (Figure 1.5; reviewed in Tanida et al., 2008). After the fusion between lysosomes and autophagosomes, LCB3II is degraded and recycled to LC3BI. Therefore, lysosomal turnover of LCBII reflects autophagic activity and can be used to monitor autophagy (reviewed in Tanida et al., 2008). LC3BII and p62 are directly related, since p62 recognizes polyubiquitinated proteins and via LC3BII interaction conduces them to the autophagy machinery (Bjorkoy et al., 2005).
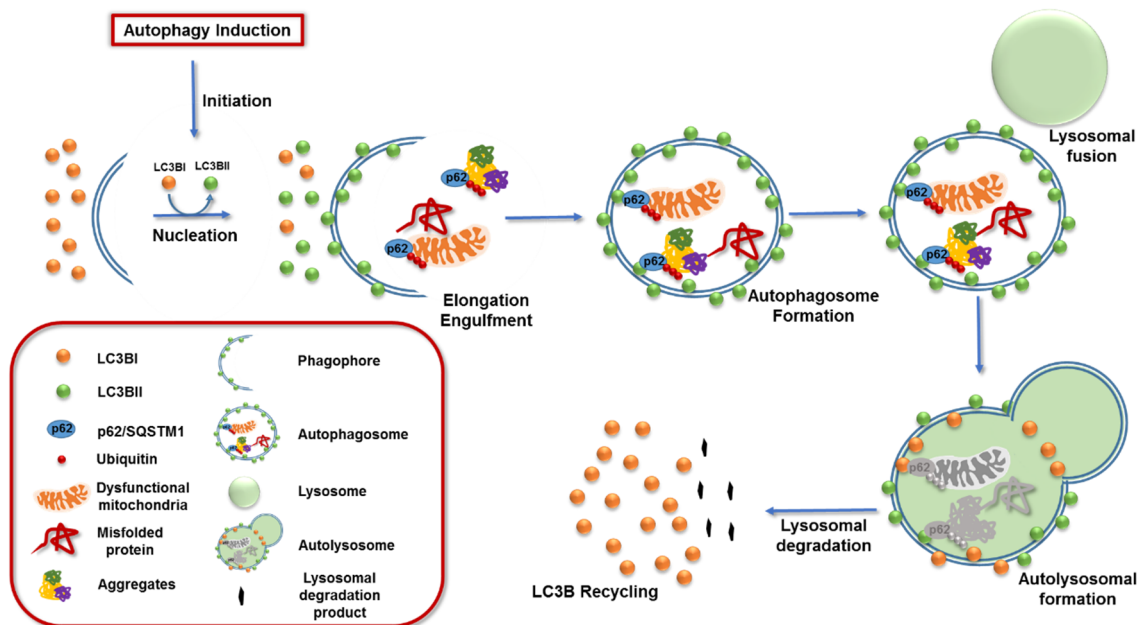
Figure 1.5 <u>Schematic diagram of the principal steps of macroautophagy.</u> Once autophagy is activated, an unidentified membrane source delivers bi-layers for the formation of the phagophore. Throughout this process, LC3BI is converted into LCBII, by the addition of a phosphatidylethanolamine group. Then, more membrane and LC3BII are recruited to the developing vacuole (elongation step). Meanwhile, as the phagophore expands, cytoplasmic components, such as organelles, aggregated proteins, and misfolded proteins are enwrapped. At the end of elongation, sequestering membrane closes and results in the formation of the autophagosome, a double-membrane vesicle. After that, autophagosome fuses with lysosome to form autolysosome for degradation. Lysosomal enzymes degrade the cargo together with the autophagosome membranes, p62 is degraded, and LC3BII is recycled into LC3BI. This process can act as a homeostatic mechanism to support cell survival. <u>LC3B:</u> Microtubule-associated protein 1 light chain 3 B light-chain 3B; <u>SQSTM1:</u> Sequestosome 1.

Mutant ataxin-3 is degraded by autophagy (Menzies et al., 2010; Nascimento-Ferreira et al., 2011; Nascimento-Ferreira et al., 2013; Dubinsky et al., 2014). As referred before, one of the main subcellular localizations of mutant ataxin-3, in the form of aggregates, is the nucleus. Nevertheless, while the UPS is present both in cytoplasm and nucleus, even with lower nuclear activity (reviewed in Li et al., 2008b), autophagy is described as a cytoplasmic mechanism, since there are no lysosomes at the nucleus (reviewed in Cuervo, 2004). Although, the autophagy activation is able to increase mutant ataxin-3 aggregates clearance. Hence, three main situations may occur: i) clearance at the cytoplasm of some precursors and microaggregates before their nuclear translocation, reducing nuclear aggregation; ii) shuttling of nuclear aggregates to the cytoplasm or perinuclear region for degradation; iii) presence of cytoplasmic inclusions besides the intranuclear inclusions (Yamada et al., 2004). Moreover, it was also showed by our group and others that intranuclear inclusions sequesters important autophagy proteins in a rodent mouse model of MJD, and their expression is abnormally altered in MJD patient's brain (Nascimento-Ferreira et al., 2011; Mori et al., 2012). Particularly, in our group we observed that endogenous autophagic markers, namely p62 and LC3B, are accumulated in the brain of MJD patients, and in the striatum of mice in the striatal lentiviral model of MJD (Nascimento-Ferreira et al., 2011). Moreover, beclin-1, a protein that participates in the early stage of nucleation was found to be reduced in the striatum of MJD mice (Nascimento-Ferreira et al., 2011). More recently, our group also demonstrated that autophagy is impaired in fibroblasts from MJD patients (Onofre et al., 2016). Likewise, therapeutic strategies that increase autophagy activation through pharmacological or molecular approaches contributed to mutant ataxin-3 clearance and had a positive role on MJD pathogenesis (Nascimento-Ferreira et al., 2011; Nascimento-Ferreira et al., 2013; Dubinsky et al., 2014; Silva-Fernandes et al., 2014; Onofre et al., 2016).

1.1.1.1.4.3 Mitochondrial impairments and oxidative stress

Mitochondrial dysfunction has been associated with aging and age-related diseases, particularly with neurodegenerative diseases (reviewed in Knott et al., 2008). Regarding polyQ diseases, evidences that mitochondrial dysfunction contributes to polyQ neurodegeneration, came firstly from studies in HD (Browne et al., 1997; Panov et al., 2002; Orr et al., 2008; Lou et al., 2016). These studies demonstrated that energy metabolism is compromised in HD and oxidative damages are increased, leading to neurodegeneration. Furthermore, due to the ATP-dependency of the protein quality control system, mitochondrial dysfunction can aggravate protein misfolding or reduce the

degradation of polyglutamine proteins (Gines et al., 2003). Mitochondrial dysfunction was also observed on other polyglutamine disorders, such as SBMA (Beauchemin et al., 2001), DRPLA (Lodi et al., 2000), SCA1 (Kish et al., 1999), and also in MJD.

Regarding MJD, in 1996, Matsuishi and colleagues described a metabolic disarrangement in the cerebrospinal fluid of MJD patients, suggesting that mitochondrial function could be affected (Matsuishi et al., 1996). In fact, later on, *in vitro* studies using cellular models of MJD showed that the expression of mutant ataxin-3 promotes mitochondrial-mediated cell death, increases oxidative stress, and reduces mitochondrial DNA copy number, suggesting an alteration on mitochondrial function, and the last two changes were also observed in human brain tissues (Tsai et al., 2004; Chou et al., 2006; Yu et al., 2009). Moreover, wild-type and mutant ataxin-3 were found in mitochondria, but regarding the fragments of ataxin-3, resulting from proteolysis, only the fragments of mutant ataxin-3 were found in mitochondria, suggesting a potential mitochondrial damage generated by changes induced by them (Pozzi et al., 2008). Another study, using a MJD mouse model, clarified that mitochondria from MJD animals are dysfunctional, particularly complex II of the respiratory chain (Laco et al., 2012). Lately, it was also shown that mtDNA is damaged in blood and brain samples from a transgenic MJD mouse model, suggesting that in fact mitochondrial function is compromised (Kazachkova et al., 2013; Ramos et al., 2015). Altogether, these results suggest that mitochondrial dysfunction contributes to MJD pathogenesis, although a clear explanation about how a pathogenesis that is mainly focused on the nucleus generates a mitochondrial dysfunction, is still lacking.

1.1.1.1.4.4 Other mechanisms underlying Machado-Joseph disease pathogenesis

As described before, several mechanisms are behind MJD pathogenesis. Besides the three mechanisms already described, other mechanisms are summarized in Figure 1.6.

Briefly, it is known that ataxin-3 interacts with other proteins and the loss or alteration on these interactions, promoted by the mutation, may contribute to its toxicity (Deriu et al., 2014). Furthermore, mutant ataxin-3 inclusions were observed in axons of several brain regions of MJD patients, suggesting an interference in normal axonal transport mechanisms, and in that way contributing to the degeneration of nerve cells in MJD (Seidel et al., 2010). Mutant ataxin-3 seems to have a negative role in the regulation of intracellular calcium and the treatment with a Ca^{2+} stabilizer (dantrolene) was able to

ameliorate the disease (Chen et al., 2008b). Moreover, some studies showed another potential mechanism behind mutant ataxin-3 toxicity. They suggest that the accumulation of nuclear inclusions of mutant ataxin-3 can induce an abnormal interaction with transcriptional factors or cofactors, leading to an erroneous transcription (McCampbell et al., 2000; Chou et al., 2008; reviewed in Yamada et al., 2000), although, further studies are needed. Furthermore, due to the changes on mutant ataxin-3 protein, it can be abnormally processed after translational, inducing an increase on its toxicity.
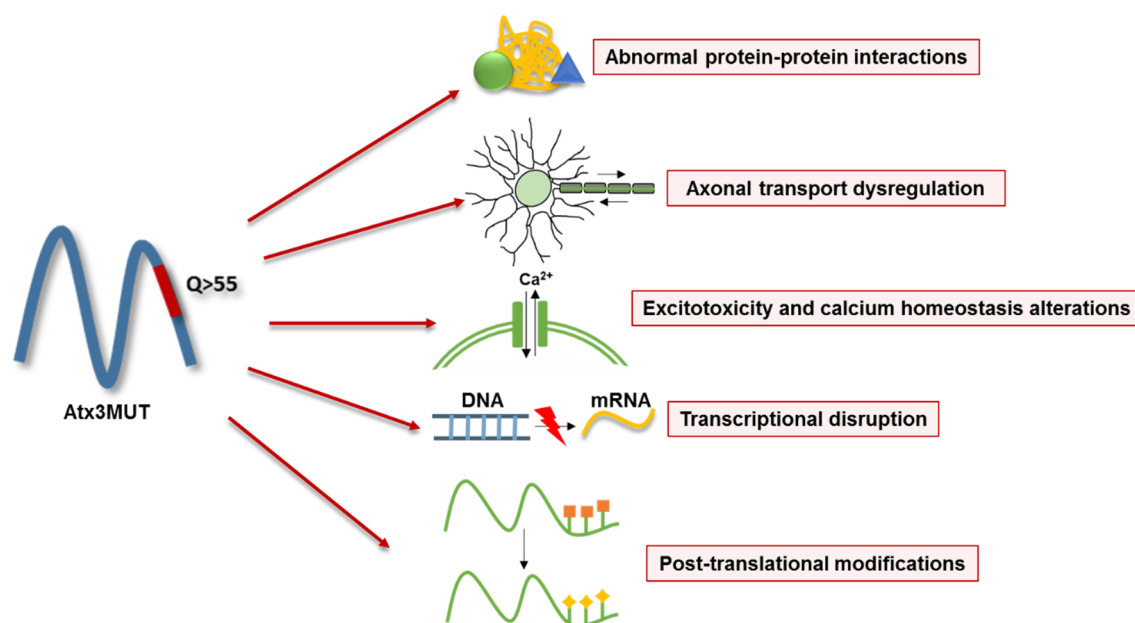
Figure 1.6 <u>Other mechanisms underlying MJD pathogenesis.</u> Besides the mechanisms related to mutant ataxin-3 protein modification by proteolysis, oligomerization and aggregation, the changes in autophagy, and in mitochondrial function, previously explained, there are several other mechanisms, such as: i) erroneous protein-protein interactions; ii) axonal transport dysregulation; iii) excitotoxicity and calcium homeostasis alterations; iv) transcriptional disruption; and v) post-translational modifications. <u>Atx3MUT:</u> Mutant ataxin-3.

1.1.1.1.5 Cellular and animal models of Machado-Joseph disease

In the past two decades several cellular and animal models of MJD were developed. These models allowed the study of the pathogenesis behind MJD and they have been used to test potential therapeutic strategies. Nevertheless, they do not entirely resemble all the pathological events in humans, principally the cellular models.

Cellular models include neuronal or non-neuronal cell lines, and primary cultures (rodent neuronal cells from cerebellum, striatum or *substantia nigra*, or fibroblasts from MJD patients) genetically modified to transiently or stably express the full-length, or truncated form of ataxin-3 (Paulson et al., 1997b; Yoshizawa et al., 2001; Chen et al., 2008b; Chou et al., 2011b). These cellular models of MJD offer suitable approaches to

study the pathological mechanisms behind MJD, although they have some limitations regarding the representation of the neuropathology associated with the disease. To overcome these limitations, animal models were developed and will be develop in the next subsections.

1.1.1.1.5.1 Animal models of Machado-Joseph disease

Regarding MJD, several studies have been focusing on the development of animal models for this disease. Animal models of MJD were developed by the generation of transgenic lineages expressing human full length expanded ataxin-3, or a truncated portion of ataxin-3. So far, the currently used MJD animal models that have been created in invertebrates include: *Caenorhabditis elegans* (Khan et al., 2006; Teixeira-Castro et al., 2011; Christie et al., 2014; Teixeira-Castro et al., 2015), and *Drosophila melanogaster* (Warrick et al., 1998; Bonini, 1999; Warrick et al., 1999; Kim et al., 2004; Warrick et al., 2005; Jung et al., 2009). These models are especially interesting for a large-scale pharmacological and genetic screening studies. MJD fruit flies models express full length or truncated mutant ataxin-3, presenting locomotor dysfunction, formation of intranuclear aggregates, and neuronal loss (Warrick et al., 1998; Warrick et al., 1999; Bonini, 1999; Kim et al., 2004; Warrick et al., 2005; Jung et al., 2009). In worms, the expression of the full length or truncated mutant ataxin-3 in the nervous system led to motor dysfunction, aggregation of mutant ataxin-3, and some neuronal abnormalities (Khan et al., 2006; Teixeira-Castro et al., 2011; Christie et al., 2014; Teixeira-Castro et al., 2015). These invertebrate models have some advantages related with their low cost, simplicity, lower time requirements, ease of maintenance and to genetically manipulate, and the absence of blood-brain barrier (reviewed in Bates and Hockly, 2003). However, invertebrate models of MJD are far away from resembling the human disease.

Rodents, namely mice and rats, are so far, the most frequently used animals to model MJD, since these mammals share some important similarities with humans that fruit flies or worms do not share.

1.1.1.1.5.1.1 Rodent models of Machado-Joseph disease

Mouse models of MJD have been very useful to explore the pathogenesis of the disease, and to test some therapies. Up to now, 15 mouse models and variants of MJD have been developed, although the majority of them expresses cDNA driven by unrelated and non-physiological promoters, such as Purkinje cells-specific L7, prion, rat huntingtin, and cytomegalovirus (CMV) promoters (Ikeda et al., 1996; Goti et al., 2004;

Bichelmeier et al., 2007; Torashima et al., 2008; Chou et al., 2008; Boy et al., 2009; Boy et al., 2010; Silva-Fernandes et al., 2010; Silva-Fernandes et al., 2014). Additionally, an N-terminal ataxin-3 cDNA gene trap model, excluding the C-terminal region of the protein and the CAG tract, has demonstrated ataxia-like alterations (Hubener et al., 2011). In 2002, a model that includes the full gene and endogenous regulatory sequences of human origin was developed, namely the yeast artificial chromosome (YAC) transgenic model (Cemal et al., 2002). Excluding the last mouse model (Cemal et al., 2002), all the other mouse models have reproduced many features of SCA3 pathogenesis, but showed an unnatural expression pattern, due to the use of unrelated promoters, a non-expression of the full length protein and the endogenous regulators, and an excessive number of transgene copies. To solve some of these problems, two knock-in mouse models were recently created (Ramani et al., 2015; Switonski et al., 2015). One of the models inserted a long CAG repeat into the endogenous ataxin-3 gene of mice (Ramani et al., 2015), and the other led to the creation of a full humanized allele's coding sequence, producing a human mutant ataxin-3 protein (Switonski et al., 2015). All these models are explored in the following Table 1.2.

Table 1.2 Mouse models of Machado-Joseph disease.

Protein expressed Number of Q repeats	Expression system Distribution	Neuropathology	Motor Phenotype	Observations	References
Truncated *vs* full length human ataxin-3 79Q	L7 Promoter Cerebellar Purkinje cells	Cerebellar atrophy of all the three cortical layers (molecular, Purkinje cells, and granular).	Gait disturbances Ataxia	Truncated mutant ataxin-3 induced clear pathological changes, but the same did not occur with the full-length. Neurotoxicity-mediated by a toxic fragment.	Ikeda et al., 1996
Full-length human ataxin-3 64, 67, 72, 76 and 84Q	YAC (native regulators) Ubiquitous	Cell death in pontine and cerebellar nuclei. Ubiquitin-positive nuclear inclusions.	Wide-based gait Tremor Motor incoordination Reduced weight Hypotonia	Gene dosage and polyQ length correlate positively with phenotype.	Cemal et al., 2002
Full-length human ataxin-3 71Q	Prion promoter Ubiquitous (but directed to brain and spinal cord)	No relevant neurodegeneration found. Nuclear inclusions in deep cerebellar, pontine nuclei, and spinal cord.	Ataxia Postural instability Weight loss Premature death	Only homozygous had the phenotype. Results support the theory that the fragments are the most toxic form of ataxin-3.	Goti et al., 2004; Colomer Gould et al., 2007
Full-length human ataxin-3 70Q/148Q	Prion promoter fragment Several brain regions (including pons and cerebellum)	Neurodegeneration of Purkinje cells. Ubiquitin-positive nuclear inclusions in several brain regions.	Tremor Gait impairments Reduced motor behavior Reduced weight Premature death	Gene dosage, number of inclusions, and polyQ length correlate positively with phenotype. Nuclear localization of inclusions is important.	Bichelmeier et al., 2007
HA-tagged full-length human ataxin-3 79Q	Prion promoter Several brain regions (including cerebellum, brainstem, striatum, and spinal cord)	No relevant neuronal death found. Nuclear inclusions in neurons of the dentate nucleus, pontine nucleus, and *substantia nigra*.	Motor incoordination Gait impairments Hypoactivity Reduced weight gain	This mouse model displayed transcriptional dysregulation even before neurological symptoms.	Chou et al., 2008

Protein expressed Number of Q repeats (Cont.)	Expression system Distribution (Cont,)	Neuropathology (Cont,)	Motor Phenotype (Cont,)	Observations (Cont.)	References (Cont,)
Truncated human ataxin-3 69Q	L7 Promoter Cerebellar Purkinje cells	Severe cerebellar atrophy of all the three cortical layers (molecular, Purkinje cells, and granular). Nuclear inclusions and affected synaptic transmission of Purkinje cells.	Gait disturbances Ataxia at early stages Imbalance Reduced body weight	Some ubiquitinated large inclusions were found close to, but outside of the soma of Purkinje cells. These Purkinje cells are not apoptotic, but are substantially impaired.	Torashima et al., 2008; Oue et al., 2009
Full-length human ataxin-3 77Q	*Tet-off* system (ataxin-3 under the control of a CMV promoter transactivated by a prion promoter) Brain (mainly cerebellum, but in glia cells)	Neurodegeneration of Purkinje cells and molecular layer of cerebellar cortex.	Gait impairments Spasticity Hyperactivity Reduced body weight	Turning off the expression of ataxin-3 in an early disease state reversed the phenotype. The glial dysfunction may explain the Purkinje cells disruption.	Boy et al., 2009
Full-length human ataxin-3 148Q	Rat huntingtin promoter Ubiquitous in brain	Nuclear inclusions in pons and cerebellum (including Purkinje cells, with degeneration of them)	Motor incoordination Hyperactivity Reduced anxiety Reduced motor learning	Weaker expression of ataxin-3 in comparison with the previous models. Later onset of the symptoms (12-14 months), and slower progression.	Boy et al., 2010
Full-length human ataxin-3 94Q	CMV promoter Ubiquitous	No nuclear inclusions were observed. Astrogliosis and atrophy of dentate and pontine nuclei, *substantia nigra*, and thalamus.	Motor incoordination Reduced locomotor activity	These animals showed somatic mosaicism. Generational instability of CAG repeats (as high is the number of CAG as worse is the phenotype).	Silva-Fernandes et al., 2010

Protein expressed Number of Q repeats (Cont.)	Expression system Distribution (Cont,)	Neuropathology (Cont,)	Motor Phenotype (Cont,)	Observations (Cont.)	References (Cont.)
Truncated mouse ataxin-3 (mutation in mouse ataxin-3 gene – Gene trap) Only N-terminus (does not have polyQ tract)	Endogenous regulators Brain and spinal cord	Prominent extranuclear protein aggregates with neuronal cell death. Altered endoplasmic reticulum-mediated unfolded response.	Tremor Gait disturbances Ataxia Weight loss Premature death	Suggests that N-terminal fragment resulting from calpain processing is toxic. Symptoms onset at 9 months.	Hubener et al., 2011
Full length human ataxin-3 135Q	CMV promoter Ubiquitous (including several brain regions)	Brain atrophy at late stages (40 weeks). Nuclear inclusions in neurons in different brain regions (pontine and dentate nuclei, pons, spinal cord, among others).	Unhealthy appearance Abnormal body posture Limb clasping Limb tonus deficit Decline in body weight Ataxia	WT and transgenic animals indistinguishable in cages before 16 weeks of age. Earlier motor phenotype than neuropathology.	Silva-Fernandes et al., 2014
Mouse full-length ataxin-3 (Knock-in) 82Q	Endogenous promoter Ubiquitous (including several brain areas)	Intranuclear inclusions mainly on striatum, hippocampus, cortex, and DCN. Extranuclear inclusions mainly on hippocampus, amygdala, and cortex.	No relevant alterations	Knockin mice display altered splicing. Ataxin-3 accumulation is noted especially in the hindbrain.	Ramani et al., 2015
Human full-length ataxin-3 (Knock-in) 91Q	Endogenous promoter Ubiquitous (including several brain areas)	Intranuclear and perinuclear inclusions in various brain regions: cerebellum, cortex, and hippocampus. Astrogliosis and neurodegeneration at cerebellum.	Late onset (90 weeks) motor incoordination and imbalance	Early transcriptional changes in the brain. Late disease onset.	Switonski et al., 2015

Summary of the main mouse models of MJD indicating particularities, such as: i) protein expressed; ii) number of repeats; iii) distribution; iv) neuropathology; and v) motor phenotype. CMV: Cytomegalovirus; DCN: Deep cerebellar nuclei; HA: Hemagglutinin; polyQ: Polyglutamine; Q: Glutamine; WT: Wild-Type; YAC: Yeast Artificial Chromosome.

There are some important particularities that arose from these studies. Boy and colleagues (2010) demonstrated that transgenic MJD mice have motor dysfunction before the formation of nuclear inclusions (Boy et al., 2010) and Maciel's group also reported that neurodegeneration can occur even in the absence of nuclear inclusions (Silva-Fernandes et al., 2010). These studies suggested that there is no clear correlation between neuronal intranuclear inclusions and MJD-like symptoms. Moreover, it was also suggested that the subcellular localization of mutant ataxin-3 is important. Bichelmeier and colleagues (2007) showed that the nuclear localization of mutant ataxin-3, driven by the expression of a nuclear localization signal (NLS) exacerbated the phenotype compared to mice that expressed nuclear export signal (NES) (Bichelmeier et al., 2007). Furthermore, it was also clear that truncated forms of ataxin-3 induces a more severe pathology with an earlier age of onset of behavioral impairments (3-4 weeks of age; Ikeda et al., 1996; Torashima et al., 2008; Oue et al., 2009), whereas the expression of the full-length mutant ataxin-3 promoted a late onset and a milder phenotype (Cemal et al., 2002; Goti et al., 2004; Bichelmeier et al., 2007; Chou et al., 2008; Boy et al., 2010; Silva-Fernandes et al., 2010; Silva-Fernandes et al., 2014). Additionally, with a *Tet-Off* system it was demonstrated that the reversion of motor symptoms is possible after shutting off the expression of the mutated protein at an early stage of the disease (Boy et al., 2009).

There are other rodent models of MJD that allow a genetic modelling of the disease through a faster and well-controlled way, namely the MJD lentiviral-based animal models that will be described in the next section.

1.1.1.1.5.1.1.1 Lentiviral rodent models of Machado-Joseph disease

As described before, regarding the rodent models of MJD, we have transgenic, knock-in, and gene trap rodent models. We also have rodent models where neurodegenerative diseases, in this particular case, MJD, can be modeled through the stereotaxic injection of viral vectors encoding for mutant ataxin-3 in specific brain regions (reviewed in Deglon and Hantraye, 2005). This is a widely used strategy to elucidate and dissect the molecular basis of diseases, reproducing the neuropathology and behavioral abnormalities of each disease, through the expression of the disease-causing protein. There are some advantages of the use of these genetic viral-mediated vectors in detriment of the use of transgenic mice. With these mouse models we can control the onset and the time-course of the neurodegeneration, and this onset can be fast due to the high transduction efficiencies, and the robust and persistent transgene expression. We can also control the levels of the disease-causing protein through the manipulation

of the titer and/or amounts of the vectors (Senut et al., 2000; reviewed in Deglon and Hantraye, 2005). Furthermore, we can select a specific brain region that we want to precisely transduce, overcoming the unexpected phenotypic effects associated with a widespread overexpression of the transgene (Senut et al., 2000; reviewed in Deglon and Hantraye, 2005). This strategy can also be used as a therapeutic approach using MJD-modifier genes or delivering RNA interference mediators to allow the shutting-down of the disease-causing gene (Alves et al., 2008a; Alves et al., 2010; Nascimento-Ferreira et al., 2011; Simoes et al., 2012; Nascimento-Ferreira et al., 2013; Nobrega et al., 2013b; Nobrega et al., 2014; Duarte-Neves et al., 2015; Nobrega et al., 2015).

There is an extensive range of viral vectors that can be used (Table 1.3), and the viral vector should be tailored accordingly to the specific properties of each one and our objectives. As detailed in Table 1.3 these properties are: i) packaging capacity; ii) ability to integrate or not in the host genome; iii) tropism; and iv) tendency to elicit immune responses. The most desired characteristics for neurodegenerative diseases modelling are long term expression, tropism to non-dividing cells, high packaging capacity, and low immunogenicity, and thus the most used option are the lentivirus. In fact, in 2002 lentivirus were used for the first time to develop a rat model of Huntington's disease (de Almeida et al., 2002).

Table 1.3 <u>Most used viral vectors.</u>

Vector	Packaging Capacity	Tropism	Inflammatory properties	Observations
Retrovirus (Enveloped)	~8 kb	Dividing cells	Low	They integrate their genetic material, and in some applications this leads to oncogenesis.
Lentivirus (Enveloped)	~8 kb	Broad	Low	They integrate their genetic material, and in some applications this leads to oncogenesis.
AAV (Non-enveloped)	<5 kb	Broad	Low	It is non-pathogenic. Generally (90%) genetic material is episomal and does not integrate.
Adenovirus (Non-enveloped)	~30 kb	Broad	High	Vector genome is episomal, but has high efficiency transducing tissues.

Four main groups of viral vectors: retrovirus, lentivirus, AAV and adenovirus, and the main characteristics of each one. <u>AAV:</u> Adeno-associated virus; <u>kb:</u> Kilo base pairs; Adapted from Thomas et al., 2003.

Regarding MJD rodent models using the stereotaxic injection of lentiviral vectors encoding for mutant ataxin-3 (Table 1.4), in 2008 in our group, it was developed the first

viral-based model for MJD (Alves et al., 2008b). This was done through the injection of recombinant lentiviruses encoding for the full-length ataxin-3 with 72 glutamines, under the control of the phosphoglycerate kinase (PGK) promoter in different brain regions: *substantia nigra*, cortex, and striatum (Alves et al., 2008b). The same vector encoding for the full-length normal ataxin-3 with 27 glutamines was used as control (Alves et al., 2008b). The injection in the *substantia nigra*, a region that is generally affected in MJD patients, induced the formation of intranuclear inclusions, the depletion of tyrosine-hydroxilase (TH) and vesicular monoamine transporter-2 (VMAT2) in dopaminergic neurons, and motor behavior impairments (Alves et al., 2008b). Interestingly, the injection of the lentiviral vectors into the striatum (a brain region that is mildly affected in the patients) also led to neuropathological changes that include the loss of DARPP-32 staining and neuronal nuclei (NeuN), and the formation of intranuclear inclusions and pyknotic nuclei, leading to neurodegeneration (Alves et al., 2008b). This model was initially developed in rats (Alves et al., 2008b) and later on in mice (Simoes et al., 2012). It was also developed a model in a different brain region – cerebellum (Nobrega et al., 2013a), all summarized in Table 1.4.

Table 1.4 <u>MJD rodent models using lentiviral vectors.</u>

Rodent specie	Brain region	Phenotype	Reference
Rat	*Substantia nigra*	Formation of ubiquitinated ataxin-3 aggregates. Loss of dopaminergic markers (TH and VMAT2) and neuronal markers (NeuN). Motor behavior impairments.	Alves et al., 2008b
Rat	Striatum	Reduction of DARPP-32 and NeuN immunoreactivity. Formation of intranuclear inclusions and pyknotic nuclei.	Alves et al., 2008b
Mouse	Striatum	Ataxin-3 aggregates. Reduction of DARPP-32 immunoreactivity.	Simoes et al., 2012
Mouse	Cerebellum	Accumulation of ataxin-3 intranuclear inclusions in the cerebellum. Neuronal dysfunction and neurodegeneration in the cerebellum. Reduced motor coordination, wide-based ataxic gait, and hyperactivity.	Nobrega et al., 2013a

Summary of the lentiviral rodent models of MJD and the main characteristics associated with each one. <u>DARPP-32:</u> Dopamine- and cAMP-regulated neuronal phosphoprotein. <u>TH:</u> Tyrosine hydroxilase. <u>VMAT2:</u> Vesicular monoamine transporter 2.

1.1.1.1.6 New perspectives in the treatment of Machado-Joseph disease

Unfortunately, until now, MJD and the other polyglutamine diseases are untreatable. Although, despite the absence of a preventive strategy for the disease, there are available some pharmacological and nonpharmacological strategies to treat symptoms. Furthermore, research groups have been tapping into the available knowledge about the specificities of these disorders in order to investigate rational therapeutic approaches.

Physiotherapy is a common option for MJD symptomatic treatment. It may help the patients to cope with the disability related with gait problems (D'Abreu et al., 2010). Walkers and wheelchairs can assist the patients in their everyday activities. Furthermore, systematic speech therapy can help on the dysarthria and dysphagia problems, as well as occupational therapies (D'Abreu et al., 2010).

Pharmacological symptomatic therapies for MJD tested in clinical trial and respective outcomes are summarized in Table 1.5. Furthermore, the pre-clinical studies with potential pharmacological or molecular treatments for MJD, and the respective main results are summarized in Table 1.6. Figure 1.7 indicates different strategies that can be developed to treat MJD and, in fact, represent the main lines of study of the pre-clinical studies summarized in Table 1.6.
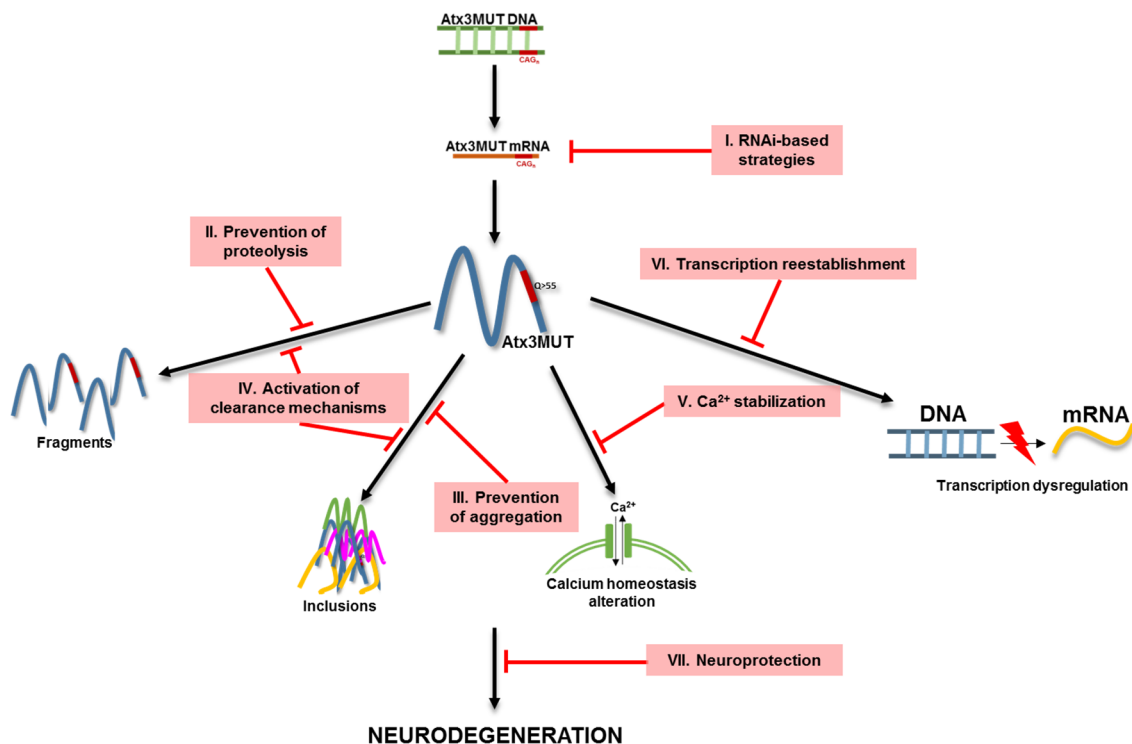
Figure 1.7 Potential therapeutic targets for MJD. As demonstrated in the previous sections, the expression of mutant ataxin-3 leads to a cascade of events culminating in the neuronal death. Some of these events include: i) formation of mutant ataxin-3

Figure 1.7 (cont.) inclusions; ii) proteolytic cleavage of mutant ataxin-3, leading to the generation of toxic fragments; iii) alterations in the calcium signaling; and iv) dysregulation of transcription. There are seven main lines of action, in which the more recent pre-clinical studies are based on: i) reduction of the levels of expanded proteins using RNAi-based strategies to promote gene silencing; ii) prevention of the proteolysis through the administration of inhibitors of proteases, such as calpastatin that inhibits calpains; iii) prevention of the aggregation, using inhibitors of aggregation or preventing the nuclear transportation; iv) activation of the clearance mechanisms, such as UPS or autophagy; v) administration of calcium stabilizers; vi) targeting transcription in order to increase it; and vii) use neuroprotective strategies that can act directly or indirectly on other mechanisms. Atx3MUT: Mutant ataxin-3; RNAi: RNA interference.

Table 1.5 Outcomes from clinical trials with drugs used as symptomatic approaches in Machado-Joseph disease.

Drug(s)	Outcomes	References
Trimethoprim + sulfamethoxazole	Reduction of the spasticity, improvement of the walker-assisted gait, improvement in hyperreflexia of knee jerks and of rigospasticity.	Mello and Abbott, 1988; Azulay et al., 1994; Correia et al., 1995; Sakai et al., 1995
Trimethoprim + sulfamethoxazole	No significant effects.	Schulte et al., 2001
Fluoxetine	No significant effects.	Monte et al., 2003
Taltirelin hydrate	Amelioration of the ataxic speech.	Shirasaki et al., 2003
Tandospirone	Reduction of the ataxia and depression, and alleviation of insomnia and leg pain.	Takei et al., 2004
Lamotrigine	Amelioration of the gait disturbances in an early stage of the disease.	Liu et al., 2005
Varenicline	Improvement of axial symptoms and alternating movements.	Zesiewicz et al., 2012
Lithium Chloride	Safe but only with slight beneficial effects on motor deficits.	Saute et al., 2014; Saute et al., 2015
Valproic acid	Improvement of locomotor function without significant side effects.	Lei et al., 2016

Summary of the clinical trials with drugs to symptomatically treat MJD, indicating the drug(s) and the observed outcomes.

Table 1.6 Results from pre-clinical studies in Machado-Joseph disease.

Drug/Therapy Strategy number	Model(s) of the disease	Results	References
CRAG overexpression through gene therapy (LV) III/IV	Transgenic mouse model of MJD	Increase of the degradation of ataxin-3 aggregates, and amelioration of neuropathology and motor deficits.	Torashima et al., 2008
Dantrolene V	Transgenic mouse model of MJD	Stabilization of intracellular calcium signaling. Reduction of neuronal loss and improvement of motor function.	Chen et al., 2008b
Tensirolimus IV	Transgenic mouse model of MJD	Reduction of the number of ataxin-3 inclusions and the levels of the soluble cytosolic ataxin-3. Improvement in motor performance.	Menzies et al., 2010
Sodium butyrate VI	Transgenic mouse model of MJD	Amelioration of motor incoordination.	Chou et al., 2011a
SKA-31 V	Transgenic mouse model of MJD	Partial correction of Purkinje cells firing and improvement of the motor impairments.	Shakkottai et al., 2011
Beclin-1 overexpression through gene therapy (LV) IV	Transgenic and lentiviral mouse models of MJD	Increase of mutant ataxin-3 clearance and amelioration of MJD neuropathology and motor deficits.	Nascimento-Ferreira et al., 2011; Nascimento-Ferreira et al., 2013
shRNA targeting ataxin-3 through gene therapy (LV) I	Transgenic and lentiviral mouse models of MJD	Reduction of ataxin-3 levels, amelioration of the neuropathology and motor phenotype.	Alves et al., 2008a; Alves et al., 2010; Nobrega et al., 2013b; Nobrega et al., 2014
PNA and LNA I	Fibroblasts of MJD patients	Reduction of ataxin-3 levels.	Hu et al., 2009; Hu et al., 2011
Oral BDA-410 or calpastatin overexpression through gene therapy (LV) II	Transgenic and lentiviral mouse models of MJD	Alleviation of MJD neuropathology with the decrease on mutant ataxin-3 fragments formation and amelioration of MJD motor phenotype.	Simoes et al., 2012; Simoes et al., 2014
Oral Caffeine VII	Lentiviral model of MJD	Amelioration of MJD neuropathology, including reduction of the neuroinflammation.	Goncalves et al., 2013

Drug/Therapy Strategy number (Cont.)	Model(s) of the disease (Cont.)	Results (Cont.)	References (Cont.)
Artificial microRNA overexpression through gene therapy (AAV) I	Transgenic mouse model of MJD	Short-term treatment decreased mutant ataxin-3 inclusions.	Rodriguez-Lebron et al., 2013; Costa Mdo et al., 2013
Valproic acid VI	Cellular, fruit fly and transgenic mouse models of MJD	Neuroprotection and attenuation of mutant ataxin-3 toxicity in the cellular and *Drosophila* models. Limited effects in the improvement of motor deficits and neuropathology in the mouse model.	Yi et al., 2013; Lin et al., 2014b; Esteves et al., 2015
17-DMAG IV	Transgenic MJD mouse model	Decrease in soluble mutant ataxin-3 levels and intranuclear inclusions.	Silva-Fernandes et al., 2014
Citalopram VII	Transgenic MJD mouse model	Reduction of ataxin-3 inclusions and astrogliosis. Amelioration of motor impairments.	Teixeira-Castro et al., 2015
Neuropeptide Y overexpression through gene therapy (AAV) VII	Transgenic and lentiviral mouse models of MJD	Amelioration of MJD neuropathology and motor performance. Reduction of the neuroinflammation.	Duarte-Neves et al., 2015
Neural stem cell transplantation in cerebellum VII	Transgenic MJD mouse model	Robust alleviation of motor behavior impairments and associated neuropathology in cerebellum.	Mendonca et al., 2015
Ataxin-2 overexpression through gene therapy (LV) III/VII	Transgenic and lentiviral mouse models of MJD	Reduction of mutant ataxin-3 levels, rescue of behavioral defects and amelioration of neuropathology of MJD.	Nobrega et al., 2015
SNALPs containing siRNA against ataxin-3 I	Transgenic and lentiviral mouse models of MJD	Amelioration of motor performance and alleviation of MJD neuropathology.	Conceicao et al., 2016

Summary of the pre-clinical studies with potential pharmacological or molecular treatments for MJD, indicating the drug/treatment, the corresponding number of the strategy used based on Figure 1.7, the model of MJD that was used, and the main results. AAV: Adeno-associated virus; CRAG: Collapsin response mediator protein (CRMP)-associated molecule (CRAM [CRMP-5])-associated GTPase; LNA: Locked nucleic acid; LV: Lentivirus; MJD: Machado-Joseph disease; PNA: Peptide nucleic acid; shRNA: short hairpin RNA; siRNA: Small interfering RNA; SNALPs: Stable nucleic acid particles.

1.2 <u>Caloric restriction</u>

Hippocrates, the father of the Western medicine, almost two and a half millenniums ago, wrote: "To eat when you are sick is to feed your sickness". Nowadays, this view is remarkably prescient. In fact, in the beginning of the 20th century, a study published in *Science*, demonstrated that the decrease of the food intake in rats is able to slow growth and to increase lifespan (Osborne et al., 1917). Despite the great discoveries, this paper had a limited impact because the survival component of the study had poor quality and also because a study, published in 1920, reported the opposite relation between growth and lifespan (Robertson and Ray, 1920). They reported that growth rate and length of life are positively related in mice (Robertson and Ray, 1920). Nevertheless, some years later, in 1935, McCay and colleagues carried out a well-executed and reliable study, clearly demonstrating that the marked reduction of food intake in rats (around 40%), without malnutrition, at or soon after weaning, resulted in an extension of lifespan (McCay et al., 1935). The uniqueness of McCay's study design compared with previous studies was that retarded growth was achieved only through the reduction of calories. Increased longevity by retarding growth in prior investigations had been achieved by the use of nutrient deficiency along with food restriction. Furthermore, later the author also reported that the main dietary factor responsible for the increase in lifespan is probably the decrease in the energy intake (McCay et al., 1939). Thus, the effects on longevity result from the restriction of total calories derived from carbohydrates, fats, and proteins. At the end of 40s and 50s the definition of the experimental diet and feeding protocol was verified. New investigations were performed in order to manipulate the amount of specific nutrients to more precisely evaluate whether or not the restriction of food or nutrients was the cause of the extended lifespan. After that, a large number of experiments were conducted in order to prove the effects of CR in different species.

The view that the beneficial effects observed in this type of diets are due to a reduction in calories and not in a specific nutrient have been challenged in the last years. Some studies have been demonstrating that the restriction of a specific dietary component, such as methionine, without a reduction in the caloric intake can result in life extension (Richie et al., 1994; Zimmerman et al., 2003; Johnson and Johnson, 2014; Lee et al., 2016). However, these findings do not necessarily invalidate the conclusion that caloric restriction (CR) induces lifespan extension. A study from 1985 demonstrated that when dietary protein is reduced by 40% without reduction in energy intake, there is an increase in lifespan, although not nearly so marked as that resulting from a 40% reduction in the caloric intake (Yu et al., 1982; Yu et al., 1985). One explanation for the

success of the reduction of proteins without reducing caloric intake remains to the fact that in the specific rodent strain used in that study, one of the main causes of death is kidney failure, thus the reduction of protein intake can be beneficial (Masoro et al., 1989). Nevertheless, this indicated that part of the life extension can result from a reduced intake of proteins. However, in another study, it was observed that restricting the caloric intake by 40% resulted in the same magnitude of life extension whether or not protein intake was restricted (Masoro et al., 1989).

Therefore, although the restriction of nutrients seems to have beneficial effects, based on the current knowledge it is generally accepted that these effects are, at least, achieved with a reduction in the intake of calories, without malnutrition. Indeed, across time the life-prolonging manipulation of restricting food intake, was initially referred as food restriction (very general), and then by a vague name of dietary restriction, and is now usually referred by a more specific name – caloric restriction, which is will be used herein after. Dietary restriction is more used as an undefined designation that englobes the CR or intermittent fasting (IF) protocols. In the IF protocols animals are fed on an alternate-day schedule. and it was previously reported that this corresponds to a CR of 30-40%, in comparison with the *ad libit\um* group (Weindruch et al., 1986).

1.2.1 Beneficial effects of caloric restriction

The data among the last 80 years support the idea that CR is not a simply passive set of effects, but is an active and dynamic conserved stress response that evolved early in life's history to increment the chance of the organisms to survive against adversity. In fact, CR has been associated with two important benefits, namely: retardation of the onset of aging and extension of lifespan, and neuroprotection. These two effects will be explored in the next sections. In addition, it also has other beneficial effects, such as it reduces metabolic rate and oxidative stress, improves insulin sensitivity, alters neuroendocrine and sympathetic nervous system function, reduces the incidence of age-related cancer, cardiovascular diseases, and immune deficiencies, among others (Lane et al., 1999; Teeuwisse et al., 2012; Marchal et al., 2012; Kitada et al., 2013). Thus, we can infer that physiological alterations promoted by CR contribute towards a condition of stout health, and these same changes trigger a greater lifespan.

1.2.1.1 Caloric restriction and lifespan

CR is the oldest and the most effective and reproducible strategy known to regulate aging and to improve the healthy lifespan in several organisms. This ranges from unicellular budding yeast *Saccharomyces cerevisiae* (Jiang et al., 2000; Lin et al., 2002), the nematode *Caenorhabditis elegans* (Houthoofd et al., 2003; Kaeberlein et al., 2006; Lee et al., 2006a), the fruit fly *Drosophila melanogaster* (Chapman and Partridge, 1996; Partridge et al., 2005) to more complex organisms, such as rodents (Weindruch et al., 1986; Turturro et al., 1999) and non-human primates (Bodkin et al., 2003; Colman et al., 2009; Mattison et al., 2012; Colman et al., 2014). An interesting meta-analysis of studies from 1934 to 2011 about the effects of CR on lifespan in rodents, reported that in rats, CR increases median lifespan by 14 to 45%, and 4 to 27% in mice (Swindell, 2012). Moreover, it was shown by microarray that CR actually forestalls many progressive alterations that occur during aging (Lee et al., 1999; Weindruch et al., 2001; Weindruch et al., 2002). In most cases of these studies, CR entails a 20-40% reduction of food consumption relative to normal intake, always without malnutrition.

Regarding the studies in *Rhesus* monkeys, the most closed specie to humans, they have some controversial data. In 2003, Bodkin and colleagues reported that dietary restriction leads to an increased lifespan in primates, which was associated with the prevention of hyperinsulinemia and the mitigation of age-related diseases (Bodkin et al., 2003). Moreover, two longitudinal studies have been investigating the benefits of long-term CR on longevity and age-related diseases in non-human primates: one at the National Institute of Aging (Mattison et al., 2003; Mattison et al., 2012) and one at the University of Wisconsin (Colman et al., 2009; Colman et al., 2014). Results from the 20-year longitudinal adult-onset CR study in the Wisconsin University concluded that monkeys in a CR diet show a decrease in the incidence of aging-related deaths (Colman et al, 2009; Colman et al., 2014). At the time point reported, 50% of *ad libitum*-fed animals survived compared with 80% of CR animals. The onset of age-related pathologies (such as diabetes, cancer, cardiovascular disease, and brain atrophy) was also delayed. But, in 2012 it was demonstrated that CR regimen implemented in young and old *Rhesus* monkeys does not improve survival (Mattison et al., 2012). This result contrasts with the previous paper. However over the years, both studies have extensively documented beneficial health effects of CR. Furthermore, caloric-restricted monkeys had lower body temperatures, higher concentration of dehydroepiandrosterone sulfate (DHEAS) and insulin than control monkeys, and all of those variables are biomarkers for longevity in rodents (Roth et al., 2002). In addition, study design, husbandry, and diet composition

may strongly affect the life-prolonging effect of CR in a long-lived non-human primate, and could contribute to the differences observed between the two studies.

Despite the absence of well-controlled and reproducible studies of CR in humans, there are some observational studies showing the effects of CR in humans. A study among Spanish nursing home residents undergoing a long-term IF led to a decrease in the morbidity and mortality (Vallejo, 1957). Kagawa (1978) analyzed the prevalence of centenarians on the island of Okinawa in Japan, and observed a high prevalence (Kagawa, 1978). Total energy consumed by schoolchildren was only 62% of the recommended intake for Japanese children. For adults, total protein and lipid intakes were about the same, but total energy intake was 20% less than Japanese national average. This population shows very low incidence of pathologies, such as cerebral vascular diseases, malignancies, and heart diseases in comparison with the rest of Japan. The people from this island when submitted at a normal diet have a mortality rate higher than those Okinawans who remained on the island (Willcox et al., 2006). Other evidence comes from the Biosphere II study in which an involuntary and unplanned severe CR was associated with several physiological alterations that resemble those observed in rodents and non-human primates (Walford et al., 1995; Verdery and Walford, 1998; Walford et al., 1999; Weyer et al., 2000; Walford et al., 2002). These data are consistent with the hypothesis that CR increases lifespan in humans.

1.2.1.2 Caloric restriction and neuroprotection

Brain aging leads to cognitive impairments and to an increased vulnerability to age-related chronic neurodegenerative diseases, such as Alzheimer's disease (AD), Parkinson's disease (PD), Huntington's disease (HD), and amyotrophic lateral sclerosis (ALS), among others. Although, there is no evidence about the potential effects of CR in MJD. As referred before, there are compelling evidence demonstrating that limiting access to food prolongs lifespan in an extremely conserved fashion throughout the evolutionary scale (from unicellular organisms, namely yeast, to mammals). In 1990 Park and colleagues revealed the role of CR in neuroprotection. They demonstrated that CR attenuates the age-related loss of spinal ganglion neurons in mice (Park et al., 1990). Moreover, in 1999, Bruce-Keller and colleagues showed, in adult rats, that CR promotes the resistance of neurons to chemically-induced neurodegeneration (Bruce-Keller et al., 1999). These results show that CR not only extends lifespan, but also increases resistance of the brain to insults that involve metabolic compromise and excitotoxicity.

As previously described, three important prospective studies conducted on monkeys have confirmed that CR induces metabolic, physiological, and behavioral changes, although with variable effects on lifespan (Colman et al., 2009; Mattison et al., 2012; Colman et al., 2014). Additionally, aged CR-treated monkeys were found to suffer less severe brain atrophy, which is a hallmark of the aging brain, compared to the *ad libitum* controls (Colman et al., 2009; Mattison et al., 2012; Colman et al., 2014). Other studies on aged monkeys demonstrated that CR is related with a preservation of the brain volume and microstructure with lower iron accumulation (Kastman et al., 2010; Willette et al., 2012b), lower levels of circulatory pro-inflammatory cytokines (Willette et al., 2010; Willette et al., 2013), improved insulin sensitivity (Willette et al., 2012a), and decreased astrogliosis, but not of amyloid plaque load (Sridharan et al., 2013). Altogether, these results support the idea that CR is neuroprotective. There are also some studies in animal models of neurodegenerative diseases that corroborate the potential beneficial effect of CR on these diseases, and are summarized on Table 1.7.

Briefly, AD is a neurodegenerative disease affecting almost an half of all people with more than 85 years (reviewed in Mayeux and Stern, 2012). It is the most common neurodegenerative disease and unlike MJD, its cause is associated with mutations involving more than one gene, namely genes encoding for β-amyloid precursor protein (APP), presenilin 1 or 2 (PS1/PS2), as well the ε4 allele of apolipoprotein E (Goate et al., 1991; St George-Hyslop et al., 1994; Barinaga, 1995). AD is characterized by specific neuropathological hallmarks, namely: i) β-amyloid plaques resulting from the cleavage of APP by β- or γ-secretase complexes, leading to the formation of β-amyloid peptides that are prone to aggregation; and ii) neurofibrillary tangles of hyper phosphorylated *tau* protein (reviewed in Serrano-Pozo et al., 2011). Transgenic mouse models resemble some or all of these abnormalities (reviewed in Onos et al., 2016). PD is the second most common neurodegenerative disease worldwide. Most cases of PD result from a complex interaction of environmental and genetic factors, such as mutations in *LRRK2*, *PARK2*, *PARK7*, *PINK1*, or *SNCA* genes (reviewed in Schulz, 2008; Blesa and Przedborski, 2014). Only approximately 15% of the cases have a family history of this disorder. Neuropathology associated with this disease includes: loss of dopaminergic neurons at *substantia nigra*; and ii) accumulation of Lewy bodies inclusions that contain α-synuclein and ubiquitin (Recasens et al., 2014; reviewed in Dehay et al., 2015). These changes lead to tremor, rigidity, postural instability, among other symptoms (reviewed in Rodriguez-Oroz et al., 2009). There are genetic mouse models of the disease, and mouse models where a neurotoxic molecule is injected, such as 1-methyl-4-phenyl-1,2,3,6-tetrahydropyridine (MPTP), resembling some features of the disease (reviewed

in Blesa and Przedborski, 2014). HD is a polyglutamine disorder, and was generally described in subsection 1.1.1 and table 1.1 of this thesis. ALS is the most common motor neuron disease affecting muscle functionality and coordination. It is associated with mutations in several genes, such as *SOD1* (reviewed in Leblond et al., 2014). As all the other neurodegenerative disorders, it does not have cure or treatment to retard its progression.

The perspective beneficial role of CR on neurodegenerative diseases has been exploited in several animal models, obtained either through experimental or genetic manipulation. For example, in mice injected with the dopaminergic toxic MPTP (rodent model of PD), both the loss of nigro-striatal dopaminergic neurons and the motor deficits were diminished in animals subjected to CR (Duan and Mattson, 1999). Moreover, in 2004, Maswood and colleagues did a similar experimental approach in monkeys that resulted in comparable neuroprotection towards striatal dopamine levels, and motor activity of dietary restricted animals (Maswood et al., 2004). Regarding animal models of AD, Wang and colleagues (2005) showed that transgenic mice expressing human mutated forms of the APP, which induces progressive development of amyloid plaques in the cortex and hippocampus, were significantly protected by long-term CR (Wang et al., 2005a). An even greater protection was obtained by 40% of CR in a double transgenic AD mice (APP/PS1; Patel et al., 2005). Halagappa and colleagues (2007) also demonstrated that in a triple transgenic mouse model of AD, carrying an additional mutation of *tau* protein, similar CR protocol induced a retardation of the development of AD hallmarks, particularly the amyloid deposition and *tau* protein phosphorylation, and an improvement of cognitive deficits (Halagappa et al., 2007). As summarized in Table 1.7 there are other studies demonstrating the beneficial effects of CR on these two diseases (PD and AD), and also on other neurodegenerative diseases, such as HD and ALS. As also showed in Table 1.7 (in the yellow and red rows), there are some studies that do not demonstrate beneficial effects of CR on some mouse models of neurodegenerative diseases, although the majority of the studies shows that CR is neuroprotective.

Table 1.7 Effects of caloric restriction on neurodegenerative diseases.

Disease Model	Diet protocol Age of mice	Outcomes	References
AD PS1M146V mouse model	3 months of IF *vs* AL 6-week-old mice	Mice maintained in the IF diet exhibited reduced excitoxicity and reduced damages on hippocampal CA1 and CA3 neurons, compared to AL mice.	Zhu et al., 1999
PD Intraperitoneally-injected MPTP mice	3 months of IF *vs* AL, prior MPTP injection 4-month-old mice	IF induced the resistance of dopaminergic neurons, in the *substantia nigra*, to the toxicity of MPTP. IF also induced an amelioration of the loss of dopaminergic neurons and motor deficits, and increased the expression of HSP70 and GRP78 in dopaminergic cells.	Duan and Mattson, 1999
ALS SODMutM mouse model	IF *vs* AL, until all mice in each group had developed complete hindlimb paralysis 6-week-old mice	There was no significant differences in the age of disease onset, and disease duration was shortened. Histological analysis shown a similar extent of motor neurons degeneration.	*Pedersen and Mattson, 1999*
HD N171-82Q Tg mouse model	12 weeks of CR *vs* AL 8-week-old mice	CR normalized glucose metabolism and BDNF levels, increased HSP70 in the striatum and cortex, and slowed the progression of the disease, increasing also the lifespan.	Duan et al., 2003
PD *Rhesus* monkeys (*Macacca mulata*) injected with MPTP in right carotid artery	6 months of 30% CR *vs* AL before of the injection of the neurotoxin to induce hemiparkinsonism Adult (9-17 years)	CR monkeys exhibited significantly higher levels of locomotor activity, dopamine and dopamine metabolites in the striatal region associated with an increased survival of dopaminergic neurons in the *substantia nigra*, in comparison with AL monkeys.	Maswood et al., 2004
AD Tg2576 mouse model	9 months of 30% CR *vs* AL 3-month-old mice	CR prevents Aβ peptides formation and neuritic plaque deposition in the brain, through the increase of anti-amyloidogenic α-secretase activity.	Wang et al., 2005a
AD Tg APP$_{swe/ind}$ and Tg APP/ PS1 mouse models	6 weeks of 40% of CR *vs* AL 14-15-week-old mice (Tg APP$_{swe/ind}$) 15 weeks of 40% CR *vs* AL 9-week-old mice (Tg APP/PS1)	CR reduced amyloid plaque number and size (40% in Tg APP$_{swe/ind}$ and 55% in Tg APP+PS1) and decreased Aβ-plaque-induced astrogliosis in both transgenic mouse models.	Patel et al., 2005
AD Tg2576 mouse model	6 months of 30% CR *vs* AL 4-month-old female mice	CR attenuated Aβ levels, mainly through the increase in NAD$^+$ and SIRT1, and regulating ROCK1 activity.	Qin et al., 2006b
AD Squirrel monkeys with AD-type brain amyloidosis	30% of CR *vs* AL across all life	CR monkeys had reduced content of Aβ1-40 and Aβ1-42 peptides in the temporal cortex, relative to AL-fed monkeys.	Qin et al., 2006a

Disease Model (cont.)	Diet protocol Age of mice (cont.)	Outcomes (cont.)	References (cont.)
AD 3xTgAD mouse model	8 or 15 months of 40% CR or IF *vs* AL 3-month-old mice	CR and IF groups exhibited a higher exploratory behavior and performed better Morris water maze test, compared to AL. CR, but not IF, decreased Aβ and phospho-*tau* levels in the hippocampus of transgenic mice.	Halagappa et al., 2007
AD cDKO PS1 and PS2 mouse model	4 months of 30% CR *vs* AL 4-month-old mice	CR attenuated lateral ventricle enlargement, caspase-3 activation, and astrogliosis. CR also increased neurogenesis-related genes, improved memory, and decreased neuroinflammation on the hippocampus.	Wu et al., 2008
AD Tg2576 mouse model	6 months of 30% CR *vs* AL 4-month-old female mice	CR alters FOXO3a activity, leading to the attenuation of AD-type amyloid neuropathology with the preservation of spatial reference memory.	Qin et al., 2008
PD Unilateral striatal infusion of 6-OHD in Sprague-Dawley rats	Two and eight weeks before the stereotaxic injection of 6-OHD mice were maintained in IF *vs* AL diets	Histological and behavioral measurements indicated an absence of alterations induced by IF, regarding for example the degree of dopaminergic neuron loss, in comparison with AL rats.	Armentero et al., 2008
AD Tg APP/ PS1 mouse model	18 weeks of 40% CR *vs* AL 13-14-month-old mice	CR reduced the total Aβ volume by about 33% in the hippocampus and the overlying neocortex.	Mouton et al., 2009
AD *Drosophila melanogaster* UAS-ArcA42 and WT 4R *tau*	Constant sugar concentration (50 g/L) and a variable yeast concentration	CR extended lifespan in both Arctic mutant A42 and WT 4R *tau*-overexpressing flies, but molecular pathology and neuronal dysfunction were not prevented.	Kerr et al., 2011
ALS G93A mouse model	40% CR diet *vs* AL until endpoint or during 50 days 40-day-old mice	CR hastened clinical onset, disease progression and shortened lifespan, while transiently improved motor performance in males. It also increased lipid peroxidation, inflammation and apoptosis, while decreased mitochondrial bioenergetics efficiency, protein oxidation, and stress response.	Hamadeh et al., 2005; Hamadeh and Tarnopolsky, 2006; Patel et al., 2010
ALS H46R/H48Q transgenic mice	40% CR *vs* AL 40-50-day-old mice	CR delayed disease onset and extended lifespan.	Bhattacharya et al., 2012
AD CK-p25 mouse model	3 months of 30% CR *vs* AL (p25 expression was induced with doxycycline, in the middle of CR protocol – 6 weeks after the beginning) 3-month-old mice	CR delayed the onset of neurodegeneration, the related synaptic loss, and the neuronal dysfunction, preserving the cognitive capacities.	Graff et al., 2013
PD SNCA mouse model	12 weeks of IF *vs* AL 12-week-old mice	IF did not reduce α-synuclein levels, but preserved cell function on DMNV.	Griffioen et al., 2013

Disease Model (cont.)	Diet protocol Age of mice (cont.)	Outcomes (cont.)	References (cont.)
AD Tg2576 mouse model	12 months of 30% CR *vs* AL 2.5-month-old mice	CR reduced Aβ burden in hippocampus and reduced the expression of presenilin enhancer 2, and presenilin components of γ-secretase, mainly on females.	Schafer et al., 2015
AD Tg4510 mouse model	4 months of CR (to achieve a reduction of 35% of body weight) *vs* AL 4-month-old mice	CR Tg4510 mice had better short-term memory and performed better in the contextual fear conditioning test, than AL mice. Although, they showed absence of effects on: motor performance, spatial memory, phospho-*tau* levels, and neuroinflammation. They also presented mitochondrial dysfunction of complex I.	Brownlow et al., 2014; Delic et al., 2015
HD YAC128 mouse model	3 months of IF *vs* AL 3-5-month-old mice	IF corrected several pathological markers of the transgenic mouse model of HD, namely the increased body weight, decreased blood glucose, and impaired motor function. It also changed the expression of mRNAs related with HD in the striatum and hypothalamus. It also decreased the expression of huntingtin in the striatum.	Moreno et al., 2016

Summary of the main studies evaluating the effects of caloric restriction in some neurodegenerative diseases, namely, Alzheimer's disease (AD), Parkinson's disease (PD), Huntington's disease (HD), and amyotrophic lateral sclerosis (ALS). The different colors in some rows represent different general effects of caloric restriction: the rows in white are from studies in which CR showed beneficial effects, the yellow rows represent positive and negative/null effects in different parameters, and the red rows represent negative effects of CR. In the intermittent fasting protocols animals are fed on an alternate-day schedule, and it was previously reported that this corresponds to a 30-40% CR, in comparison with the *ad libitum* group (Weindruch et al., 1986). Aβ: β-amyloid protein; AL: *Ad libitum*; APP: Amyloid precursor protein; BDNF: Brain-derived neurotrophic factor; CA1: Region I of hippocampus proper; CA3: Region III of hippocampus proper; cDKO: Conditional double knockout; CR: Caloric restriction; DMNV: Dorsal motor nucleus of the vagus; FOXO3a: Forkhead box protein 3a; GRP78: Glucose-related protein 78; HSP70: Heat-shock protein 70; IF: Intermittent fasting; MPTP: 1-methyl-4-phenyl-1,2,3,6-tetrahydropyridine; NAD$^+$: Nicotinamide adenine dinucleotide; OHD: 6-hydroxydopamine; PS1: Presenilin 1; Q: Glutamine; ROCK1: Rho-associated protein kinase 1; SIRT1: Sirtuin 1; SNCA: Alpha-synuclein; SOD: Superoxide dismutase; Tg: Transgenic; WT: Wild-type; YAC: Yeast artificial chromosome.

1.2.2 Pathways underlying the beneficial effects of caloric restriction

CR has many beneficial effects in the retardation of aging and in the prevention of age-related diseases, but it is not a practical treatment option for humans. As a consequence, considerable efforts have been invested to understand the mechanisms underlying its benefits, hoping to develop alternative therapeutic approaches for diseases, and to prevent age-related health problems. All the specific mechanisms underlying CR have not yet been definitively demonstrated. Indeed, there are several

hypothesis that still must be tested before all the mechanisms are fully understood. In the next sections will be described some of the main mechanisms already described that could be underlying the beneficial effects of CR on neurodegenerative diseases.

1.2.2.1 Autophagy regulation

Autophagy is a highly regulated intracellular process for the degradation of cellular constituents, and is essential for the maintenance of important biological functions. It is emerging as a central regulator of cellular health and disease. In the central nervous system (CNS) this homeostatic process appears to influence synaptic growth and plasticity (reviewed in Alirezaei et al., 2011). Accumulating evidence shows that aggregated and misfolded proteins may have impact on autophagy function, suggesting that this could be a secondary pathogenic mechanism in many neurodegenerative diseases, such as AD, PD, HD, and ALS, and also on MJD (Nascimento-Ferreira et al., 2011; Nascimento-Ferreira et al., 2013; Dubinsky et al., 2014; reviewed in Hochfeld et al., 2013;). It is known that autophagy decreases with aging in many tissues and organs, including the brain (Keller et al., 2004). Up-regulation of autophagy may prevent, delay or ameliorate, at least, some neurological disorders.

Mammalian target of rapamycin (mTOR) pathway is a nutrient-sensor signaling pathway known to regulate longevity (reviewed in Ehninger et al., 2014). It is a well-known amino acid sensor that is evolutionarily conserved from yeast to mammals (reviewed in Lee and Min, 2013). Amino acids can activate mTOR, promoting protein synthesis (Kimball et al., 1999). mTOR complex 1 (mTORC1) directly phosphorylates and inactivates a complex related with the initiation of autophagy (reviewed in Cohen and Hall, 2009). Therefore, the inactivation of mTOR promotes degradation of damaged proteins and intracellular organelles, via autophagy. Decreased expression or activity of the mTOR signaling pathway is known to extend lifespan in a large variety of species, from yeast to fruit flies and rodents (Jia et al., 2004; Kapahi et al., 2004; Kaeberlein et al., 2005b; Powers et al., 2006; Harrison et al., 2009). There are some studies showing that CR mediates mTOR pathway, since mTOR works as an amino acid sensor, and CR influences circulating nutrient levels (Dogan et al., 2011). In fact, there are different studies demonstrating that CR inhibits mTOR pathway, and by this way activates autophagy in different tissues, namely brain, liver, kidney, heart, skeletal muscle, among others (Alirezaei et al., 2010; Ning et al., 2013; Yang et al., 2014; Dong et al., 2015). Moreover, the activation of autophagy was confirmed by the decrease in p62/SQSTM1 levels and the increase in LC3BII levels, and consequently in the number of

autophagosomes, demonstrated by the different studies (see Figure 1.8; Alirezaei et al., 2010; Cui et al., 2013; Ning et al., 2013; Yang et al., 2014; Dong et al., 2015). One study demonstrated that the activation of autophagy promoted by CR is tightly related with the increase in lifespan (Morselli et al., 2010). In fact, in *C. elegans*, CR only prolonged lifespan on autophagy-proficient nematodes, whereas these beneficial effects were abolished by the knockdown of beclin-1, an important player on initial steps of autophagy (Morselli et al., 2010). Another interesting study showed that the stimulatory effect of CR on autophagy, and consequently on lifespan, is verified in autotrophs and in heterotrophs, since the CR promoted by the decrease of the light sensitivity in *Arabidopsis* was related with an increased lifespan and activation of autophagy (Minina et al., 2013). Thus, it is clear that one of the underlying mechanisms related with CR is the activation of autophagy, as summarized in Figure 1.8.
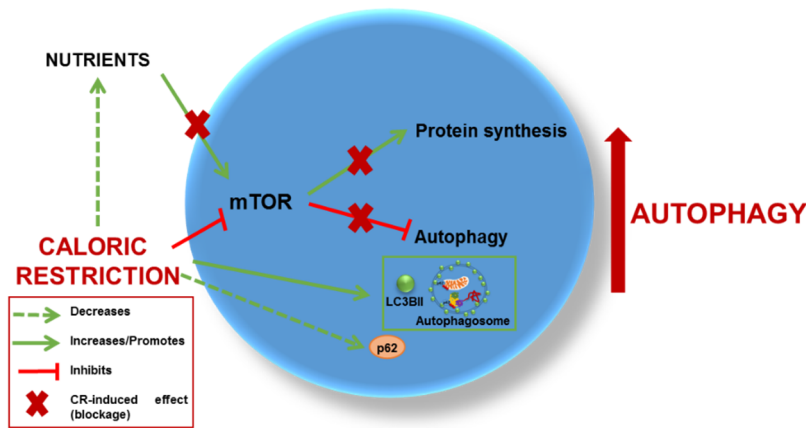
Figure 1.8 Caloric restriction activates autophagy. mTOR works as a nutrient-sensor. The minimum increase in the nutrient-content reflects in an mTOR activation and a consequent promotion of protein synthesis, and autophagy inhibition. Caloric restriction induces a decrease in the nutrient-content, inhibiting mTOR pathway, and consequently activating autophagy. Moreover, this activation of autophagy is also denoted by the increase in LC3BII levels and autophagosomes number, and the decrease in p62 levels. LC3B II: Microtubule-associated protein 1 light chain 3B II; mTOR: Mammalian target of rapamycin; p62: Sequestosome 62.

1.2.2.2 Inflammatory pathway

During normal aging and in some neurodegenerative diseases, such as MJD, a progressive neuroinflammatory state occurs in brain, involving astrocytes and microglia, which are the primary components of neuroinflammation(Evert et al., 2001; Evert et al., 2006b). In fact, microarray gene expression profiling showed that inflammation-related genes are increased during aging (Lee et al., 1999). Although, CR prevents this increase in 65% of those genes involved in the inflammatory network in the neocortex (Lee et al., 1999). Other studies have demonstrated that CR decreases the circulating levels of inflammatory cytokines and inflammatory signaling activities in a wide variety of tissues

(Ugochukwu et al., 2006; Ugochukwu and Figgers, 2007; Horrillo et al., 2011; MacDonald et al., 2014; Mulrooney et al., 2011; Harvey et al., 2013; Chujo et al., 2013; Harvey et al., 2014).

Nuclear factor kappa B (NF-κB) is a transcription factor that induces the expression of pro-inflammatory cytokines, such as the tumor necrosis factor alpha (TNF-α), interleukin-1 beta (IL-1β), and interleukin-6 (IL-6). CR attenuates the age-related upregulation of NF-κB, and consequently reduces the inflammation (Lee et al., 1999; Ugochukwu et al., 2006). It is known that insulin growth factor 1 (IGF-1) activates NF-kB, and interestingly CR is able to decrease IGF-1, and consequently to reduce NF-kB, attenuating the pro-inflammatory network that is present during aging and in neurodegenerative diseases (Harvey et al., 2013; Harvey et al., 2014). In the central nervous system interferon gamma (INF-γ) is an important mediator of neuronal plasticity (Vikman et al., 2001). INF-γ enhances synaptogenesis, regulates synaptic plasticity, and controls neurogenesis (Vikman et al., 2001, Wong et al., 2004). Mascarucci and colleagues (2002) reported that levels of INF-γ are increased in circulating leukocytes of monkeys that had been maintained on a CR diet (Mascarucci et al., 2002). Moreover, Lee and colleagues (2006) also showed that INF-γ is increased in the hippocampus in response to IF, where it exerts a protective role against excitotoxicity (Lee et al., 2006b). The excessive release of INF-γ has been associated with the pathogenesis of chronic inflammatory and autoimmune diseases (reviewed in Muhl and Pfeilschifter, 2003). Although, a small increase in INF-γ, such as the generated by CR, can lead to the induction of the anti-inflammatory network (reviewed in Muhl and Pfeilschifter, 2003). CR is also able to increase other anti-inflammatory players, such as interleukin 10 (IL-10), nuclear factor of kappa light polypeptide gene enhancer in B-cells inhibitor, alpha (IκBα), among others (MacDonald et al., 2014). Moreover, CR leads to an increase in glucocorticoids due to the increase in the catabolism of fatty acids and cholesterol (Sabatino et al., 1991; Klebanov et al., 1995; discussed in Patel and Finch, 2002). Glucocorticoids have broad anti-inflammatory effects by the direct interaction between the glucocorticoid receptor and the transactivation domain of NF-κB, contributing to the decrease of the patent inflammation.

Generally, it is known that CR reduces inflammation in several tissues, including brain, due to an increase in the anti-inflammatory network and a decrease in the pro-inflammation (see Figure 1.9).
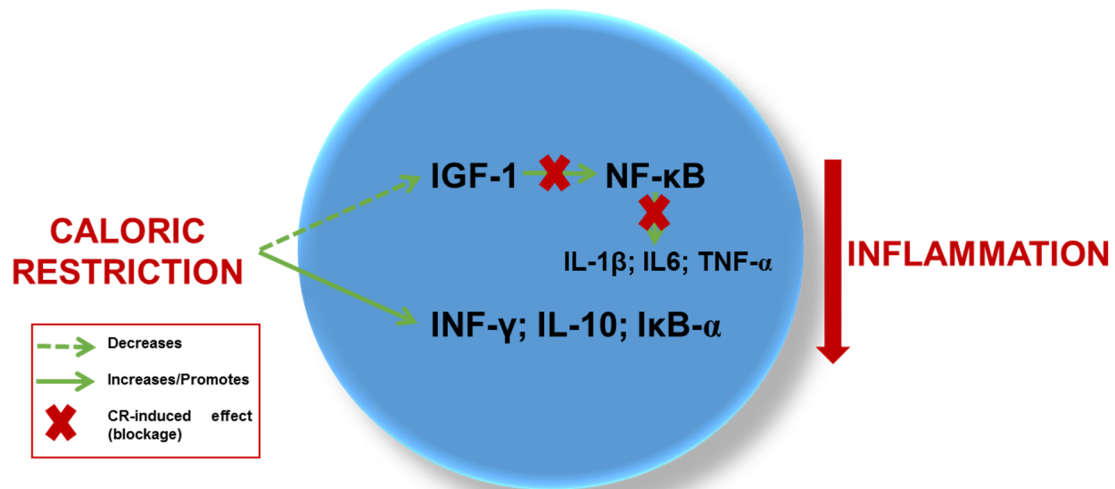
Figure 1.9 <u>Caloric restriction effects on inflammatory network.</u> Caloric restriction decreases the levels of IGF-1, contributing to a decrease in the activation of NF-kB, and consequently to a reduction in the levels of pro-inflammatory cytokines (IL-1β, IL-6, and TNF-α). On the other hand, CR induces the expression of anti-inflammatory players, such as INF-γ, IL-10, and IκB-α. Altogether, the reduction of the pro-inflammatory network and the activation of the anti-inflammatory network induces a decrease in the patent inflammation. <u>IGF-1:</u> Insulin Growth Factor 1; <u>IκB-α:</u> Nuclear factor of kappa light polypeptide gene enhancer in B-cells inhibitor, alpha; <u>IL-1β:</u> Interleukin 1 beta; <u>IL-6/10:</u> Interleukin 6/10; <u>INF-γ:</u> Interferon gamma; <u>NF-κB:</u> Nuclear Factor kappa B; <u>TNF-α:</u> Tumor Necrosis Factor alpha.

1.2.2.3 Mitochondrial function and oxidative stress

Neurons are excitable cells that require large amounts of energy to survive and to function. During aging and in age-related diseases, such as neurodegenerative disorders, occurs an increase of mitochondrial free radical generation due to a decrease of mitochondrial function and an increase in the oxidative stress (reviewed in Wang and Hekimi, 2015).

Aging is associated with oxidative damages arising from corresponding changes in mitochondrial oxidant production. Thus, protein carbonyl content, mitochondrial superoxide formation, and hydrogen peroxide are indices of aging, and CR can change their levels (Sohal et al., 1994a; Sohal et al., 1994b). There are some studies demonstrating that CR applied at early or late middle age can induce an amelioration of the mitochondrial dysfunction due to a reduction of protein carbonyl content, a decrease in superoxide and hydrogen peroxide formation, an amelioration of mitochondrial abnormalities, and a reduction in the accumulation of mtDNA deletions in different tissues of rodents, such as kidney, heart, skeletal muscle, and also brain (Sohal et al., 1994a; Sohal et al., 1994b; Aspnes et al., 1997; Lee et al., 1998; Gredilla et al., 2001a; Gredilla et al., 2001b; Bevilacqua et al., 2004; Sanz et al., 2005). It was demonstrated that the mechanism behind the described effects of CR is not a simple reduction in the

mitochondrial oxygen consumption, but is a reduction of oxygen radicals release *per* unit of electron flow in the respiratory chain, mainly in complex I (Gredilla et al., 2001a; Gredilla et al., 2001b; Lopez-Torres et al., 2002). Another important study also demonstrated that 36 weeks of 40% CR enhanced the transcripts of genes involved in radical oxygen free scavenging function, tissue development, and energy metabolism, while lowered the genes involved in signal transduction, and stress response (Sreekumar et al., 2002). Furthermore, Lopez-Lluch and colleagues (2006) reported that CR increases the efficiency of the electron transport system in regard to ATP generation, while decreases the generation of reactive oxygen species, and thus suggested that CR increases biogenesis and bioenergetics efficiency (Lopez-Lluch et al., 2006). In fact, results from the CALERIE (Comprehensive Assessment of Long term Effects of Reducing Intake of Energy) study in humans, indicate that muscle mitochondrial biogenesis is increased in calorie-restricted healthy humans (Civitarese et al., 2007). Another relevant study demonstrated that 3 or 12 months of CR increases endothelial nitric oxide synthase (eNOS) expression, mitochondrial biogenesis, oxygen consumption, and ATP production, in white adipose tissue of mice (Nisoli et al., 2005). More recently, it was also shown that neuronal energy production and neurotransmission rates were significantly reduced in aging, but were preserved in old caloric-restricted rats (Lin et al., 2014a).

Altogether, these results suggest that CR decreases aging rate and neurodegeneration, in part by lowering the degree of free radical generation and mitochondrial abnormalities, and by increasing the mitochondrial biogenesis and energy production efficiency (summarized on Figure 1.10).
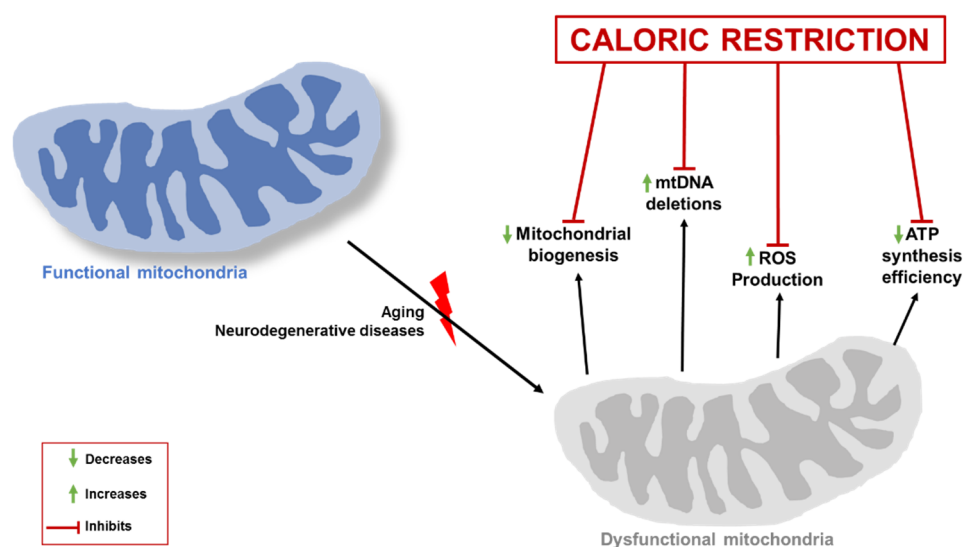
Figure 1.10 Mechanisms underlying caloric restriction effects on mitochondrial function. During aging and in some neurodegenerative disease, such as Machado-Joseph disease, mitochondria are dysfunctional. This is translated into a reduction in

Figure 1.10 (cont.) mitochondrial biogenesis, in ATP synthesis efficiency, and an increase in mtDNA deletions and ROS production. Caloric restriction is able to oppose against these changes, contributing to a better mitochondrial function. <u>ATP:</u> Adenosine triphosphate; <u>mtDNA:</u> Mitochondrial DNA; <u>ROS:</u> Reactive oxygen species.

1.2.2.4 Changes in regulatory proteins

CR changes some regulatory proteins, such as sirtuins and forkhead box (FOXOs) proteins. These changes can be associated with the beneficial effects triggered by CR on longevity and neuroprotection (see Figure 1.11).

Sirtuins are a family of proteins that belong to the class III of histone deacetylases (HDACs) and contribute to the coordination of energy metabolism by directing cellular processes in accordance with the availability of the metabolic currency - NAD^+. In fact, sirtuins are NAD^+-dependent enzymes (Imai et al., 2000; Landry et al., 2000) that have their activity increased with low energy conditions, such as CR. Since 2004, it was clarified that the beneficial effects of CR in mammals are strongly related with the increase in the levels and activity of one of the seven mammalian sirtuins – sirtuin 1 (SIRT1; Cohen et al., 2004). In the section 1.3 sirtuins and their connection with CR will be further developed.

Forkhead box (FOX) proteins are multifaceted transcription factors that are responsible for fine-tuning the spatial and temporal expression of a broad range of genes (reviewed in Lam et al., 2013). There are several subfamilies of FOX proteins, and the subgroup "O" (FOXO) are transcription factors that have been postulated to influence lifespan and to have a role in the beneficial effects of CR on lifespan (Shimokawa et al., 2015). There are four main families of FOXO proteins, namely, FOXO1, FOXO3, FOXO4, and FOXO6 (reviewed in Lam et al., 2013). These proteins control a wide array of genes linked by a common mechanism that serve to control energy metabolism in response to external stimulus, such as CR. In 2002, it was demonstrated that 30% of CR was able to increase FOXO1, 3, and 4 levels in muscle tissue (Furuyama et al., 2002). Although, in 2008, it was shown in *Drosophila melanogaster* that lifespan extension promoted by CR does not require dFOXO, but its activity interferes with CR response (Giannakou et al., 2008). Although, flies with dFOXO overexpressed in the adult body fat have an altered response to CR and partially behaved as though dietary restricted (Giannakou et al., 2008). These results proposed that while CR extends longevity in the absence of dFOXO, the presence of an active FOXO modulates the response to CR, potentially by the modification of the expression of its target genes, mediating the normal response of CR (Giannakou et al., 2008). While, more recently it was shown in mice that the presence of FOXO3 is necessary for the beneficial effects of CR on lifespan, since

the absence of FOXO3 led to a blockage of CR-induced lifespan extension (Shimokawa et al., 2015), highlighting the importance and the role of FOXO3 in the effects of CR. Moreover, regarding the mechanism behind the control mediate by CR, it is known that during CR the circulating levels of insulin/IGF-1 are attenuated in order to improve euglicemia (Breese et al., 1991; Smith et al., 1995). As demonstrated in Figure 1.11, in these conditions, FOXO proteins are non-phosphorylated and are translocated to the nucleus, where they act as transcription factors, regulating the expression of important proteins (reviewed in Martin et al., 2006).
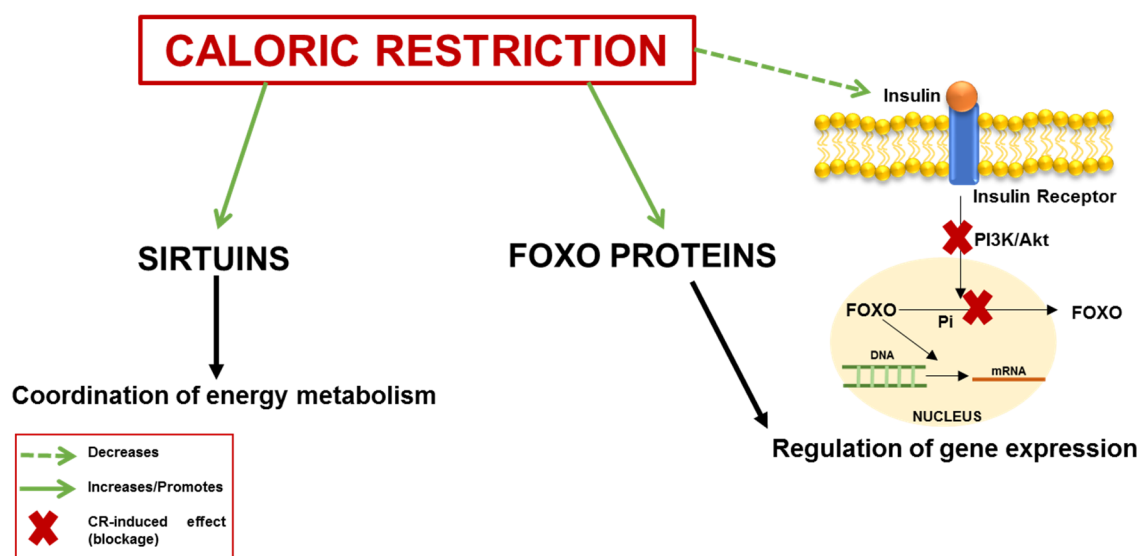
Figure 1.11 Effects of caloric restriction on two groups of regulatory proteins: sirtuins and FOXO proteins. Caloric restriction is able to increase the levels and activity of sirtuins, and to regulate energy metabolism through the deacetylation of several substrates, that will be discussed in section 1.3. It is also able to regulate the activity of FOXO proteins, and consequently to regulate gene expression. The normal activation of insulin receptor induces the activation of PI3K/Akt pathway, resulting in the phosphorylation of FOXO proteins. Phosphorylated FOXO proteins are translocated to the cytoplasm, resulting a decrease of its activity in the regulation of gene transcription. Although, during caloric restriction, the circulating levels of insulin are lower, decreasing the phosphorylation of FOXO, and consequently, FOXO proteins stay in the nucleus, resulting a regulation of their transcriptional activity. FOXO: Forkhead box O; Pi: Phosphate; PI3K/Akt: Phosphatidilinositol-3 kinase/Protein kinase B.

1.2.2.5 Other mechanisms behind caloric restriction beneficial effects

We described some of the mechanisms underlying the beneficial effects of CR related with autophagy, inflammation, mitochondrial function and oxidative stress, and some regulatory proteins. Other mechanisms could also be involved, as instance changes in stress response proteins and in neurotrophic factors, and the alterations in glucose/insulin signaling, and consequently on PPARs. Nevertheless, there are other mechanisms described (for more details see the following reviews: Sinclair, 2005;

Bordone and Guarente, 2005; Martin et al., 2006; Redman and Ravussin, 2009; Fontana and Partridge, 2015).

It is known that the decrease in food availability causes a certain degree of psychological and physiological stress in the organism. This leads to an increase of some proteins, such as heat shock proteins, glucose-regulated proteins, and also neurotrophic factors, in order to respond to the mild stress imposed by CR (Aly et al., 1994; Heydari et al., 1996; Lee et al., 1998; Yu et al., 1999; Duan et al., 2003; Maswood et al., 2004). At a neuronal level, all these factors are related with neuroprotection and neurotrophic factors are also associated with the induction of neurogenesis (Lowenstein et al., 1991; Lee et al., 2002). CR is also associated with a decrease in glucose and insulin levels, increasing the insulin responsiveness and glucose effectiveness (Masoro et al., 1992; Dunn et al., 1997; Anson et al., 2003). Moreover, the decrease on insulin levels leads to an activation of the expression of PGC-1α and β, inducing the regulation of the energy metabolism and balance in the organism, providing extra energy supplies (Herzig et al., 2001; Puigserver and Spiegelman, 2003). Figure 1.12 summarizes these other mechanisms that underlies the beneficial effects of CR.
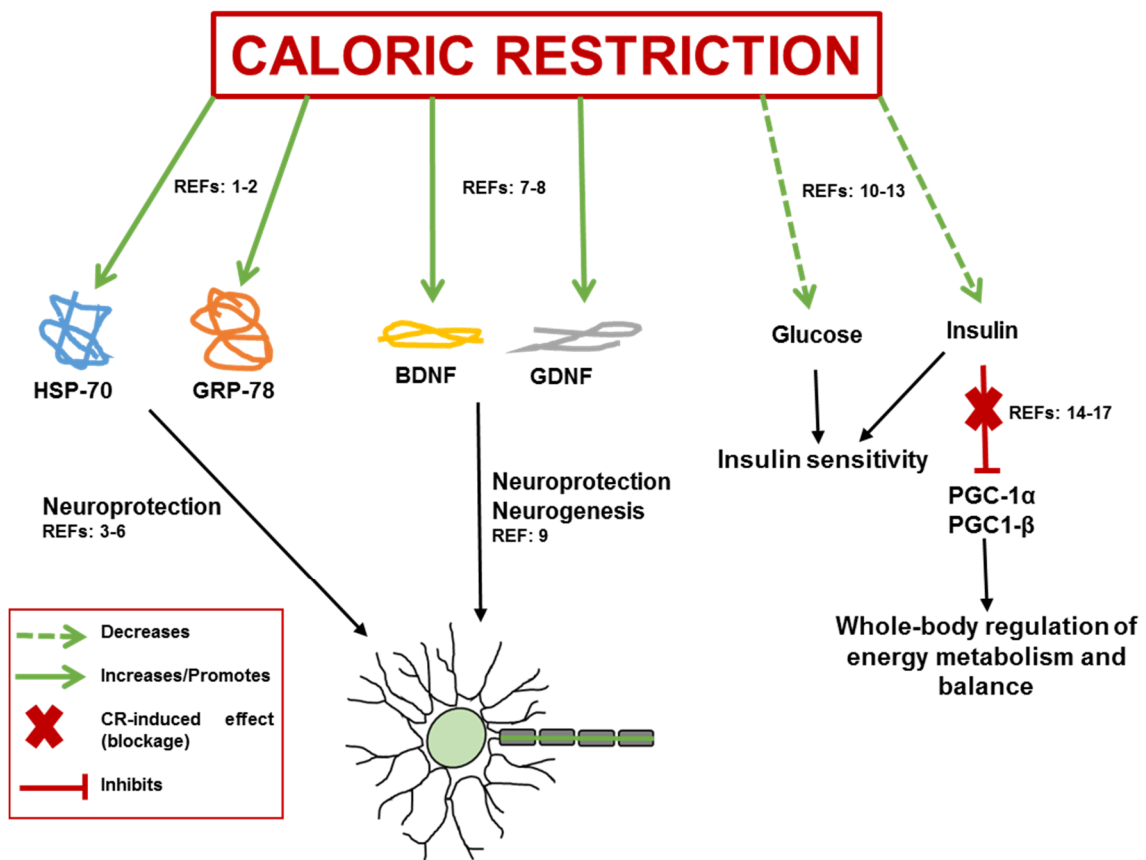
Figure 1.12 Some of other mechanisms underlying the beneficial effects of caloric restriction. Caloric restriction induces a mild stress response in neurons, presumably due to a decrease in energy, increasing the levels of stress-response proteins and factors, such as HSP-70, GRP-78, BDNF, and GDNF. All of them contribute to neuroprotection

Figure 1.12 (cont.) and the last two are also linked with the induction of neurogenesis. Caloric restriction decreases glucose and insulin circulating levels, leading to an amelioration of the insulin sensitivity. The decrease in insulin is related with an upregulation of PGC-1α and β leading to a better coordination of the energy metabolism and balance. REF: 1- Lee et al., 1998; 2- Heydari et al., 1996; 3- Lowenstein et al., 1991; 4- Yu and Mattson, 1999; 5- Warrick et al., 1999; 6-Yu et al., 1999; 7- Duan et al., 2003; 8- Maswood et al., 2004; 9- Lee et al., 2002; 10- Dunn et al., 1997; 11- Anson et al., 2003; 12- Masoro et al., 1992; 13- Kemnitz et al., 1993; 14- Weindruch et al., 2002; 15- Kayo et al., 2001; 16- Puigserver and Spiegelman, 2003; 17- Herzig et al., 2001. BDNF: Brain-derived neurotrophic factor; GDNF: Glial-derived neurotrophic factors; GRP-78: Glucose-related protein 78; HSP-70: Heat-shock protein 70; PGC-1α: Peroxisome proliferator-activated receptor gamma coactivator 1-alpha; PGC-1β: Peroxisome proliferator-activated receptor gamma coactivator 1-beta.

1.2.3 Limitations and disadvantages of caloric restriction

CR is able to extend lifespan in several species and also mediates neuroprotection. Although, CR is a severe intervention that results in both beneficial and detrimental effects, which sometimes could outweigh the positive effects. For example, in non-obese subjects, CR can induce an excessive loss of body fat (Mitchell et al., 2015a; Mitchell et al., 2015b; Mitchell et al., 2015c) and the concomitant decline in sex steroids can lead to menstrual irregularities, amenorrhea, dysfunction in sex drive, bone thinning, and development of osteoporosis in females (Dos Santos et al., 2011; Devlin et al., 2010; Colman et al., 2012; Williams et al., 2015). Moreover, the majority of mammalian CR experiments are conducted in animals housed in pathogen-free and environmentally protected facilities. However, when challenged with polymicrobial environment, calorie restricted animals performed significantly worse (Sun et al., 2001). Indeed, some researchers are skeptical whether CR will work in humans. In this point of view, individuals practicing CR should be cautious, and it may be more sensible and beneficial, to utilize therapies based in specific genetic mechanisms of CR action. Thus, the development of a chemical CR mimetic may be a promising therapeutic strategy for the treatment of some neurodegenerative diseases, and to delay the aging process, extending health- and lifespan. However, a CR mimetic could not be a feasible drug to produce, especially since the appreciation of the processes whereby CR exerts its protective effects, are still somewhat complex. Hence, it is imperative the knowledge of the main mechanisms underlying CR beneficial effects on specific diseases, in order to develop new potential therapies for them.

1.3 <u>Sirtuins</u>

The history of sirtuins is not as long as CR's history. It initiates more than three decades ago with the identification of Silent information regulator 2 (Sir2), a protein that belongs to a complex that enables gene silencing at specific regions of the yeast genome (Shore et al., 1984; Ivy et al., 1985; Rine and Herskowitz, 1987). Later on, sirtuins were identified by Guarente and colleagues in a genetic screening of genes involved in yeast "replicative lifespan" (Kennedy et al., 1995). In fact, the discovery of sirtuins as regulators of aging started in yeast. In Kennedy's study at Guarente's laboratory, it was observed that in the absence of normal telomere length, silent information regulator 4 complex localizes to an unknown aging regulator locus (Kennedy et al., 1995). Afterward, this site was discovered in the yeast genome as the ribosomal DNA (rDNA) locus, a tandem repeat of the coding sequences for the ribosomal RNA (rRNA; Kennedy et al., 1997). This observation contributed to the discovery that the basis of yeast aging is the recombination events within rDNA that release a single repeat in the circular form, since the accumulation of these extrachromosomal rDNA circles (ERCs) can contribute to the cell death (Sinclair and Guarente, 1997). After that, it was demonstrated that Sir2, that belongs to Sir4 complex in yeast, coordinates the rate of ERC formation and therefore the rate of yeast aging (Figure 1.13; Kaeberlein et al., 1999). This last study, that was also performed at Guarente's laboratory, demonstrated that deletion of Sir2 shortens yeast lifespan, and Sir2 overexpression extends longevity of yeast (Kaeberlein et al., 1999). A first glimpse about the real function of Sir2 and its orthologues, was grasped when Shin Imai and Leonard Guarente revealed for the first time the real enzymatic activity of Sir2: a NAD$^+$-histone deacetylase (Imai et al., 2000). This simultaneously explains how Sir2 and its homologs act as nutrient sensors (Guarente, 2000).
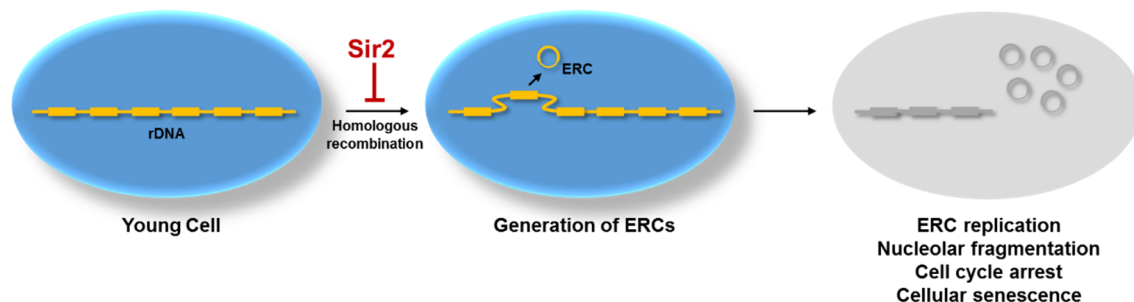
Figure 1.13 <u>ERC formation in yeast cells leads to cellular senescence and death.</u> As cells age, a single repeat of rDNA can be released by a homologous recombination reaction, leading to the formation of ERCs. The accumulation of ERCs during time induces nucleolar fragmentation, cell cycle arrest, and consequently cellular senescence. Yeast Sir2, through its deacetylase activity, slows the formation of ERCs, thereby reducing these effects. <u>ERCs:</u> Extrachromosomal rDNA circles; <u>rDNA:</u> Ribosomal DNA; <u>Sir2:</u> Silent information regulator 2.

Sir2, and the mammalian orthologues sirtuins, became more attractive to the scientific community when several publications showed that sirtuins are pivotal in the regulation of lifespan in different species. Similarly to the finding in yeast, the increase in sirtuins in *C. elegans* (Tissenbaum and Guarente, 2001) and *Drosophila melanogaster*, using either genetic (Rogina and Helfand, 2004) or chemical approaches (Wood et al., 2004), also extend their lifespan, at least 15%. Furthermore, this was linked with CR (Lin et al., 2000; Cohen et al., 2004). It was showed that Sir2 could be a critical mediator of the effects of CR on yeast longevity (Lin et al., 2000). This because reduced glucose amounts were enough to increase replicative lifespan, but only in the presence of Sir2, and similar outcomes were obtained with Sir2 overexpression (Lin et al., 2000). Moreover, in 2004 Cohen at the Sinclair's laboratory, demonstrated that SIRT1, the most closed Sir2 orthologue in mammals, is involved on CR-response on lifespan in rats (Cohen et al., 2004). Thus, these results suggested that sirtuins regulate lifespan in an evolutionarily conserved way, and the understanding of their regulation at the molecular level may contribute to the development of new therapeutic possibilities.

1.3.1 Subcellular localization and activities

Seven Sir2 homologues, also referred as sirtuins (SIRT1-7), have been described for mammals (Frye, 2000). All of them present a conserved catalytic core domain, but have different cellular localizations and the protein sequences flanking their catalytic core are also different (Figure 1.14). Three sirtuins, namely SIRT1, SIRT6, and SIRT7 are primarily found in the nucleus, but not exclusively, and display different subnuclear localizations. SIRT1 is found in non-nucleolar regions (Michishita et al., 2005), as well as in the cytosol in certain conditions, such as during tumor progression (Byles et al., 2010), apoptosis (Jin et al., 2007), and neuronal differentiation (Hisahara et al., 2008; Tanno et al., 2007). SIRT6 and SIRT7 are mostly located in heterochromatic regions and nucleoli, respectively (Michishita et al., 2005; Mostoslavsky et al., 2006). SIRT2 is normally found in the cytosol and during mitosis binds to chromatin becoming enriched in the nucleus (North and Verdin, 2007). SIRT3, SIRT4, and SIRT5 are present in mitochondria (Michishita et al., 2005), but SIRT3 can also shuttle to the nucleus (Scher et al., 2007). Figure 1.14 summarizes the primary structure and the subcellular localization of the seven sirtuins.
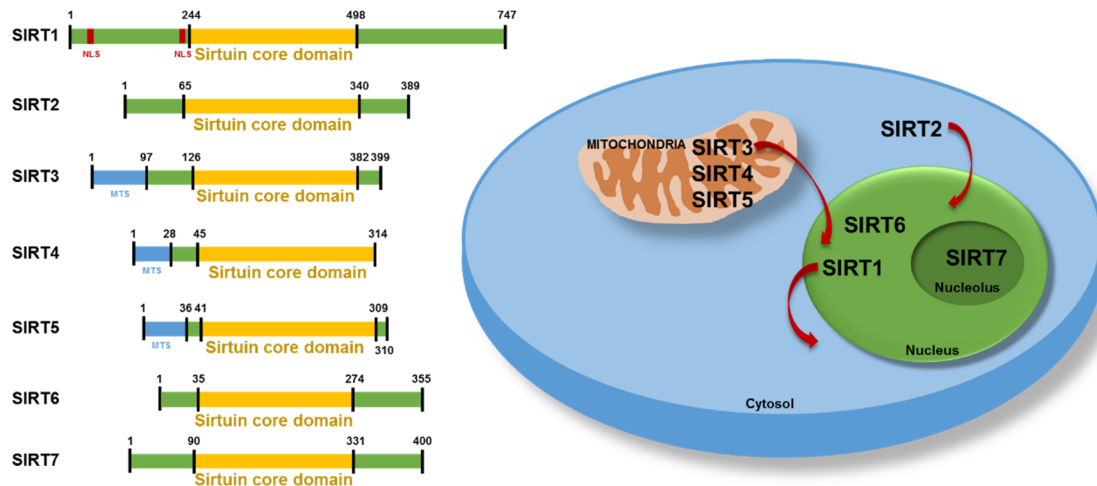
Figure 1.14 <u>Primary structure and subcellular localization of sirtuins.</u> The conserved catalytic domain of the seven mammalian sirtuins (SIRT1-7) is represented in yellow. NLSs (in red) and MTSs (in blue) of specific sirtuins are also indicated. Numbers refer to amino acid residues in the proteins. SIRT1 is primarily located at the nucleus, but in some conditions can be found at the cytosol. SIRT6 is found at the nucleus and SIRT7 at the nucleolus. SIRT2 is a well-known cytosolic sirtuin that during mitosis can translocate to the nucleus. SIRT3, 4, and 5 are mitochondrial proteins. SIRT3 in some conditions can shuttle to the nucleus. <u>MTS:</u> Mitochondrial targeting sequence; <u>NLS:</u> Nuclear localization sequence; <u>SIRT:</u> Sirtuin.

Originally, sirtuins were included in the group of NAD$^+$-dependent type III histone deacetylases (HDACs class III) due to the deacetylation of histone H3 and H4 on specific genomic loci of Sir2 in yeast (Imai et al., 2000; Parsons et al., 2003; Shankaranarayana et al., 2003; reviewed in Toiber et al., 2011). Nowadays, it is known that this is not the unique activity of sirtuins and their deacetylase activity targets broaden beyond histones, to include many transcription factors and enzymes (see Section 1.3.2 for more details). There is a growing list of reactions that mammalian sirtuins catalyze, including demalonylation, desuccinylation, deacylation, and mono-ADP-ribosylation. Table 1.8 summarizes the main reactions associated with each sirtuin and the class that each sirtuin belongs, due to a sequence-based phylogenetic analysis (Frye, 2000).

Table 1.8 <u>Sirtuin's class and main activities.</u>

Sirtuin	Class	Activity/ies	Reference
SIRT1	I	Deacetylase ADP-ribosylase (weak)	Imai et al., 2000; Landry et al., 2000; Smith et al., 2000; Vaziri et al., 2001
SIRT2	I	Deacetylase	North et al., 2003; Jing et al., 2007
SIRT3	I	Deacetylase	Lombard et al., 2007; Hirschey et al., 2010; Shimazu et al., 2010
SIRT4	II	ADP-ribosylase	Haigis et al., 2006
SIRT5	III	Deacylase (succinyl, malonyl groups) Deacetylase (weak)	Nakagawa and Guarente, 2009; Du et al., 2011; Zhou et al., 2012
SIRT6	IV	Deacylase (long-chain fatty acyl groups) Deacetylase (weak) ADP-ribosylase (weak)	Liszt et al., 2005; Michishita et al., 2008
SIRT7	IV	Deacetylase	Chen et al., 2013; Chen et al., 2016

SIRT1-7 description of the phylogenetic class that each sirtuin belongs and the main known activities. <u>ADP</u>: Adenosine diphosphate; <u>SIRT</u>: Sirtuin.

The enzymatic reaction catalyzed by sirtuins necessitates NAD^+ as a co-substrate (Imai et al., 2000; Landry et al., 2000). This is then converted into nicotinamide, and the concentration of which is determined by the nutritional state of the cell (reviewed in Houtkooper et al., 2010). For example, during CR is observed an increase in $NAD^+/NADH$ ratio, increasing sirtuins' activity.

This thesis is centered on SIRT1 and on its deacetylase activity. Herein after, we will describe the particularities referred in each section focusing on SIRT1.

1.3.2 Substrates and physiological effects

As referred before, in yeast, Sir2 deacetylates histones H3 and H4 (Imai et al., 2000; Parsons et al., 2003; Shankaranarayana et al., 2003; reviewed in Toiber et al., 2011). Besides histones, substrates of nuclear sirtuins include transcription factors and cofactors. Moreover, all the seven sirtuins deacetylate several metabolic players, and particularly, mitochondrial sirtuins (SIRT3-5) play important roles in the deacetylation and activation of enzymes involved in fatty oxidation, in the tricarboxylic acid cycle, and in

other oxidative pathways (reviewed in Parihar et al., 2015). Therefore, the main functions related with sirtuins are: transcription regulation, control of energy metabolism, regulation of several processes including, cell survival, DNA repair, tissue regeneration, inflammation, neuronal signaling, and circadian rhythms (reviewed in Haigis and Sinclair, 2010). Nakagawa and Guarente's review (2014) describes the different known substrates of the each sirtuin (reviewed in Nakagawa and Guarente, 2014).

SIRT1 has been the most extensively sirtuin studied. As referred before, it is predominantly nuclear, but can also be present at cytosol. SIRT1 deacetylates more than 50 non-histone targets (reviewed in Nakagawa and Guarente, 2014), including transcription factors (Luo et al., 2001; Vaziri et al., 2001; Yeung et al., 2004; Rodgers et al., 2005; Walker et al., 2010), autophagy-related proteins (Lee et al., 2008; Huang et al., 2015), among others. It is an important enzyme, since the whole-body SIRT1 knockout (KO) mice display developmental and growth defects, as well as altered birth rate, and only infrequently postnatally survival (Cheng et al., 2003; McBurney et al., 2003). The SIRT1 KO mice that survived until adulthood do not display some of the metabolic responses normally triggered by CR (Chen et al., 2005a). At McBurney's lab it was also showed that SIRT1 KO mice are metabolically inefficient and the increase in longevity in response to CR is absent in these mice (Boily et al., 2008). In contrast, transgenic mice that constitutively express SIRT1, display several phenotypes that resemble caloric restricted mice, namely: i) they are leaner; ii) they are metabolically more active; and iii) they show decreased insulin and fasted blood glucose combined with an increased glucose tolerance (Bordone et al., 2007).

Regarding the main substrates of SIRT1 we can highlight five important nuclear targets: p53, PGC-1α, NF-κB, FOXOs, and CRTC2 and three cytosolic targets: AceCS-1, eNOS, and Atgs (see Figure 1.15). In fact, the identification of p53 as a SIRT1 substrate enlightened the scientific community on the versatility of SIRT1. Indeed, it was the first-described non-histone target for SIRT1. Two different independent groups described how SIRT1 interacts with and deacetylates p53 (Luo et al., 2001; Vaziri et al., 2001). This deacetylation attenuates its activity on the p21 promoter and inhibits p53-dependent apoptosis (Luo et al., 2001; Vaziri et al., 2001). Unexpectedly, SIRT1 suppresses tumor formation (reviewed in Herranz and Serrano, 2010). SIRT1 also deacetylates PGC-1α and this event is very important for PGC-1α activation (Rodgers et al., 2005; Lerin et al., 2006), inducing mitochondrial gene expression. SIRT1 has also a marked anti-inflammatory effect in diverse tissues and cell models (Pfluger et al., 2008; Purushotham et al., 2009; Yoshizaki et al., 2009; Yoshizaki et al., 2010), possibly through the negative regulation of the NF-κB pathway (Yeung et al., 2004). It is also known that

SIRT1 plays key roles modulating cognitive function and synaptic plasticity (Gao et al., 2010; Michan et al., 2010). Additionally, as will be explored in the section 1.3.5.2, enhanced SIRT1 activity could be beneficial in neurodegenerative diseases (Araki et al., 2004; Chen et al., 2005b; Kim et al., 2007a).

The FOXO family, as referred before, is an important family of transcription factors. SIRT1 interacts with and deacetylates FOXO family of transcription factors (Brunet et al., 2004; Motta et al., 2004). Interestingly, the deacetylation of a member of FOXO family – FOXO3 – inhibited its activity on apoptosis-related gene expression, while driving its action towards the induction of oxidative stress resistance genes (Brunet et al., 2004). It also deacetylates and regulates CREB-protein regulated transcriptional co-activators (CRTCs) (Liu et al., 2008). This is related to the regulation of the hepatic gluconeogenesis and to an adaptation to the nutrient environment and oxidative stress (Liu et al., 2008).

As aforementioned SIRT1 is also located at the cytosol in many cell types, especially when insulin signals are lacking (Tanno et al., 2007). This suggests that SIRT1 also modifies the activity of some cytosolic proteins. One of the cytosolic substrates is acetyl-CoA synthetase 1 (AceCS-1) enzyme. AceCS-1 is deacetylated by SIRT1, but not by other sirtuins (Hallows et al., 2006), regulating the formation of acetyl-CoA. Moreover, SIRT1 also deacetylates endothelial nitric oxide synthase (eNOS; Mattagajasingh et al., 2007). This leads to an inefficient vasodilation, a key process for proper nutrient supply to tissues.

In addition, a study demonstrated that SIRT1 deacetylates Atg5, Atg7, and Atg8, key players on autophagy pathway (Lee et al., 2008). This study highlighted the relevant role of SIRT1 on autophagy, since its activation by starvation was impeded in embryonic fibroblasts of SIRT1$^{-/-}$ mice and was also associated with the accumulation of damaged organelles, mainly mitochondria (Lee et al., 2008). A more recent study also demonstrated that SIRT1 is necessary for LC3B nuclear deacetylation, and consequent autophagy activation driven by starvation (Huang et al., 2015). SIRT1 has other substrates and they are reviewed in Nakagawa and Guarente, 2014.

Therefore, the deacetylation driven by SIRT1 can lead to a direct activation or inhibition of several transcription regulators and other proteins, and contribute to the modification of their interaction profiles, depending on the cellular context.
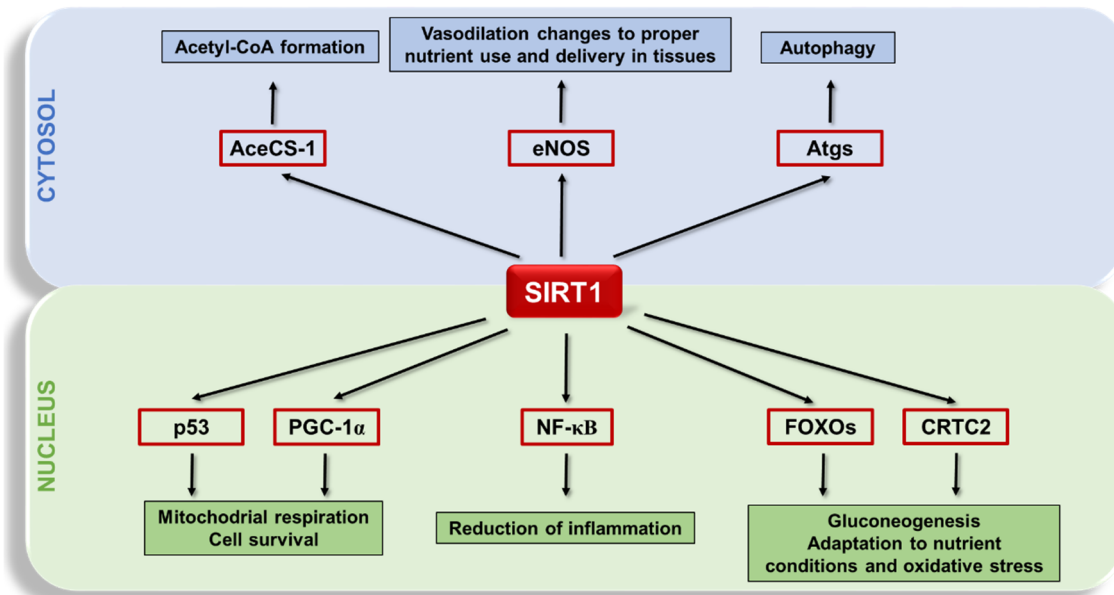
Figure 1.15 Representation of some SIRT1 nuclear and cytosolic substrates and the main resulting physiological effects. SIRT1 can deacetylate a large array of protein targets involved in different cellular processes: metabolism, cell survival, inflammation, oxidative stress, nutrient use response, and autophagy. SIRT1's cytosolic targets are illustrated in the top of the figure and nuclear targets in the bottom of the figure. AceCS-1: Acetyl-CoA Synthetase 1; Atgs: Autophagy-related proteins; CRTC2: CREB protein-regulated transcriptional co-activator 2; eNOS: Endothelial nitric oxide synthase; FOXOs: Forkhead box O proteins; NF-κB: Nuclear factor kappa B; p53: Tumor protein p53; PGC-1α: Peroxisome proliferator-activated receptor gamma coactivator 1-alpha.

1.3.3 Regulation of sirtuin 1 activity and levels

Sirtuins are some of the most highly regulated enzymes described until now. As referred before, subcellular localization partially influences activity. Additional regulation is required at different levels, namely: transcription, post-transcription, translation, post-translation, protein-protein interactions, protein stability, and with inhibitory molecules. The substrate and co-substrate availability also influence sirtuins' activity. There are also nutrients and small molecules that modulate sirtuins activity, opening new opportunities for therapeutic interventions. The particular regulation of SIRT1 will be the focus of this section.

There are several physiological conditions that affect SIRT1's activity. For example, nutrient starvation increases SIRT1 expression (Nemoto et al., 2004), whereas high-fat diet reduces SIRT1 expression (Heyward et al., 2012; Choi et al., 2013). In table 1.9 we summarized the main points of SIRT1 regulation, the main effectors, and respective outcomes in SIRT1's expression or activity. All in all, this is a complex mechanism involving different players, and it is not completely understood.

Table 1.9 <u>Activators and repressors of SIRT1's expression and activity.</u>

Point of regulation	Effectors	Outcome	References
Transcription	FOXO1, PPARα/β, CREB	Increased expression	Chen et al., 2005c; Zhang et al., 2007; Hayashida et al., 2010; Han et al., 2010; Okazaki et al., 2010; Bai et al., 2011a; Noriega et al., 2011
	PPARγ, ChREBP, HIC, PARP2	Decreased expression	
Post-Transcription	miR 34a, miR 199	Repression	Yamakuchi et al., 2008; Rane et al., 2009; Lee et al., 2010
Post-Translational	Phosphorylation Sumoylation	Activation/Repression	Yang et al., 2007b; Sasaki et al., 2008; Nasrin et al., 2009; Guo et al., 2010
Protein-protein complexes	AROS	Activation	Picard et al., 2004; Kim et al., 2007b; Kim et al., 2008; Zhao et al., 2008; Escande et al., 2010; Mulligan et al., 2011
	NCoR1, SMRT, DBC1, LSD1	Repression	

SIRT1 can be regulated at different levels that are represented in the table. To each point of regulation is indicated the effectors and the respective outcome. <u>AROS:</u> Active regulator of SIRT1; <u>ChREBP:</u> Carbohydrate response-element-binding protein; <u>CREB:</u> cAMP-responsive element binding; <u>DBC1:</u> Deleted in breast cancer 1; <u>FOXO:</u> Forkhead box O; <u>HIC:</u> Hypermethylated in cancer; <u>miR:</u> microRNA; <u>LSD1:</u> Lysine-specific demethylase 1; <u>NCoR1:</u> Nuclear receptor co-repressor 1; <u>PARP2:</u> Poly-(ADP-ribose) polymerase 2; <u>PPAR:</u> Peroxisome proliferator-activated receptor; <u>SMRT:</u> Silencing mediator of retinoid and thyroid hormone receptors.

Moreover, SIRT1 activity also depends on cofactor NAD^+, and therefore the availability of NAD^+ is another point of regulation. In the next sections this regulation will be better explored.

1.3.3.1 Sirtuin NAD^+-dependency

As referred before, NAD^+ is an important cofactor for SIRT1 activity. NAD^+ levels can be regulated by several pathways. For example, the reduced form NADH, generated during glycolysis, can limit NAD^+ levels, thereby conditioning the use of NAD^+ in SIRT1 enzymatic reactions (Canto et al., 2009). Another example is during fasting and exercise, in which muscle NAD^+ levels rise, with a parallel activation of SIRT1 (Canto et al., 2010). Furthermore, CR also leads to an increase in NAD^+ levels in several tissues, such as muscle, liver, and white adipose tissue, and in contrast high-fat diet reduces the NAD^+/NADH ratio, affecting SIRT1 activity (Chen et al., 2008a; Kim et al., 2011).

The by-products generated by deacetylase activity of SIRT1, resulting from the transformation of NAD^+ molecule, can also regulate SIRT1 activity (Figure 1.16).

Nicotinamide in high concentrations can non-competitively bind, and therefore trough a negative feedback, inhibit SIRT1 activity (Bitterman et al., 2002; Anderson et al., 2003). The another by-product of the sirtuin deacetylase reaction – 2'-O-acetyl-ADP-ribose – was also reported as a signaling molecule, but likewise nicotinamide its exact role in metabolic control is not completely understood (Tanner et al., 2000; Liou et al., 2005).
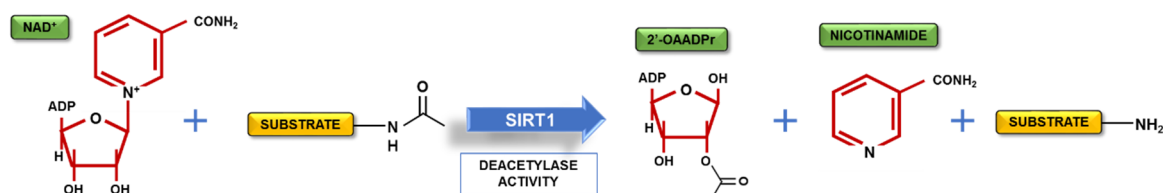
Figure 1.16 <u>SIRT1 deacetylase activity.</u> SIRT1 activity is regulated by the levels of NAD^+ co-factor. It deacetylates the substrates and generates 2'-OAADPr and nicotinamide. Both by-products are signaling molecules that can regulate SIRT1 activity. <u>2'-OAADPr:</u> 2'-O-acetyl-ADP-riboside; <u>ADP:</u> Adenosine diphosphate; <u>NAD^+:</u> Oxidized nicotinamide adenine dinucleotide; <u>SIRT1:</u> Sirtuin 1.

NAD^+ levels also depend on the pathways related with its biosynthesis, degradation, and regeneration, and will be explored in the next section.

1.3.3.1.1 NAD$^+$ biosynthesis, degradation, and salvage pathways

NAD^+ can be synthesized from several precursors by two important pathways: *de novo* biosynthesis and regeneration pathways. *De novo* biosynthesis that begins with amino acid tryptophan is known as kynurenine pathway (Krehl et al., 1946; reviewed in Houtkooper et al., 2010), and the pathway that begins with nicotinic acid is known as the Preiss-Handler pathway (Preiss and Handler, 1958a; Preiss and Handler, 1958b). NAD^+ can be also regenerated from nicotinamide, nicotinamide riboside (NR; naturally found in milk), or from nicotinamide mononucleotide (NMN; not naturally found in food) (Bieganowski and Brenner, 2004; Yoshino et al., 2011). Further studies should be done in order to determine whether the naturally occurring nicotinic acid, nicotinamide and/or NR can activate SIRT1 *in vivo*, and to clarify the physiological relevance of these molecules.

Regarding *de novo* biosynthetic pathways, as described before, NAD^+ can be synthesized from dietary sources, such as nicotinic acid and tryptophan (Figure 1.17). The major dietary source is nicotinic acid, which is a form of vitamin B_3 (niacin), that can be transformed into NAD^+ through three steps in the Preiss-Handler pathway, described in Figure 1.17. In sum, the key enzyme of this pathway is nicotinamide mononucleotide adenylyltransferase (NMNAT), which also plays an important role in the salvage

pathway. Three isoforms of the enzyme have distinct subcellular localizations: NMNAT1 in the nucleus, NMNAT2 in the cytosol, and NMNAT3 in the mitochondria (Zhang et al., 2003; Berger et al., 2005). The synthesis from tryptophan occurs in the kynurenine pathway, as demonstrated in Figure 1.17 (Bogan and Brenner, 2008). This is linked with the Preiss-Handler pathway since the excess of tryptophan induces the formation of quinolinic acid that is transferred to the Preiss-Handler pathway, through the formation of nicotic acid mononucleotide. Although, the NAD^+-salvage pathway is the key pathway for the maintenance of cellular NAD^+ levels. The NAD^+-consuming enzymes, namely, sirtuins, poly-(ADP-ribose) polymerases (PARPs), and cyclic ADP-ribose (cADPR) synthases (CD38 and CD157), generate nicotinamide as a by-product of their enzymatic activities (Figure 1.17). As referred before, nicotinamide inhibits sirtuin activity by binding in a conserved NAD^+-pocket, and is a precursor of the NAD^+-regeneration pathway. As demonstrated in Figure 1.17, the NAD^+-salvage pathway is a two-step pathway. In the first step nicotinamide is converted into NMN, through the participation of nicotinamide phosphoribosyltransferase (NAMPT), and then NMNAT regenerates NAD^+ from NMN (reviewed in Verdin, 2015). This is an important pathway that recycles nicotinamide into NAD^+ and relieves its inhibitory effect. NR can also be converted into NAD^+, entering directly into the NAD^+-salvage pathway after the action of nicotinamide riboside kinase (NRK) (Figure 1.17; reviewed in Verdin, 2015).

There is a competitive relationship between the three NAD^+-consuming enzymes. For instance, PARP1 activity increases with aging, due to the accumulation of DNA damages, and in response to high energy intake (Braidy et al., 2011; reviewed in Mouchiroud et al., 2013a). PARP1 and SIRT1 have relatively similar values of K_m for NAD^+, and thus the decrease in NAD^+ that occurs when PARP1 is over activated leads to a reduction on SIRT1 activity (Bai et al., 2011b; Braidy et al., 2011). Deletion of *Parp1* or *Parp2* in mice activates SIRT1, because PARP1 competes for NAD^+ and PARP2 decreases SIRT1 expression, because as denoted before, it is a SIRT1 repressor (Bai et al., 2011a). Consistent with nuclear localization of both SIRT1 and PARPs, *Parp1* deletion does not increase deacetylation activity of non-nuclear sirtuins (Bai et al., 2011b). Cyclic ADP-ribose synthases (CD38 and CD157) produce ADP-ribose from NAD^+, in different cell types, not only on lymphocytes. CD38 is a major NAD^+-consuming enzyme, and its decrease is associated with increased NAD^+ concentrations in the brain, lung, and kidney (Young et al., 2006; Aksoy et al., 2006). Moreover, it was recently demonstrated that CD38 not only consumes NAD^+, and dictates a decrease of NAD^+-pool during aging, but also degrades NMN, contributing to the decrease of NAD^+ in different tissues, where brain is included (Camacho-Pereira et al., 2016).
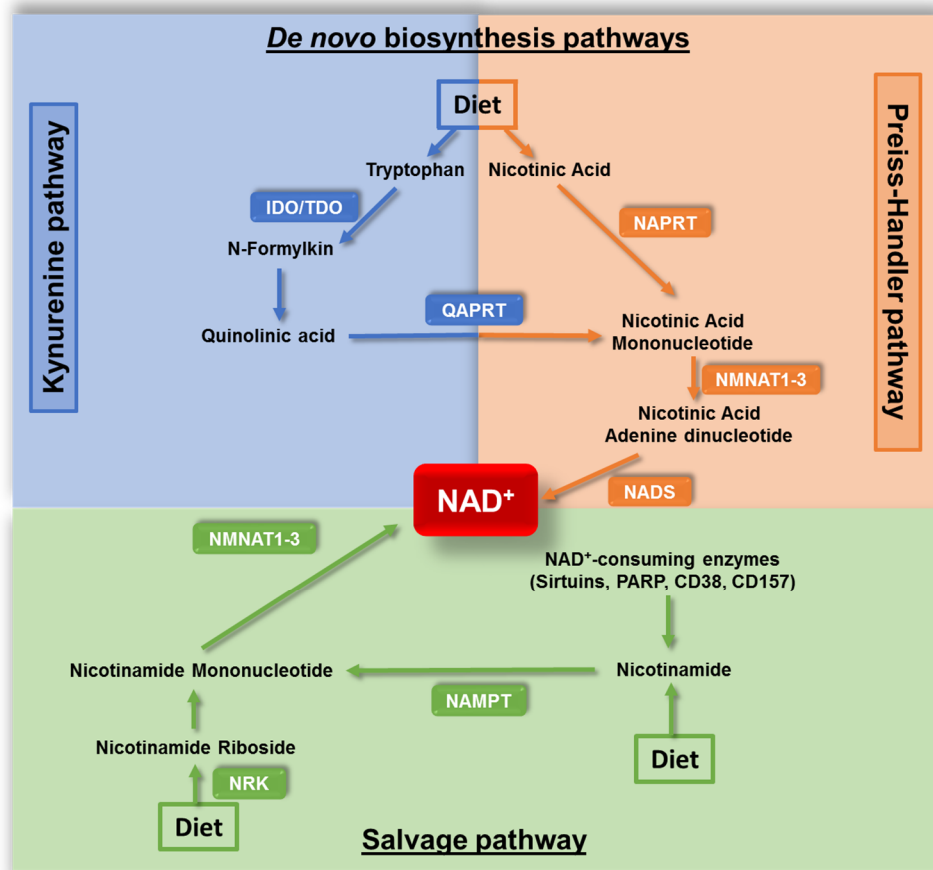
Figure 1.17 <u>NAD$^+$ *de novo* biosynthetic and salvage pathways.</u> NAD$^+$ levels are maintained through three different processes: i) kynurenine pathway; ii) Preiss-Handler pathway; and iii) salvage pathway. In the Preiss-Handler pathway, dietary nicotinic acid is converted into nicotinic acid mononucleotide through the action of NAPRT. This product is then converted into nicotinic acid adenine dinucleotide by the NMNAT1-3 enzymes (isoform 1 at the nucleus, isoform 2 at the cytosol, and isoform 3 at the mitochondria). NADS converts nicotinic acid adenine dinucleotide into NAD$^+$. Furthermore, tryptophan can be used to *de novo* synthesize NAD$^+$. In the kynurenine pathway, tryptophan is converted into N-formylkinurenine (N-formylkin) by either IDO or TDO. When tryptophan levels are high, this product is converted into quinolinic acid, which is transformed into nicotinic acid mononucleotide by the QAPRT enzyme, entering in the Preiss-Handler pathway. The NAD$^+$-salvage pathway recycles nicotinamide (naturally found in food and by-product of the enzymatic activities of NAD$^+$-consuming enzymes, such as sirtuins, PARPs, CD38, and CD157). Initially, NAMPT converts nicotinamide into nicotinamide mononucleotide, and then recycles it into NAD$^+$ via NMNATs. Nicotinamide riboside from the diet can also be converted into nicotinamide mononucleotide, through the action of NRK, entering in the salvage pathway. <u>CD38:</u> Cluster of differentiation 38; <u>CD157:</u> Cluster of differentiation 157; <u>IDO:</u> Indoleamine 2,3-dioxygenase; <u>NADS:</u> NAD$^+$ synthase; <u>NAMPT:</u> Nicotinamide phosphoribosyltransferase; <u>NAPRT:</u> Nicotinic acid phosphoribosyltransferase; <u>NMNAT:</u> Nicotinamide mononucleotide adenylyltransferase; <u>NRK:</u> Nicotinamide riboside kinase; <u>PARP:</u> Poly-(ADP-ribose) polymerase; <u>QAPRT:</u> Quinolinate phosphoribosyltransferase; <u>TDO:</u> Tryptophan 2,3-dioxygenase.

In the next chapters pharmacological strategies to manipulate SIRT1 activity, through direct or indirect (for example manipulating NAD$^+$ levels) pathways will be explored.

1.3.4 Strategies to increase sirtuin 1 activity and/or expression

An evident approach to artificially enhance SIRT1 would be the chemical or molecular approaches that directly activate SIRT1 or induce its expression. Another option is to increase the availability of its co-factor – NAD^+ –, therefore indirectly contributing to the increase in SIRT1 activity. Although, it is important to have in mind whether these strategies are specific for SIRT1, or whether more sirtuins will be influenced. In the next subsections will be explored strategies to increase SIRT1 activity and/or expression, mainly with direct (acting on SIRT1) and indirect (acting on NAD^+) pharmacological approaches, although the possibility of doing it with gene therapy strategies should be taken into account.

It is also well-known that CR activates SIRT1 (Cohen et al., 2004). The mechanism by which CR controls SIRT1 activity is still under debate. The most well accepted hypothesis came from Guarente's lab where they propose that the metabolic shift that occurs in response to CR, results in an increased intracellular NAD^+ levels, leading to SIRT1 activation (Lin et al., 2002). This respiratory increase would decrease NADH, which acts as a SIRTs inhibitor (Lin et al., 2004), even though whether NADH at physiological levels control sirtuins' activity is still under debate (Schmidt et al., 2004). This hypothesis was challenged due to the fact that the cells that are not able to shift from fermentation to respiration should not respond to CR, although this was not observed (reviewed in Kaeberlein and Powers, 2007). Moreover, some studies in worms also suggest that the reduction in mitochondrial function may also promote longevity (Dillin et al., 2002; Lee et al., 2003). On the other hand, there is also compelling evidence demonstrating that mitochondrial function is also positively correlated with lifespan (reviewed in Dilova et al., 2007). This suggests that mitochondrial respiration might be fine-tuned during different stages, while the metabolic shift might not be mandatory for the effects of CR. Therefore, NAD^+/NADH levels are regulated by a complex network of reactions, consequently regulating SIRT1 activity.

1.3.4.1 Sirtuin activating compounds

The discovery of a molecule that activates SIRT1 was desired in the early 2000's, with the observation that Sir2 was linked to an extension of lifespan. Although, if we think in the entire history of pharmaceutical industry, less than dozen examples of allosteric activators were developed (reviewed in Zorn and Wells, 2010). This can be allied to the fact that there is a small number of enzymes that can be allosterically activated, and also because sometimes the activation is seen as an artifact, and researchers avoid the use

of these type of molecules. Besides that, in 2003 the first sirtuin activating compounds (STACs) were discovered, in which resveratrol was the most potent (Howitz et al., 2003). Subsequently, different groups developed synthetic molecules (Feige et al., 2008; Wu et al., 2013), which are in fact more potent than the first generation of STACs (polyphenols) and some of them are already in human clinical trials (Libri et al., 2012; Hoffmann et al., 2013).

As abovementioned, high-throughput screening for SIRT1-activating compounds led to the identification of SIRT1 activators (Howitz et al., 2003). Indeed, the screen of 18,000 compounds identified 21 that are able to activate SIRT1 *in vitro*, lowering its K_m for the peptide substrate (Howitz et al., 2003). Most of these compounds belong to the polyphenol family of natural products characterized by planar multi-phenyl rings bearing hydroxyl groups, such as resveratrol, piceatannol, quercetin, and butein. Resveratrol was the most potent and increased SIRT1 activity approximately tenfold (Howitz et al., 2003). Resveratrol increases SIRT1 activity and enhances mitochondrial function in mice (Lagouge et al., 2006; Baur et al., 2006). Resveratrol also increased lifespan of obese mice (Baur et al., 2006) and improved mitochondrial activity and metabolic control in humans, as well (Timmers et al., 2011). More intensive high-throughput screening identified several novel synthetic compounds that can be more active than resveratrol (reviewed in Milne et al., 2007). As resveratrol, these compounds lower the K_m for the substrate peptide. Interestingly, these STACs comprise numerous scaffolds, such as imidazothiazole, benzimidazoles, thiazolopyridines, and urea-based scaffolds (Hubbard et al., 2013; reviewed in Milne et al., 2007). Pharmaceutical chemistry has developed thousands of analogs of these scaffolds, which can be up to three orders of magnitude more potent than resveratrol (reviewed in Szczepankiewicz and Ng, 2008). The most potent is SRT1720, which as resveratrol extends lifespan of obese mice (Minor et al., 2011), and improves mitochondrial function (Feige et al., 2008).

Even though the physiological effects of resveratrol and the synthetic STACs are widely accepted, there was a strong debate about the mechanisms behind them. Two opposing models were proposed for STAC activity: i) direct allosteric activation of SIRT1 through a decrease of peptide substrate and NAD^+ K_m (Howitz et al., 2003; Dai et al., 2010); and ii) coincidental, and indirect activation due to off-targets effects, such as cAMP phosphodiesterases (Pacholec et al., 2010; Park et al., 2012). In fact, in 2012 Sinclair's group demonstrated that in the particular case of resveratrol, regarding skeletal muscle mitochondrial function, resveratrol can activate SIRT1 or AMPK (independently of SIRT1), and this was dose dependent (Price et al., 2012). High doses induced an AMPK activation, independently of SIRT1, whereas low doses of resveratrol induced an

effect where SIRT1 was the central player (Price et al., 2012). Thus, whether or not resveratrol acts directly on SIRT1 seems to be dose-dependent. Moreover, skepticism about the mechanism behind STACs arose from some particularities regarding the assay used. "Fluor de Lys" assay was the fluorometric assay used in initial screen for STACs (Howitz et al., 2003). In this assay an acetylated peptide substrate was conjugated with aminomethylcoumarin (AMC), a fluorescence labelling (Howitz et al., 2003). Separately, synthetic SIRT1 activators (e.g. SRT1460, SRT1720, SRT2183, SRT2106) were discovered in a fluorescence polarization assay using a carboxytetramethylrhodamine (TAMRA)-tagged substrate (Dai et al., 2010; Hubbard et al., 2013). The validity of STACs as direct SIRT1 activators was called into question when some reports suggested that fluorescent moieties on the substrates used in these studies were required for the activation of SIRT1 (Borra et al., 2005; Kaeberlein et al., 2005a; Pacholec et al., 2010), leading to the conclusion that SIRT1 activation could be an *in vitro* artifact (Pacholec et al., 2010). Since then, the direct mode of SIRT1 activation was strengthened. The first study against the skeptics reported that the fluorescent moiety on substrates is indeed dispensable for activation, because its replacement by hydrophobic amino acids led to an activation, and also demonstrated that synthetic STACs physically interact with SIRT1 (Dai et al., 2010). Another study demonstrated that native peptide substrates of SIRT1, such as PGC-1α and FOXO3, mediate the activation promoted by resveratrol and other STACs *in vitro*, due to the presence of hydrophobic residues in the same positions as the fluorophores (Hubbard et al., 2013). These studies suggested that are structural and positional requirements in the natural substrates that facilitate SIRT1 activation. Sinclair's group proposed an assisted-allosteric activation mechanism in which STACs can bind to a substrate-induced exosite on SIRT1, consequently stabilizing the substrate binding, and subsequently activating SIRT1 (Figure 1.18; Hubbard et al., 2013). Additional clues came from the analysis that a single base mutation in SIRT1 (E230K) blocks its activation induced by 117 tested STACs from distinct chemical classes (Hubbard et al., 2013). Further insights into the beneficial effects of STACs *in vivo* have come from the studies that explore their effects on aging and aging-related diseases, effects that are very similar to the effects resulting from the overexpression of SIRT1 (see section 1.3.5).
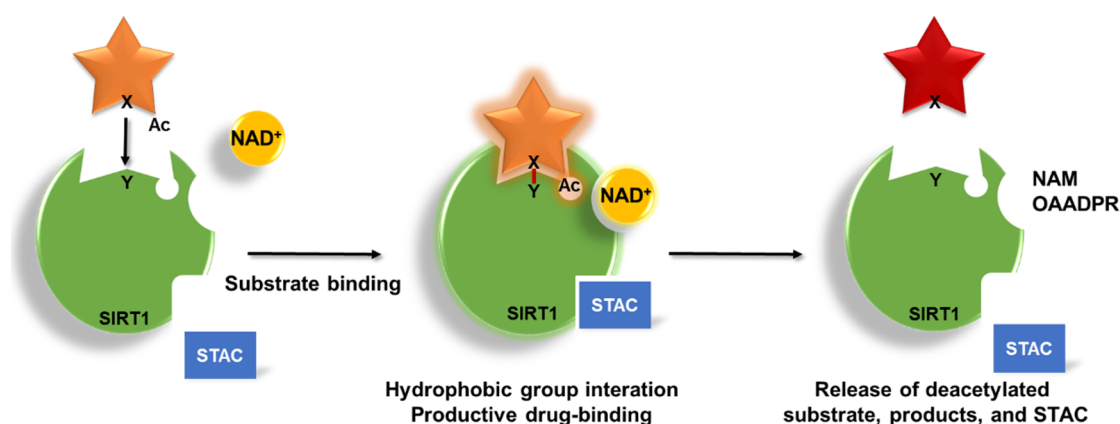
Figure 1.18 <u>Proposed mechanism for the allosteric activation of SIRT1 by STACs.</u> Representation of the activity of SIRT1 indicating that SIRT1 deacetylates the target protein (in orange) using NAD$^+$ to generate a deacetylated product (red), OAADPR, and NAM. Studies demonstrate that the mechanism of activation is a direct-assisted allosteric mechanism (Hubbard et al., 2013). Binding of substrates with hydrophobic motifs near the acetyl site (represented by X in the substrate) with SIRT1 (represented by Y in the image), induces a conformational change after interaction, leading to the alteration and creation of a specific exosite, that allows STACs to bind in a productive manner, stabilizing the docked substrate and facilitating the deacetylation. <u>Ac:</u> Acetyl group; <u>NAM:</u> Nicotinamide; <u>OAADPR:</u> O-acetyl-ADP-ribose; <u>STAC:</u> Sirtuin-activating compound.

1.3.4.1.1 Resveratrol

Resveratrol (3,5,4'-trihydroxystilbene) is the most potent polyphenol of all the natural SIRT1 activators discovered to date. In 1940, it was identified as a phenolic molecule present in the roots of white hellebore, *Veratrum grandiflorum* (Takaoka, 1940), and later from the roots of *Polygonum cuspidatum*, a plant used in alternative medicine (reviewed in Baur and Sinclair, 2006). It is present on grapes, blueberries, blackberries, peanuts, pistachios, rhubarb, and other dietary sources. Resveratrol has two geometric isomers – *cis* and *trans*. *Trans-* configurations undergoes isomerization to the *cis-* form with ultraviolet light (Rodriguez-Cabo et al., 2015). *Trans*-isomer is the most abundant and stable isomer of resveratrol (Trela and Waterhouse, 1996).

Before described as a SIRT1 activator, resveratrol and other related polyphenolic compounds had been documented to exhibit many health-enhancing effects, due to their antioxidant properties (reviewed in Baur and Sinclair, 2006). Although, initially resveratrol was characterized as a phytoalexin (Langcake and Pryce, 1977), and attracted little interest until 1992, when it was hypothesized the role of red wine on cardioprotection (Renaud and de Lorgeril, 1992). In fact, in the 90's, resveratrol and other polyphenols in the red wine were proposed as the potential reason for the "French paradox", in which the high consumption of red wine was associated with a low incidence of cardiovascular diseases, despite the fat-rich diets (Renaud and de Lorgeril, 1992; Renaud et al., 1998).

Although, some studies demonstrated that the dose of resveratrol present on red wine, considering a daily ingestion of 300 mL, is too far away from the therapeutic dose usually used (0.1 to 1500 mg per kg body weight; reviewed in Baur and Sinclair, 2006). Since then, several reports have shown the effects of resveratrol on different illnesses, including cancer (Jang et al., 1997), cardiovascular diseases (reviewed in Bradamante et al., 2004), and others (see section 1.3.5.).

Regarding resveratrol pharmacokinetics, the chemical structure of resveratrol leads to low hydro solubility, which positively affects its absorption. At an intestinal level, resveratrol is absorbed by passive diffusion or through the formation of complexes with membrane transporters, such as integrins (reviewed in Gambini et al., 2015). Once in the bloodstream, resveratrol can be metabolized, and thus the forms essentially found in bloodstream are: glucuronide, sulfate, or free. These three forms can bind to albumin and lipoproteins (reviewed in Delmas et al., 2011). In fact, resveratrol has a high metabolism leading to the rapid formation of conjugated glucuronides and sulfates, which retain some biological activity (Wang et al., 2004). Low bioavailability is a factor that may reduce the efficacy of resveratrol. Despite its low bioavailability, resveratrol shows *in vivo* efficacy, maybe due to the activity of the conjugates produced by the liver. Another potential explanation could be the enterohepatic recirculation of resveratrol metabolites, followed by its deconjugation in the small intestine and reabsorption (Walle et al., 2004). In fact, two of the first human studies on resveratrol bioavailability using a single dose of 25 mg showed that it was difficult to find non-metabolized resveratrol at circulating plasma (Goldberg et al., 2003; Walle et al., 2004).

Moreover, as described in the previous section, resveratrol and other STAC have not a clear and whole-accepted mechanism. So this arose a question: "Are the beneficial effects of resveratrol merely a result of an unforeseen interaction with other proteins?" As described before, since the middle of 30's it is known that a reduction of the caloric intake slows the rate of aging in mammals and delays the onset of some age-related diseases (McCay et al., 1935). In fact, these effects were also observed for resveratrol (see section 1.3.5). So an attractive hypothesis is that resveratrol might use the same pathways activated by CR in mammals that are more than one and both include the activation of SIRT1 pathway. Unquestionably, to prove this hypothesis we need to have a better understanding of both processes, but the results obtained until now have been corroborating this hypothesis.

1.3.4.2 NAD⁺ boosters

In 2002 it was demonstrated that the upregulation of NAD⁺-salvage pathway extends lifespan and mimics CR in yeast (Anderson et al., 2002; Anderson et al., 2003). NR is a naturally occurring precursor of NAD⁺, and as described before (section 1.3.3.1.1), enters directly on the salvage pathway after being converted into NMN, by NRK. NMN is also an intermediate of the NAD⁺ salvage pathway, resulting from the conversion of nicotinamide. CD38 and CD157 are glyco-hydrolases that degrade NAD⁺, contributing to the maintenance of NAD⁺ levels. PARPs are enzymes related with DNA repair, and they also use NAD⁺, on their enzymatic activity. Therefore, NMN, NR, PARP inhibitors, and CD38 or CD157 inhibitors, can be used as NAD⁺-boosters, indirectly activating SIRT1.

NAD⁺-boosting molecules, such as NMN, NR, PARP inhibitors, and CD38 inhibitors (e.g., apigenin, quercetin, GSK 897-78c; Escande et al., 2013; Haffner et al., 2015) increase NAD⁺ levels, and may simultaneously activate sirtuins. In recent studies, they have been administered through intraperitoneal route, oral gavage, or in drinking water, at doses from 100 up to 1000 mg/kg body weight/day (Gomes et al., 2012; Mouchiroud et al., 2013b; Escande et al., 2013; Gong et al., 2013; Haffner et al., 2015). However, it is not completely know the stability of these compounds. It also remains to be determined how safe and effective is the chronic dosing with these compounds, although initial studies seem to be promising. In fact, Gong and colleagues demonstrated that administration of NMN or NR for 180 days in AD mouse models did not produce toxicity, and in addition several beneficial effects were observed (Gong et al., 2013).

Targeting the enzymes that participate in the NAD⁺-salvage pathway (NAMPT and NMNAT) may also have some therapeutic potential. A recent study demonstrate that the activation of NAMPT equivalent in yeast (PCN1) is possible with P7C3 compound (Wang et al., 2014), and more recently it was also demonstrated some neuroprotective effects of a P7C3 derivative (Wang et al., 2016). Moreover, the use of CD38 inhibitors can have dual positive effects on NAD⁺ levels, since CD38 is a NAD⁺-consuming enzyme, but recently it was also demonstrated that it degrades NMN *in vivo*, in several tissues, including the brain (Camacho-Pereira et al., 2016).

1.3.5 Impact of sirtuin 1 on human health

Sirtuins play major roles in several features of physiology, mainly in pathways related to aging, and consequently to neurodegenerative diseases. In the next two subsections we will focus the current understanding of the role of sirtuins, particularly

SIRT1, in the longevity and in pathological processes behind neurodegenerative diseases, with special emphasis on AD, PD, HD, and ALS.

1.3.5.1 Sirtuin 1 and longevity

Studies at the end of the 90's demonstrated that the lifespan of yeast was shortened through the deletion of *Sir2*, but extended by its overexpression (Kaeberlein et al., 1999). Moreover, the increase in Sir2 orthologs, SIR-2.1 and dSIR2, also lengthened longevity or worms, and flies, respectively (Tissenbaum and Guarente, 2001; Rogina and Helfand, 2004; Wood et al., 2004). More recently, the effect of Sir2 on aging has been challenged (Burnett et al., 2011) and reaffirmed (Viswanathan and Guarente, 2011; Banerjee et al., 2012). Burnet and colleagues (2011) reported that metazoan Sir2 overexpression is not able to increase lifespan, as reported by Guarente's lab, referring also that the observed lifespan extension was the apparent result of improper controls (Burnett et al., 2011). In the same issue of the journal, Guarente's lab, published that the magnitude of the original lifespan (30-50%) was overestimated due to an unlinked "*Dyf*" mutation, but still a highly reproducible 15% in multiple lines was observed (Viswanathan and Guarente, 2011). Another independent study demonstrated in flies that fat-body specific dSir2 overexpression extends lifespan (Banerjee et al., 2012). Later, in Blackwells's lab it was demonstrated that Sir2 and PNC1 (NAMPT homolog) are required for a full calorie-induced lifespan extension (Moroz et al., 2014). It seems that the levels of sirtuins overexpression are very important, since the dSir2 overexpression levels influenced the presence (2-5 fold) or absence (<2 or >5 fold) of effects on the promotion of lifespan (Whitaker et al., 2013). Nevertheless, compelling evidence shows that sirtuins play a major role in many aspects of physiology in different species (reviewed in Baur et al., 2012; Libert and Guarente, 2013).

Moreover, the *in vivo* administration of resveratrol and other STACs, lengthened longevity in several species, as instance yeast (Howitz et al., 2003; Jarolim et al., 2004; Yang et al., 2007a; Morselli et al., 2009), *C. elegans* (Wood et al., 2004; Viswanathan and Guarente, 2011; Zarse et al., 2010), *Drosophila melanogaster* (Bauer et al., 2004; Bauer et al., 2009; Wang et al., 2013), fish (Valenzano et al., 2006), and bees (Rascon et al., 2012). In yeast, worms, and also flies, the effects were dependent on the presence of *SIR2* gene. Unlike the yeast case, experiments with transgenic overexpression or pharmacological activation of SIRT1 improved metabolic parameters later in life (Baur et al., 2006; Alcendor et al., 2007; Milne et al., 2007; Herranz et al., 2010), although they failed to significantly increase lifespan in mice (Herranz et al., 2010). Other reports have

collectively provided reliable evidence that sirtuins are able to prolong lifespan of mice. For example, whole-body transgenic mice overexpressing SIRT6 had an increased lifespan (males only; Kanfi et al., 2012). Notably, mice with brain-specific transgenic overexpression of SIRT1 (BRASTO mice) had also an extension on lifespan (Satoh et al., 2013). Moreover, the specific activation of SIRT1 with SRT1720, extended lifespan of mice even when they were fed a standard diet (Mitchell et al., 2014). These changes induced by SIRT1 can positively regulate not only lifespan, but also neurodegenerative diseases.

1.3.5.2 Sirtuin 1 and neuroprotection

SIRT1 has been linked to neuroprotective effects in a myriad of neuronal injuries and neurodegeneration paradigms (reviewed in Tang, 2009; Zhang et al., 2011; Herskovits and Guarente, 2014). More than regulation of neurite outgrowth and synaptic processes (Sugino et al., 2010; Guo et al., 2011; Li et al., 2013; Liu et al., 2013), SIRT1 was also shown to play an important role in cognitive function and synaptic plasticity (Gao et al., 2010; Michan et al., 2010), counteracting cognitive decline associated with aging and neurodegenerative diseases. In fact, several studies using genetic and pharmacological strategies to manipulate SIRT1 activity and/or expression in invertebrates and mouse models of neuronal injuries and disorders, have been reported.

Mice overexpressing SIRT1 in the brain exhibit neuroprotection mediated by SIRT1 in mouse models of some neurodegenerative diseases, as instance AD, PD, HD, and ALS (Kim et al., 2007a; Jiang et al., 2012; Jeong et al., 2012; Guo et al., 2016). Moreover, in another mouse model of neurodegeneration, namely the Wallerian degeneration slow (WldS), it was demonstrated that Wld S protein requires NMNAT activity to have its neuroprotective properties (Mack et al., 2001; Araki et al., 2004; Wang et al., 2005b; Conforti et al., 2009; Sasaki et al., 2009). Therefore, it seems that SIRT1 and NAD^+ may be neuroprotective.

In AD multiple evidences indicate that SIRT1 increase or activation is beneficial. An early *in vitro* study suggested that SIRT1 is able to attenuate NF-κB signaling in microglia, and is protective against neuronal death induced by Aβ peptides (Chen et al., 2005b). This effect is linked with CR, since CR reduces Aβ peptides generation and amyloid plaque deposition in other transgenic AD mice (Wang et al., 2005a) and also in primates (Qin et al., 2006a), and this process is SIRT1-dependent. Moreover, SIRT1 activation by resveratrol seems to protect neurons in another AD mouse model (Kim et al., 2007a). In the same study it was shown that the direct injection of SIRT1-expressing

lentivirus in CA1 hippocampal region of AD transgenic mice is also able to protect against neurodegeneration (Kim et al., 2007a). Although, another study challenged the field, reporting that the pan-sirtuin inhibitor nicotinamide is able to ameliorate cognitive defects of 3xTg-AD mice (triple transgenic for mutant presenilin-1, APP and *Tau*), through the reduction of *Tau* phosphorylation (Green et al., 2008). While later, different studies reported and highlighted the positive role of SIRT1 on the disease, demonstrating beneficial effects associated with the use of resveratrol in mouse models of AD (Porquet et al., 2013; Feng et al., 2013), suggesting a paradox in the effects of nicotinamide. NAD^+ boosters, as NMN and NR, also exhibited potential beneficial effects for AD treatment (Gong et al., 2013; Long et al., 2015a). NR supplementation led to an increase in PGC-1α and a decrease in β-secretase, which is the enzyme responsible for the generation of the toxic β-amyloid peptides (Gong et al., 2013). Therefore, it is relevant to evaluate whether NAD^+ declines in some, or all of the neurodegenerative diseases, and whether NAD^+ restauration, will be broadly beneficial.

In PD the activation and/or overexpression of SIRT1 and its homologs through genetic or pharmacological (resveratrol) approaches has been shown to be neuroprotective *in vitro*, and *in vivo*, particularly in worms and also in mouse models of PD (van Ham et al., 2008; Albani et al., 2009; Wu et al., 2011).

Moreover, in HD an early study demonstrated that resveratrol is able to protect both *C. elegans* and mouse neurons against the toxicity associated with mutant huntingtin (Parker et al., 2005). Later on, a study using a transgenic mouse model of HD demonstrated that resveratrol is able to protect against only the peripheral, but not central deficits (Ho et al., 2010). Meanwhile, genetic manipulations of SIRT1 confirmed the SIRT1's beneficial effects in HD (Jeong et al., 2012; Jiang et al., 2012). Although, the SIRT1-specific inhibitor EX-527 (or selisistat) was also linked to an alleviation of the HD pathology in *Drosophila* and mouse models (Smith et al., 2014), bringing some controversy to the field. Even though, preliminary results from a clinical trial using selisistat in HD patients revealed that circulating levels of soluble huntingtin are not affected by selisistat, supporting the idea that SIRT1 activation and not its inhibition can be beneficial for HD (Sussmuth et al., 2015). Additionally, a more recent study demonstrated that resveratrol treatment during 28 days, in a transgenic mouse model of MJD, is able to ameliorate motor impairments and to improve learning of HD mice, although, nicotinamide, a SIRT1 inhibitor, worsened motor deficits of HD mice (Naia et al., 2016). Another recent study indicated that SIRT1 activity is down-regulated in the brain of two complementary HD mouse models (Tulino et al., 2016), justifying the relevance of its increase.

Furthermore, the beneficial effect of SIRT1 increased levels or activation for models of ALS is more consistent (Kim et al., 2007a; Song et al., 2014). In cellular and different mouse models of ALS it was demonstrated that the genetic or pharmacological SIRT1 activation is able to protect motor neurons from the toxicity induced by the causative protein – SOD1, and ameliorates disease progression, increasing survival (Kim et al., 2007a; Wang et al., 2011; Mancuso et al., 2014; Song et al., 2014; Watanabe et al., 2014). Recently, it was also demonstrated, using primary cultures of astrocytes isolated from human SOD1-overexpressing mice, as well as human post-mortem ALS spinal cord-derived astrocytes, that the NAD^+ increase, through the increase of NAMPT or giving NR or NMN, reduces the toxicity associated with mutant SOD1 (Harlan et al., 2016).

As aforementioned neurodegenerative diseases have distinct clinical manifestations, due to the impairment of specific neural networks. However, neurodegenerative diseases share some key pathophysiological mechanisms, such as loss of protein homeostasis, mitochondrial dysfunction, and neuroinflammation. In these diseases occur the accumulation of protein aggregates, such as Aβ (AD), hyperphosphorylated *tau* (AD), α-synuclein (PD), huntingtin (HD), among others. In fact, SIRT1 is also able to activate autophagy due to the deacetylation of substrates that play major roles on autophagy (Lee et al., 2008; Huang et al., 2015), alleviating some diseases through this pathway (van Ham et al., 2008; Shin et al., 2013; Mancuso et al., 2014). Accumulating evidence suggest that mitochondrial dysfunction is a hallmark of neurodegenerative diseases (reviewed in Lin and Beal, 2006), and SIRT1 is able to ameliorate mitochondrial function, and consequently alleviate some neurodegenerative diseases (Jiang et al., 2012; Jeong et al., 2012; Wang et al., 2011; Long et al., 2015a; Naia et al., 2016). Many neurodegenerative disorders exhibit prolonged inflammatory responses (reviewed in Glass et al., 2010), and SIRT1 is able to regulate the inflammatory network (Yeung et al., 2004), and thus the anti-inflammatory effects of sirtuins could have broad relevance in neurodegeneration (Chen et al., 2005b; Porquet et al., 2013). Figure 1.19 summarizes the main mechanisms behind SIRT1 neuroprotection.

Unfortunately, there is currently no effective therapy to treat or retard the development of any of these neurodegenerative diseases. A broad therapy to treat several of these diseases would be crucial and the combination of sirtuin activation and NAD^+ intermediate supplementation to restore NAD^+ may be an interesting way to start down one such path.
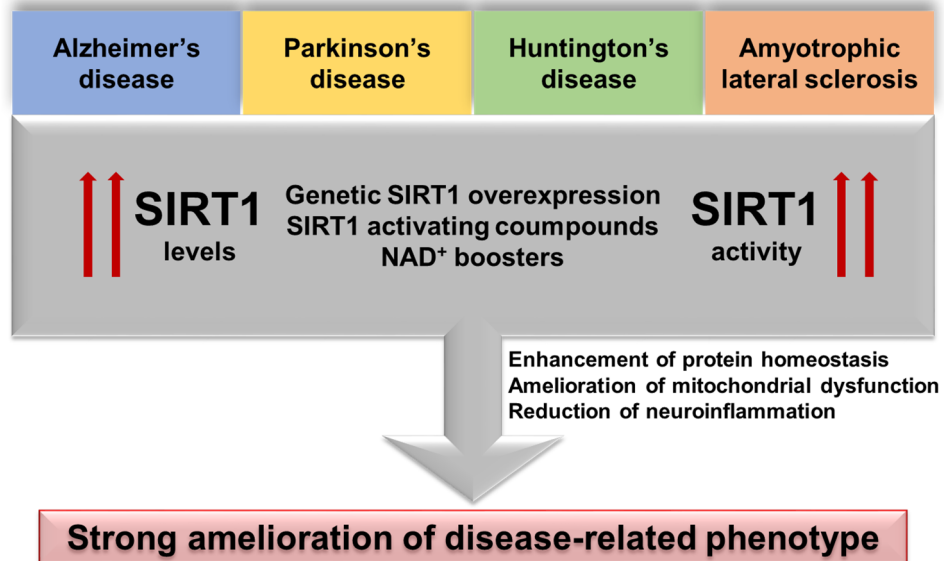
Figure 1.19 <u>New potential therapeutic approaches for neurodegenerative diseases, based on SIRT1 increase.</u> Studies demonstrate that Alzheimer's disease, Parkinson's disease, Huntington's disease, and amyotrophic lateral sclerosis are neurodegenerative diseases in which the increase in SIRT1 levels and/or activity improved their phenotype. This can occur through the genetic SIRT1 overexpression, using for example lentiviral vectors encoding for SIRT1, by the use of SIRT1 activating compounds, such as, resveratrol, or using NAD^+ boosters, as instance NR and NMN supplementation. This induces the activation of autophagy, increasing the elimination of altered protein, induces the amelioration of mitochondrial dysfunction, and reduces the neuroinflammation. All in all, SIRT1 can lead to a robust amelioration of the disease-related phenotype.

1.4 <u>Objectives</u>

The central aim of this thesis was to investigate the putative beneficial effects of CR on neurodegeneration, and particularly on a rare and incurable neurodegenerative disease - the MJD. Moreover, it was also intended to explore the underlying mechanisms, trying to develop new therapeutic strategies, in order to modify or block the disease progression.

The specific objectives behind this thesis were the following:

- To assess and characterize the neuronal changes induced by CR, in lentiviral and transgenic mouse models of MJD (Chapter 2);

- To dissect the mechanisms by which CR mediates the beneficial effects in the brain of MJD mouse models, particularly the mechanisms related with SIRT1 (Chapter 2);

- To measure the levels of SIRT1 and its cofactor NAD^+ in the cerebellum of transgenic MJD mice (Chapters 2 and 3);

- To investigate the relevance of SIRT1 increased expression or activity in the effects of CR through molecular and pharmacological approaches (Chapters 2 and 4);

- To evaluate the particular changes induced by SIRT1 in the autophagy and neuroinflammation (Chapter 2);

- To study the putative link between the mitochondrial dysfunction patent in MJD, and nuclear changes in SIRT1 and/or NAD^+ levels, unraveling the potential nuclear-mitochondrial disruption at a neuronal level, in the disease (Chapter 3);

- To clarify the mechanistic underlying the nuclear-mitochondrial dysregulation, at a molecular level (Chapter 3);

- To investigate the potential beneficial effects resulting from the pharmacological manipulation of SIRT1 and NAD^+ in transgenic MJD mice (Chapter 4).

In the end, with this thesis we aim to contribute to the development of new translational approaches to delay and/or prevent MJD progression.

CHAPTER 2

Caloric restriction ameliorates neuropathology and motor deficits in Machado-Joseph disease mouse models through the activation of SIRT1 pathway

Everything is theoretically impossible until is done.

(Robert Heinlein)

2.1 <u>Abstract</u>

Machado-Joseph disease (MJD), also known as spinocerebellar ataxia type 3 (SCA3), is a neurodegenerative disorder characterized by an abnormal expansion of the cytosine-adenine-guanine (CAG) triplet in the *ATXN3* gene, translating into a polyglutamine tract within the ataxin-3 protein. The available treatments only ameliorate symptomatology and do not block disease progression. Caloric restriction (CR) has neuroprotective properties and slows down the occurrence of age-dependent diseases. The mechanisms underlying these effects are intrinsically related to sirtuin 1 (SIRT1), a NAD^+-dependent enzyme with a deacetylase activity. The putative beneficial role of CR and SIRT1 on MJD progression was not investigated before.

In this study, we evaluated the impact of CR in the motor impairments and neuropathology of mouse models of MJD. We observed that CR dramatically rescues the motor incoordination, imbalance, and the associated neuropathology in transgenic MJD mice. We also observed that such effects are majorly mediated by SIRT1, as CR reverts abnormal decrease of SIRT1 levels in transgenic MJD mice, and these effects are blocked upon SIRT1 genetic silencing. Additionally, the increase of SIRT1 levels in a MJD mouse model, through gene delivery approach, significantly ameliorated neuropathology, reducing total number of aggregates and consequently, decreasing neuronal dysfunction. The mechanisms underlying these effects include the decrease of neuroinflammation and the activation of autophagy.

This study shows that SIRT1 activation delays disease progression, in different MJD mouse models. Therefore, a therapy based on SIRT1 activation is a promising approach to treat MJD.

2.2 <u>Introduction</u>

The polyglutamine (polyQ) diseases are a group of genetic neurodegenerative pathologies triggered by an over-repetition of the trinucleotide cytosine-adenine-guanine (CAG) within the open reading frame of different genes, and encoding long polyQ tracts in the respective proteins. The translated proteins tend to misfold and aggregate causing dysfunction and degeneration of specific neuronal subpopulations (reviewed in Todd and Lim, 2013).

Machado-Joseph disease (MJD), also known as spinocerebellar ataxia type 3 (SCA3; Haberhausen et al., 1995), is one of these polyglutamine diseases whose mutation is mapped to chromosome 14q32.1, particularly in *ATXN3* gene (Takiyama et al., 2013; Kawaguchi et al., 1994). Despite rare, it is the most common autosomal dominantly-inherited ataxia worldwide and reaches high prevalence in certain regions of Portugal, particularly in the islands of Azores (Coutinho and Andrade, 1978; Sequeiros et al., 1994). The disorder has its onset at adult age and involves neurodegeneration within cerebellar systems, *substantia nigra*, cranial nerve motor nuclei (Durr et al., 1996; Rub et al., 2008), as well as striatum (Klockgether et al., 1998), resulting in clinical hallmarks that include motor incoordination, postural instability, dysarthria, and dysphagia, among other symptoms (Maruyama et al., 1995). Neurodegeneration is associated with the accumulation of the polyglutamine-expanded ataxin-3 (stretch over 55 repeats) in the cells (Maciel et al., 1995; Ikeda et al., 1996; Paulson et al., 1997a). To this contributes the cleavage of the mutated protein in toxic fragments, mediated by calpains (Simoes et al., 2012; Hubener et al., 2013; Simoes et al., 2014), and the inefficient activation of autophagy to clear the mutant ataxin-3 (Nascimento-Ferreira et al., 2011; Nascimento-Ferreira et al., 2013; Dubinsky et al., 2014; Onofre et al., 2016). This mutant ataxin-3 can aggregate and is accumulated in the nucleus of neuronal cells, and the presence of these aggregates leads to neuronal dysfunction (Paulson et al., 1997b). There is no treatment to prevent or to slow down the progression of MJD, and only symptomatic treatments for the disease currently exist.

Caloric restriction (CR) is a dietary regimen involving consumption of fewer calories than usual but containing all the essential nutrients, without malnutrition. Since 1935, it is known that CR increases longevity in rats (McCay et al., 1935), and over the last years it has been proved that CR extends lifespan in a wide spectrum of species, including rodents (Weindruch et al., 1986). Emerging data show that this effect is conserved in nonhuman primates, although some controversy subsists (Colman et al.,

2012; Mattison et al., 2012; Colman et al., 2014). The role of CR in neuroprotection was first revealed in 1990, when Park and colleagues showed that CR attenuated the age-related loss of spinal ganglion neurons in mice (Park et al., 1990) and its application in neurodegenerative disorders, such as Alzheimer's, Parkinson's, and Huntington's diseases, has been explored from that time on (Duan et al., 2003; Maswood et al., 2004; Qin et al., 2006b). How CR exerts its beneficial effects has been the object of several hypotheses, and its knowledge may contribute to open new therapeutic strategies for neurodegenerative diseases and other age-related diseases. One of the most explored and accepted hypothesis is that CR increases the levels of regulatory proteins named sirtuins (Cohen et al., 2004).

Sir2 or silent information regulator 2 was found in yeast, and its mammalian orthologues are known as sirtuins. Sirtuins (SIRTs) are NAD^+-dependent deacetylases found to slow down aging in yeast and higher organisms, including mammals (Kaeberlein et al., 1999; Imai et al., 2000; Kanfi et al., 2012). Their activity is required for the effects of CR in many organisms (reviewed in Guarente, 2013). In mammals seven sirtuins have been identified, namely SIRT1-7. Each sirtuin has a specific cellular localization and function. SIRT1 is the most closed orthologue of Sir2, and as Sir2 is a NAD^+-dependent deacetylase that is mainly located in the nucleus (Michishita et al., 2005) and is so far the most studied member of this family. It has been reported that SIRT1 plays a neuroprotective role in Huntington's disease (Jeong et al., 2012; Jiang et al., 2012) and spinal and bulbar muscular atrophy (Montie et al., 2011), both polyglutamine diseases. Nevertheless, until now the protective role of SIRT1 in other polyglutamine diseases, namely spinocerebellar ataxias, had not been investigated.

Here, taking advantage of two different mouse models of MJD, namely the transgenic MJD mouse model and the striatal lentiviral model of MJD, we set out to study the potential beneficial effects of CR in MJD. Moreover, with lentiviral vectors encoding for SIRT1, or for a short hairpin RNA targeting SIRT1 (shRNA SIRT1), and the respective controls, we intended to investigate the role of SIRT1 in the effects of CR in the disease. In the present study we provide compelling evidence demonstrating that CR not only robustly mitigates the neuropathology, but also ameliorates motor impairments in mouse models of MJD. The knowledge of the main mechanism(s) underlying these effects is crucial to develop a new therapeutic strategy to be applied in humans. We show that CR alleviation of MJD is mediated by SIRT1, highlighting the potential benefits of increasing SIRT1 expression or activity to alleviate this and potentially other spinocerebellar ataxias.

2.3 <u>Materials and Methods</u>

2.3.1 Animals

C57Bl/6-background transgenic MJD mice and age-matched wild-type control mice were obtained from backcrossing heterozygous males with C57Bl/6 females (obtained from Charles River, Barcelona, Spain). Transgenic mice were initially acquired from Hirokazu Hirai from Kanazawa University, Japan (Torashima et al., 2008; Oue et al., 2009), and a colony of these transgenic mice was established in the Center for Neuroscience and Cell Biology of University of Coimbra. Transgenic mice express a N-terminal-truncated human ataxin-3 with 69 repeats, and a N-terminal hemagglutinin (HA) epitope specifically in cerebellar Purkinje cells, driven by a L7 promotor. Genotyping was performed by PCR analysis of DNA from ears. Five-week-old C57Bl/6 mice submitted to the stereotaxic surgery (obtained from Charles River, Barcelona, Spain) were also used. Mice were housed under conventional 12-hour light-dark cycle in a temperature-controlled room with water provided *ad libitum* and food restricted or *ad libitum*, depending on the group of study. The experiments were carried out in accordance with the European Community directive (2010/63/EU) for the care and use of laboratory animals. Researchers received adequate training (FELASA certified course) and certification to perform the experiments from Portuguese authorities (Direção Geral de Veterinária).

2.3.2 Caloric restriction diet

Mice were fed with a standard AIN-93G diet. In CR studies, young caloric-restricted mice were fed with an amount of food equal to 90% of that consumed by mice in *ad libitum*-fed corresponding group in the first period (10% of CR), 80% in the second period (20% of CR), and 70% from third period until end of the study (30% of CR), without malnutrition. During the different dietary regimens body weight was daily measured.

2.3.3 Viral vectors production

Lentiviral vectors encoding for i) mutant ataxin 3 (LV-PGK-Atx3 72Q) (Alves et al., 2008b); ii) sirtuin 1 (LV-PGK-SIRT1); iii) a SIRT1 that does not have deacetylase activity – H363Y (LV-PGK-H363Y); iv) a negative short hairpin RNA (LV-PGK-EGFP-H1-shRNA CNTL); and v) a short hairpin RNA targeting SIRT1 (LV-PGK-EGFP-H1-shRNA SIRT1) were produced in HEK293T cell line with a four-plasmid system, as previously

described (de Almeida et al., 2001). Lentiviral particles were suspended in sterile 1% bovine serum albumin (BSA) in phosphate buffered solution (PBS). The viral particle content of batches was evaluated by assessing HIV-1 p24 antigen levels by ELISA (Retro Tek, Gentaur, Paris, France). Concentrated viral stocks were stored at -80ºC, until use.

2.3.4 *In vivo* injection into striatum

Mice were anesthetized with avertin (250 mg/kg body weight, intraperitoneally). Concentrated viral stocks were thawed on ice, and diluted viral suspensions were prepared. We stereotaxically co-injected in striatum, 400 ng of p24 antigen of each lentiviral vector, encoding for mutant ataxin-3 (Atx3 72Q) and H363Y (left hemisphere), or Atx3 72Q and SIRT1 (right hemisphere) in one experiment, and Atx3 72Q and a negative shRNA (left hemisphere) or Atx3 72Q and a shRNA targeting SIRT1 (right hemisphere), in the other experiment, in a final total volume of 2.5 µL. The coordinates that we used were: anteroposterior: +0.6 mm; lateral: ±1.8 mm; ventral: -3.3 mm; tooth bar: 0. These coordinates correspond to the internal capsule, a large fiber passing through the middle of the striatum dividing both dorsoventral and mediolateral structures. After the surgery mice were maintained in their home cages and were sacrificed four or six weeks later for immunohistochemical analysis, and morphological and neurochemical changes in the striatum.

2.3.5 Behavioral testing

Six-week-old mice were submitted to a battery of motor tests, starting two days before the beginning of the study (t=0), and every three weeks until the ninth week. Although, open-field was only performed in the beginning and in the last time-point. All tests were performed in a dark room with, at least, 60 minutes of acclimatization to the experimental room. The same phenotyping tests were conducted at the same time of the day, particularly in the first half of the day (during the morning, until early afternoon).

2.3.5.1 Stationary and accelerated rotarod tests: Rotarod tests allowed the assessment of the motor coordinative abilities and balance of mice between the different groups (Nobrega et al., 2013b). Rotarod apparatus (Letica Scientific Instruments, model LE 8200, Panlab, Barcelona, Spain) was used. In accelerated rotarod, mice were placed at accelerating speed (from 4 r.p.m. and accelerating to 40 r.p.m. over a period of 5

minutes). On stationary rotarod, mice were placed on the rotarod at a constant velocity (5 r.p.m. for a maximum of 5 minutes). The time during which mice remained running in the rotation roll was recorded. For each test and time point, each animal performed two sets of two trials with a 20-minute inter-trial interval. For statistical analysis we used the mean latency to fall off the rotarod of 3-4 trials.

2.3.5.2 Vertical pole test: The vertical pole test was used to assess motor coordination and balance of mice (Matsuura et al., 1997). Each mouse was positioned head-upward on the top of a round rough-surfaced pole (with 52 cm of height and 1 cm of diameter). The vertical pole was initially positioned horizontally, and then slowly inclined to 90º. The time to orient downward (t-turn) and the time to reach the floor (t-descend) was recorded, and the accepted maximum observation time was 2 min. Five consecutive trials were performed with an inter-trial interval of 60 seconds. The best 3 scores for each parameter were statistically analyzed.

2.3.5.3 Swimming test: Mice were placed in the border of a rectangular aquarium (length: 70 cm; height: 20 cm; width: 15 cm) with a safe platform 9 cm upper the floor (length: 7cm; width: 6 cm) in the opposite side. The aquarium was filled up to the area of the platform with water at 24-26ºC. The time that mice took to reach the platform was recorded. We performed four trials with an inter-trial interval of 60 seconds. The first trial was considered an exploratory trial and the results were expressed as the average of the other 3 trials.

2.3.5.4 Beam walking test: In order to evaluate motor coordination and balance of mice, the ability of mice to cross a graded series of narrow beams to reach an enclosed escape platform was evaluated, as previously described (Nobrega et al., 2013b). Briefly, this test was performed in four long wood beams (1 m): two square beams with an 18 or 9 mm square wide, and two round beams with 9 and 6 mm diameter. Tests were performed sequentially from the widest to the narrowest beam. Therefore, the first beam was the 18 mm square beam, followed by the 9 mm square beam, and the 9 mm round beam, ending with the 6 mm round beam. Each beam was placed horizontally, 25 cm above the bench surface, with one end attached on a narrow support, and the other end fixed to a bounded box (20 cm square) into which the mouse could escape. Mice were allowed up to 60 seconds to transverse each beam, and the time was recorded. As mice became progressively impaired, they gripped tightly onto the beam to prevent the

consequent fall. Any animal that did not cross in 60 seconds was assigned the maximum value of 60 seconds for analysis. We repeated twice each trial, with no inter-trial interval in the same beam, and statistical analysis was performed with average values. We let 60 minutes of inter-trial interval between each beam.

2.3.5.5 Footprint pattern: Different parameters of gait can be simply and effectively evaluated tracking the walk (Nobrega et al., 2013b). This test was used to evaluate the effect of CR in mice gait. To obtain footprints, mice feet were coated with black and white non-toxic paints, respectively in the hind and forefeet. Then, animals walked along 100 cm long, in a 10 cm wide runaway fresh sheet of green paper, in an apparatus with 15 cm high walls. A fresh sheet of green paper was replaced on the floor for each new mouse. In order to analyze footprint patterns, some parameters were explored (all measured in centimeters). Stride length, the average distance of forward movement between each stride, was measured. This parameter was determined by the measurement of the perpendicular distance of a given step to a line connecting its opposite preceding and proceeding steps. The average of three strides was obtained. To explore uniformity of step alternation the distance from left or right front footprint/hind footprint overlap was measured. A perfect overlap, recorded as zero, was considered when the center of the hind footprint fell on the top of the center of the preceding front footprint. When the footprint did not overlap, the distance between the centers of footprints was verified. A sequence of four consecutive steps was chosen for evaluation, excluding footprints made at the beginning and the end of the run, where the animal was initiating or finishing the movement, respectively. The same operator made all footprints measurements blindly.

2.3.5.6 Open-field test: Open-field test was used to explore locomotor horizontal activity, and anxiety-like behaviors of mice (Nobrega et al., 2013b). Mice were placed in the center of a 50x50 cm arena with 50 cm high walls, and movement activity was recorded for 40 min with Acti-Track System (PanLab, Barcelona, Spain). In order to reduce any type of novelty it was guaranteed that cage changes were performed, at least, 24 hours prior to test. Arena was cleaned with 10% ethanol before the first mouse and between each animal. All the experiments were performed by the same operator and during the experiment the operator was outside of the experimental room. Total distance travelled in the experimental time, mean velocity of mice, and time and distance travelled in the center of arena was recorded.

2.3.6 Histological processing

2.3.6.1 Tissue preparation: Mice were sacrificed with an overdose of avertin (625 mg/kg body weight, intraperitoneally). Transcardial perfusion with PBS and fixation with 4% paraformaldehyde was performed. Brains were collected and post-fixed in 4% paraformaldehyde for 24 hours, and cryoprotected by incubation in 25% sucrose/phosphate buffer for 36/48 hours. After that, dry brains were frozen at -80ºC and 25-μm coronal sections from stereotaxically injected mice or 35-μm sagittal sections from transgenic MJD and corresponding wild-type littermate mice, were sliced using a cryostat (LEICA CM3050S, Leica Microsystems) at -21ºC. Slices were collected in anatomical series, and stored in 48-well trays as free-floating sections in PBS supplemented with 0.05% (m/v) sodium azide. The trays were stored at 4º C until immunohistochemical, and other procedures.

2.3.6.2 Immunohistochemical processing: After the blockage of endogenous peroxidases with phenylhidrazyne/phosphate solution and incubation in blocking solution, composed by PBS/0.1% Triton X-100 with 10% normal goat serum (Gibco), free-floating sections were overnight incubated at 4ºC in blocking solution with primary antibodies: mouse monoclonal anti-ataxin 3 antibody (1H9; 1:5000; #5360 Merck Millipore), rabbit anti-dopamine and cyclic AMP-regulated neuronal phosphoprotein 32 (DARPP-32) antibody (1:1000; AB#10518 Merck Millipore); followed by incubation with respective biotinylated secondary goat anti-mouse or anti-rabbit antibodies (1:200; Vector Laboratoires). Bound antibodies were visualized using the VECTASTAIN® ABC kit, with 3',3'-diaminobenzidine tetrahydrocloride (DAB metal concentrate; Pierce) as substrate. Dry sections were mounted in gelatin-coated slides, dehydrated with ethanol solutions and xylene, and mounted in Eukit (Sigma-Aldrich).

In immunofluorescence staining, free-floating sections were incubated in PBS/0,1% Triton X-100 containing 10% normal goat serum (Gibco), and then incubated overnight at 4ºC in blocking solution with primary antibodies: mouse polyclonal anti-glial fibrillary acidic protein (GFAP) antibody (1:1000; Z0334 Dako, Glostrup, Denmark); rabbit anti-ionized calcium binding adaptor molecule 1 (Iba-1) antibody (1:1000; #019-19741 Wako Chemicals USA); rabbit anti-sirtuin 1 antibody (1:250; #2028 Cell Signaling Technology); mouse monoclonal anti-HA antibody (1:1000; ab-hatag InvivoGen, San Diego, CA, USA). Sections were washed and incubated for 2 h at room temperature with the corresponding secondary antibodies coupled to fluorophores: goat anti-mouse, goat anti-rabbit Alexa Fluor 488 or Alexa Fluor 594 (1:200, Molecular Probes-Invitrogen,

Eugene, OR), diluted in the respective blocking solution. The sections were washed and incubated during 10 min with 4',6'-diamidino-2-phenylindole (DAPI; Sigma; St. Louis; MO), washed, and mounted in mowiol on microscope slides.

In sections from injected mice definition and analysis of protein immunoreactivities were made as previously described (Goncalves et al., 2013).

Staining was visualized with Zeiss Axioskop 2 plus or Zeiss Axiovert 200 imaging microscopes (Carl Zeiss MicroImaging, Oberkochen, Germany) equipped with AxioCam HR color digital cameras (Carl Zeiss Microimaging) and 35, 320, 340, and 363 Plan-Neofluor or 363 Plan/Apochromat objectives using the AxioVision 4.7 software package (Carl Zeiss Microimaging). Quantitative analysis of fluorescence was performed with a semiautomated image-analysis software package, and images were taken under identical image acquisition conditions, and uniform adjustments of brightness and contrast were made to all images (ImageJ, NIH, USA).

2.3.6.3 Cresyl violet staining: Dry pre-mounted sections were stained with the basic dye cresyl violet solution for 3 minutes, differentiated in 70% ethanol, dehydrated twice by passing through 95% ethanol, 100% ethanol solutions and xylene solution, before mounting onto microscope slides with Eukit (Sigma).

2.3.7 Analysis of the volume of DARPP-32 depletion region

Mutant ataxin-3 induces striatal neurons dysfunction characterized by a decrease in DARPP-32 staining, as previously described (Alves et al., 2008b). The extent of striatal mutant ataxin-3 lesions was evaluated by photographing, with a x5 objective, 12 sections stained with DARPP-32 per animal (25 μm-thick sections at 200 μm intervals), selected so as to obtain rostrocaudal sampling of the striatum. The area of the lesion was quantified with a semi-automated image-analysis software package (ImageJ, NIH, USA). The area of the striatum showing a loss of DARPP-32 staining was measured for each animal, with an operator-independent macro. The volume was then estimated with the following formula: volume = $d(a_1+a_2+\ldots+a_{11}+a_{12})$, where d is the distance between serial sections (200 μm) and a_{1-12} are DARPP-32 depleted areas for individual serial sections, as previously described (de Almeida et al., 2002). The depleted area corresponds to the area with a gray-scale value lower than the mean gray-scale value of all pixels measured around the lesioned area.

2.3.8 Cell counts of ataxin-3 inclusions

Coronal sections showing entire striatum (12 sections per animal) were scanned with x20 objective. The analyzed areas of the striatum encompassed the entire region containing ataxin-3 inclusions, as revealed by staining with an anti-ataxin-3 antibody. The number of striatal inclusions was estimated by the formula: total number = $s(n_1+n_2+n_3+\ldots+n_{12})$, where s represents the number of intermediate sections (8), and $n_{1\text{-}12}$ represents the number of aggregates present in each section. All inclusions were blindly manually counted using a semiautomated image analysis software package (Image J, NIH, USA).

2.3.9 Pyknotic nuclei counting

After a cresyl violet staining, the number of pyknotic nuclei in the area under the needle tract was evaluated. Specific eight regions under the needle tract of each injection were photographed, with x40 objective. The total number of the pyknotic nuclei in this area was blindly counted for each animal and each hemisphere using a semiautomated image analysis software (Image J, NIH, USA).

2.3.10 Quantitative analysis of HA aggregates

Quantification of hemagglutinin-tagged ataxin-3 positive inclusions was performed after an anti-HA immunohistochemistry, and imaging of 8 sagittal sections with 35 µm-thick spread over the lateral extent of cerebellum of each animal, using a x20 objective on a Zeiss Axioskop 2 plus imaging microscope. The number of HA inclusions in Purkinje cells was blindly counted. The number of inclusions in Purkinje cells in the cerebellum was estimated by the formula: total number = $2s(n_1+n_2+n_3+\ldots+n_8)$, where s represents the number of intermediate sections (8), $n_{1\text{-}8}$ represents the number of aggregates present in each section and this was multiplied by 2 to estimate the total number in two hemispheres.

2.3.11 Quantification of granular and molecular layers size and cerebellar volume

Quantification was made over 8 cresyl violet stained sagittal sections with 35 µm-thick spread over lateral extent of cerebellum in a blind fashion. For each section, cerebellar cortex of lobule V and lobule IX was digitalized in x20 objective. For each

acquired field, four measurements were blindly made in the same region for all animals. Results were converted to µm using Image J software (NIH, USA). The results are shown as the average of the thickness of each layer in lobule V and IX together. For cerebellar volume evaluation, x5 objective images of each section were obtained, and area of cerebellum was blindly evaluated, using Image J software (NIH, USA). Cerebellar volume was estimated using the following formula: $2d(a_1+a_2+...+a_8)$, where d represents the distance between two followed sections (280 µm), a_{1-8} represents the calculated area of each section, and this was multiplied by two to estimate the volume of the whole cerebellum.

2.3.12 Immunoblot Procedure

2.3.12.1 Tissue preparation: Mice were sacrificed by a lethal dose of avertin (625 mg/kg body weight) and cervical dislocation. Cerebellum or striatal dissection was performed and tissues were incubated in a radioimmunoprecipitation assay-buffer solution (RIPA; 50 mM Tris-HCl pH=8; 150 nM NaCl; 1% NP-40; 0.5% sodium deoxycholate; 0.1% sodium dodecyl sulphate - SDS) containing protease inhibitors (Roche Diagnostics GmbH), and supplemented with 1 mM phenylmethylsulphonyl fluoride, 10 µg/mL dithiothreitol, 5 µM sodium fluoride, 1 µg/mL sodium orto-vanadate, and 1 mM nicotinamide. Tissue lysates were prepared by 2 series of 4 seconds ultra-sound pulse (1 pulse/sec). *In vitro* samples were obtained scrapping cells with supplemented RIPA solution (described before) and collecting cellular lysates. Total protein lysates were stored at -80ºC and protein concentration was determined with BCA protein assay (Pierce Biotechnology, Thermo Fisher Scientific).

2.3.12.2 Western blot procedure: Samples were previously denatured with 2x sample buffer (10% β-mercaptoethanol, 4% SDS, 0.25 M Tris-HCl, 8 M urea) and incubated during 5 min at 95ºC. Equal amounts of protein (50 µg or 25 µg) were resolved on 12% SDS-PAGE and transferred onto polyvinylidene fluoride (PVDF) membranes (GE Healthcare), according to standard protocols. Membranes were blocked by incubation in 5% non-fat milk powder in 0.1% Tween 20 in Tris buffered saline (TBS-T), and incubated overnight at 4ºC with primary antibody: mouse monoclonal anti-ataxin-3 antibody (1H9; 1:3000; #5360 Merck Millipore); rabbit anti-sirtuin 1 antibody (1:1500; #2028 Cell Signaling Technology); rabbit monoclonal anti-p62 antibody (1:1000; #5117 Cell Signaling Technology); rabbit monoclonal anti-LC3B antibody (1:1000; #2775 Cell Signaling Technology); mouse anti-polyclonal glial fibrillary acidic protein (GFAP)

antibody (1:1000; #3670 Cell Signaling Technology); mouse anti-β-actin antibody (clone AC74; 1:5000; A5316 Sigma-Aldrich); mouse anti-HA antibody (1:1500; ab-hatag InvivoGen, San Diego, CA, USA); rabbit anti-AcFOXO1 antibody (1:1000; sc-49437 Santa Cruz Biotech); mouse anti-β-tubulin antibody (1:10.000; T7816 Sigma-Aldrich), followed by the incubation with the corresponding alkaline phosphatase-linked secondary goat anti-mouse or anti-rabbit antibody (Thermo Fisher Scientific). Bands were visualized with enhanced chemifluorescence substrate (ECF, GE Healthcare) and chemifluorescence imaging (VersaDoc Imaging System Model 3000, Bio-Rad). Semi-quantitative analysis was carried out based on the optical density of scanned membranes (Quantity One; 1-D image analysis software version 4.6.6; Bio-Rad). The specific optical density was then normalized with respect to the amount of β-actin or β -tubulin loaded in the corresponding lane of the same gel.

2.3.13 Quantitative Real-Time Polymerase Chain Reaction (qRT-PCR)

2.3.13.1 Isolation of total RNA from mice tissues and cDNA synthesis: Animals were sacrificed with a lethal dose of avertin (625 mg/Kg body weight) and cervical dislocation. Cerebellum or striatum of mice were dissected and stored in tubes containing RNA*later* RNA stabilization reagent (QIAGEN), and were kept at -80ºC until RNA isolation. Total RNA was isolated with NucleoSpin RNA isolation kit (Machery-Nagel) according to manufacturer's instructions and was preceded by homogenization of the tissue with Qiazol reagent (Qiagen) and d-clorophorm. Total amount of RNA was quantified by optical density (OD) using a Nanodrop 2000 Spectrophotometer (Thermo Fisher Scientific), and RNA was stored at -80ºC. cDNA was then obtained by conversion of total RNA with iScript Selected cDNA Synthesis kit (Bio-Rad) according to manufacturer's instructions, and stored at -20ºC.

2.3.13.2 qRT-PCR procedure: qRT-PCR was performed in the StepOne Plus Real-Time PCR System (Applied Biosystems) using 96-well microliter plates and the SsoAdvanced SYBR Green Supermix (Bio-Rad). PCR was carried out in 10 μL reaction volume. Primers for mouse SIRT1, IL-6, IL-1β, TNF-α, IL-10, and GADPH were pre-designed and validated by QIAGEN (QuantiTect Primers, QIAGEN). Primers for human SIRT1 and human GADPH were designed using PrimerBlast Software, and oligonucleotide sequences are in Table 2.1. We also prepared the adequate negative controls. All reactions were performed in duplicate and according to the manufacturer's recommendations: 95ºC for 30 seconds, followed by 45 cycles at 95ºC for 5 seconds,

and 60ºC for 30 seconds. The amplification rate for each target was evaluated from the cycle threshold (Ct) numbers obtained with cDNA dilutions, with correction for GADPH levels. The mRNA fold increase or fold decrease with respect to control samples was determined by the Pfäffl method.

Table 2.1. Oligonucleotides sequences

Gene		Sequence
hSIRT1	F	5' TGCTCGCCTTGCTGTAGACTTC 3'
	R	5' GGCTATGAATTTGTGACAGAGAGATGG 3'
hGAPDH	F	5' TGTTCGACAGTCAGCCGCATCTTC 3'
	R	5' CAGAGTTAAAAGCAGCCCTGGTGAC 3'

2.3.14 Engineering of short hairpin RNA

A negative shRNA (control) and shRNA targeting mouse sirtuin 1 and mouse autophagy-related protein 5 (Atg5) were created. For each one, a pair of oligomers was designed. The sequences of each pair of oligomers used are below, in Table 2.2. Each pair of oligomers were annealed and inserted in linearized (with BglII and HindIII restriction enzymes) pENTR/pSUPER⁺ plasmid (AddGene 575-1). The H1-shRNA cassette was then transferred, with LR clonase recombination system, into SIN-cPPT-PGK-EGFP-WHV-LTR gateway vector.

Table 2.2. Oligonucleotides sequences

Gene		Sequence
shRNA CNTL	Top	5' GATCCCCCAACAAGATAAGAGCACCAATTCAAGAGATTGG TGCTCTTCATCTTGTTG3TTTTTA 3'
	Bot	5' AGCTTAAAAACAACAAGATGAAGAGCACCAATCTCTTGAA TTGGTGCTCTTCATCTTGTTGGGG 3'
shRNA SIRT1	Top	5' GATCCCCGCCATGTTTGATATTGAGTATTTCAAGAGAATA CTCAATATCAAACATGGC3TTTTTA 3'
	Bot	5' AGCTTAAAAAGCCATGTTTGATATTGAGTATTCTCTTGAAA TACTCAATATCAAACATGGCGGG 3'
shRNA Atg5	Top	5' GATCCCCAGCCGAAGCCTTTGCTCAATGTTCAAGAGACAT TGAGCAAAGGCTTCGGCTTTTTTA 3'
	Bot	5' AGCTTAAAAAAGCCGAAGCCTTTGCTCAATGTCTCTTGAA CATTGAGCAAAGGCTTCGGCTGGG 3'

2.3.15 Neuroblastoma cell culture

Mouse neuroblastoma cell line (Neuro-2a cells) was obtained from the American Type Culture Collection cell biology bank (ATCC, CCL-131). This cell line was incubated in Dulbecco's modified Eagle's medium supplemented with 10% foetal bovine serum, 100 U/mL penicillin, and 100 mg/mL streptomycin (Gibco) (complete medium) at 37ºC in 5% CO_2/air atmosphere. Cells were plated in a six-well plate and 24 hours later were co-infected with lentiviral vectors encoding for mutant ataxin-3 (LV-PGK-Atx3 72Q), and for H363Y (LV-PGK-H363Y) or lentiviral vectors encoding for mutant ataxin-3 (LV-PGK-Atx3 72Q), and for SIRT1 (LV-PGK-SIRT1) at the ratio of 50 ng of p24 antigen/10^5 cells of each vector. At 2 weeks post-infection, cells were incubated or not with 100 µM of chloroquine during three hours, and then were lysed for western blot processing.

2.3.16 Human fibroblasts culture

Human fibroblast cells were obtained from Coriell cell repositories and skin biopsy of six individuals, namely three healthy and three diseased individuals with different gender and age (controls: 44 years, female, not affected; 47 years, male, not affected; 52 years, female, not affected; Machado-Joseph disease: 31 years, female, 79 CAG; 22 years, male, 80 CAG; 69 years, male, 70 CAG). Cells were maintained in culture in Dulbecco's modified Eagle's medium supplemented with 10% foetal bovine serum, 1% nonessential amino acids, 2 mM L-glutamine, 100 U/mL penicillin and 100 mg/mL streptomycin (Gibco) at 37ºC in 5% CO_2/air atmosphere.

2.3.17 Statistical analysis

Statistical analysis was performed with paired or unpaired Student's t-test and one-way or two-way Analysis of Variance (ANOVA) followed by the adequate post-hoc test, for multiple comparisons. Results are expressed as mean±standard error of the mean (SEM). Significant thresholds were set at $p<0.05$, $p<0.01$ and $p<0.001$, as defined in the text.

2.4 Results

2.4.1 A progressive caloric restriction regimen does not change mice body weight but reduces adipose tissue accumulation in young mice

It is well known that the reduction of caloric intake interferes with body weight (McCay et al., 1935). In this study, young mice (6-week-old mice) were submitted to a CR diet during nine weeks (Figure 2.1A) and one of our initial objectives was to evaluate the effects of CR on their body weight. Nine weeks after the beginning of CR regimen, we observed that: i) AL transgenic MJD mice exhibited a lower body weight, in comparison with age-matched AL wild-type mice (Figure 2.1B; Tg MJD-AL: 21.95±0.34 g *vs* WT-AL: 25.33±0.69 g; p<0.01); ii) caloric-restricted mice, diseased or non-diseased, had a significantly lower body weight in comparison with animals in the same condition and with the same age (Figure 2.1B; WT-CR: 17.38±0.38 g *vs* WT-AL: 25.33±0.69 g; p<0.001 and Tg MJD-CR: 16.00±0.21 g *vs* Tg MJD-AL: 21.95±0.34 g; p<0.001); iii) diseased and non-diseased mice in the CR diet did not exhibit differences in body weight (Figure 2.1B; WT-CR: 17.38±0.38 g *vs* Tg MJD-CR: 16.00±0.21 g; p>0.05). These results are in accordance with the changes observed in epididymal adipose tissue, where we also observed the same changes (Figure 2.1C). Although, in Figure 2.1D, where we have represented the percentage body weight changes relative to the initial body weight of mice, we clearly observe that these differences are not achieved by a weight loss of caloric-restricted mice, but by a maintenance of their body weight to the values observed in the beginning of the study.
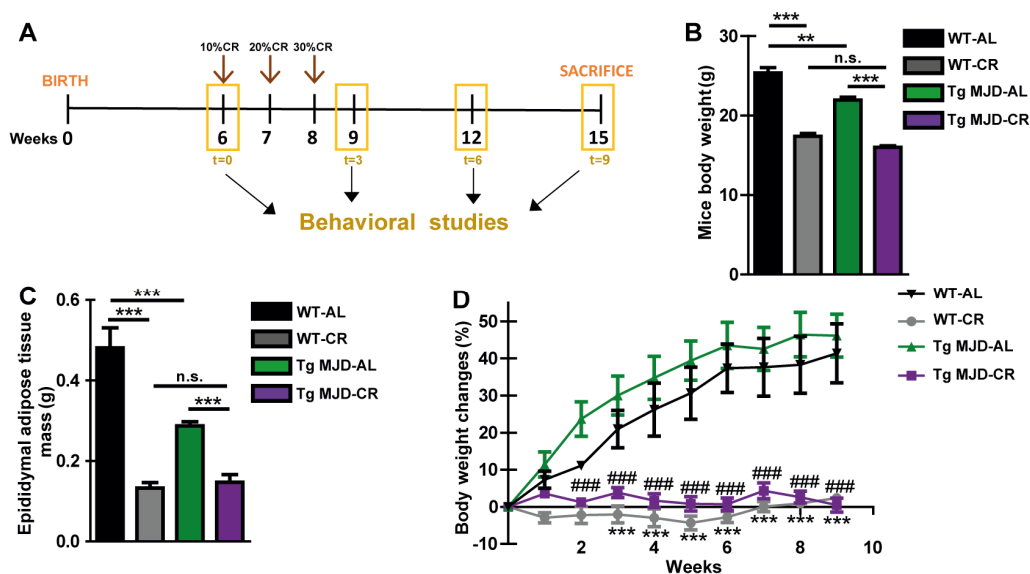
Figure 2.1 Caloric restriction maintains mice body weight, but reduces epididymal adipose tissue mass. **(A)** Representative study design. 6-week-old transgenic MJD and

Figure 2.1 (cont.) wild-type littermate mice were divided in two groups: *ad libitum* group and caloric-restricted group. Every three weeks behavioral tests were performed, until animals achieved 15-week-old. Body weight and food intake were daily measured. **(B)** Average body weight of 15-week-old mice, nine weeks after the beginning of caloric restriction regimen. **(C)** Epididymal adipose tissue mass of 15-week-old wild-type and transgenic MJD mice, in AL or CR diets. **(D)** Weekly body weight change (%) normalized with the initial body weight of mice. Mice were daily weighed and weekly body weight average was calculated. <u>WT-AL:</u> Wild Type *Ad Libitum*; <u>WT-CR:</u> Wild-Type Caloric Restriction; <u>Tg MJD-AL:</u> Transgenic MJD *Ad Libitum*; <u>Tg MJD-CR:</u> Transgenic MJD Caloric Restriction. Data represent mean ± SEM. n.s. $p > 0.05$; **$p < 0.01$; ***/### $p < 0.001$. **(B-C)** One-way Analysis of Variance (ANOVA) with Bonferroni's post-hoc test. **(D)** Two-way ANOVA with Bonferroni's post hoc test. WT-CR relative to WT-AL (#); Tg-CR relative to Tg-AL (*). WT-AL n=5; WT-CR n=7; Tg MJD-AL n=6; Tg MJD-CR n=7.

Overall, these results demonstrate that CR do not reduce body weight of mice. They also show that the differences in the body weight between wild-type mice and MJD transgenic mice were lost when mice from each group were submitted to the CR diet.

2.4.2 Caloric restriction drastically alleviates motor deficits of transgenic Machado-Joseph disease mice

Previously, it was shown that the transgenic MJD mouse model used in this study exhibits a marked cerebellar atrophy and a severe loss of motor coordination and balance, since at least the third week of age (Torashima et al., 2008; Nobrega et al., 2013b; Nascimento-Ferreira et al., 2013; Simoes et al., 2014; Mendonca et al., 2015; Duarte-Neves et al., 2015; Conceicao et al., 2016). In the present study the motor coordination and balance of transgenic MJD mice maintained in an AL diet or with CR diet were evaluated by beam walking test, stationary and accelerated rotarod tests, pole test, and swimming test. We started the CR regimen in 6-week-old mice, thus in a post-symptomatic stage of the disease. In order to follow the effects of CR during the progressive stages of the disease, behavioral outcomes were measured every three weeks until the end of the study (Figure 2.1A).

Six weeks after the beginning of CR diet, transgenic MJD mice showed a clear improvement in motor coordination and balance, evaluated by beam walking test, which reached significance for the 6 and 9 mm round and square beams, at this time point. At nine weeks' time-point, 15-week-old caloric-restricted transgenic MJD mice showed a robust improvement of motor coordination and balance in all beams, compared to AL mice (Figure 2.2A-D).
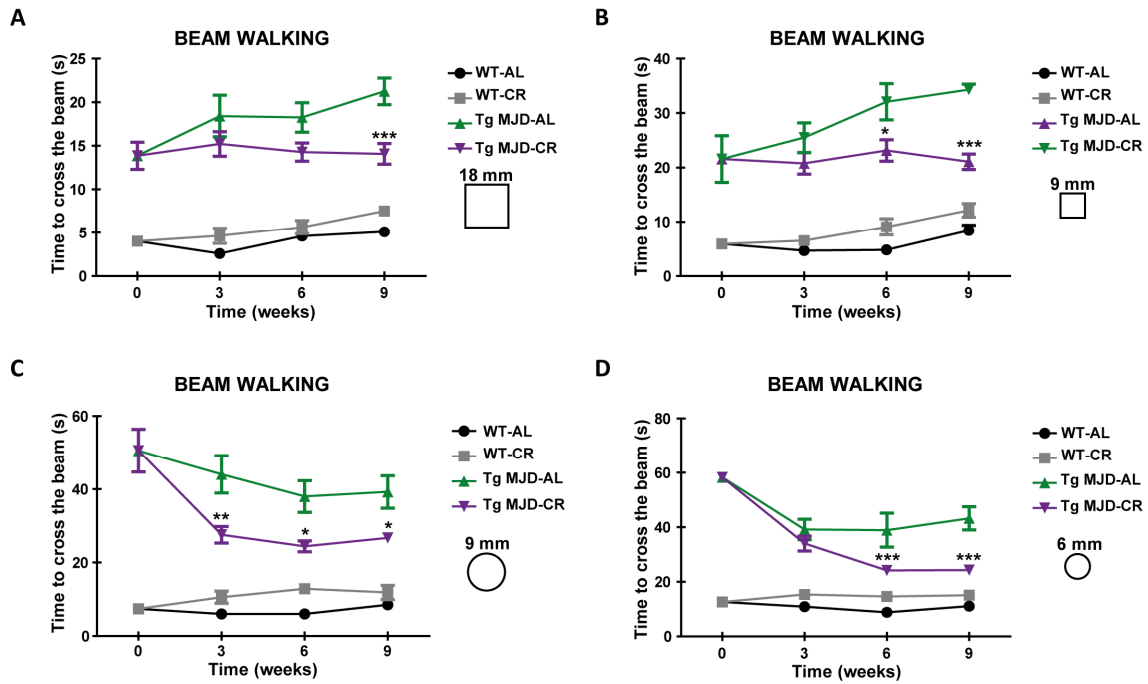
Figure 2.2 <u>Caloric restriction alleviates MJD motor incoordination.</u> **(A-D)** Beam walking test performance in four different beams, with different diameter and shape (square beam with 18 mm side, square beam 9 mm side, round beam 9 mm diameter, and round beam 6 mm diameter), during the experimental time course. <u>WT-AL:</u> Wild Type *Ad Libitum*; <u>WT-CR:</u> Wild-Type Caloric Restriction; <u>Tg MJD-AL:</u> Transgenic MJD *Ad Libitum*; <u>Tg MJD-CR:</u> Transgenic MJD Caloric Restriction. Data represent mean ± SEM. *$p<0.05$; **$p<0.01$; ***$p<0.001$ compared to Tg MJD-AL. **(A-D)** Two-way Analysis of Variance (ANOVA) with Bonferroni's post-hoc test. WT-AL n=5; WT-CR n=7; Tg MJD-AL n=6; Tg MJD-CR n=7.

To further assess motor coordination and balance, stationary and accelerated rotarod tests were performed. In stationary rotarod, transgenic MJD mice maintained in the AL diet quickly fell off the stationary rotarod, while caloric-restricted transgenic MJD mice exhibited an impressive improvement of performance (4.5 times) from the sixth week on (Figure 2.3A; t=6 weeks; Tg MJD-AL: 33.7±7.0 s *vs* Tg MJD-CR: 132.7±29.9 s; p<0.001). Similar results were obtained with the accelerated rotarod (Figure 2.3B; t=6 weeks; Tg MJD-AL: 25.3±3.0 s *vs* Tg MJD-CR: 51.4±4.2 s; p<0.05), which persisted along the experimental time course in both protocols.

This improvement in motor coordination and balance was additionally investigated with pole test. Transgenic MJD mice in the control group showed a markedly prolonged t-turn, compared with the caloric-restricted group, from the sixth week on (Figure 2.3C; t=6 weeks; Tg MJD-AL: 28.7±9.4 s *vs* Tg MJD-CR: 10.0±2.4 s; p<0.01). Moreover, caloric-restricted transgenic mice descended the vertical beam faster than mice in the AL diet, and this difference was statistically different since the third week (Figure 2.3D; t=3 weeks; Tg MJD-AL: 20.6±1.4 s *vs* Tg MJD-CR: 15.0±1.5 s; p<0.01),

and was maintained along the experimental time.

Using the swimming test, we observed that caloric-restricted transgenic MJD mice, since the third week after the beginning of the study, spent less time and had less difficulties to reach the safe platform, in comparison to the control group (Figure 2.3E; t=3 weeks; Tg MJD-AL: 30.3±1.3 s *vs* Tg MJD-CR: 18.7±2.4 s; p<0.01). Importantly, at six and nine weeks after the beginning of the study, performance of caloric-restricted transgenic MJD mice did not differ from the performance of wild type mice, suggesting that a complete rescue of the phenotype occurred (Figure 2.3E; t=6 weeks; Tg MJD-CR: 10.8±1.1 s vs [WT-CR: 6.3±0.8 s OR *vs* WT-AL: 6.3±0.9 s]; p>0.05).

Furthermore, gait was studied by the analysis of footprint patterns. Nine weeks after the beginning of the CR diet, transgenic mice in the CR diet showed a rescue of the affected footprint overlap (Figure 2.3F; t=9 weeks; Tg MJD-AL: 1.12±0.05 cm *vs* Tg MJD-CR: 0.57±0.06 cm; p<0.001; WT-AL: 0.39±0.028 cm *vs* Tg MJD-CR: 0.57±0.06 cm; p>0.05). A similar outcome was registered upon the analysis of stride length. Caloric-restricted transgenic MJD mice showed a consistently longer stride length in comparison with the control group (Figure 2.3G; Tg MJD-AL: 5.6±0.15 cm *vs* Tg MJD-CR: 6.09±0.14 cm; p<0.05). These results indicate a significant improvement in the affected gait of transgenic MJD mice with a CR diet.
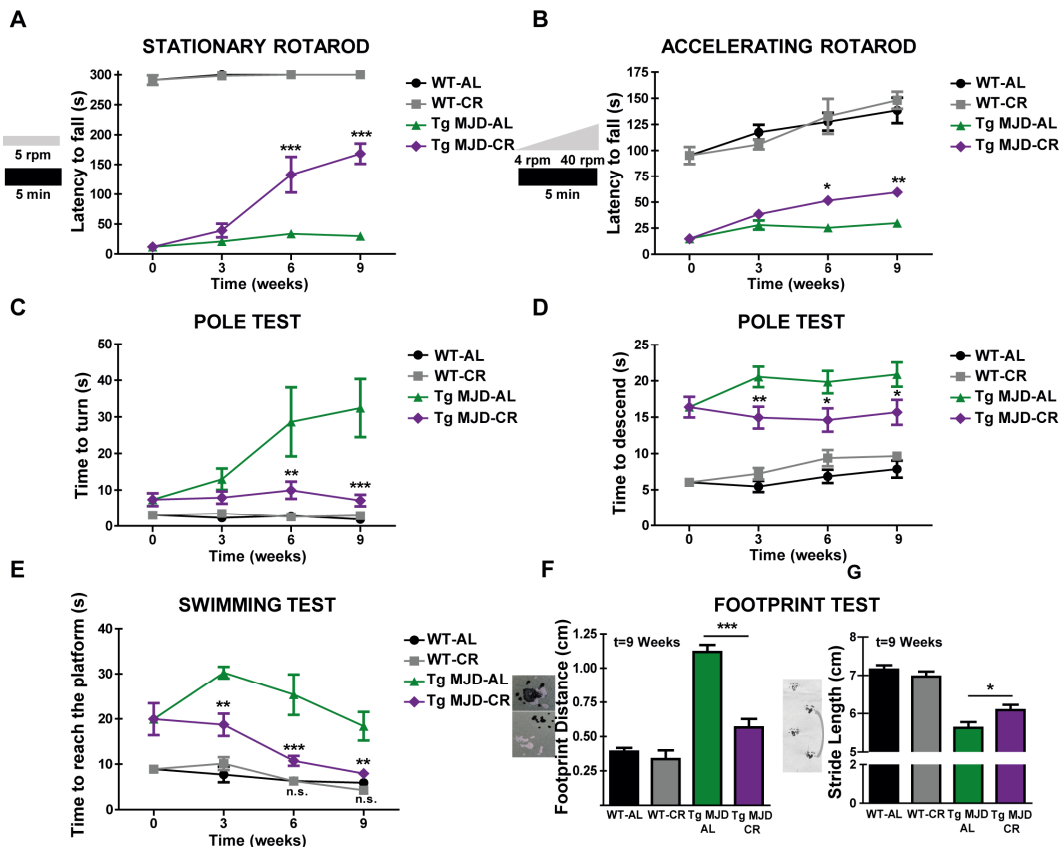
Figure 2.3. Caloric restriction alleviates balance and motor coordination impairments, and ameliorates gait in a transgenic MJD mouse model. **(A-B)** Wild-type and transgenic

Figure 2.3. (cont.) MJD mice in *ad libitum* or caloric restriction diet performance in stationary (5 r.p.m. – **A**) and accelerated (from 4 r.p.m. to 40 r.p.m. - **B**) rotarod, showing the time that mice took to fall off the rotarod. **(C-D)** Performance of wild-type and transgenic MJD mice in *ad libitum* or caloric restriction diet, in pole test. In **(C)** is represented the time that mice took to turn downwards and in **(D)** the time that mice took to descend the vertical beam. **(E)** Time that wild-type and transgenic MJD mice in *ad libitum* or caloric restriction diet spent to reach the safe platform on the swimming pool. **(F-G)** Quantitative analysis of the footprint patterns of wild-type and transgenic MJD mice in the different regimens, nine weeks after the beginning of the study. In **(F)** is represented the average distance between the hindpaw and forepaw during four consecutive steps, and in **(G)** the average stride length. WT-AL: Wild Type *Ad Libitum*; WT-CR: Wild-Type Caloric Restriction; Tg MJD-AL: Transgenic MJD *Ad Libitum*; Tg MJD-CR: Transgenic MJD Caloric Restriction. Data represent mean ± SEM. n.s. $p > 0.05$; *$p < 0.05$; **$p < 0.01$; ***$p < 0.001$ compared to Tg-AL, or WT-AL in **(E)**. **(A-E)** Two-way Analysis of Variance (ANOVA) with Bonferroni's post-hoc test. **(F-G)** One-way ANOVA with Bonferroni's post-hoc test. WT-AL n=5; WT-CR n=7; Tg MJD-AL n=6; Tg MJD-CR n=7.

Finally, horizontal locomotor activity was evaluated by the open-field test. Caloric-restricted transgenic MJD mice completely reverted the typical hypoactivity of this model (Figure 2.4A,B), travelling consistently longer distances than the AL mice (Figure 2.4A; t=9 weeks; Tg MJD-AL: 45.15±2.40 m *vs* Tg MJD-CR: 56.02±3.11 m; $p < 0.05$), with a higher mean velocity (Figure 2.4B; t=9 weeks; Tg MJD-AL: 1.972.0±0.14 cm.s^{-1} *vs* Tg MJD-CR: 2.36±0.12 cm.s^{-1}; $p < 0.05$), in both cases reaching the values observed for WT mice. Altogether, these results show that CR improves locomotor activity. Furthermore, we also evaluated the time that mice spent in the central area of the arena, and the distance travelled in this area. We observed that transgenic MJD in the AL diet avoided this area, spending less time in this central area relative to the total time, and travelling significantly less, in comparison with wild-type mice (Figure 2.4C,D; t=9 weeks; WT-AL: 7.1±1.1% *vs* Tg MJD-AL: 4.9±0.8%; WT-AL: 14.0±1.4 cm *vs* Tg MJD-AL: 10.1±1.0 cm; $p < 0.05$). These results demonstrate that transgenic MJD mice are more anxious in comparison with wild-type age-matched mice. Interestingly, caloric-restricted mice, wild-type or transgenic, did not significantly avoid this area, suggesting that nine weeks of CR did not cause an increase in anxiety on the animals. Moreover, caloric-restricted transgenic MJD mice showed a reversion of the phenotype to the normal levels of a wild-type mice (Figure 2.4D).
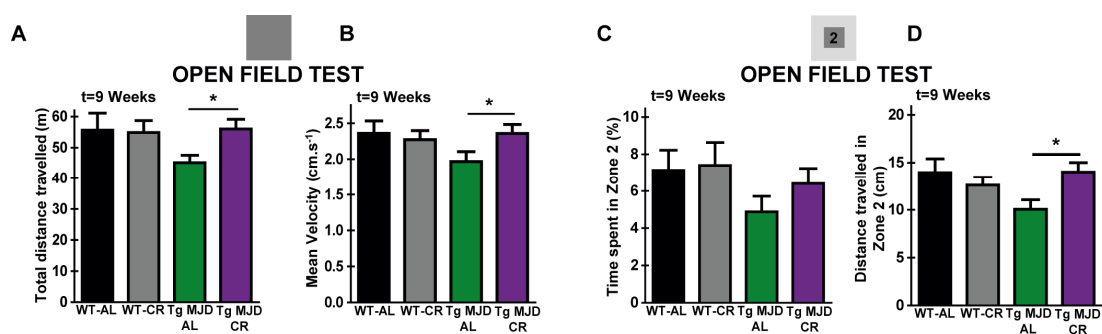
Figure 2.4 <u>Caloric restriction ameliorates locomotor hypoactivity and does not interfere with anxiety.</u> **(A-B)** Distance travelled **(A)** and mean velocity **(B)** of 40 minutes of experiment in open-field arena of wild-type and transgenic MJD mice. **(C-D)** Percentage of time spent in the central area of the arena (represented by the 2 in dark grey in the scheme; in **(C)**), and distance travelled by the animals from the different groups in this area **(D)**, during 40 minutes. <u>WT-AL:</u> Wild Type *Ad Libitum*; <u>WT-CR:</u> Wild-Type Caloric Restriction; <u>Tg MJD-AL:</u> Transgenic MJD *Ad Libitum*; <u>Tg MJD-CR:</u> Transgenic MJD Caloric Restriction. Data represent mean ± SEM. *p<0.05. **(A-D)** One-way Analysis of Variance (ANOVA) with Bonferroni's post-hoc test. WT-AL n=5; WT-CR n=7; Tg MJD-AL n=6; Tg MJD-CR n=7.

Importantly, no differences were found for wild type mice submitted to CR or AL diets in any behavioral test. This finding suggests that caloric-restricted animals do not perform better in these tests simply because they are leaner. Altogether, these data demonstrate that nine weeks of CR robustly reduces the severe motor deficits in a post-symptomatic transgenic mouse model of MJD.

2.4.3 Caloric restriction ameliorates neuropathology of transgenic Machado-Joseph disease mice

Next we wanted to investigate if motor improvements, triggered by CR, correlate with histopathological changes in the cerebellum. Transgenic MJD mice used in this study present severe cerebellar atrophy and Purkinje cells are specifically affected (Torashima et al., 2008). Representative images of cerebellar lobule V confirm the generalized cerebellar atrophy in transgenic MJD mice (Figure 2.5A). We evaluated neuropathology at the last time-point (nine weeks after the beginning of CR), when we observed the most prominent CR effects in motor behavior.

In agreement with the behavioral data, 15-week-old caloric-restricted transgenic MJD mice exhibited significantly larger layers thickness, in comparison with AL mice (Figure 2.5B; Molecular layer - Tg MJD-AL: 55.1±3.0 µm *vs* Tg MJD-CR: 70.3±1.5 µm; p<0.05; Figure 2.5C; Granular layer - Tg MJD-AL: 69.5±0.7 µm *vs* Tg MJD-CR: 89.9±3.2 µm; p<0.05), which suggests prevention of neurodegeneration. In contrast, no difference

was found in layers thickness within the two groups of wild-type mice (Figure 2.5B; Molecular layer - WT-AL: 122.9±3.1µm *vs* WT-CR: 114.3±6.2 µm; p>0.05; Figure 2.5C; Granular layer - WT-AL: 123.8±6.7 µm *vs* WT-CR: 117.9±2.5 µm; p>0.05). Cerebellar volume was also evaluated and caloric-restricted transgenic MJD mice had a significantly higher cerebellar volume, in comparison with the AL transgenic group (Figure 2.5D; Tg MJD-AL: 10.1±0.1 mm^3 *vs* Tg MJD-CR: 12.6±0.4 mm^3; p<0.05). Again, there was no difference between the two groups of wild-type mice (Figure 2.5D; WT-AL: 37.4±1.2 mm^3 *vs* WT-CR: 36.9±1.5 mm^3; p>0.05).

The polyQ expansion in mutant ataxin-3 leads to the formation of intranuclear inclusions, one of the main hallmarks of MJD (Paulson et al., 1997b; Schmidt et al., 1998). Therefore, we investigated whether beneficial effects of CR in motor abnormalities are related with changes in the number of mutant ataxin-3 aggregates, in the cerebellum. The number of aggregates in Purkinje cells of the cerebellar cortex, in caloric-restricted transgenic MJD mice was reduced around 30% in comparison with the AL transgenic mice (Figure 2.5E; Tg MJD-AL: 4680±393 *vs* Tg MJD-CR: 3214±271; p<0.05), as well the levels of soluble mutant ataxin-3 (Figure 2.5F).
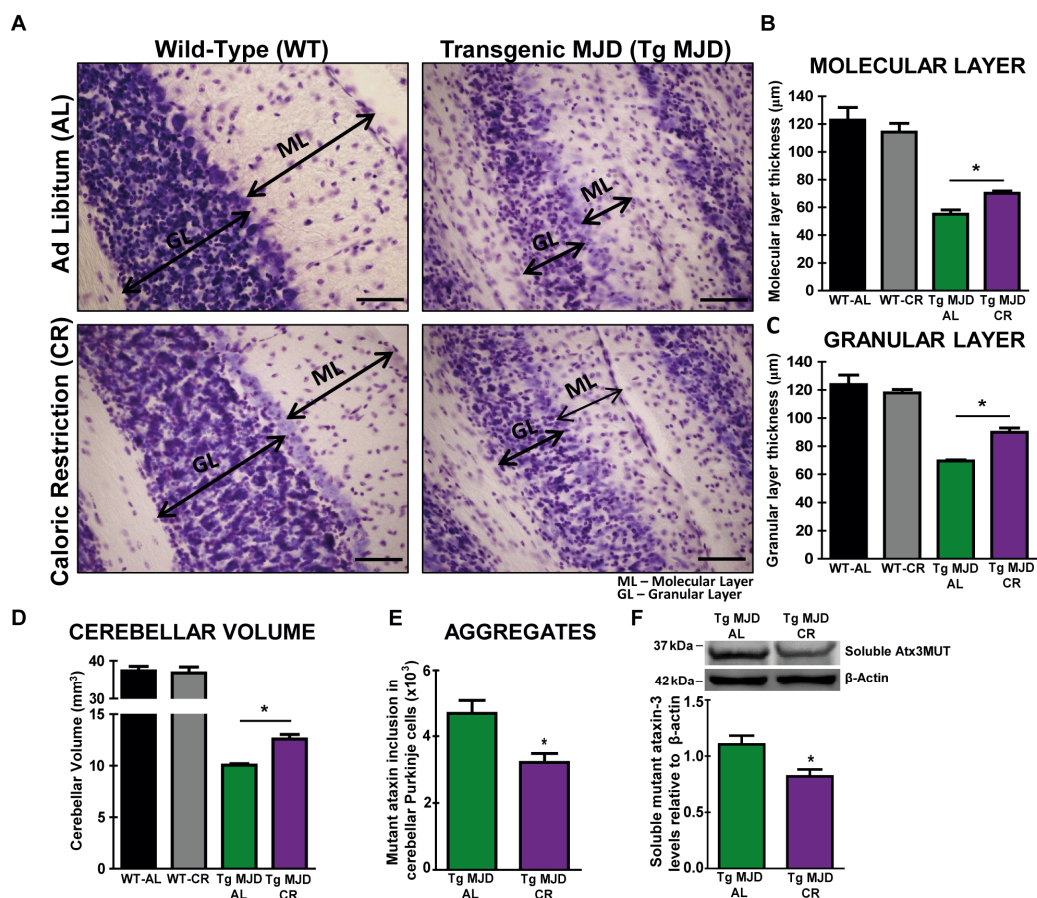
Figure 2.5 Nine weeks of caloric restriction ameliorates cerebellar neuropathology in transgenic MJD mice. **(A)** Cresyl violet-stained sections demonstrate the thickness of molecular and granular layers of lobule V of cerebellum in 15-week-old littermate wild-

Figure 2.5 (cont.) type (WT) and transgenic MJD (Tg MJD) mice in *ad libitum* (AL) or caloric restriction (CR) diet, quantified in **(B)** and **(C)**. **(D)** Quantification of cerebellar volume in cresyl violet-stained sections from wild-type and transgenic MJD mice in *ad libitum* or caloric restriction diet. **(E)** Immunohistochemistry analysis of the number of mutant ataxin-3 inclusions in the cerebellar Purkinje cells of transgenic MJD mice. **(F)** Western blot analysis of the relative levels of the soluble form of mutant ataxin-3, normalized with β-actin, from *ad libitum* and caloric-restricted transgenic MJD mice. WT-AL: Wild Type *Ad Libitum*; WT-CR: Wild-Type Caloric Restriction; Tg MJD-AL: Transgenic MJD *Ad Libitum*; Tg MJD-CR: Transgenic MJD Caloric Restriction. Data represent mean ± SEM. *$p<0.05$. Relative to Tg-AL. **(B-D)** One-way Analysis of Variance (ANOVA) with Bonferroni's post-hoc test. **(E-F)** Unpaired Student's t-test. WT-AL n=3; WT-CR n=4; Tg-AL n=4; Tg-CR n=4. Scale bar: 50 μm.

Altogether, these results demonstrate that CR prevents cerebellar neurodegeneration in MJD mice, while it simultaneously decreases the levels of mutant ataxin-3.

2.4.4 Caloric restriction reestablishes compromised sirtuin 1 levels in the cerebellum of transgenic Machado-Joseph disease mice

Since the increase in SIRT1 levels and activity are intrinsically related to the effects on lifespan and neuroprotection mediated by CR (Cohen et al., 2004; Graff et al., 2013), we evaluated SIRT1 levels in human fibroblasts from healthy controls and MJD patients, and in the cerebellum of 15-week-old wild-type vs *ad libitum* or caloric-restricted transgenic MJD mice.

We observed that SIRT1 mRNA in fibroblasts of patients was compromised around 42.9±3.6 %, in comparison with healthy controls (Figure 2.6A). We also observed a dramatic decrease of 58.4±8.3 % in mRNA levels and 38.5±8.8 % in protein levels of SIRT1 in transgenic MJD mice, in comparison with wild-type littermate mice (Figures 2.6B,C). Upon CR, SIRT1 mRNA and protein levels were completely reestablished to the levels observed in the non-diseased mice (Figures 2.6B,C). As expected, CR also induced the activation of SIRT1, evaluated by the decrease in acetylated levels of the SIRT1 substrate, Forkhead box protein O1 (Ac-FOXO1, Figure 2.6D).
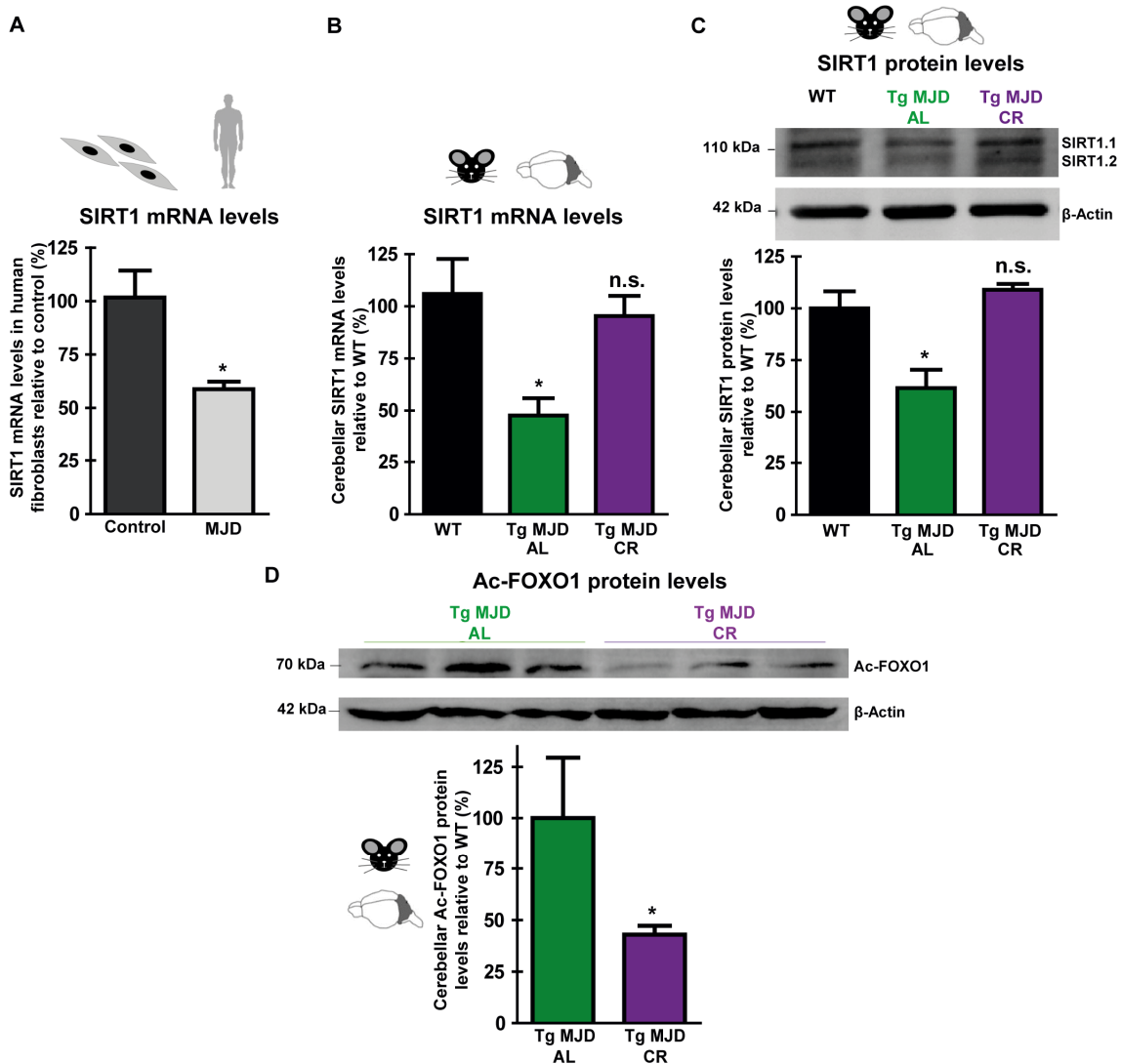
Figure 2.6 <u>SIRT1 levels are abnormally reduced in human MJD fibroblasts and in cerebellum of transgenic MJD mice, and caloric restriction reestablishes normal cerebellar SIRT1 levels.</u> **(A)** SIRT1 mRNA levels in human MJD fibroblasts, in comparison with healthy controls, evaluated by qRT-PCR. **(B-C)** SIRT1 mRNA levels and SIRT1 protein levels in the cerebellum of wild-type and *ad libitum* or caloric-restricted transgenic MJD mice. **(D)** Acetylated levels of FOXO1 relative to β-actin, evaluated by western blot, in *ad libitum* and caloric-restricted MJD mice. <u>WT:</u> Wild Type; <u>Tg MJD-AL:</u> Transgenic MJD *Ad Libitum*; <u>Tg MJD-CR:</u> Transgenic MJD Caloric Restriction. Data represent mean ± SEM. n.s. $p>0.05$; * $p<0.05$. Relative to controls. **(A)** Unpaired Student's t-test. Control n=3; MJD n=3. **(B-C)** One-way Analysis of Variance (ANOVA) with Dunnet's post hoc test. WT n=5; Tg MJD-AL n=5; Tg MJD-CR n=4. SIRT1.1 (SIRT1 isoform 1) SIRT1.2 (SIRT1 isoform 2). **(D)** Unpaired Student's t-test. Tg MJD-AL n=3; Tg MJD-CR n=3.

Overall, these results suggest that SIRT1 expression is compromised in Machado-Joseph disease, and CR can revert this defect, reinstating normal SIRT1 levels.

2.4.5 Genetic overexpression of sirtuin 1 reduces the number of mutant ataxin-3 inclusions and neuronal dysfunction in the striatal lentiviral model of Machado-Joseph disease

Previously, we showed that CR robustly mitigated MJD phenotype and reverted the compromised cerebellar levels of SIRT1 in mice. We then investigated whether lentiviral overexpression of SIRT1 would be sufficient to mimic the effects of CR, and mediate similar alleviation of MJD pathology. For this purpose we took advantage of a genetic mouse model of MJD generated by the localized lentiviral-mediated expression of mutant ataxin-3 in the striatum, another affected brain region in MJD (Alves et al., 2008b; Simoes et al., 2012). This model is particularly useful as it allows a precise quantification of neuropathology regarding the loss of the dopamine- and cAMP-regulated phosphoprotein 32 (DARPP-32) marker, and the number of ataxin-3 aggregates in specific regions of interest. Therefore, in 5-week-old wild-type mice, we stereotaxically co-injected in the left hemisphere lentiviral vectors encoding for mutant ataxin-3 and an inactive mutant SIRT1 - H363Y - as control (control hemisphere), while in the right hemisphere, we co-injected lentiviral vectors encoding for mutant ataxin-3 and for SIRT1 (Figure 2.7A). SIRT1 overexpression was specifically located at striatum, and as expected, induced a decrease in the acetylated levels of a SIRT1 substrate (FOXO1) in striatum (Figures 2.7B,C).

Despite the unclear role in the pathology, insoluble aggregates of ataxin-3 are a hallmark of the disease that can be used as a surrogate marker. By immunohistochemistry (Figures 2.7D,E) and by western blotting (Figure 2.7F), we observed that SIRT1 overexpression induced a 60.9±4.8% decrease in the total number of aggregates (Figure 2.7E; Non treated: 136960±26808 *vs* SIRT1 50480±5960) and a significant decrease in the levels of aggregated and soluble forms of mutant ataxin-3 (Figure 2.7F). Interestingly, the ~34 kDa and ~26 kDa toxic fragments, resulting from the processing of mutant ataxin-3 (Simoes et al., 2012), were also decreased in the hemisphere where SIRT1 was overexpressed, indicating an interference of SIRT1 in the process of formation or degradation of these fragments. No changes were observed regarding the mRNA levels of mutant ataxin-3 (Figure 2.7G). Altogether, these results suggest that SIRT1 overexpression decreases the accumulation and aggregation of mutant ataxin-3, and decreases the levels of toxic fragments, contributing to the decrease of mutant ataxin-3 toxicity.

In the control hemisphere, DARPP-32 immunoreactivity decreased, with a depleted staining volume of 0.78±0.10 mm^3, while in the contralateral hemisphere SIRT1 overexpression reduced the volume depletion of DARPP-32 by 52% (Figure 2.7H-I),

clearly demonstrating its neuroprotective activity.

Furthermore, brightfield images showed that in the control hemisphere occurred a small condensation of the internal capsule of the striatum, triggered by the neuronal dysfunction induced by mutant ataxin-3 (Figure 2.7J, left). This was not observed in the hemisphere where SIRT1 was overexpressed (Figure 2.7J, left). Importantly, SIRT1 overexpression reduced by 42.0±10.7% the number of pyknotic nuclei (Figures 2.7J right and K).
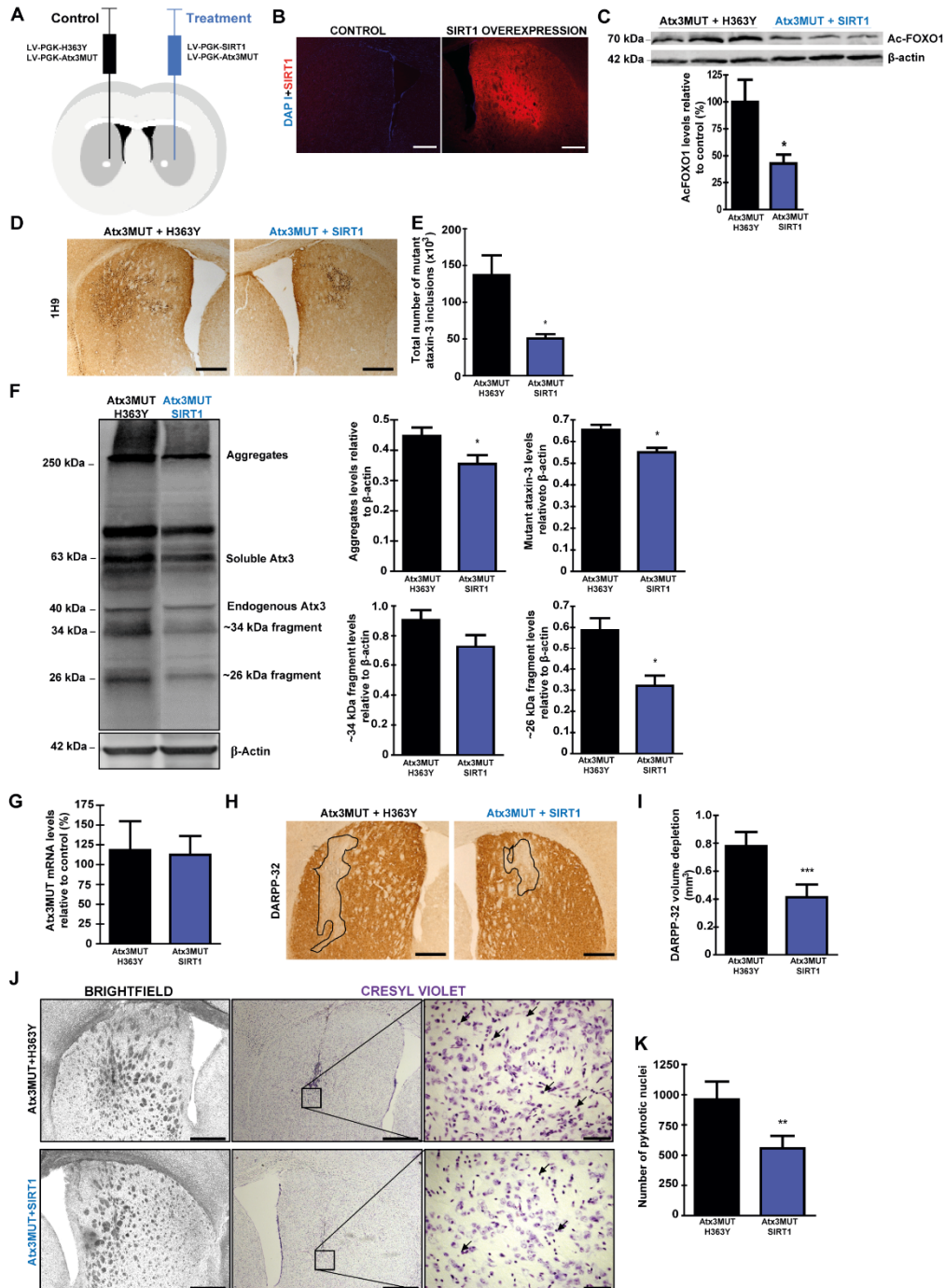
Figure 2.7 <u>SIRT1 overexpression reduces mutant ataxin-3 toxicity, neuronal dysfunction, and neurodegeneration in a striatal lentiviral model of MJD.</u> **(A)** Schematic

Figure 2.7 (cont.) representation of the strategy used to create the *in vivo* striatal lentiviral model of MJD, and to overexpress SIRT1/H363Y. Five-week-old C57Bl/6J mice were bilaterally injected with lentiviral vectors encoding for mutant ataxin-3. In left hemisphere were co-injected lentiviral vectors encoding for H363Y and in right hemisphere for SIRT1. Four weeks after the surgery mice were sacrificed. **(B)** SIRT1 immunoreactivity (red) in striatum of animals of the striatal lentiviral model of MJD co-injected with SIRT1 *versus* a control animal. DAPI, blue, nuclei. **(C)** Western blot representing percentage change of acetylated levels of FOXO1 relative to β-actin, in striata of mice of the lentiviral model of MJD overexpressing H363Y, in comparison with SIRT1 overexpression. **(D)** By immunohistochemistry (with an anti-ataxin-3 antibody - 1H9), total number of mutant ataxin-3 inclusions were counted, and are quantified in **(E)**. **(F)** Western blot analysis of the levels of aggregated, soluble, and ~34 kDa and ~26 kDa fragments of ataxin-3, normalized with β-actin. **(G)** qRT-PCR analysis of mutant ataxin-3 mRNA. **(H-I)** DARPP-32 immunohistochemistry and quantification of the volume of the depleted region of striatal DARPP-32. **(J)** Brightfield images of coronal sections of mice of the lentiviral model of MJD overexpressing H363Y, in comparison with SIRT1 overexpression. Cresyl violet staining indicating pyknotic nuclei, and its quantification is demonstrated in **(K)**. 1H9: Anti-ataxin-3 antibody; Ac-FOXO1: Acetylated Forkhead box protein 1; Atx3MUT: Mutant ataxin-3; DARPP-32: Dopamine- and cAMP-Regulated Neuronal Phosphoprotein; SIRT1: Sirtuin 1. Data represent mean±SEM. *$p < 0.05$; **$p < 0.01$; ***$p < 0.001$ compared to Atx3MUT+H363Y hemisphere. **(C,E-G,I,K)** Paired student's t-test. n=4. Scale bar: 500 μm **(B,D,H,4 left panels of J)**; Scale bar: 50 μm **(2 right panels of J)**.

Altogether, these data suggest that specific and localized SIRT1 overexpression prevents cell injury and striatal degeneration, triggered by mutant ataxin-3.

2.4.6 Genetic overexpression of sirtuin 1 decreases neuroinflammation in the striatal lentiviral model of Machado-Joseph disease

To explore the mechanism(s) by which SIRT1 overexpression produced beneficial effects on MJD mouse models, we investigated whether SIRT1 interferes with the characteristic neuroinflammation observed in the lentiviral MJD mouse model (Alves et al., 2008b; Goncalves et al., 2013).

In the non-treated hemisphere, we observed a local glial fibrillary acidic protein (GFAP) immunoreactivity, suggestive of astrocytic activation. Although, SIRT1 overexpression reduced GFAP immunoreactivity and levels (Figures 2.8A-C). Additionally, in the non-treated hemisphere, a strong immunoreactivity for the microglial marker Ionized calcium binding protein 1 (Iba-1) was observed, revealing microglial recruitment, which was robustly and significantly reduced in the hemisphere where we overexpressed SIRT1 (Figures 2.8D,E). These results suggest that SIRT1

overexpression prevents reactive gliosis associated with MJD.

Furthermore, we analyzed the changes in the mRNA levels of inflammatory cytokines, namely interleukin-1 beta, -6, and -10 (IL-1β, -6, and -10) and tumor necrosis factor alpha (TNF-α). We found a strong and significant decrease in the mRNA levels of the pro-inflammatory cytokines (IL-1β, IL-6, and TNF-α) in the hemisphere where we overexpressed SIRT1, relative to the non-treated hemisphere (Figures 2.8F-H). Interestingly, the levels of one anti-inflammatory cytokine, IL-10, were not different between non-treated and SIRT1 overexpressing striata (Figure 2.8I). These results suggest that SIRT1 has a specific downregulating effect over pro-inflammatory cytokines, but does not have effects on the anti-inflammatory network.
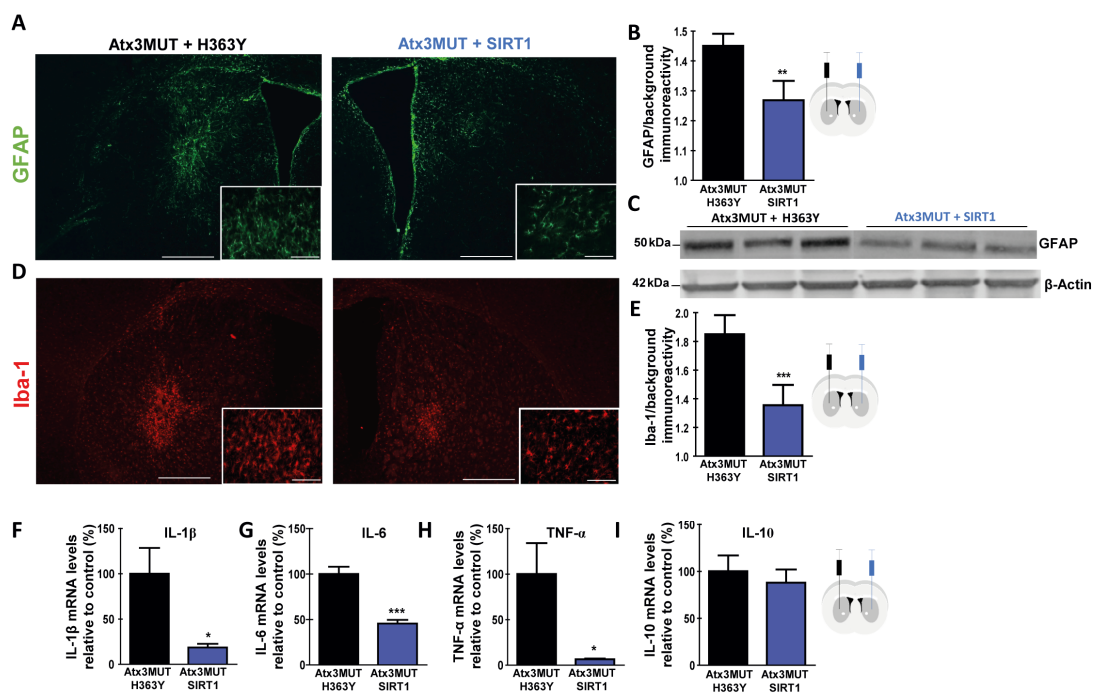
Figure 2.8 SIRT1 overexpression reduces MJD-associated neuroinflammation. **(A-C)** Analysis of GFAP immunoreactivity by immunohistochemistry, quantified in **(B)**, and by western blot **(C)** in the striatum of the striatal lentiviral model of MJD, co-injected with lentiviral vectors encoding for H363Y in the left hemisphere, and SIRT1 in the right hemisphere. **(D-E)** Iba-1 immunoreactivity evaluated by immunohistochemistry. **(F-H)** mRNA levels of pro-inflammatory cytokines (IL-1β, IL-6 and TNF-α) were evaluated by qRT-PCR. **(I)** mRNA levels of the anti-inflammatory IL-10 cytokine, evaluated by qRT-PCR. Atx3MUT: Mutant ataxin-3; GFAP: Glial Fibrillary Acidic Protein; H363Y: Mutated SIRT1 without deacetylase activity; Iba-1: Ionized calcium-binding adapter molecule 1; IL-1β: Interleukin-1 beta; IL-6: Interleukin-6; IL-10: Interleukin-10; SIRT1: Sirtuin 1; TNF-α: Tumoral Necrosis Factor alpha. Data represent mean ± SEM. *p<0.05; **p<0.01; ***p<0.001 compared to Atx3MUT+H363Y hemisphere. **(B,E-I)** Paired student's t-test. n=4. Scale bar 500 μm **(A,D larger panels)**; Scale bar: 125 μm **(A,D smaller panels)**.

Overall, data indicate that, at least, one of the mechanisms by which SIRT1 ameliorates MJD neuropathology is by the decrease of neuroinflammatory markers.

2.4.7 Genetic overexpression of sirtuin 1 activates autophagy in Machado-Joseph disease models

It is known that SIRT1 deacetylase activity is crucial for autophagy activation induced by starved conditions (Lee et al., 2008; Huang et al., 2015). Additionally, we previously demonstrated that autophagy is compromised in MJD and its activation can alleviate MJD (Nascimento-Ferreira et al., 2011; Nascimento-Ferreira et al., 2013). We also previously demonstrated that the increase in SIRT1 through CR or gene therapy decreases the levels of mutant ataxin-3. Therefore, we hypothesized that SIRT1 increases mutant ataxin-3 clearance by activating autophagy.

Firstly, in order to explore if autophagy could be activated by CR, we evaluated LC3BII and p62 protein levels in the cerebella of 15-week-old transgenic animals fed during nine weeks with a CR diet *vs* an AL diet. We observed a significant increase in LC3BII levels and a decrease of p62 levels in cerebella of transgenic MJD mice fed with CR diet, in comparison with transgenic MJD AL-fed animals (Figure 2.9A,B). Moreover, we evaluated the same parameters in the striatum of the lentiviral model of MJD mice, where SIRT1 was overexpressed, in comparison to the control hemisphere (overexpression H363Y – see Figure 2.7A). Interestingly, we also observed a significant increase in LC3BII and a decrease in p62 levels, in the striatum where SIRT1 was overexpressed, in comparison with H363Y overexpression (Figures 2.9C,D). These results suggest that, in fact, SIRT1 activates autophagy in MJD mice.
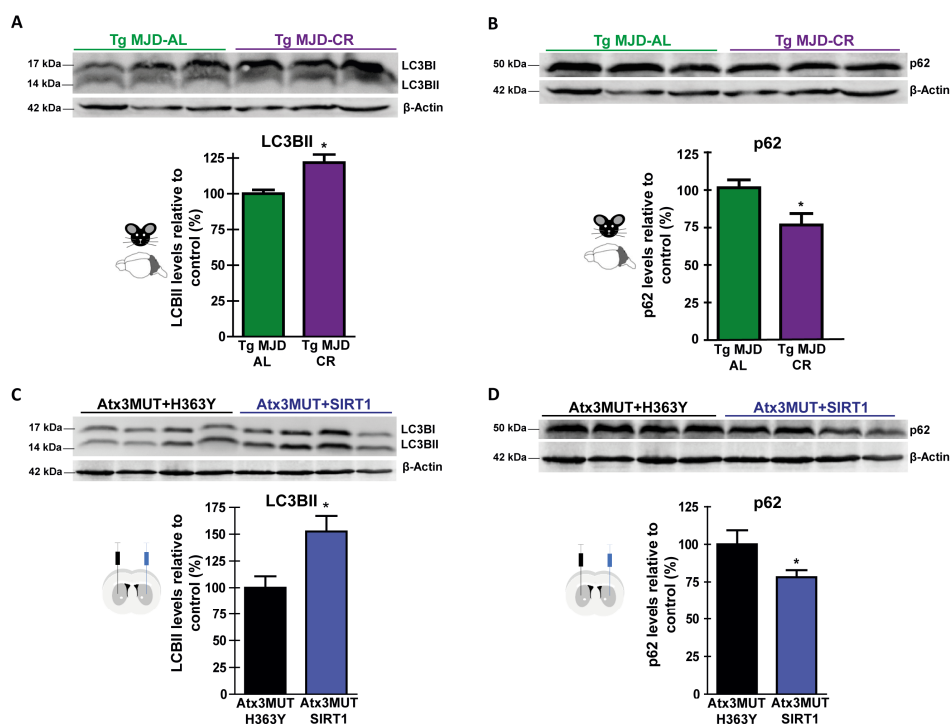
Figure 2.9 Caloric restriction or lentiviral SIRT1 overexpression stimulates autophagy in MJD mouse models. **(A-B)** Cerebellar LC3BII **(A)** and p62 **(B)** levels normalized to β-

Figure 2.9 (cont.) actin of caloric-restricted transgenic MJD mice, evaluated by western blot. **(C-D)** Striatal LC3BII **(C)** and p62 **(D)** levels normalized to β-actin of mice from the striatal lentiviral model of MJD, co-injected with lentiviral vectors encoding for SIRT1 or H363Y as control, evaluated by western blot. LC3B: Microtubule-associated protein 1 light chain 3 B; p62: Sequestosome 1. Data represent mean ± SEM. *p<0.05. Relative to controls. **(A-B)** Unpaired Student's t-test. n=6. **(C-D)** Paired Student's t-test. n=4.

To further assess the impact of SIRT1 on autophagic flux, we performed an *in vitro* study using Neuro2a cells expressing mutant ataxin-3. We co-infected these cells with lentiviral vectors encoding for H363Y or SIRT1 and we incubated them in the presence or absence of chloroquine that is an autophagy inhibitor. Interestingly, in cells overexpressing SIRT1, we observed an increase in LC3BII levels, in comparison to control cells (overexpressing H363Y; Figure 2.10A). To confirm if SIRT1 is activating autophagy, we evaluated LC3BII levels in the presence of the lysosomal degradation inhibitor (chloroquine 100 μM), and again an increase in LC3BII levels was observed, comparing to the control condition (Figure 2.10A). Cells overexpressing SIRT1 also exhibited a significant decrease in p62 or sequestosome 1 (SQSTM1), in comparison to control condition, which as expected, was prevented in the presence of chloroquine (Figure 2.10B). Additionally, SIRT1 overexpression induced a decrease of mutant ataxin-3 that was also prevented by chloroquine (Figure 2.10C).
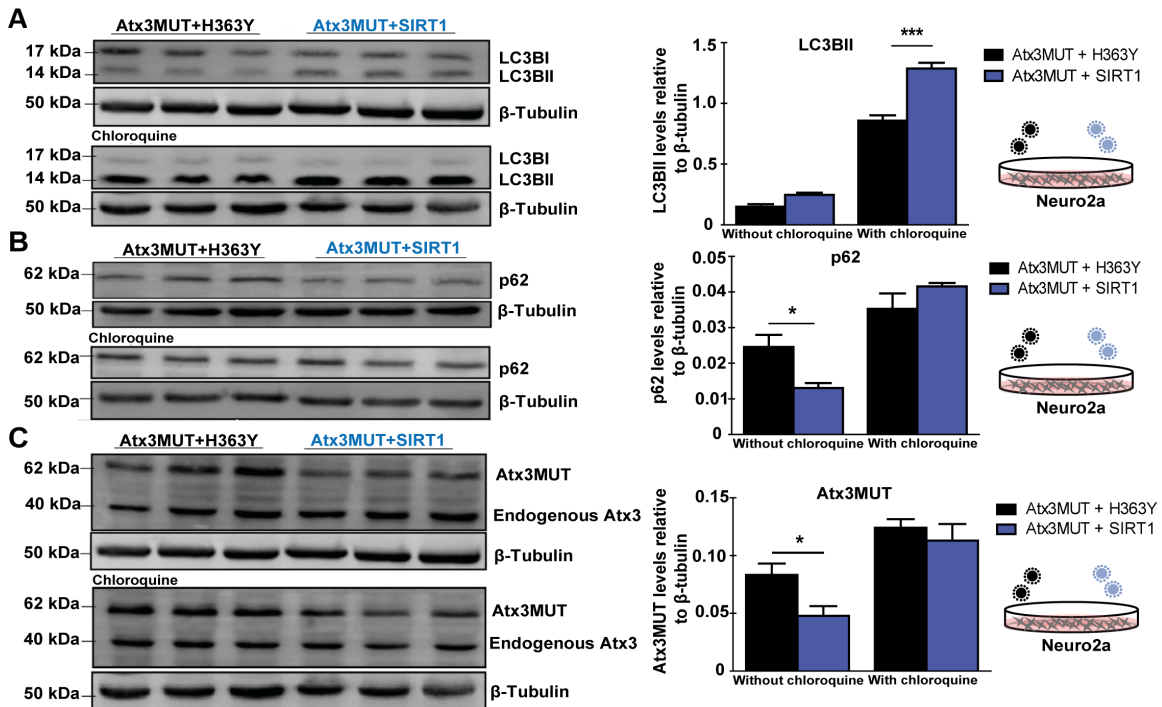
Figure 2.10 SIRT1 is able to increase autophagic flux, contributing to mutant ataxin-3 clearance. **(A-C)** Neuro 2a cells were co-infected with lentivirus encoding for mutant ataxin-3 and for H363Y (control condition) or co-infected with lentivirus encoding for mutant ataxin-3 and for SIRT1. LC3BII **(A)**, p62 **(B)** and mutant ataxin-3 **(C)** levels were

Figure 2.10 (cont.) evaluated by western blot, in two different conditions: in the presence and in the absence of chloroquine. <u>LC3B</u>: Microtubule-associated protein 1 light chain 3 B; <u>p62</u>: Sequestosome 1. Data represent mean ± SEM. *p<0.05; ***p<0.001. Relative to control. **(A-C)** Two-way ANOVA with Bonferroni's post hoc test. n=3

Furthermore, to better understand the direct effect of SIRT1 on autophagy pathway and on MJD pathology, we performed additional experiments using the same *in vitro* model of MJD that is suitable to address autophagy features - Neuro2a cells expressing mutant ataxin-3 - and we molecularly manipulated autophagy. We generated and validated a shRNA targeting Atg5 (shAtg5) in addition to a shRNA targeting SIRT1 (shSIRT1). In the Neuro2a cell line expressing a mutated form of ataxin-3, we genetically silenced SIRT1 or Atg5, in comparison with a control shRNA that does not have any known target. We evaluated, by western blot, the protein levels of LC3BII and p62. As expected, we observed that the genetic silencing of Atg5 significantly decreased the conversion of LC3BI to LC3BII (Figure 2.11A) and induced an accumulation of p62 (Figure 2.11B), and consequently of mutant ataxin-3 (Figure 2.11C). Similar results were obtained upon autophagy inhibition by SIRT1 knockdown, indicating that SIRT1 inhibition causes autophagic flux disruption. To further clarify the mechanism through which SIRT1 deacetylase activity stimulates autophagy and clears mutant ataxin-3, in cells expressing mutant ataxin-3, we genetically silenced Atg5 (or not) and overexpressed SIRT1 or the non-functional SIRT1 - H363Y. Interestingly, we made the following observations: i) as expected, when autophagy is not disrupted, SIRT1 activates autophagy, demonstrated by the increase in LCBII levels and the decrease in p62 (Figures 2.11D,E); ii) SIRT1 induces mutant ataxin-3 clearance and to do this its deacetylase activity is crucial because its inactive form (H363Y) had no effects (Figure 2.11F); iii) if autophagy is disrupted (here promoted by Atg5 genetic silencing) SIRT1 is not able to reduce mutant ataxin-3 levels, indicating that it is by the activation of autophagy that SIRT1 mediates the clearance of mutant ataxin-3 (Figures 2.11D-F). This study suggests that SIRT1 plays an important role in ataxin-3 clearance through the participation on autophagy, because the reduction of mutant ataxin-3, promoted by SIRT1, is reverted when Atg5 is genetically silenced.
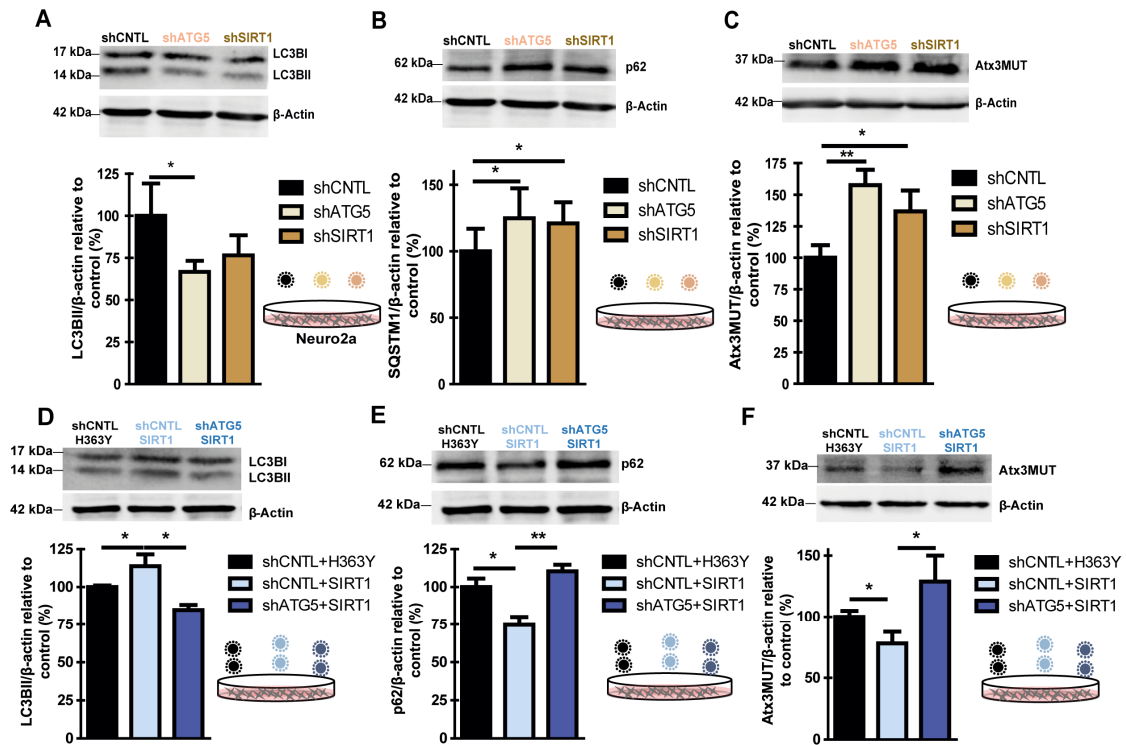
Figure 2.11 <u>The genetic blockage of autophagy, through ATG5 knockdown, reverts the beneficial effects of SIRT1.</u> **(A-C)** LC3BII **(A)**, p62 **(B),** and mutant ataxin-3 **(C)** levels in Neuro 2a cells expressing mutant ataxin-3 and a control shRNA (shCNTL), or a shRNA targeting SIRT1 (shSIRT1), or targeting Atg5 (shATG5). **(D-F)** LC3BII **(D)**, p62 **(E)** and mutant ataxin-3 **(F)** levels in Neuro2a cells expressing a mutant ataxin-3 and shCNTL and H363Y *vs* shCNTL and SIRT1 *vs* shATG5 and SIRT1. <u>Atg5:</u> Autophagy-related protein 5; <u>LC3B</u>: Microtubule-associated protein 1 light chain 3 B; <u>p62</u>: Sequestosome 1. Data represent mean ± SEM. *p<0.05; **p<0.01. Relative to control. **(A-F)** One-way ANOVA with Bonferroni's post hoc test. n=3.

Overall, these results suggest that SIRT1 activates autophagy, resulting on mutant ataxin-3 clearance, and consequently the decrease in mutant ataxin-3 levels.

2.4.8 Sirtuin 1 genetic silencing abolishes caloric restriction beneficial effects on the striatal lentiviral model of Machado-Joseph disease

To investigate whether the mechanism of CR is mediated by SIRT1 we evaluated if silencing SIRT1 would prevent the neuroprotective effects of CR in the striatal lentiviral model of MJD (see Figure 2.12A). Thus, we considered the following conditions: i) control animals from the lentiviral model of MJD (co-injected with shCNTL), in an AL diet (identified in the Figure 2.12 as shCNTL AL); ii) the same but caloric-restricted (identified in Figure 2.12 as shCNTL CR); iii) CR-fed animals, but instead of shCNTL, were co-

injected with lentiviral vectors encoding for the shSIRT1 (identified in Figure 2.12 as shSIRT1 CR).

As expected the number of mutant ataxin-3 inclusions and DARPP-32 volume depletion were significantly reduced in caloric-restricted mice compared to AL mice (Figures 2.12B,C; shCNTL AL: 80200±3040 *vs* shCNTL CR: 53720±10190; p=0.050; Figures 2.12D,E; shCNTL AL: 0.37±0.05 mm^3 *vs* shCNTL CR: 0.22± 0.03 mm^3; p<0.05). Furthermore, protein levels of SIRT1 were also increased by 63.2±12.5 % in the striatum of caloric-restricted mice (Figure 2.12F).

In contrast, silencing striatal SIRT1 (shSIRT1 CR) blocked the beneficial effects of CR as compared to control (shCNTL CR) (Figures 2.12G-J). In fact, in SIRT1-silenced mice, CR did not change the pathological striatal features induced by mutant ataxin-3, such as the number of aggregates in the striatum (Figures 2.12B,H; shCNTL AL: 80200±3040 *vs* shRNA SIRT1 CR: 94830±15810; p>0.05), neither DARPP-32 volume depletion (Figures 2.12D,J; AL: 0.37±0.05 mm^3 *vs* shRNA SIRT1 CR: 0.34±0.07 mm^3; p>0.05), completely reverting the neuropathology to the one observed in AL mice.
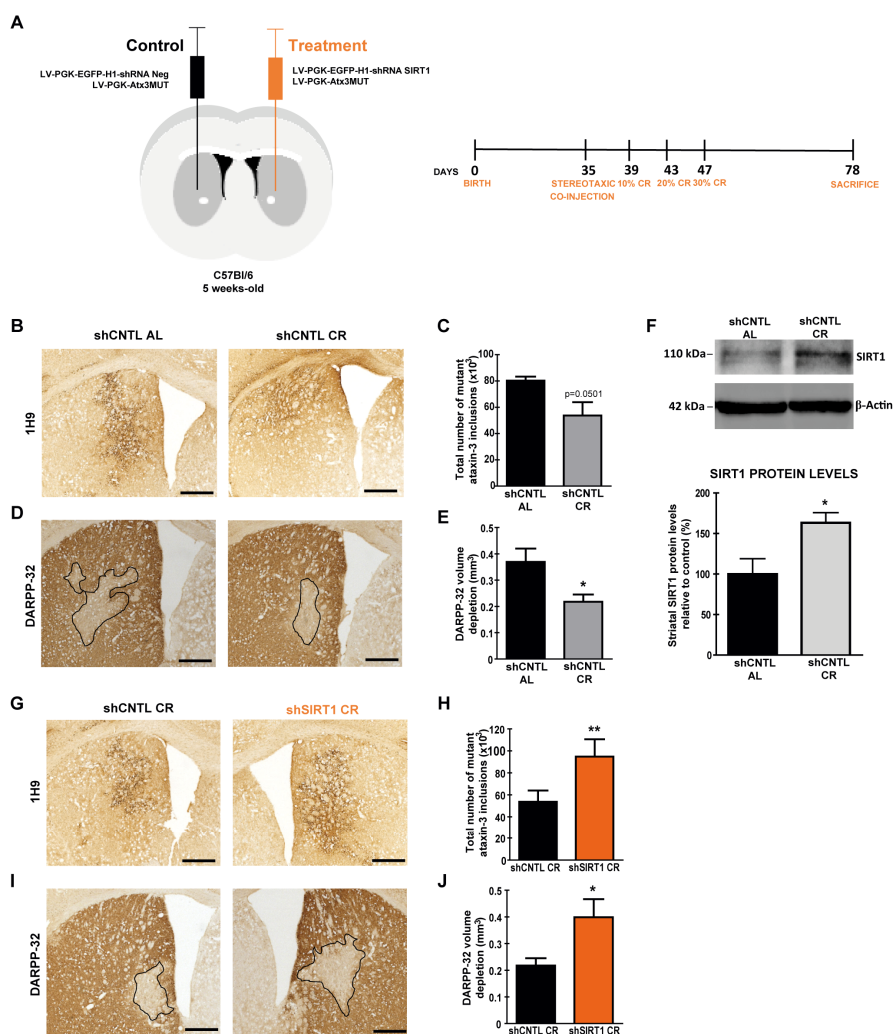
Figure 2.12 Caloric restriction alleviates MJD neuropathology by the SIRT1 pathway, in

Figure 2.12 (cont.) <u>the striatal lentiviral model of MJD.</u> **(A)** Schematic representation of the study. Five-week-old C57Bl/6J mice were stereotaxically injected in the striatum. In each hemisphere we injected lentiviral vectors encoding for mutant ataxin-3 and in the left hemisphere were co-injected lentiviral vectors encoding for a control shRNA and in the right hemisphere were co-injected lentiviral vectors encoding for the shRNA targeting SIRT1. Four days after the surgeries animals were divided in two groups. One group of mice was maintained in an *ad libitum* diet and the other was in a caloric restriction diet of 10% in the first four days, 20% in the next four days, and 30% after these period of adaptation and until the end of the study. **(B)** Immunohistochemistry for mutant ataxin-3 in the control hemisphere (shCNTL) of caloric-restricted and *ad libitum*-fed animals, and the resulting counting of inclusions are in **(C)**. **(D)** DARPP-32 immunohistochemistry and quantification of the volume depletion region of striatal DARPP-32 **(E)**. **(F)** Immunoblotting for SIRT1 in striatal samples from *ad libitum* and caloric-restricted mice. **(G)** Immunohistochemistry for mutant ataxin-3, and the number of inclusions are represented in **(H)**. **(I)** DARPP-32 immunohistochemistry and quantification of the volume depletion region of striatal DARPP-32 **(J)**. <u>1H9:</u> Anti-ataxin-3 antibody; <u>DARPP-32:</u> Dopamine- and cAMP-Regulated Neuronal Phosphoprotein. Data represent mean ± SEM. *p<0.05; **p<0.01; compared to control. **(C,E,F)** Unpaired student's t-test. n=5 **(H,J)** Paired Student's t-test. n=5.

Altogether, these results suggest that SIRT1 mediates the robust neuroprotective effects of CR in MJD.

2.5 <u>Discussion</u>

In the present study we provide strong evidence demonstrating that CR robustly alleviates the neuropathology in two MJD mouse models (transgenic and lentiviral MJD mouse models), and rescues the motor impairments by a mechanism involving the upregulation of SIRT1, and the consequent inhibition of neuroinflammation and activation of autophagy.

The cerebellum is one of the brain regions where neuropathology is most prominent in MJD, and cerebellar damages cause motor incoordination, explaining the disabling clinical features of MJD (Durr et al., 1996). The MJD transgenic mice that we used in this study (Torashima et al., 2008) display a specific expression of the mutant ataxin-3 in Purkinje cells of the cerebellar cortex. Mice of this MJD model exhibit a severe cerebellar atrophy and an early pronounced ataxic motor behavior. We started the study after the development of the ataxic behavior, in other words, in a post-symptomatic stage of the disease. In the present work, we show with several behavioral tests, that CR strongly ameliorates the severe motor deficits of this transgenic MJD mice. Furthermore, in comparison to the AL-fed MJD mice, we observed that CR also decreases the neuropathology features of these mice, mediating an amelioration of cerebellar atrophy, preserving molecular and granular layers thickness in the cerebellar cortex, while promoting a significant decrease in the aggregated and soluble forms of mutant ataxin-3 in Purkinje cells within cerebellar tissue. Our results suggest that the Purkinje cells preservation observed in caloric-restricted MJD mice resulted from the decrease in mutant ataxin-3 toxicity, and this may explain the preserved larger molecular and granular layers thickness in comparison to AL-fed animals. Moreover, we also evaluated the effects in the striatal lentiviral model of MJD. In this model of MJD we stereotaxically injected lentiviral vectors encoding for a mutated form of ataxin-3 in the striatum of five-week-old mice, inducing neuropathology from the second week on, including striatal mutant ataxin-3 inclusions, synaptic loss, and astrogliosis (Simoes et al., 2012; Goncalves et al., 2013; Duarte-Neves et al., 2015; Conceicao et al., 2016). In the CR and in the SIRT1 lentiviral overexpression experiments using this model of the disease, we started the treatments at an early stage of the disease, namely before the development of the aforementioned alterations, complementing the observations made with the previous mouse model of the disease. Therefore, using two complementary MJD mouse models, we observed that CR and the specific SIRT1 overexpression ameliorate the neuropathology in two stages of the disease: post-symptomatic and at an initial stage.

Some previous studies described benefits of CR in neurodegenerative disorders, such as Parkinson's, Alzheimer's, and Huntington's diseases (Duan et al., 2003; Maswood et al., 2004; Qin et al., 2006b). Specifically, Qin and colleagues (2006) demonstrated that in Alzheimer's disease, the neuroprotection mediated by CR can be reproduced by manipulating cellular SIRT1 expression/activity, highlighting the role of SIRT1 in the effects of CR (Qin et al., 2006b). Another more recent study showed that CR induced the expression of SIRT1, and pharmacological activation of SIRT1 replicated the effects of CR in a neurodegeneration mouse model (Graff et al., 2013). The increase in SIRT1 seems to be neuroprotective, and thus to ameliorate neuropathology in some diseases. Interestingly, in the transgenic mouse model of MJD used in the present study we observed that SIRT1 protein levels were compromised in the cerebellum, and that CR restored its levels, ameliorating MJD neuropathology. Besides that, we wanted to investigate the potential beneficial effects resulting from SIRT1 overexpression in the striatum of MJD mice from the lentiviral model, in order to clarify the importance of SIRT1. The results show that SIRT1 overexpression significantly reduced the characteristic MJD neuropathology, highlighting the role and importance of SIRT1 in the disease.

The mechanism underlying the neuroprotective effects promoted by CR is not fully understood. In fact, there is a myriad of mechanisms, in which CR participates. It is described that CR increases the levels of neurotrophic factors and stress-resistance proteins, such as heat shock protein 70 (HSP70), induces changes in regulatory proteins, namely in FOXOs proteins and also in sirtuins and that these changes contribute to neuroprotection (Duan et al., 2003; Maswood et al., 2004; Cohen et al., 2004; Qin et al., 2008). In order to further explore whether SIRT1 is the major mediator of CR beneficial effects, we genetically silenced SIRT1 in the striatum of *ad-libitum vs* caloric-restricted mice of the lentiviral model of MJD. We found compelling evidence demonstrating that CR drives its benefits mainly through the effects on SIRT1, due to the absence of neuroprotection in mice where SIRT1 was genetically silenced.

Recently, we described that neuroinflammation and reactive gliosis is a feature of MJD, in the two genetic mouse models of MJD that we used in this study (Goncalves et al., 2013; Mendonca et al., 2015; Conceicao et al., 2016). Moreover, it was previously suggested that the decrease in neuroinflammation, at least in part, underlies the neuroprotective action of CR and/or SIRT1 (Chen et al., 2005b). Taking this information into account, we evaluated neuroinflammatory markers in the affected brain region of MJD mouse models after SIRT1 overexpression, and we observed in the striatum of the lentiviral MJD mouse model, a significant decrease of gliosis markers and mRNA levels of pro-inflammatory cytokines (IL-1β, IL-6 and TNF-α), but no change on anti-

inflammatory cytokine levels (IL-10). Since others showed that SIRT1 deacetylates and inactivates NF-κB, a transcription factor that controls the gene expression of pro-inflammatory cytokines genes, such as IL-1β, IL-6, and TNF-α (Yeung et al., 2004), our results suggest an effect of SIRT1 on the pro-inflammatory network, probably related with this pathway.

It was also described that SIRT1 activates autophagy, through the deacetylation and activation of important autophagy-related proteins, namely Atg5, Atg7, and Atg8 (Lee et al., 2008). Moreover, it was recently shown that SIRT1 plays a crucial role in autophagy, contributing to nuclear LC3 deacetylation, driving its transportation for the cytoplasm and the initiation of autophagy under starvation conditions (Huang et al., 2015). Accordingly, we observed an activation of autophagy, triggered by SIRT1, which was specifically mediated by its deacetylase activity, given the absence of effects in the control condition (H363Y), where deacetylase activity was not present. We also observed a decrease in mutant ataxin-3 levels, suggesting that the reduction of mutant ataxin-3 toxicity is associated to autophagy activation, and promotion of mutant ataxin-3 clearance. Thus, SIRT1 can deacetylate important autophagic substrates, leading to autophagy activation, mutant ataxin-3 clearance, and reduction of toxic fragments, thereby ameliorating neurodegeneration. Moreover, we observed that SIRT1 decreases the levels of neurotoxic fragments of ~26 kDa and ~32 kDa. This hypothesis is in accordance with previous evidence showing that calpains are enzymes that participate in the proteolysis of mutant ataxin-3 leading to the formation of the toxic fragments of mutant ataxin-3 (Simoes et al., 2012; Hubener et al., 2013; Simoes et al., 2014) and also participate in the neuroinflammatory network (Liu et al., 1996). Overactivation of calpains increases the cleavage of mutant ataxin-3 into fragments containing the expanded polyglutamine tract. These fragments are translocated to the nucleus, contributing to the formation of aggregates and neurodegeneration. With SIRT1 overexpression and the decrease in neuroinflammation, we hypothesized that calpain activity could be reduced, leading to a decrease in the toxic fragments. The reduction in fragments described before can also be linked to the activation of autophagy. In fact, the faster turnover of soluble mutant ataxin-3 contributes to the decrease of mutant ataxin-3 fragment levels. These results are in accordance to the absence of changes in mutant ataxin-3 mRNA, that is suggestive of a decrease of different forms of ataxin-3 independently of transcriptional alterations.

In conclusion, the present study shows that SIRT1 activation strongly improves motor deficits and neuropathology in mouse models of MJD by SIRT1-mediated effects. Thus, a therapy based on SIRT1 increase, is a promising approach to treat MJD.

CHAPTER 3

NAD⁺ decrease induces nuclear-mitochondrial communication disruption in Machado-Joseph disease mouse models

The important thing is to never stop questioning…

(Einstein)

3.1 <u>Abstract</u>

Machado-Joseph disease (MJD) is a fatal neurodegenerative disorder caused by a mutation in the *ATXN3* gene. This mutation leads to the expression of a mutated protein - mutant ataxin-3 - that induces the formation of nuclear aggregates. Regarding the pathogenesis behind MJD, some mechanisms have been proposed, including mitochondrial dysfunction. However, it is not well understood how a mainly nuclear-focused disease is associated with mitochondrial dysfunction. Aiming the development of new therapeutic targets to treat MJD, we studied the potential dysregulation of the communication between nucleus and mitochondria, using MJD models.

In this study we provide evidence that nuclear-mitochondrial communication is altered in the cerebellum of transgenic MJD mice, due to the decrease of mitochondrial transcription factor A (TFAM). Furthermore, we also observed that this alteration is strongly related with the reduced levels of oxidized nicotinamide adenine dinucleotide (NAD$^+$), found in the cerebellum of these mice. We observed that the decrease in NAD$^+$ is associated with a debility in the NAD$^+$-salvage pathway, given the low levels of nicotinamide mononucleotide adenylyltransferase 1 (NMNAT1), and is also associated with a strong increase in the cluster of differentiation 38 (CD38), a NAD$^+$-consuming enzyme. Furthermore, the increase in NAD$^+$ levels through lentiviral-mediated overexpression of NMNAT1, is able to reestablish nuclear-mitochondrial communication, and to restore mitochondrial function.

Overall, this study suggests a new potential target to treat MJD, based on the increase in NAD$^+$.

3.2 <u>Introduction</u>

Machado-Joseph disease (MJD), also known as spinocerebellar ataxia type 3 (SCA3; Haberhausen et al., 1995), was described for the first time in 1972 on American families with Portuguese ancestry, particularly with Azorean ancestry (Machado's family from São Miguel island and Joseph's family from Flores island; Nakano et al., 1972; Rosenberg et al., 1976). MJD is a polyglutamine disease and is the most common autosomal dominant ataxia worldwide (Coutinho and Andrade, 1978; Schols et al., 2004). MJD is caused by an unstable mutation in the *ATXN3* gene leading to the expansion of the CAG tract in the C-terminal region of the ataxin-3 protein (Kawaguchi et al., 1994). Clinically, MJD is a heterogeneous disease, but the main symptoms include: cerebellar ataxia and neuromuscular dysfunction causing dystonia, dysarthria, spasticity, rigidity, among others (Rosenberg, 1992; Sudarsky and Coutinho, 1995; Riess et al., 2008). These symptoms are linked to the neurodegeneration that affects specific brain regions, mainly the cerebellum, but also the *substantia nigra*, striatum, thalamus, among others (Coutinho and Andrade, 1978; Durr et al., 1996; Rub et al., 2008). Unfortunately, there is no therapy to cure or even to retard the progression of this fatal disease.

Numerous mechanisms underlying MJD pathogenesis have been proposed, which could be explored as potential therapeutic targets. One of the phenomena that is intrinsically related with aging and also with some neurodegenerative diseases, in which MJD is included, is the decline in mitochondrial function. The mitochondrial dysfunction observed in MJD is supported by some evidences. In 1996, Matsuishi and colleagues described that lactate/pyruvate ratio is increased in the cerebrospinal fluid of MJD patients, suggesting a metabolic disarrangement (Matsuishi et al., 1996). Moreover, *in vitro* studies using cellular models of MJD, particularly SH-SY5Y cell line and neuronal cultures of cerebellum, striatum, and *substantia nigra* expressing the mutated protein, demonstrated that the expression of mutant ataxin-3 promotes mitochondrial-mediated cell death, suggesting an alteration of mitochondrial function (Tsai et al., 2004; Chou et al., 2006). Later, in another *in vitro* model of MJD, it was demonstrated that the specific expression of a mutant ataxin-3 with 78 glutamines induces oxidative stress, and also revealed that mitochondrial DNA (mtDNA) copy is decreased in the *in vitro* model of MJD, as well in MJD patients (Yu et al., 2009). Another study, using a MJD mouse model, clarified that mitochondria from MJD animals are dysfunctional (Laco et al., 2012). More recently, it was shown that mtDNA is damaged in blood and brain samples from a transgenic MJD mouse model, suggesting that in fact mitochondrial function can be compromised (Kazachkova et al., 2013; Ramos et al., 2015). Altogether, these results

suggest that mitochondrial dysfunction is underlying MJD pathogenesis. Although, a clear explanation about how a pathogenesis that is mainly focused on the nucleus generates a mitochondrial dysfunction, is still lacking. Furthermore, the late onset of Machado-Joseph disease suggests that an accumulation of changes can contribute to the pathogenesis of the disease.

Regarding mitochondrial assembly, there are approximately 90 genes that codify the subunits of the oxidative phosphorylation system (OXPHOS). Thirteen subunits of the OXPHOS system remain codified by mitochondrial DNA (mtDNA) and the other are codified by the nuclear DNA (reviewed in Tao et al., 2014). For a perfect OXPHOS subunits assembly, it is necessary a functional communication between the nucleus and mitochondria, to form stoichiometric OXPHOS complexes. There are two main nuclear transcriptional factors, namely nuclear respiratory factor 1 and 2 (NRF-1 and NRF-2), that regulate the expression of nuclear-encoded proteins, such as mitochondrial transcription factor A (TFAM) that carry out the replication, transcription, and translation of the mtDNA. It was demonstrated, in muscle cells, that with aging there is a decrease of the nuclear oxidized nicotinamide adenine dinucleotide (NAD+) levels, leading to a disruption between nuclear- and mitochondrial-encoded OXPHOS subunits stoichiometry (Gomes et al., 2013). This decrease in nuclear NAD+ led to a reduction on SIRT1 activity and to a consequent decrease of TFAM expression, generating a dysregulation on the mtDNA replication, transcription, and translation (Gomes et al., 2013). This process was prevented by caloric restriction and was completely reversed by raising NAD+ levels (Gomes et al., 2013). All these evidences show that, in muscle cells, nuclear NAD+ decrease is the underlying mechanism related with the mitochondrial dysfunction associated with aging.

Mammalian sirtuins (SIRT1-7) are a conserved family of NAD+-dependent deacetylases that regulate physiological responses to the environment (Haigis and Sinclair, 2010). Some of the health benefits associated with SIRTs, particularly with SIRT1, the most studied sirtuin that is mainly located at nucleus, have been linked to improved mitochondrial function (Baur et al., 2006; Gerhart-Hines et al., 2007; Price et al., 2012). Besides its role as coenzyme in redox reactions, NAD+ is an important substrate not only for sirtuins, but also for the following enzymes: 1) poly (ADP-ribose) polymerases (PARPs); and 2) cyclic ADP-ribose (cADPR) synthases (CD38 and CD157) (reviewed in Verdin, 2015). These enzymes consume NAD+ and to maintain homeostatic NAD+ levels, cells primarily use the NAD+-salvage pathway (reviewed in Verdin et al., 2015). This salvage pathway starts with nicotinamide (NAM) that regulates the activity of NAD+-consuming enzymes. Nicotinamide phosphoribosyltransferase (NAMPT) recycles

NAM into nicotinamide mononucleotide (NMN), and nicotinamide mononucleotide adenylytransferase (NMNAT) recycles NMN into NAD^+ (see Figure 1.17 of Introduction section). Changes in NAD^+ levels can be related with the dysregulation of the regeneration or consumption pathways of NAD^+. In Chapter 2 we demonstrated that SIRT1 is compromised, but nothing is known regarding NAD^+ and about how can this interfere with MJD pathogenesis. Therefore, we aimed to unravel the potential nuclear changes that are on the basis of the mitochondrial dysfunction.

Here, we provide evidences suggesting that nuclear-mitochondrial communication is dysregulated in the cerebellum of a transgenic MJD mouse model. We also demonstrate that NAD^+ is strongly reduced in the cerebellum of these animals and this decrease could be related to the changes in nuclear-mitochondrial communication. Furthermore, we also provide evidence suggesting that this NAD^+ decrease is related with the reduction of NMNAT1 and with the increase in CD38 levels. The increase of NAD^+ was able to restore the normal nuclear-mitochondrial communication markers, and also to restore the normal mitochondrial function. Altogether, these results open a window for new targets to treat MJD.

3.3 <u>Materials and Methods</u>

3.3.1 Animals

As referred in Chapter 2, C57Bl/6-background transgenic MJD mice and age-matched wild-type control mice were obtained from backcrossing heterozygous males with C57Bl/6 females (obtained from Charles River, Barcelona, Spain). Transgenic mice were initially acquired from Hirokazu Hirai from Kanazawa University, Japan (Torashima et al., 2008; Oue et al., 2009), and a colony of these transgenic mice was established in the Center for Neuroscience and Cell Biology of University of Coimbra. Transgenic mice express N-terminal-truncated human ataxin-3 with 69 repeats and an N-terminal hemagglutinin (HA) epitope specifically in cerebellar Purkinje cells, driven by a L7 promotor. Genotyping was performed by PCR analysis of DNA from ears. Five-week-old C57Bl/6 mice submitted to the stereotaxic surgery (obtained from Charles River, Barcelona, Spain) were also used. Mice were housed under conventional 12-hour light-dark cycle in a temperature controlled room with water and food provided *ad libitum*. The experiments were carried out in accordance with the European Community directive (2010/63/EU) for the care and use of laboratory animals. Researchers received adequate training (FELASA certified course) and certification to perform the experiments from Portuguese authorities (Direção Geral de Veterinária).

3.3.2 Viral vectors production

Lentiviral vectors encoding for: i) mutant ataxin 3 (LV-PGK-Atx3 72Q) (Alves et al., 2008b); ii) normal ataxin 3 (LV-PGK-Atx3 27Q) (Alves et al., 2008b); iii) NMNAT1 (LV-PGK-NMNAT1); iv) EGFP (LV-PGK-EGFP); v) a negative short hairpin RNA (LV-PGK-EGFP-H1-shRNA CNTL); and vi) a short hairpin RNA targeting NMNAT1 (LV-PGK-EGFP-H1-shRNA NMNAT1) were produced in HEK293T cell line with a four-plasmid system, as previously described (de Almeida et al., 2001). Lentiviral particles were suspended in sterile 1% bovine serum albumin in phosphate buffered solution (PBS). The viral particle content of batches was evaluated by assessing HIV-1 p24 antigen levels by ELISA (Retro Tek, Gentaur, Paris, France). Concentrated viral stocks were stored at -80ºC, until use.

3.3.3 *In vivo* injection into striatum

As described in Chapter 2, mice were anesthetized with avertin (250 mg/kg body weight, intraperitoneally). Concentrated viral stocks were thawed on ice and diluted viral suspensions were prepared. We stereotaxically injected in striatum, 400 ng of p24 antigen of each lentiviral vector in a final total volume of 2.5 μL. We performed a total of three independent experiments, where we injected lentiviral vectors encoding for: i) shRNA CNTL (left hemisphere) or shRNA NMNAT1 (right hemisphere); ii) Atx3 72Q + shRNA CNTL (left hemisphere) or Atx3 72Q + shRNA NMNAT1 (right hemisphere); iii) Atx3 72Q + EGFP (left hemisphere) or Atx3 72Q + NMNAT1 (right hemisphere). The coordinates that we used were: anteroposterior: +0.6 mm; lateral: ±1.8 mm; ventral: -3.3 mm; tooth bar: 0. These coordinates correspond to the internal capsule, a large fiber passing through the middle of the striatum dividing both dorsoventral and mediolateral structures. After the surgery, mice were maintained in their home cages and were sacrificed four weeks later for immunohistochemical analysis, and morphological and neurochemical changes in the striatum.

3.3.4 Histological processing

3.3.4.1 Tissue preparation: As described in Chapter 2, with some modifications, mice were sacrificed with an overdose of avertin (625 mg/kg body weight, intraperitoneally). Transcardial perfusion with PBS and fixation with 4% paraformaldehyde were performed. Brains were collected and post-fixed in 4% paraformaldehyde for 24 hours, and cryoprotected by incubation in 25% sucrose/phosphate buffer for 36/48 hours. After that, dry brains were frozen at -80ºC and 25 μm coronal sections were sliced using a cryostat (LEICA CM3050S, Leica Microsystems) at -21ºC. Slices were collected in anatomical series and stored in 48-well trays, as free-floating sections in PBS supplemented with 0.05% (m/v) sodium azide. The trays were stored at 4º C, until immunohistochemical and other procedures.

3.3.4.2 Immunohistochemical processing: As described in Chapter 2, after the blockage of endogenous peroxidases with phenylhidrazyne/phosphate solution and incubation in PBS/0.1% Triton X-100 with 10% normal goat serum (Gibco), free-floating sections were overnight incubated at 4ºC in blocking solution with primary antibodies: mouse monoclonal anti-ataxin 3 antibody (1H9; 1:5000; #5360 Merck Millipore), rabbit anti-dopamine and cyclic AMP-regulated neuronal phosphoprotein 32 (DARPP-32) antibody (1:1000; AB#10518 Merck Millipore); followed by incubation with respective

biotinylated secondary goat anti-mouse or anti-rabbit antibodies (1:200; Vector Laboratoires). Bound antibodies were visualized using the VECTASTAIN® ABC kit, with 3',3'-diaminobenzidine tetrahydrocloride (DAB metal concentrate; Pierce) as substrate. Dry sections were mounted in gelatin-coated slides, dehydrated with ethanol solutions and xylene, and mounted in Eukit (Sigma-Aldrich).

In brain sections from injected mice, area definition and analysis of protein immunoreactivities were made as previously described (Goncalves et al., 2013).

Staining was visualized with Zeiss Axioskop 2 plus or Zeiss Axiovert 200 imaging microscopes (Carl Zeiss MicroImaging, Oberkochen, Germany) equipped with AxioCam HR color digital cameras (Carl Zeiss Microimaging) and 35, 320, 340, and 363 Plan-Neofluor or 363 Plan/Apochromat objectives using the AxioVision 4.7 software package (Carl Zeiss Microimaging). Quantitative analysis of fluorescence was performed with a semiautomated image-analysis software package and images were taken under identical image acquisition conditions, and uniform adjustments of brightness and contrast were made to all images (ImageJ; NIH; Bethesda, MD).

3.3.5 Analysis of the volume of DARPP-32 depletion region

The analysis of the volume of DARPP-32 depletion area was done as described in section 2.3.7 of Chapter 2.

3.3.6 Cell counts of ataxin-3 inclusions

The counting of ataxin-3 inclusions was done as described in section 2.3.8 of Chapter 2.

3.3.7 Immunoblot procedure

3.3.7.1 Tissue preparation: Tissue preparation for immunoblot procedure was done as described in section 2.2.12.1 of Chapter 2.

3.3.7.2 Western blot procedure: As described in Chapter 2, with some modifications, samples were previously denatured with 2x sample buffer (10% β-mercaptoethanol, 4% sodium dodecyl sulphate (SDS), 0,25 M Tris-HCl, 8 M urea) and incubated during 5 min at 95ºC. Equal amounts of protein (50 μg or 25 μg) were resolved

on 12% SDS-PAGE, and transferred onto polyvinylidene fluoride (PVDF) membranes (GE Healthcare) according to standard protocols. Membranes were blocked by incubation in 5% non-fat milk powder in 0.1% Tween 20 in Tris buffered saline (TBS-T), and incubated overnight at 4ºC with primary antibody: rabbit anti-NMNAT1 antibody (1:500; #ARP48889 Aviva Systems Biology); rabbit monoclonal anti-CD38 antibody (1:500; #GTX37752 GeneTex); rabbit monoclonal anti-PARP1 antibody (1:1000; #9532 Cell Signaling Technology); mouse anti-polyclonal NAMPT antibody (1:1000; #PA5-23198 Thermo Fisher Scientific); mouse anti-β-actin antibody (clone AC74; 1:5000; A5316 Sigma-Aldrich), followed by the incubation with the corresponding horseradish peroxidase-conjugated anti-mouse, anti-rabbit or anti-goat antibody (Thermo Fisher Scientific) for 1h at room temperature. Bands were revealed using Amersham ECL detection system (GE Healthcare).

3.3.8 Quantitative Real-Time Polymerase Chain Reaction (qRT-PCR)

3.3.8.1 Isolation of total RNA from mice tissues and cDNA synthesis: The isolation of total RNA from tissue and cDNA synthesis was done as described in section 2.3.13.1 of Chapter 2.

3.3.8.2 Mitochondrial DNA analysis: Animals were sacrificed with a lethal dose of avertin (625 mg/Kg body weight) and cervical dislocation. Striatum of mice was dissected, stored in tubes, frozen immediately in liquid nitrogen, and kept at -80ºC until gDNA isolation. Total DNA was extracted from striatal tissue using Quick-gDNA Miniprep kit (Zymo Research) according to manufacturer's instructions. Mitochondrial DNA (mtDNA) was amplified using primers specific for the mitochondrial cytochrome c oxidase subunit 2 (COX2) gene and normalized to genomic DNA by amplification of the ribosomal protein s18 (rsp18) nuclear gene (Table 3.1).

Table 3.1 Oligonucleotide Sequences

Gene		Sequence
Rsp18	F	5' TGTGTTAGGGGACTGGTGGACA 3'
	R	5' CATCACCCACTTACCCCCAAAA 3'
COX2	F	5' ATAACCGAGTCGTTCTGCCAAT 3'
	R	5' TTTCAGAGCATTGGCCATAGAA 3'

3.3.8.3 qRT-PCR procedure: As described in Chapter 2, with some modifications, qRT-PCR was performed in the StepOne Plus Real-Time PCR System (Applied Biosystems) using 96-well microliter plates and the SsoAdvanced SYBR Green Supermix (Bio-Rad). PCR was carried out in 10 µL reaction volume. Primers for mouse TFAM, NRF-1, NRF-2, ND1, Cytb, COX1, ATP6, NDUFS8, SDHb, Uqcrc1, COX5b, ATP5a1, NAMPT, NMNAT1, and GADPH were designed using PrimerBlast Software and oligonucleotide sequences are in Table 3.2. We also prepared the adequate negative controls. All reactions were performed in duplicate and according to the manufacturer's recommendations: 95ºC for 30 sec, followed by 45 cycles at 95ºC for 5 sec and 60ºC for 30 sec. The amplification rate for each target was evaluated from the cycle threshold (Ct) numbers obtained with cDNA dilutions, with correction for GADPH levels. The mRNA fold increase or fold decrease with respect to control samples was determined by the Pfäffl method.

Table 3.2 Oligonucleotide Sequences

Gene		Sequence
ATP5a1	F	5' CATTGGTGATGGTATTGCGC 3'
	R	5' TCCCAAACACGACAACTCC 3'
ATP6	F	5' TCCCAATCGTTGTAGCCATC 3'
	R	5' TGTTGGAAAGAATGGAGTCGG 3'
COX1	F	5' CCCAGATATAGCATTCCCACG 3'
	R	5' ACTGTTCATCCTGTTCCTGC 3'

Gene (cont.)		Sequence (cont.)
COX5b	F	5' ACCCTAATCTAGTCCCGTCC 3'
	R	5' CAGCCAAAACCAGATGACAG 3'
Cytb	F	5' CCCACCCCATATTAAACCCG 3'
	R	5' GAGGTATGAAGGAAAGGTATAAGGG 3'
GAPDH	F	5' TGGAGAAACCTGCCAAGTATGA 3'
	R	5' GGTCCTCAGTGTAGCCCAAG 3'
NAMPT	F	5' TGGCCTTGGGGTTAATGTGT 3'
	R	5' TAACAAAGTTCCCCGCTGGT 3'
ND1	F	5' TGCACCTACCCTATCACTCA 3'
	R	5' GGCTCATCCTGATCATAGAATGG 3'
NDUFS8	F	5' GTTCATAGGGTCAGAGGTCAAG 3'
	R	5' TCCATTAAGATGTCCTGTGCG 3'
NMNAT1	F	5' CCTTCAAGGCCTGACAACATC 3'
	R	5' TAAAAGAGCCACAGGCCAGG 3'
NRF-1	F	5' TGGAACAGCAGTGGCAAGATCTCA 3'
	R	5' GGCACTGTACAGGATTTCACTTGC 3'
NRF-2	F	5' AAAGCACAGCCAGCACATTC 3'
	R	5' GGGATTCACGCATAGGAGCA 3'
SDHb	F	5' ACCCCTTCTCTGTCTACCG 3'
	R	5' AATGCTCGCTTCTCCTTGTAG 3'
TFAM	F	5' TAGGCACCGTATTGCGTGAG 3'
	R	5' GTGCTTTTAGCACGCTCCAC 3'
Uqcrc1	F	5' ATCAAGGCACTGTCCAAGG 3'
	R	5' TCATTTTCCTGCATCTCCCG 3'

3.3.9 Engineering of short hairpin RNA

A negative short hairpin RNA (shCNTL) and a shRNA targeting mouse NMNAT1 (shNMNAT1) were created. For each one, a pair of oligomers was designed. The sequences of each pair of oligomers used are below, in Table 3.3. Each pair of oligomers was annealed and inserted in linearized (with BglII and HindIII restriction enzymes) pENTR/pSUPER+ vector (AddGene 575-1). The H1-shRNA cassette was then transferred, with LR clonase recombination system, into SIN-cPPT-PGK-EGFP-WHV-LTR gateway vector.

Table 3.3 Oligonucleotide sequences.

Oligo		Sequence
shCNTL	F	5'GATCCCCCAACAAGATAAGAGCACCAATTCAAGAGATTGGTGCTCTTCATCTTGTTG3TTTTTA 3'
	R	5'AGCTTAAAAACAACAAGATGAAGAGCACCAATCTCTTGAATTGGTGCTCTTCATCTTGTTGGGG 3'
shNMNAT1	F	5'GATCCCCTGACGCTCAGAAATTCATCTATTCAAGAGATAGATGAATTTCTGAGCGTCATTTTTA 3'
	R	5'AGCTTAAAAATGACGCTCAGAAATTCATCTATCTCTTGAATAGATGAATTTCTGAGCGTCAGGG 3'

3.3.10 NMNAT1 gene cloning

To clone NMNAT1 into a lentiviral vector, a pair of oligomers was designed. The sequences of the pair of oligomers were: forward - 5'GTCCAGATGGACTCATCCAAGA AGACAGAG3' and reverse – 5'GCGGCCGCTCACAG AGTGGAATGGTTGTG3'. Using these primers and with a mouse cerebellar cDNA as template, a polymerase chain reaction was conducted using *Phusion* polymerase, under standard conditions. The PCR product was then purified from an 1% agarose gel. This product was annealed and inserted in a linearized (with BamHI and XhoI restriction enzymes) pENTR/FLAG vector (Addgene 17423). The FLAG-NMNAT1 cassette was then transferred, with LR clonase recombination system, into SIN-cPPT-PGK-attL1-cCDB-attL2-WPRE-LTR gateway vector.

3.3.11 NAD⁺ measurement

Animals were sacrificed and tissues were dissected, and immediately preserved in liquid nitrogen. NAD^+ levels from cerebellar and striatal tissues were quantified with a commercially available kit (Promega), according to the manufacturer's instructions. Total protein concentration was determined in each sample with BCA protein assay (Pierce Biotechnology, Thermo Fisher Scientific) and was used to normalize NAD^+ levels. Values were expressed as pmol NAD^+/µg protein.

3.3.12 Neuroblastoma cell culture

As described in Chapter 2, with some modifications, mouse neuroblastoma cell line (Neuro-2a cells) was obtained from the American Type Culture Collection cell biology bank (ATCC, CCL-131). This cell line was incubated in Dulbecco's modified Eagle's medium supplemented with 10% foetal bovine serum, 100 U/mL penicillin, and 100 mg/mL streptomycin (Gibco) (complete medium) at 37ºC in 5% CO_2/air atmosphere. Cells were plated in a six-well plate and 24 hours later were co-infected with lentiviral vectors encoding for: i) normal ataxin-3 (LV-PGK-Atx3 27Q), ii) mutant ataxin-3 (LV-PGK-Atx3 72Q) and for EGFP (LV-PGK-EGFP), iii) for mutant ataxin-3 (LV-PGK-Atx3 72Q) and for NMNAT1 (LV-PGK-NMNAT1) at the ratio of 100 nf (for i) condition) or 50 ng (for ii) and iii) conditions) of p24 antigen/10^5 cells of each. At 2 weeks post-infection, cells were used for respirometry analysis.

3.3.13 Neuroblastoma cell respirometry

Two weeks after Neuro2a cells infection with the specific lentiviral vectors, cells were plated in a Seahorse 24-well XF cell culture microplates. Prior to measurements, cells were gently rinsed in pre-warmed (37ºC) XF cell Mito stress test assay medium, supplemented with glucose and L-glutamine. Cells were then placed in an unbuffered, humidified incubator at 37ºC for one hour to allow temperature and pH calibration. We observed the cells prior and after the media addition, and after the calibration of the sensor cartridge, we loaded the cells onto the Seahorse XF24 analyzer (Seahorse Bioscience). After an equilibration step, basal oxygen consumption rate (OCR, pmoles/min) was recorded using 3-min mix, 2-min wait, and 3-min measure (looped 3 times) cycles prior to the injection of oligomycin to inhibit the ATP synthase. After that, three more measurement loops were recorded before the injection of carbonyl cyanide p-(trifluoromethoxy)phenylhydrazone (FCCP) to induce maximal OCR. Again, after that,

we recorded 3 more measurement loops, and pyruvate was injected to determine if maximal OCR following FCCP addition was substrate limited. To assess non-mitochondrial OCR, inhibitors of mitochondrial complex III and I, respectively antimycin A and rotenone were injected after 3 measurement loops. Two measurement loops after this last addition were recorded. The injectates were prepared in the same XF cell Mito stress test assay medium. Then they were sequentially injected as indicated, through ports in the XF24 calibration cartridge, as indicated by the manufacturer's, to final concentrations of: 1 µg/mL oligomycin, 1 µM FCCP, 10 mM pyruvate, 1µM antimycin, and 500 nM rotenone.

3.3.14 Statistical Analysis

Statistical analysis was performed with paired or unpaired Student's t-test and one-way or two-way Analysis of Variance (ANOVA), followed by the adequate post-hoc test, for multiple comparisons. Results are expressed as mean±standard error of the mean (SEM). Significant thresholds were set at $p < 0.05$, $p < 0.01$ and $p < 0.001$, as defined in the text.

3.4 <u>Results</u>

3.4.1 Nuclear-mitochondrial communication is disrupted in Machado-Joseph disease mouse models

Mitochondrial dysfunction is one of the mechanisms inherent to MJD pathogenesis (Tsai et al., 2004; Chou et al., 2006; Yu et al., 2009; Laco et al., 2012). Although, it is not completely understood how a mainly nuclear-related pathogenesis can lead to the mitochondrial dysfunction. In order to understand if in MJD the nuclear-mitochondrial communication is dysregulated, we used cerebellar samples from a transgenic MJD mouse model that expresses mutant ataxin-3, specifically in cerebellar Purkinje cells (Torashima et al., 2008). We evaluated three main nuclear-encoded transcription factors that are related with the regulation of mitochondrial DNA (mtDNA) replication, transcription and translation, namely mitochondrial transcription factor A (TFAM) and its downstream regulators, the nuclear respiratory factor 1 and 2 (NRF-1 and NRF-2; Campbell et al., 2012).

We evaluated the mRNA levels of NRF-1, NRF-2, and the mRNA and protein levels of principal marker - TFAM - in the cerebellum of eight weeks-old transgenic MJD mice, in comparison with age-matched littermate wild-type mice (Figures 3.1A-D). We observed that in MJD cerebellum, the mRNA levels of NRF-1, NRF-2, and TFAM are significantly lower compared to WT mice (Figures 3.1A-C). Furthermore, by western blot, we observed that the protein levels of TFAM, the major final player in the nuclear-mitochondrial communication, are also reduced in the cerebellum of MJD mice, compared to WT (Figure 3.1D).
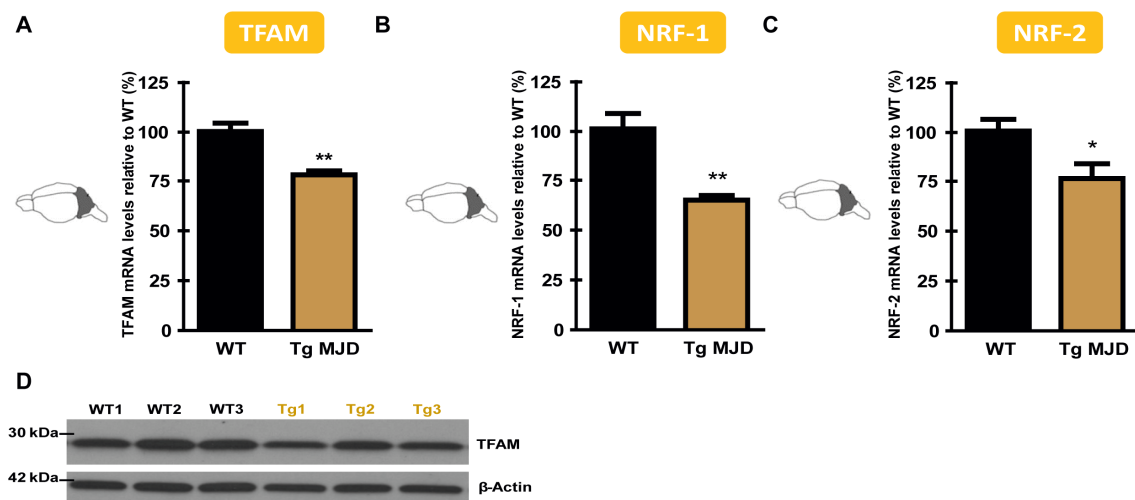
Figure 3.1 <u>Nuclear-mitochondrial communication markers are changed in the cerebellum of transgenic MJD mice, in comparison with age-matched wild type-mice.</u>

Figure 3.1 (cont.) (A-C) mRNA levels of TFAM, NRF-1, and NRF-2 in the cerebellum of transgenic MJD mice, in comparison with wild-type. **(D)** Immunoblotting of TFAM in cerebellar samples of transgenic MJD mice, in comparison with wild-type. NRF-1: Nuclear Respiratory Factor 1; NRF-2: Nuclear Respiratory Factor 2; TFAM: Mitochondrial Transcription Factor A; Tg MJD: Transgenic MJD; WT: Wild-Type. Data represent mean ± SEM. *p<0.05; **p<0.01 compared to WT. **(A-C)** Unpaired Student's t-test. WT n=5; Tg MJD n=5.

We decided to evaluate one subunit of each complex codified by nuclear DNA and one codified by mitochondrial DNA. Complex II is only composed by subunits codified by nuclear DNA, so we evaluated the mRNA levels of a total of 9 subunits (Figure 3.2A). We evaluated whether OXPHOS decline in MJD cerebella samples might be due to a specific loss of mitochondrially-encoded genes expression. To do this we used cerebellar samples from transgenic MJD mice and we observed that only the levels of the transcripts of the subunits codified by mtDNA (ND1, Cytb, COX1, and ATP6) were decreased (Figures 3.2B-E), and no significant changes were observed in the transcripts of the subunits encoded by the nuclear genome (NDUFS8, SDHb, Uqcrc1, COX5b, and ATP5a1) (Figures 3.2F-J). These results indicate that in MJD occurs a specific decrease of the mitochondrially-encoded subunits, suggesting an alteration in the regulation of the mtDNA transcription, corroborating the previous results (Figure 3.1).
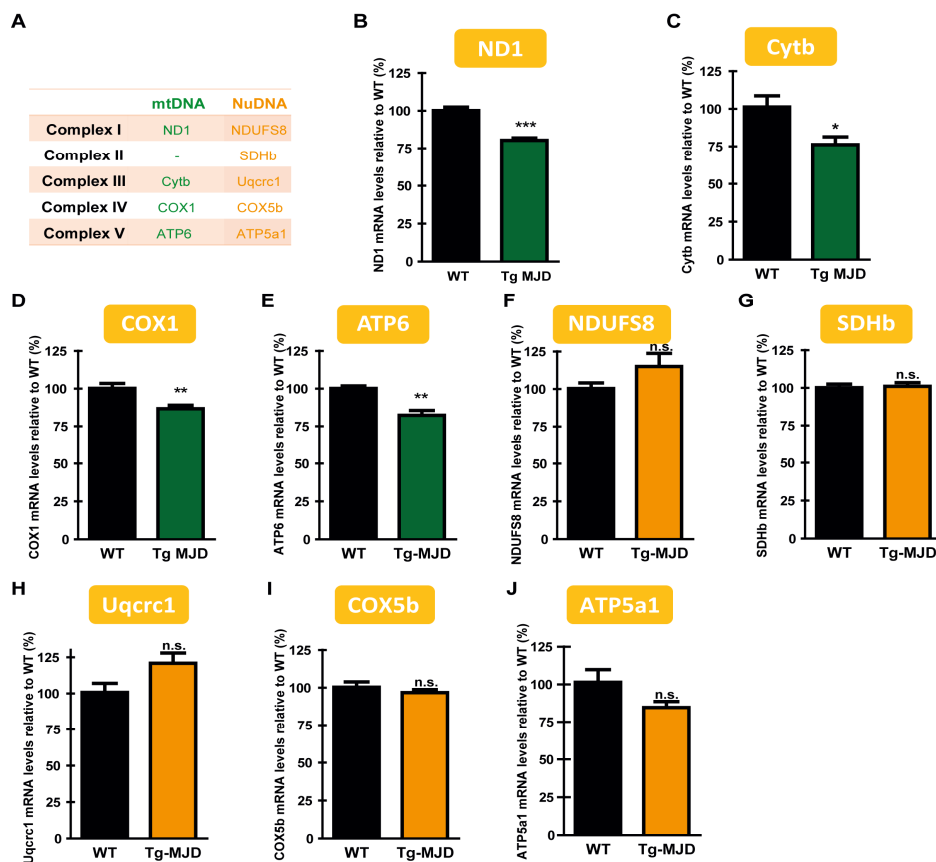
Figure 3.2 Cerebella from MJD mice have lower levels of mRNA of mitochondrial-encoded OXPHOS subunits with no difference in mRNA of nuclear-encoded OXPHOS

Figure 3.2 (cont.) <u>subunits, in comparison to cerebella from wild-type mice.</u> **(A)** Summary of the subunits indicating the complex that each belong and if they are encoded by nuclear or mitochondrial DNA. **(B-E)** mRNA levels evaluated by qRT-PCR of ND1, Cytb, COX1, and ATP6, that are OXPHOS subunits encoded by mitochondrial DNA, that belong to the complexes I, III, IV, and V, respectively. **(F-J)** mRNA levels evaluated by qRT-PCR of NDUFS8, SDHb, Uqcrc1, COX5b, and ATP5a1, that are OXPHOS subunits encoded by nuclear DNA, that belong to the mitochondrial complexes I, II, III, IV, and V, respectively. <u>ATP5A1</u>: ATP synthase subunit 5 alpha 1; <u>ATP6</u>: ATP synthase Fo subunit 6; <u>COX1</u>: Cytochrome c oxidase subunit I; <u>COX5b</u>: Cytochrome c oxidase subunit 5b; <u>Cytb</u>: Cytochrome b; <u>mtDNA:</u> Mitochondrial DNA; <u>ND1</u>: NADH-ubiquinone oxidoreductase core subunit 1; <u>NDUFS8</u>: NADH-ubiquinone oxidoreductase core subunit S8; <u>NuDNA:</u> Nuclear DNA; <u>SDHb</u>: Succinate dehydrogenase [ubiquinone] iron-sulfur subunit; <u>Tg MJD</u>: Transgenic MJD; <u>WT</u>: Wild-Type. Data represent mean ± SEM. n.s. $p > 0.05$; *$p < 0.05$; **$p < 0.01$; ***$p < 0.001$; compared to WT. **B-J.** Unpaired Student's t-test. WT n=5; Tg MJD n=5.

These results suggest that the mitochondrial dysregulation observed in MJD can be related to nuclear alterations in the expression of nuclear-mitochondrial communication markers, particularly TFAM. These nuclear alterations that will disrupt the nuclear-mitochondrial communication, lead to mitochondrial changes in the replication, transcription, and translation of mtDNA, being negatively translated in the expression of the mtDNA-encoded OXPHOS subunits.

3.4.2 NAD$^+$ is severely compromised in the cerebellum of transgenic Machado-Joseph disease mice

Sinclair's group showed that in aged muscle cells, decreased levels of NAD$^+$ explains nuclear-mitochondrial communication dysregulation (Gomes et al., 2013). Moreover, NAD$^+$ decline led to a decrease in SIRT1 activity that consequently decreased TFAM expression (Gomes et al., 2013). This mechanism was described in muscle cells, but it is not known if it also occurs in neurons undergoing neurodegeneration. Therefore, to find a possible mechanism for the nuclear-mitochondrial communication changes observed in the transgenic MJD mice, we evaluated NAD$^+$ levels in the cerebellum, the main affected brain area, of young adult transgenic MJD mice.

We observed that cerebella of transgenic MJD mice have 90.0±3.4% lower NAD$^+$ levels, in comparison with age-matched wild-type mice (Figure 3.3A). In order to understand if this strong decline is specific of the affected MJD brain region, we also measured the NAD$^+$ levels at a non-affected brain region of this mouse model of MJD - the striatum. We did not observe any difference between the NAD$^+$ levels in the striata of transgenic MJD and WT animals (Figure 3.3B). These results suggest that the lower levels of NAD$^+$ are specifically associated with MJD neuropathology.
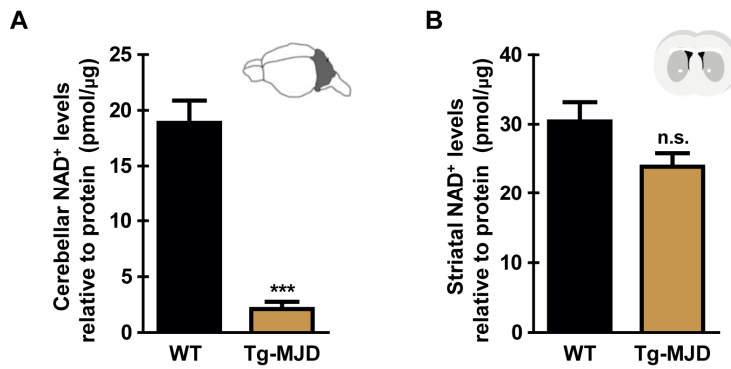
Figure 3.3 <u>NAD⁺ levels in two different brain regions – cerebellum and striatum - revealed that NAD⁺ levels are strongly declined specifically in the cerebellum of diseased mice.</u> **(A)** Cerebellar or striatal **(B)** NAD⁺ levels in transgenic MJD, in comparison with age-matched wild-type mice normalized for the protein content of each sample. Results are expressed as pmol of NAD⁺ for μg of protein. <u>Tg MJD</u>: Transgenic MJD; <u>WT</u>: Wild-Type. Data represent mean ± SEM. n.s. $p > 0.05$; ***$p < 0.001$ compared to WT. **(A-B)** Unpaired Student's t-test. WT n=5; Tg MJD n=4.

These results demonstrate that NAD⁺ is severely compromised in the cerebellum of transgenic MJD mice, which could be related with the nuclear-mitochondrial dysregulation abovementioned.

3.4.3 NAD⁺-salvage pathway is compromised and NADases are increased in the cerebellum of transgenic Machado-Joseph disease mice

Afterwards, we investigated the mechanisms that could explain the lower levels of NAD⁺ in the cerebellum of transgenic MJD mice. The very low levels of NAD⁺ in the cerebellum of MJD mice could be related to a low rate of NAD⁺ regeneration or its high consumption by different enzymes. The regeneration pathway is the major contributor to the maintenance of NAD⁺ levels and two enzymes are involved, namely: nicotinamide phosphoribosyltransferase (NAMPT) and nicotinamide mononucleotide adenylyltransferase (NMNAT). NMNAT has 3 isoforms (NMNAT1-3), and NMNAT1 is the nuclear isoform (Berger et al., 2005). The decrease on NMNAT1 levels was associated to nuclear NAD⁺ levels decline in aged muscle cells (Gomes et al., 2013). Besides that, the increase in NAD⁺ consumption could also contribute to the decrease of NAD⁺ levels. Plus sirtuins, there are other enzymes that consume NAD⁺, namely poly-ADP ribose polymerases (PARPs) and cyclic ADP-ribose (cADPR) synthases (CD38 and CD157). In order to understand why NAD⁺ is so decreased in MJD cerebella, we evaluated the levels of key enzymes responsible for NAD⁺ regeneration (NAMPT and

NMNAT1) and the main enzymes that are competitors in the consumption of NAD⁺ (PARP1 and CD38).

We evaluated by western blot and qRT-PCR, protein and mRNA levels of NAMPT, the rate-limiting enzyme that converts NAM into NMN, in the first step of the NAD⁺-salvage pathway. We did not observe any difference in the mRNA and protein levels of NAMPT between the cerebellar samples from young adult transgenic MJD and wild-type mice (Figures 3.4A,B). Furthermore, we evaluated the levels of NMNAT, the second enzyme that converts NMN into NAD⁺, and particularly, due to our nuclear-centered hypothesis, we evaluated the isoform specifically located at the nucleus, the NMNAT1 (Berger et al., 2005). We observed that mRNA and protein levels were lower in the cerebellum of transgenic MJD mice, compared to WT mice (Figures 3.4C,D). These results suggest that NAD⁺ regeneration pathway is compromised in the nucleus. We decided to evaluate, by western blot, two main NAD⁺-consuming enzymes: PARP1 and CD38. We did not observe any difference regarding PARP1 expression, although a higher levels of CD38 were found in the cerebellum of young adult transgenic MJD mice, in comparison with WT mice (Figures. 3.4E,F).
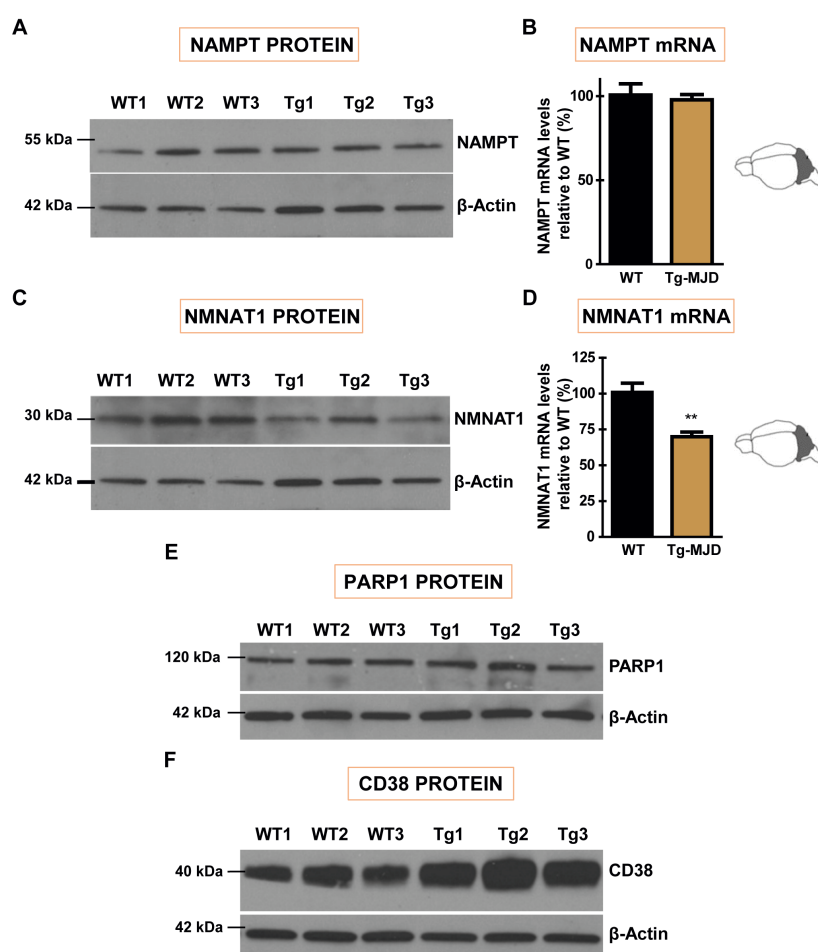
Figure 3.4 <u>Alterations in the expression of cerebellar NAMPT and NMNAT1 enzymes involved in NAD⁺-salvage pathway, and cerebellar PARP1 and CD38 enzymes that</u>

Figure 3.4 (cont.) consume NAD$^+$. **(A-B)** Protein **(A)** and mRNA **(B)** levels of NAMPT, evaluated by immunoblot and qRT-PCR, respectively, in the cerebellum of transgenic MJD mice, in comparison with age-matched non-diseased mice. **(C-D)** Protein and mRNA levels of NMNAT1 evaluated by immunoblotting **(C)** and qRT-PCR **(D)**, in the cerebellum of transgenic MJD mice, in comparison with age-matched non-diseased mice. **(E-F)** Immunoblot for PARP1 **(E)** and CD38 **(F)** in the cerebellum of transgenic MJD mice, in comparison with wild-type mice. CD38: Cluster of Differentiation 38; NAMPT: Nicotinamide Phosphoribosyltransferase; NMNAT1: Nicotinamide Mononucleotide Adenylyltransferase 1; PARP1: Poly-ADP Ribose Polymerase 1; Tg MJD: Transgenic MJD; WT: Wild-Type. Data represent mean ± SEM. **p<0.01 compared to WT. **(B,D)** Unpaired Student's t-test. WT n=5; Tg MJD n=4.

In sum, these results suggest that changes in two different pathways are in the basis of NAD$^+$ depletion. In one hand NMNAT1 is compromised, and thus the NAD$^+$-salvage pathway is not properly functioning, contributing to a decrease on nuclear NAD$^+$. On the other hand, the high CD38 levels indicate that NAD$^+$ is not available because CD38 is consuming it.

3.4.4 NAD$^+$ decrease through NMNAT1 genetic silencing resembles nuclear-mitochondrial communication changes observed in Machado-Joseph disease and induces the disease progression

We wondered whether the specific decline in the nuclear-mitochondrial communication components in transgenic MJD mice might be due, at least in part, to the decrease of nuclear NAD$^+$ levels. To test this, we designed and developed a short hairpin RNA targeting the specific nuclear enzyme responsible for the conversion of NMN into NAD$^+$, namely NMNAT1. Reducing NMNAT1 levels, nuclear NAD$^+$ levels will be reduced (Gomes et al., 2013), and we can test the effect in nuclear-mitochondrial communication.

We constructed lentiviral vectors encoding for a negative short hairpin RNA (shRNA CNTL) that does not have any known target in mouse, and we also constructed lentiviral vectors encoding for a short hairpin RNA targeting NMNAT1 (shRNA NMNAT1). We stereotaxically injected the lentiviral vectors in a specific brain region, namely striatum. We injected shRNA CNTL in the left hemisphere and shRNA NMNAT1 in the right hemisphere (Figure 3.5A). Four weeks after the surgery animals were sacrificed, we dissected the striatum and evaluated, by qRT-PCR, the mRNA levels of NMNAT1. We observed that NMNAT1 mRNA levels were decreased around 63% (Figure 3.5B) in the hemisphere where the shRNA NMNAT1 was overexpressed, indicating that our strategy was efficient in terms of NMNAT1 knockdown. Furthermore, when we evaluated

the mRNA levels of the three nuclear transcription factors related with nuclear-mitochondrial communication (TFAM, NRF-1, and NRF-2) we observed a decrease in all of them, at a percentage similarly observed in the cerebellum of the transgenic MJD mice (Figures 3.1A-C and 3.5C-E). We also observed a decline in the mtDNA content, supporting the idea that mitochondria are dysregulated (Figure 3.5F). Moreover, we aimed to investigate whether a higher decrease in the NMNAT1 levels would interfere with MJD progression. To do this in the striatal lentiviral model of MJD, we stereotaxically co-injected in the left hemisphere lentiviral vectors encoding for the shRNA CNTL and for the shRNA NMNAT1 in the right hemisphere, each one together with lentiviral vectors encoding for mutant ataxin-3 (Figure 3.5G). Four weeks after the surgery we sacrificed the mice, and we performed some analysis of neuropathology. By immunohistochemistry we counted the number of striatal mutant ataxin-3 inclusions and we observed a significant increase of their number in the hemisphere where NMNAT1 was genetically silenced (Figures 3.5H-I). We also evaluated the striatal DARPP-32 volume depletion and we observed a significant increase in the hemisphere where NMNAT1 was genetically silenced (Figures 3.5J-K). These results indicate that NMNAT1 knockdown, and consequently nuclear NAD$^+$ decrease, has a negative effect on MJD progression.
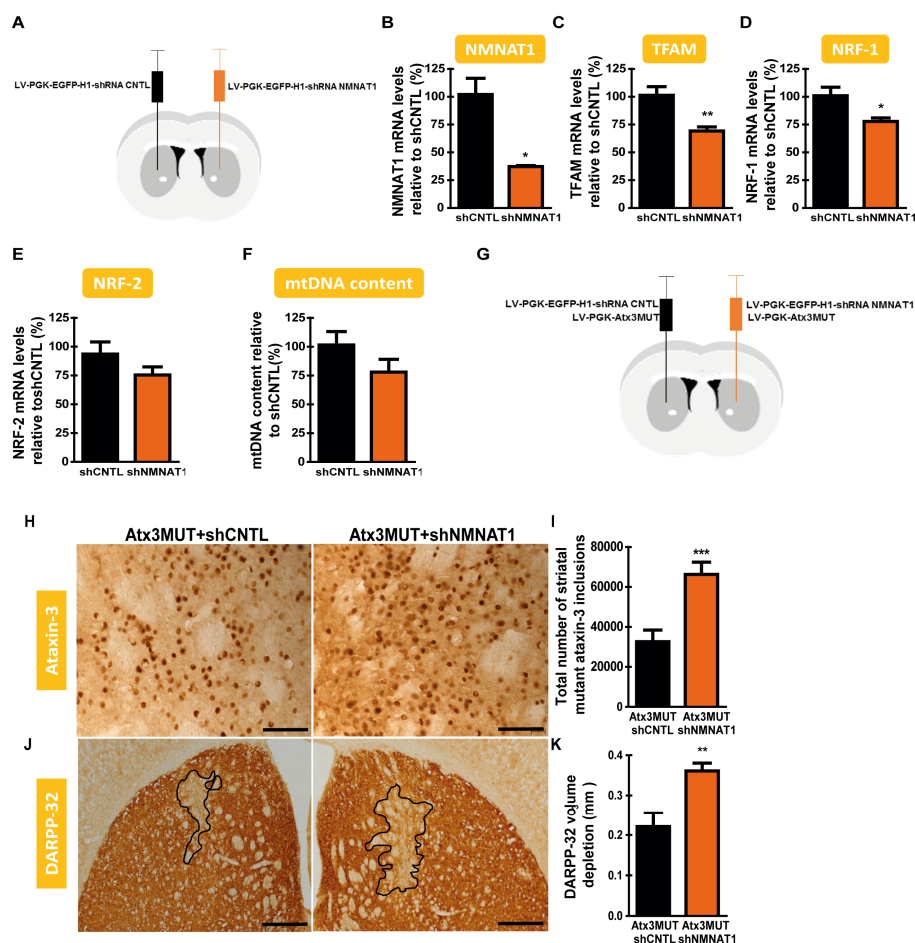
Figure 3.5 NMNAT1 genetic silencing resembles nuclear-mitochondrial alterations observed in MJD, and accelerates the disease progression. **(A)** Schematic

Figure 3.5 (cont.) representation demonstrating that we stereotaxically injected in the striatum of 5-week-old C57Bl/6 mice, lentiviral vectors encoding for a negative shRNA (left hemisphere) and for a shRNA targeting NMNAT1 (right hemisphere). **(B)** mRNA levels of NMNAT1 in the striatum, showing a knockdown around 60% in the hemisphere where NMNAT1 was genetically silenced, in comparison with the control hemisphere. **(C-E)** TFAM, NRF-1, and NRF-2 mRNA levels, evaluated by qRT-PCR in the striatal hemisphere where a negative shRNA was transduced, in comparison with the hemisphere where NMNAT1 was genetically silenced. **(F)** Mitochondrial DNA content based on COX2 *vs* Rsp18 expression in the striatal hemisphere where a negative shRNA was transduced, in comparison with the hemisphere where NMNAT1 was genetically silenced. **(G)** Schematic representation demonstrating that we stereotaxically co-injected in the striatum lentiviral vectors encoding for a mutant ataxin-3 and a negative shRNA (left hemisphere) and in the other hemisphere for mutant ataxin-3 and a shRNA targeting NMNAT1. **(H-I)** By immunohistochemistry (with an anti-ataxin-3 antibody - Ab 1H9; **H**), total number of mutant ataxin-3 inclusions were counted **(I)**. **(J-K)** DARPP-32 immunohistochemistry **(J)** and quantification of the volume depletion region **(K)**. Atx3MUT: Mutant ataxin-3; DARPP32: Dopamine- and cAMP-regulated phosphoprotein 32; mtDNA: Mitochondrial DNA; NMNAT1: Nicotinamide Mononucleotide Adenylyltransferase 1; NRF-1,2: Nuclear Respiratory Factor 1 and 2; TFAM: Mitochondrial Transcription Factor A; shCNTL: negative short hairpin RNA; shNMNAT1: short hairpin RNA targeting NMNAT1; shRNA: short hairpin RNA. Data represent mean±SEM. *$p<0.05$; **$p<0.01$; ***$p<0.001$ compared to shCNTL. **(B-F,I,K)** Paired Student's t-test. shCNTL n=5; shNMNAT1 n=5. **H.** Scale bar 125 μm. **J.** Scale bar: 500 μm.

As a whole, these results suggest that in fact, the decrease of NAD+ in the nucleus is related with the disruption of the nuclear-mitochondrial communication, and a higher decrease in NAD+ levels negatively contributes to MJD progression.

3.4.5 NAD+ increase through NMNAT1 overexpression reestablishes nuclear-mitochondrial communication and reinstates mitochondrial function

Next we sought to investigate if the increase on nuclear NAD+ would be sufficient to reestablish nuclear-mitochondrial communication and to recover mitochondrial dysfunction. To do this we used the same strategy than before, namely we manipulated NMNAT1 levels, and particularly this time we overexpressed NMNAT1, in order to increase NMN conversion into NAD+ in the nucleus. We also used Seahorse equipment to evaluate the potential changes induced by NMNAT1 overexpression on mitochondrial respiration.

In order to evaluate the potential changes induced by the increase in the intranuclear NAD+ levels, in the lentiviral mouse model of MJD, we stereotaxically co-injected in the right hemisphere lentiviral vectors encoding for a NMNAT1 and in the left

hemisphere encoding for EGFP, as control (Figure 3.6A). Four weeks after surgery, animals were sacrificed and striatum was dissected. To explore the potential changes on nuclear-mitochondrial communication induced by NMNAT1 overexpression, we evaluated the mRNA of the three nuclear transcription factors: TFAM, NRF-1, and NRF-2, related with mitochondrial regulation. We observed that in comparison with the negative control, that in this case was an animal injected into the striatum with lentiviral vectors encoding for the normal ataxin-3 (with 27 glutamines), the mRNA levels of all of them were reestablished in the striatum where NMNAT1 was overexpressed (Figures 3.6B-D). Furthermore, we decided to recreate the same experiment, but this time transducing a cell line, namely the Neuro2a cell line. We infected the cells with lentiviral vectors encoding for normal ataxin-3 (WT), or mutant ataxin-3 and EGFP (Atx3MUT+EGFP), or mutant ataxin-3 and NMNAT1 (Atx3MUT+NMNAT1) (Figure 3.6E). We observed that the expression of mutant ataxin-3 led to a decrease in the oxygen consumption rate (OCR), in comparison with the expression of normal ataxin-3 (Figure 3.6F). This decrease was statistically significant when we had FCCP and pyruvate, thus when we stimulated the maximal respiration (Figure 3.6G). Importantly, when NMNAT1 was overexpressed there was a completely reestablishment of all of the altered states (Figures 3.6F,G).
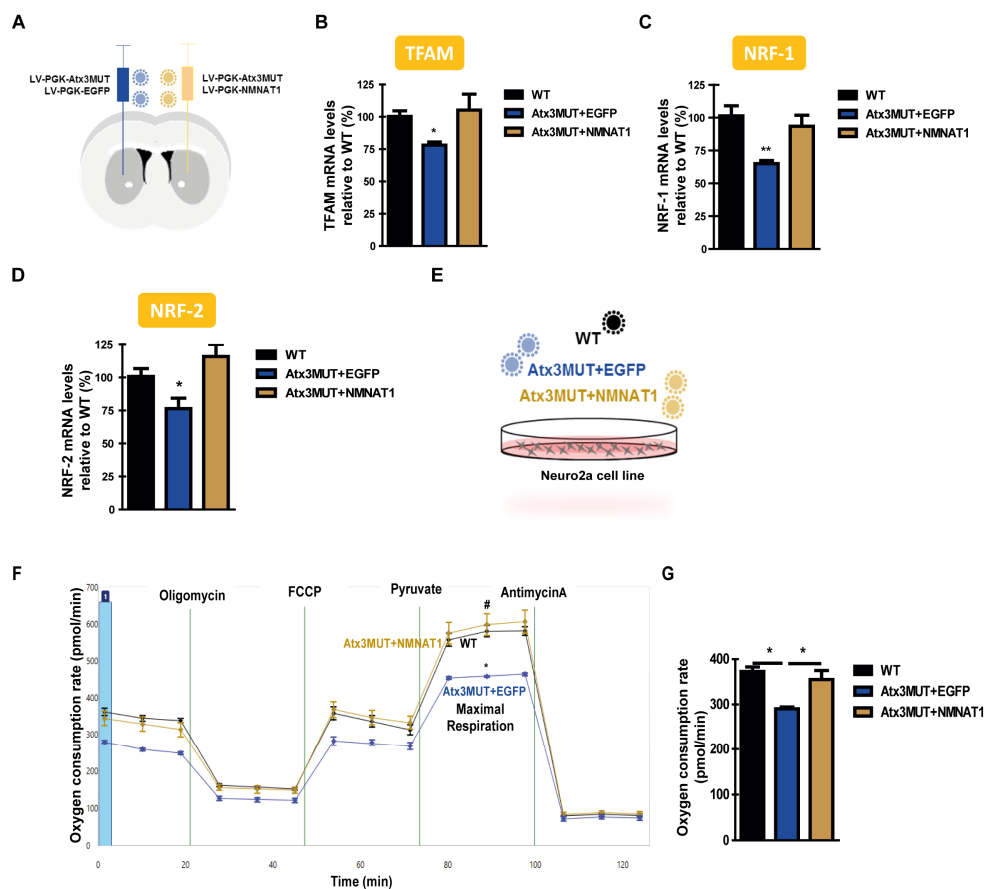
Figure 3.6 <u>NMNAT1 overexpression reestablishes nuclear-mitochondrial communication and restores mitochondrial dysfunction.</u> **(A)** Schematic representation of

Figure 3.6 (cont.) the study where we stereotaxically co-injected into the striatum lentiviral vectors encoding for mutant ataxin-3 and for EGFP (left hemisphere) or mutant ataxin-3 and NMNAT1 (right hemisphere) or wild-type ataxin-3 (not represented) in 5-week-old C57Bl/6 mice. **(B-D)** mRNA levels of TFAM, NRF-1, and NRF-2 in three groups: i) expressing normal ataxin-3 in the striatum (WT); ii) expressing mutant ataxin-3 and EGFP (Atx3MUT+EGFP) in the striatum; and iii) expressing mutant ataxin-3 and NMNAT1 (Atx3MUT+NMNAT1). **(E)** Schematic representation of the *in vitro* study where we infected Neuro2a cells with lentiviral vectors encoding for: i) normal ataxin-3 (WT); ii) mutant ataxin-3 and EGFP (Atx3MUT+EGFP); and iii) mutant ataxin-3 and NMNAT1 (Atx3MUT+NMNAT1). **(F)** Baseline-normalized oxygen consumption rate (OCR) of Neuro2a neuroblastoma cells exposed to successive additions of mitochondrial respiratory modulators that are shown. Cells received 1 μg/mL oligomycin, 1 μM FCCP, 10 mM pyruvate, and 1 μM antimycin A + 1 μM of rotenone. **(G)** Average oxygen consumption rate after the addition of FCCP and pyruvate, when maximal respiration was achieved. Atx3MUT: Mutant ataxin-3; NMNAT1: Nicotinamide Mononucleotide Adenylyltransferase 1; NRF-1,2: Nuclear Respiratory Factor 1 and 2; TFAM: Mitochondrial Transcription Factor A. Data represent mean ± SEM. */#$p < 0.05$; **$p < 0.01$; *compared to WT; #compared to Atx3MUT+EGFP. **(B-D,G)** One-way ANOVA with Bonferroni's post hoc test. **(B-D)** WT n=5; Atx3MUT+EGFP n=5; Atx3MUT+NMNAT1 n=5. **(G)** WT n=3; Atx3MUT+EGFP n=3; Atx3MUT+NMNAT1 n=3.

Altogether, these results suggest that NMNAT1 overexpression is able to reestablish nuclear-mitochondrial communication markers and this can be related with the recovery of the mitochondrial respiratory deficiency.

3.5 <u>Discussion</u>

With these studies we provide evidences demonstrating that mitochondrial dysfunction, associated with Machado-Joseph disease (MJD), is linked with a disruption in the nuclear-mitochondrial communication. We also observed that these changes are strongly related with a robust decline in the NAD^+ levels, caused by a malfunction of the NAD^+-salvage pathway and an increase in CD38, an enzyme that consumes NAD^+. The increase in nuclear NAD^+ levels, through the overexpression of NMNAT1, restored normal nuclear-mitochondrial communication, reinstating mitochondrial respiration. Hence, a nuclear dysregulation interferes with mitochondrial function and its resolution is able to restore the normal mitochondrial function.

Mitochondria are essential regulators of energy metabolism and apoptotic pathways. They do not only participate in energy conversion, through the oxidative phosphorylation pathway, but also play major roles in some cellular pathways, such as in metabolism, calcium buffering, regulation of signaling cascades, and apoptosis regulation (Nicholls, 2002). Mitochondria have been closely linked with normal aging and also with the pathogenesis of neurodegenerative diseases. During aging there is a loss of cellular homeostasis and organismal health that is strongly associated with a progressive decline in mitochondrial function (Lanza and Nair, 2010; Wallace, 2010). In age-related neurodegenerative diseases, mitochondria appear to be a dominant site for initiation and/or propagation of disease processes. There are some neurodegenerative diseases that primarily involve mitochondrial neurodegeneration. This neurodegeneration is associated with mitochondrial DNA mutations, or with mutations of nuclear-encoded mitochondrial proteins, or mutated proteins localized in multiple intracellular compartments (reviewed in Kwong et al., 2006). Furthermore, there are some diseases in which nuclear changes are involved with mitochondrial dysfunction. For example, Parkinson's disease involves mutations in the nuclear-encoded mtDNA polymerase *g*, which is associated with parkinsonism and multiple mtDNA deletions (Luoma et al., 2004). In Machado-Joseph disease the neuropathology is strongly associated with the presence of intranuclear mutant ataxin-3 aggregates (Paulson et al., 1997b). The mitochondrial dysfunction observed in MJD can have a secondary role, and is potentially related with nuclear changes. In fact, we provided evidences suggesting that in MJD occurs nuclear changes, particularly in the expression of transcription factors related with the regulation of mtDNA replication, transcription, and translation, namely TFAM and its downstream regulators (NRF-1 and NRF-2). Another clue suggesting that mitochondrial dysfunction observed in MJD is strongly related with an abnormal mtDNA

expression, potentially driven by nuclear-mitochondrial communication alterations, came from the evidence that only the transcripts of the mitochondrial OXPHOS subunits encoded by mitochondrial DNA are significantly compromised, and not the OXPHOS subunits encoded by nuclear DNA (Figure 3.2).

Recently, it was also reported that in aged muscle cells, some nuclear changes, particularly the decrease in nuclear NAD+, are associated with nuclear-mitochondrial communication disruption, and consequently with mitochondrial dysfunction (Gomes et al., 2013). Previously, we demonstrated that SIRT1 is decreased in the cerebellum of transgenic MJD mice (Figure 2.6), and this could be related with the decline in SIRT1 levels that we also observed in the same brain region (Figure 2.6). Although, we also sought to investigate if this decrease in SIRT1 activity could be also related with changes in NAD+ levels. Therefore, we evaluated the NAD+ levels in the cerebellum of transgenic MJD mice and we observed a sturdy decrease of around 90%, in comparison with age-matched non-diseased mice, and this decrease was specific of the affected brain region. Previously, it was demonstrated that NAD+ levels decrease in degenerating axons and that the prevention of this decline, for example with the increase in NMNAT1, efficiently protects axons from degeneration (Wang et al., 2005b). Although, the reason behind this decrease is still not understood. Therefore, we sought after to investigate the potential explanations for this strong decrease. When we focused on the NAD+-salvage pathway, we observed that NMNAT1 levels where significantly decreased, suggesting that NMN conversion into NAD+ is compromised in the nucleus. Likewise, we observed that CD38 is strongly upregulated in the cerebellar samples from transgenic MJD mice. It will be interesting to understand why these changes happen in the nucleus. Mutant ataxin-3 aggregates inside the nucleus (Paulson et al., 1997b), so it could be related with the decrease on NMNAT1, at a transcriptional level and/or sequestering the protein, and further work should be done to address this question. Regarding CD38, it is known that CD38 is strongly related with neuroinflammation (Banerjee et al., 2008; Mamik et al., 2011). The strong neuroinflammation present in this disease (Evert et al., 2001; Evert et al., 2006b; Mendonca et al., 2015; Goncalves et al., 2013) could be related with the increase in CD38. We provided evidence that the specific decline of nuclear NAD+ levels are strongly related with the nuclear-mitochondrial communication changes that we observed in the disease. It is not clear how the decrease in NAD+ levels are directly linked to the decrease of TFAM expression, and potentially there is some SIRT1-mediated effect on the regulation of its downstream regulators – NRF-1 and NRF-2.

There are some studies demonstrating the relevant positive role of NMNAT1 on neurodegeneration (Araki et al., 2004; Wang et al., 2005b; Sasaki et al., 2009; Avery et

al., 2009; Yahata et al., 2009; Verghese et al., 2011; Zhu et al., 2013). In fact, the NMNAT1 overexpression through gene therapy reestablished the levels of the transcription factors related with nuclear-mitochondrial communication and reestablished mitochondrial respiration, suggesting a relevant role for the disease pathogenesis.

In summary, these findings provide, for the first time, evidence of a new pathway that explains mitochondrial dysfunction in Machado-Joseph disease pathogenesis, identifying future potential targets, with implications for the treatment of MJD.

CHAPTER 4

Pharmacological activation of sirtuin 1 ameliorates neuropathology and improves motor function in a transgenic Machado-Joseph disease mouse model

Scientific advancement should aim to affirm and to improve human life.

(Nathan Deal)

4.1 <u>Abstract</u>

Machado-Joseph disease (MJD) is a neurodegenerative disease that affects mainly the cerebellum. It is a monogenic and autosomal dominant disease that results from the mutation of the *ATXN3* gene, leading to the expression of a mutated form of ataxin-3, a protein with a polyglutamine tail. As yet, there is no efficient therapy to cure or slow down the progression of this fatal disease. Therefore, the development of translational therapies that are easy and fast to implement, is imperative.

For this purpose we tested two pharmacological compounds, namely resveratrol, a well-known sirtuin 1 (SIRT1) activator, and nicotinamide mononucleotide (NMN), an intermediate of the oxidized nicotinamide adenine dinucleotide (NAD^+)-salvage pathway, and thus a NAD^+ booster. We observed that a low dose of resveratrol of 10 mg/kg of body weight/day, administered by intraperitoneal route, is able to robustly ameliorate the motor impairments, improving the motor incoordination and imbalance of transgenic MJD mice. These results were observed early in the treatment and were maintained during the entire study, suggesting a sturdy effect of resveratrol on MJD. Moreover, eight weeks after the treatment with resveratrol, we also observed a significant amelioration of the neuropathology of MJD mice. Intraperitoneally-injected NMN slightly ameliorated motor deficits in the transgenic MJD mice. Although, the treatment with NMN did not significantly alleviate neuropathology, and also did not restore cerebellar NAD^+ levels.

Altogether, these studies, essentially the results obtained with resveratrol, open new avenues for future MJD therapies.

4.2 <u>Introduction</u>

Machado-Joseph disease (MJD), also known as spinocerebellar ataxia type 3 (SCA3; Haberhausen et al., 1995), is the most common dominantly inherited ataxia worldwide, and it was originally described in families of Portuguese-Azorean ancestry (Nakano et al., 1972; Lima and Coutinho, 1980). It is a monogenic autosomal dominant neurodegenerative disease that results from the mutation in the *ATXN3* gene. This mutation involves the expansion of the CAG repeat in the C-terminal coding region of the gene (Sequeiros et al., 1994; Kawaguchi et al., 1994). The resultant mutated protein – mutant ataxin-3 – has an unstable and expanded polyglutamine tail of more than 55 glutamines (Ikeda et al., 1996; Paulson et al., 1997), conferring a toxic gain of function to the ubiquitin-binding protein ataxin-3 (Rubinsztein et al., 1999; Wang et al., 2000; Burnett et al., 2003). Neurodegeneration results from the cleavage of the mutated protein in toxic fragments, mediated mainly by calpains (Simoes et al., 2012; Hubener et al., 2013; Simoes et al., 2014), and nuclear aggregation of ataxin-3 (Paulson et al., 1997b). MJD has a late-onset that manifests with cerebellar ataxia and pyramidal and extrapyramidal signs (Lima and Coutinho, 1980; Sudarsky and Coutinho, 1995; Maruyama et al., 1995), due to neurodegeneration in cerebellum, brainstem, basal ganglia, and spinal cord (Durr et al., 1996; Sudarsky and Coutinho, 1995), as well as striatum (Klockgether et al., 1998). There is neither a cure to treat or to prevent and slow down the progression of this fatal disease, and only symptomatic treatments for the disease currently exist.

Besides the results presented in Chapter 2 demonstrating the importance of SIRT1 in MJD, other studies also showed the relevance of SIRT1 in other neurodegenerative diseases (Kim et al., 2007a; Jeong et al., 2012; Guo et al., 2016), and also in the aging field (Cohen et al., 2004). Therefore, it was desired the discovery of a molecule that activates SIRT1. In fact, since 2003 it is possible to pharmacologically activate sirtuins with sirtuin activating compounds (STACs; Howitz et al., 2003). The first reported STACs were a group of natural polyphenols: quercetin, piceatannol, butein, and resveratrol (Howitz et al., 2003). The most potent and non-toxic compound discovered in this group was resveratrol. During the last years several studies showed that resveratrol increases longevity in yeast (Yang et al., 2007a; Morselli et al., 2009), worms (Wood et al., 2004; Zarse et al., 2010), fish (Yu and Li, 2012; Genade and Lang, 2013; Liu et al., 2015), and flies (Bauer et al., 2004; Bauer et al., 2009). In rodent models it was also demonstrated that resveratrol protects against the injurious effects of high-calorie diet, and can delay most of the diseases associated with aging (Baur et al., 2006; Calliari

et al., 2014; Mishra et al., 2015; Braidy et al., 2016; Naia et al., 2016), mimicking the transcriptional changes induced by CR (Barger et al., 2008a; Barger et al., 2008b; Park et al., 2009). Regarding the mechanism of resveratrol, in 2013, Hubbard and colleagues clarified that specific hydrophobic motifs found in SIRT1 substrates facilitate SIRT1 activation by resveratrol (Hubbard et al., 2013). This study demonstrated that SIRT1 can be directly activated through allosteric mechanisms, lowering the bind affinity for the enzyme's substrate, increasing its activity ten-fold (Howitz et al., 2003). Moreover, some recent studies also suggest that resveratrol is able to increase SIRT1 expression (Cote et al., 2015).

Oxidized nicotinamide adenine dinucleotide (NAD^+) is a coenzyme present in all cells. It is a key cellular factor in metabolism. To maintain stable cellular NAD^+ levels, cells primarily use a NAD^+-salvage pathway, but also rely on several biosynthetic pathways. Since 2002 it is known that the increase in NAD^+ through the upregulation of the NAD^+-salvage pathway, mimics CR and extends lifespan (Anderson et al., 2002; Anderson et al., 2003). In mammals, NAD^+ can be regenerated from nicotinamide (NAM), through the action of two enzymes: nicotinamide phosphoribosyltransferase (NAMPT) that converts NAM into nicotinamide mononucleotide (NMN), and nicotinamide mononucleotide adenylyltransferase (NMNAT) that regenerates NAD^+ from NMN. Nicotinamide riboside (NR) is a naturally occurring precursor of NAD^+ that needs to be converted to NMN by NR kinases (NRK). Moreover, besides sirtuins there are other NAD^+-consuming enzymes, such as poly-(ADP)-ribose polymerases (PARP), cluster of differentiation 38 (CD38), and its homologue cluster of differentiation 157 (CD157; Escande et al., 2013; Haffner et al., 2015). NMN, NR, and CD38 inhibitors, such as, apigenin (Escande et al., 2013), quercetin (Escande et al., 2013) and GSK 897-78c (Haffner et al., 2015), are NAD^+ boosting molecules, increasing NAD^+ levels, and indirectly activating SIRTs. Moreover, rodent treatments with NMN or NR, have shown no toxicity when dosed for over 180 days (Gong et al., 2013). It was already shown some beneficial effects associated with these compounds, namely improvements in glucose metabolism, mitochondrial function, and recovery from heart, ears and eyes injuries, as well as reducing indicators of inflammation and muscle wasting, in a SIRT1-dependent manner (Yoshino et al., 2011; Gomes et al., 2012; Mouchiroud et al., 2013b; Khan et al., 2014; de Picciotto et al., 2016).

Here, taking into account the importance of SIRT1 and nuclear NAD^+ for MJD pathogenesis, demonstrated in Chapter 2 and 3, we show that a therapy based on the pharmacological SIRT1 activation can be a promising therapy to treat MJD patients in the near future.

4.3 <u>**Materials and Methods**</u>

4.3.1 Animals

As referred in Chapters 2 and 3, C57Bl/6-background transgenic MJD mice and age-matched wild-type control mice were obtained from backcrossing heterozygous males with C57Bl/6 females (obtained from Charles River, Barcelona, Spain). Transgenic mice were initially acquired from Hirokazu Hirai from Kanazawa University, Japan (Torashima et al., 2008; Oue et al., 2009), and a colony of these transgenic mice was established in the Center for Neuroscience and Cell Biology of the University of Coimbra. Transgenic mice express N-terminal-truncated human ataxin-3 with 69 repeats and an N-terminal hemagglutinin (HA) epitope specifically in cerebellar Purkinje cells, driven by a L7 promotor. Genotyping was performed by PCR analysis of DNA from ears. Mice were housed under conventional 12-hour light-dark cycle in a temperature controlled room with water and food provided *ad libitum*. The experiments were carried out in accordance with the European Community directive (2010/63/EU) for the care and use of laboratory animals. Researchers received adequate training (FELASA certified course) and certification to perform the experiments from Portuguese authorities (Direção Geral de Veterinária).

4.3.2 Drug treatments

Resveratrol was daily and intraperitoneally administered in a 25% DMSO, diluted in a saline solution, at a dose of 10 mg/kg body weight/day in a final volume of 50-70 µl, depending on mouse body weight. Nicotinamide mononucleotide (NMN) was daily and intraperitoneally administered in a saline solution at a dose of 500 mg/kg body weight/day, also in a final volume of 50-70 µl depending on mouse body weight. Body weight and food intake were frequently evaluated.

4.3.3 Behavioral testing

Five-week-old mice were submitted to a battery of motor tests starting two days before the beginning of the study (t=0) and every two weeks until the eighth week. All tests were performed in a dark room with, at least, 60 minutes of acclimatization to the experimental room. The same phenotyping tests were conducted at the same time of the day, particularly in the first half of the day (during the morning until early afternoon).

4.3.3.1 Stationary and accelerating rotarod tests, swimming test, and beam walking test: Stationary and accelerated rotarod tests, swimming test, and beam walking test were performed as described in sections 2.3.5.1, 2.3.5.3, and 2.3.5.4 of Chapter 2.

4.3.3.2 Grip strength: We used this test to evaluate neuromuscular function indicated by mouse limb strength (Simoes et al., 2014). The setup consisted of a 300-g metal grid positioned on a scale. The animal was hung with its forepaws on the central position of the grid. Its strength was represented as the weight lifted (g) from the scale. The grip test was performed 9 times and the mean was taken for the higher 4 values. Mice body weight was used as a normalization factor.

4.3.4 Histological processing

4.3.4.1 Tissue preparation: As described in Chapter 2, with some modifications, mice were sacrificed with an overdose of avertin (625 mg/kg body weight, intraperitoneally). Transcardial perfusion with phosphate buffered solution (PBS) and fixation with 4% paraformaldehyde were performed. Brains were collected and post-fixed in 4% paraformaldehyde for 24 hours and cryoprotected by incubation in 25% sucrose/phosphate buffer for 36/48 hours. After that, dehydrated brains were frozen at -80ºC and 35 µm sagittal sections from transgenic MJD and corresponding wild-type littermate mice were sliced using a cryostat (LEICA CM3050S, Leica Microsystems) at -21ºC. Slices were collected in anatomical series and stored in 48-well trays as free-floating sections in PBS supplemented with 0.05% (m/v) sodium azide. The trays were stored at 4º C until immunohistochemical and other procedures.

4.3.4.2 Immunohistochemical processing: As described in Chapter 2, free-floating sections were incubated in PBS/0.1% Triton X-100 containing 10% normal goat serum (Gibco), and then incubated overnight at 4ºC in blocking solution with the primary antibody: mouse monoclonal anti-HA antibody (1:1000; ab-hatag InvivoGen, San Diego, CA, USA). Sections were washed and incubated for 2 h at room temperature with the corresponding secondary antibodies coupled to fluorophores goat anti-mouse Alexa Fluor 488 (1:200, Molecular Probes-Invitrogen, Eugene, OR) diluted in the respective blocking solution. The sections were washed and incubated during 10 min with 4',6'-

diamidino-2-phenylindole DAPI (Sigma; St. Louis; MO), washed again and mounted in mowiol on microscope slides.

Staining was visualized with Zeiss Axioskop 2 plus or Zeiss Axiovert 200 imaging microscopes (Carl Zeiss MicroImaging, Oberkochen, Germany) equipped with AxioCam HR color digital cameras (Carl Zeiss Microimaging) and 35, 320, 340, and 363 Plan-Neofluor or 363 Plan/Apochromat objectives using the AxioVision 4.7 software package (Carl Zeiss Microimaging). Quantitative analysis of fluorescence was performed with a semiautomated image-analysis software package and images were taken under identical image acquisition conditions and uniform adjustments of brightness and contrast were made to all images (ImageJ; NIH; Bethesda, MD).

4.3.4.3 Cresyl violet staining: Cresyl violet staining was done as described in section 2.3.6.3 of Chapter 2.

4.3.5 Quantitative analysis of HA aggregates

Quantification of haemagglutinin-tagged ataxin-3 positive inclusions was done as described in section 2.3.10 of Chapter 2.

4.3.6 Quantification of granular and molecular layers size and cerebellar volume

Quantification of granular and molecular layers of cerebellum and of cerebellar volume was done as described in Section 2.3.11 of Chapter 2.

4.3.7 Immunoblot procedure

4.3.7.1 Tissue preparation: Tissue preparation for immunoblot procedure was done as described in section 2.2.12.1 of Chapter 2.

4.3.7.2 Western blot procedure: As described in Chapter 2, samples were previously denatured with 2x sample buffer (10% β-mercaptoethanol, 4% sodium dodecyl sulphate (SDS), 0,25 M Tris-HCl, 8 M urea), and incubated during 5 min at 95ºC. Equal amounts of protein (50 µg or 25 µg) were resolved on 12% SDS-PAGE and transferred onto polyvinylidene fluoride (PVDF) membranes (GE Healthcare) according

to standard protocols. Membranes were blocked by incubation in 5% non-fat milk powder in 0.1% Tween 20 in Tris buffered saline (TBS-T), and incubated overnight at 4ºC with primary antibody: mouse anti-HA antibody (1:1500; ab-hatag InvivoGen, San Diego, CA, USA); mouse anti-β-actin antibody (clone AC74; 1:5000; A5316 Sigma-Aldrich), rabbit anti-sirtuin 1 antibody (1:1500; #2028 Cell Signaling Technology), followed by the incubation with the corresponding alkaline phosphatase-linked secondary goat anti-mouse or anti-rabbit antibody (Thermo Scientific). Bands were visualized with enhanced chemifluorescence substrate (ECF, GE Healthcare) and chemifluorescence imaging (VersaDoc Imaging System Model 3000, BioRad). Semi-quantitative analysis was carried out based on the optical density of scanned membranes (Quantity One; 1-D image analysis software version 4.6.6; Bio-Rad). The specific optical density was then normalized with respect to the amount of β-actin loaded in the corresponding lane of the same gel.

4.3.8 Quantitative Real Time Polymerase Chain Reaction (qRT-PCR)

4.3.8.1 Isolation of total RNA from mice tissues and cDNA synthesis: The isolation of total RNA from tissue and cDNA synthesis was done as described in section 2.3.13.1 of Chapter 2.

4.3.8.2 qRT-PCR procedure: As described in Chapter 2, with some modifications, qRT-PCR was performed in the StepOne Plus Real-Time PCR System (Applied Biosystems) using 96-well microliter plates and the SsoAdvanced SYBR Green Supermix (Bio-Rad). PCR was carried out in 10 µL reaction volume. Primers for mouse SIRT1 and GADPH were pre-designed and validated by QIAGEN (QuantiTect Primers, QIAGEN). We also prepared the adequate negative controls. All reactions were performed in duplicate and according to the manufacturer's recommendations: 95ºC for 30 sec, followed by 45 cycles at 95ºC for 5 sec, and 60ºC for 30 sec. The amplification rate for each target was evaluated from the cycle threshold (Ct) numbers obtained with cDNA dilutions, with correction for GADPH levels. The mRNA fold increase or fold decrease with respect to control samples was determined by the Pfäffl method.

4.3.9 NAD⁺ measurement

As described in Chapter 3, with some modifications, animals were intraperitoneally injected with NMN or PBS, depending on the group, and 3-4 hours later

were sacrificed and tissues were dissected and immediately preserved in liquid nitrogen. NAD^+ levels from cerebellar and striatal tissues were quantified with a commercially available kit (Promega) according to the manufacturer's instructions. Total protein concentration was determined in each sample with BCA protein assay (Pierce Biotechnology, Thermo Scientific) and was used to normalize NAD^+ levels. Values were expressed as pmol NAD^+/μg protein.

4.3.10 Statistical analysis

Statistical analysis was performed with paired or unpaired Student's t-test and one-way or two-way ANOVA followed by the adequate post-hoc test, for multiple comparisons. Results are expressed as mean±standard error of the mean (SEM). Significant thresholds were set at $p<0.05$, $p<0.01$ and $p<0.001$, as defined in the text.

4.4 <u>Results</u>

4.4.1 Resveratrol treatment does not change body weight and food intake of transgenic Machado-Joseph disease mice

Resveratrol is referred as a caloric restriction (CR) mimetic, so we sought to investigate if resveratrol changes transgenic MJD mice body weight. We observed that eight weeks of intraperitoneal administration of resveratrol (Figure 4.1A) did not change body weight (Figure 4.1B) neither food intake (Figure 4.1C), in mice fed with a standard diet (AIN-93D), which is in accordance with others (Pearson et al., 2008). No significant differences were also observed in external characteristics (such as in the fur condition, energy, etc.). Therefore, the potential beneficial effects of resveratrol on MJD are not associated with body weight changes.
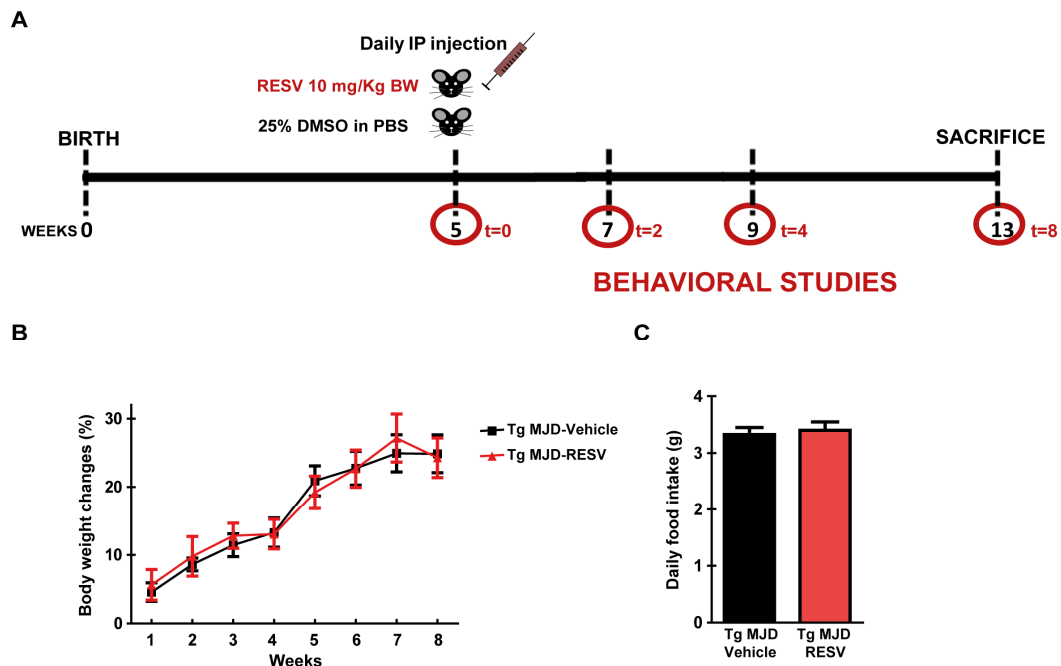
Figure 4.1 <u>Eight weeks of resveratrol treatment does not change body weight or food intake of transgenic MJD mice.</u> **(A)** Five-week-old transgenic MJD mice were divided in two groups. One group of animals was daily and intraperitoneally injected with resveratrol, diluted in a 25% DMSO in a saline solution, or with the vehicle. Eight weeks after the beginning of the study animals were sacrificed. Motor behavioral tests were frequently performed. **(B)** Weekly average of body weight of vehicle- or resveratrol-treated MJD mice. Body weight was measured 5 times per week and weekly average is represented. **(C)** Daily food intake average of mice on vehicle or resveratrol group. Food intake was measured 5 times per week and total average is represented. <u>Tg MJD-RESV:</u> Transgenic MJD treated with resveratrol; <u>Tg MJD-Vehicle:</u> Transgenic MJD treated with vehicle. Compared to Tg MJD-Vehicle. **(B)** Two-way Analysis of Variance (ANOVA) with Bonferroni's post hoc test. **(C)** Unpaired Student's t test. Tg MJD-Vehicle: n=8; Tg MJD-RESV: n=9.

4.4.2 Resveratrol ameliorates motor deficits and imbalance of transgenic Machado-Joseph disease mice

We previously demonstrated in Chapter 2 that the increase in SIRT1 promoted by CR robustly ameliorates motor incoordination and imbalance of transgenic MJD mice. Next we investigated if the pharmacological activation of SIRT1 with a well-known compound that activates SIRT1 – resveratrol – could also provide beneficial effects for the disease. For this purpose, five-week-old transgenic MJD mice were daily and intraperitoneally injected with resveratrol diluted in 25% DMSO in saline solution *vs* a vehicle-injected group (Figure 4.1A). Behavioral tests to evaluate motor outcomes were frequently performed (Figure 4.1A).

To evaluate motor coordination and balance, accelerated and stationary rotarod tests and beam walking test, were performed. With stationary rotarod test we clearly observed a significant improvement in the motor performance of mice, since the second week after the beginning of the treatment (Figure 4.2A; t=2 weeks; Tg MJD-Vehicle: 15.2±2.3 s *vs* Tg MJD-RESV: 75.4±15.0 s; p<0.001), and the effect was maintained across the experimental time course. Moreover, similar results were obtained in accelerated rotarod test, where resveratrol-treated mice showed a better performance than vehicle-treated animals, since the second week after the beginning of the study (Figure 4.2B; t=2 weeks; Tg MJD-Vehicle: 21.3±2.4 s *vs* Tg MJD-RESV: 44.3±3.9 s; p<0.001). In beam walking test we clearly observed that four weeks after the beginning of the treatment, resveratrol-treated mice demonstrated a significantly better performance, crossing three of the four beams faster than mice injected with vehicle solution (Figure 4.2C). Altogether, these results demonstrate that a treatment based on resveratrol robustly alleviates the motor incoordination and imbalance of transgenic MJD mice, suggesting that resveratrol is a promising therapeutic approach to treat MJD.
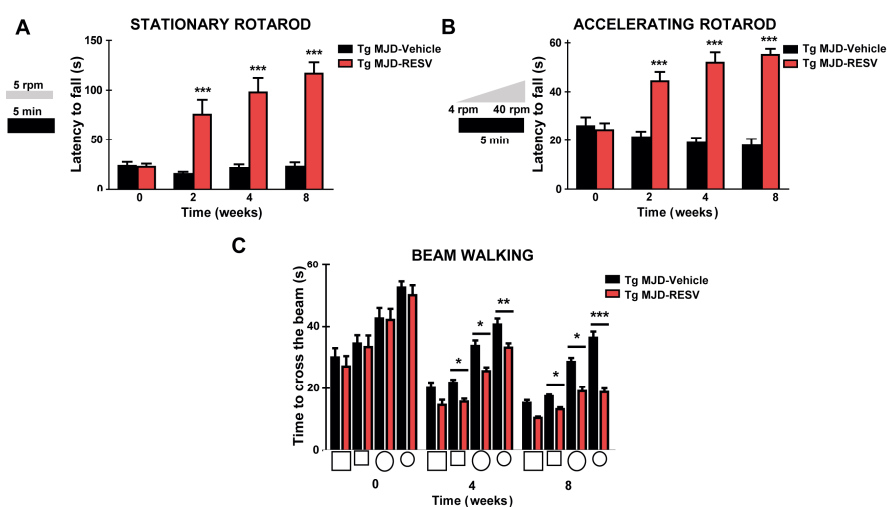
Figure 4.2 Resveratrol alleviates motor incoordination and imbalance of Machado-Joseph disease mice. **(A-B)** Transgenic MJD mice were placed in the stationary rotarod

Figure 4.2 (cont.) (with 5 r.p.m. of velocity) or in the accelerating rotarod (from 4 to 40 r.p.m. of velocity in 5 minutes), and the time that mice maintained walking/running on the rolling cylinder was recorded. **(C)** Beam walking performance of transgenic MJD mice. Two square beams (18 and 9 mm of width) and two round beams (9 and 6 mm of diameter) were used, and time that mice took to cross each beam was recorded. Tg MJD-RESV: Transgenic MJD treated with resveratrol; Tg MJD-Vehicle: Transgenic MJD treated with vehicle. Data represent mean ± SEM. *$p<0.05$; **$p<0.01$; ***$p<0.001$ compared to Tg MJD-Vehicle. **(A-C)** 2-way Analysis of Variance (ANOVA) with Bonferroni's post-hoc test. Tg MJD-Vehicle: n=8; Tg MJD-RESV: n=9.

Moreover, we evaluated mouse strength and motor coordination in MJD mice, using swimming and grip strength tests. In both tests, we did not observe statistically significant differences between the two groups, although we observed a tendency to an improvement of the performance in the resveratrol-treated group, in comparison with the vehicle-injected group, which is in accordance with the previous results (Figures 4.3A,B).
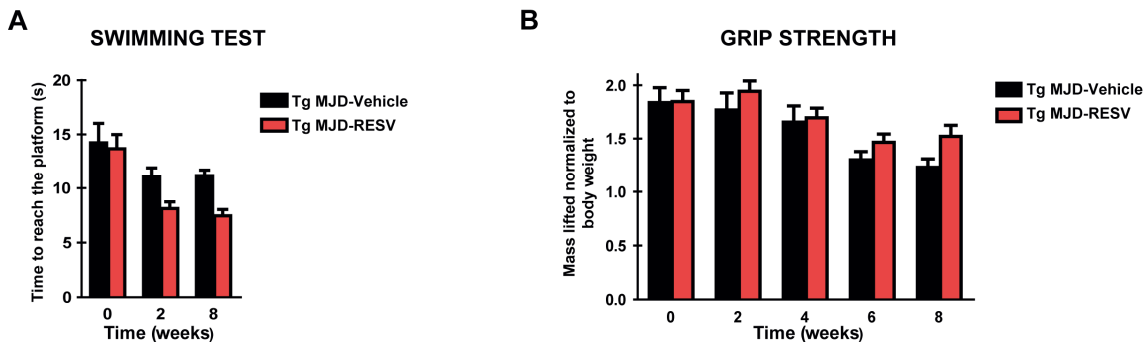
Figure 4.3 Resveratrol slightly, but not significantly improves motor coordination and strength of transgenic MJD mice. **(A)** Representation of the time that vehicle- or resveratrol-treated transgenic MJD mice took to cross the swimming pool and reach the safe platform. **(B)** Grip strength of transgenic MJD mice, represented by the mass that mice can lift (in grams) normalized with their body weight (also in grams). Tg MJD-RESV: Transgenic MJD treated with resveratrol; Tg MJD-Vehicle: Transgenic MJD treated with vehicle. Data represent mean ± SEM. Compared to Tg MJD-Vehicle. **(A-B)** Two-way Analysis of Variance (ANOVA) with Bonferroni's post-hoc test. Tg MJD-Vehicle: n=8; Tg MJD-RESV: n=9.

Overall, these results demonstrate that eight weeks of treatment with resveratrol robustly ameliorate motor coordination and balance impairments of transgenic MJD mice.

4.4.3 Eight weeks of resveratrol treatment ameliorate cerebellar Machado-Joseph disease neuropathology

To determine whether transgenic MJD mice phenotype was correlated with neuropathological changes, we evaluated some neuropathological markers. As described before, transgenic MJD mice used in this study exhibit an early and severe

cerebellar neuronal loss, and consequently cerebellar atrophy, due to the expression of mutant ataxin-3 in Purkinje cells of cerebellar cortex (Torashima et al., 2008). We evaluated cerebellar volume and the morphology of cerebellar layers, particularly the molecular and granular layers thickness. Furthermore, we also counted the number of mutant ataxin-3 aggregates in Purkinje cells. We evaluated neuropathology only eight weeks after the beginning of the treatment, namely in the time-point where we observed the most prominent effect in motor performance.

We observed that eight weeks of resveratrol treatment were able to protect transgenic MJD mice cerebella from shrinkage, demonstrated by the higher cerebellar volume, and molecular and granular layers thickness (Figures 4.4A-C). We also observed a significant decrease in the number of mutant ataxin-3 aggregates, suggesting that the neuroprotective effects might be related to a better neuronal survival (Figures 4.4D,E). Additionally, by western blot we observed a decrease of soluble mutant ataxin-3 levels, corroborating the previous results (Figure 4.4F).
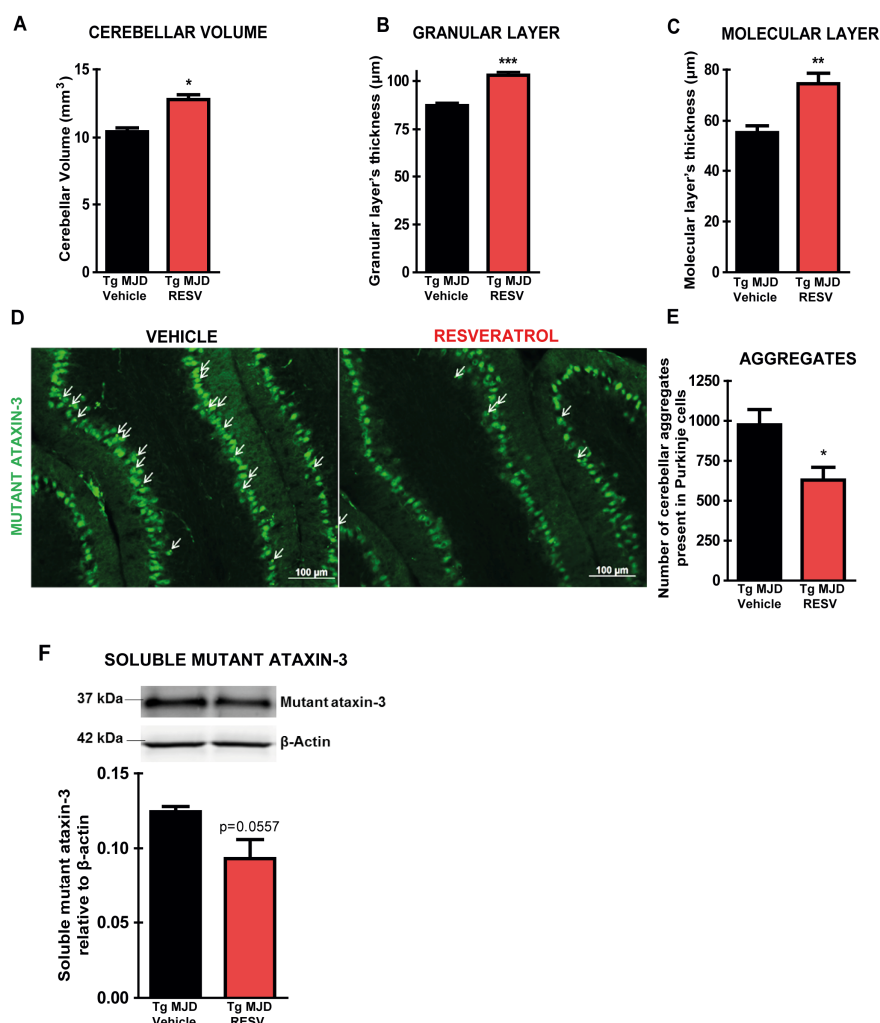
Figure 4.4 <u>Resveratrol reduces the number of mutant ataxin-3 inclusions and soluble levels, contributing to the neuronal survival and preventing cerebellar atrophy.</u> **(A)** Volume of cerebellum of transgenic MJD mice treated during eight weeks with resveratrol

Figure 4.4 (cont.) or vehicle. **(B-C)** Granular or molecular layers thickness of lobules V and IX of cerebellar cortex of vehicle- or resveratrol-treated transgenic MJD mice. **(D)** Number of mutant ataxin-3 inclusions present in Purkinje cells of cerebellar cortex (inclusions indicated by the arrows) and quantified in **(E)**. **(F)** Soluble mutant ataxin-3 protein levels in cerebellum of transgenic MJD mice treated or not with resveratrol, normalized with β-actin. <u>Tg MJD-RESV:</u> Transgenic MJD treated with resveratrol; <u>Tg MJD-Vehicle:</u> Transgenic MJD treated with vehicle. Data represent mean ± SEM. *p<0.05; **p<0.01; ***p<0.001 compared to Tg MJD-Vehicle. **(A-C,E,F)** Unpaired Student's t-test. Tg MJD-Vehicle: n=4; Tg MJD-RESV: n=5.

In sum, these results demonstrate that resveratrol is able to preserve cerebellar cortex, potentially through the decrease of mutant ataxin-3 toxicity.

4.4.4 Resveratrol increases sirtuin 1 activity and reestablishes cerebellar sirtuin 1 levels

It is well known that resveratrol activates SIRT1 (Howitz et al., 2003). In 2013 Hubbard and colleagues demonstrated that specific hydrophobic motifs found in SIRT1 substrates are important for the activation of SIRT1 by resveratrol (Hubbard et al., 2013). Moreover, a recent study suggested that resveratrol is also able to increase SIRT1 mRNA and protein levels (Cote et al., 2015). The mechanism underlying this effect is not yet fully understood.

We evaluated the mRNA levels of SIRT1 in the cerebellum of wild-type and transgenic MJD mice treated, or not, with resveratrol. The results show that resveratrol was able to reestablish mRNA and protein SIRT1 levels, suggesting an effect on SIRT1 expression besides the increase on its activity (Figure 4.5A-B).
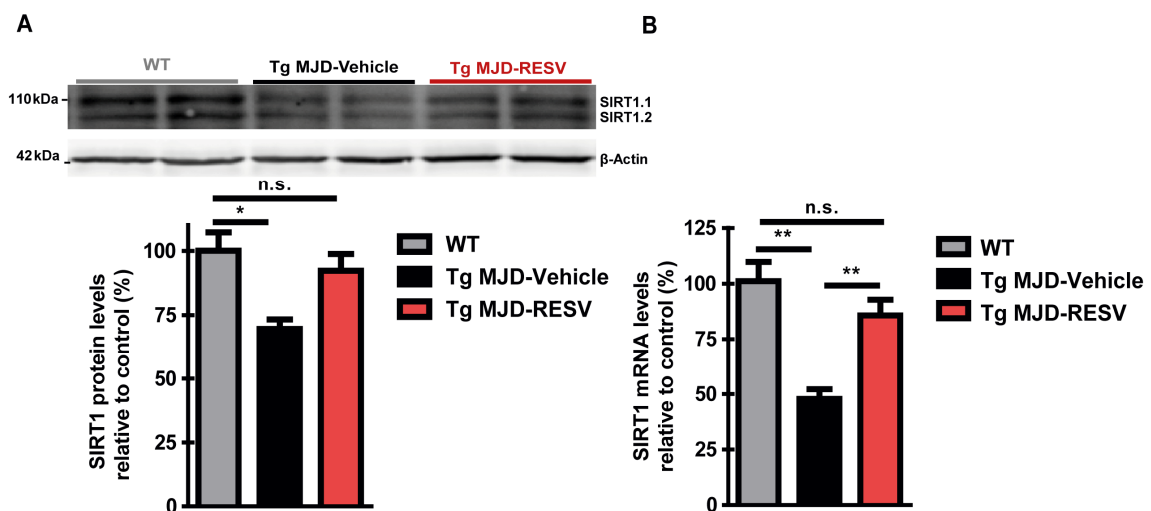
Figure 4.5 <u>Resveratrol reestablishes SIRT1 levels in the cerebellum of transgenic MJD mice.</u> **(A-B)** SIRT1 protein levels evaluated by western blot **(A)** and SIRT1 mRNA levels evaluated by qRT-PCR **(B)**, in the cerebellum of wild-type mice *vs* vehicle- or resveratrol-

Figure 4.5 (cont.) treated transgenic MJD mice. <u>Tg MJD-RESV:</u> Transgenic MJD treated with resveratrol; <u>Tg MJD-Vehicle:</u> Transgenic MJD treated with vehicle. Data represent mean ± SEM. n.s. p>0.05; *p<0.05; **p<0.01, compared to Tg MJD-Vehicle or Wild-type. **(A-B)** One-way Analysis of Variance (ANOVA) with Bonferroni's post-hoc test. Tg MJD-Vehicle: n=4; Tg MJD-RESV: n=4.

Taking everything into account, these results indicate that the beneficial effects of resveratrol are potentially related with the changes in SIRT1 levels.

4.4.5 Nicotinamide mononucleotide treatment does not significantly change body weight and food intake

Nicotinamide mononucleotide (NMN) is an intermediate of the NAD^+-salvage pathway. The supplementation with NMN increases NAD^+ levels, and consequently can increase SIRT1 activity, so we can also consider NMN as a CR mimetic. We intraperitoneally and daily injected NMN, at a dose of 500 mg/kg body weight/day diluted in a saline solution (PBS), and we compared with animals injected with the saline solution alone (control; Figure 4.6A). We also evaluated food intake and body weight five times per week.

We did not observe any significant difference in mice body weight gain in the NMN-treated transgenic MJD mice, in comparison with mice injected with vehicle alone (Figure 4.6B). Moreover, we did not observe any difference in the average food intake of transgenic MJD mice from the two groups (Figure 4.6C). No significant differences in external characteristics (such as in the fur condition, energy, etc.) were observed between NMN- and vehicle-treated transgenic MJD mice. Strikingly, we observed that gonadal white adipose tissue weight, was significantly lower in the transgenic MJD mice treated with NMN, in comparison with vehicle-treated mice (Figure 4.6D), resembling in part the changes induced by CR.
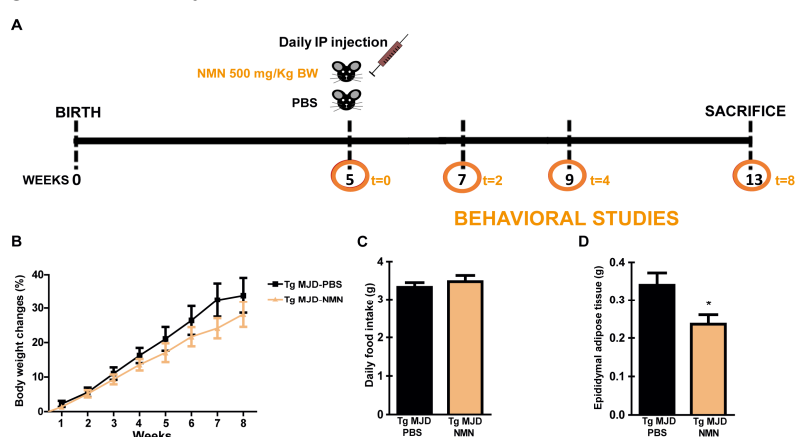
Figure 4.6 <u>Eight weeks of NMN treatment does not change body weight or food intake of MJD transgenic mice, but decreases gonadal white adipose tissue.</u> **(A)** Five-week-old

Figure 4.6 (cont.) transgenic MJD mice were divided in two groups. One group of mice was daily and intraperitoneally injected with a solution with 500 mg/kg body weight of NMN, and the other group was administered with the saline solution (PBS – vehicle). Motor behavioral tests were frequently performed. **(B)** Weekly average of body weight of vehicle- or NMN-treated mice. Body weight was measured 5 times per week, and weekly average is represented. **(C)** Daily food intake average of mice on vehicle or resveratrol group. Food intake was measured 5 times per week, and total average is represented. **(D)** Epididymal adipose tissue mass of PBS-treated transgenic MJD mice, in comparison with NMN-treated animals. <u>NMN</u>: Nicotinamide Mononucleotide; <u>PBS</u>: Phosphate Buffered Saline; <u>Tg MJD-NMN:</u> Transgenic MJD treated with NMN; <u>Tg MJD-PBS:</u> Transgenic MJD treated with vehicle. *$p<0.05$ compared to Tg MJD-PBS. **(B)** Two-way Analysis of Variance (ANOVA) with Bonferroni's post hoc test. **(C-D)** Unpaired Student's t test. Tg-PBS: n=8; Tg-NMN: n=9.

4.4.6 Intraperitoneal nicotinamide mononucleotide injection increases NAD⁺ levels in the cerebellum and striatum of transgenic Machado-Joseph disease mice

It was previously shown that peripheral administration of NMN is able to ameliorate metabolic impairments and mitochondrial dysfunction associated with aging in muscle cells (Ramsey et al., 2008; Yoshino et al., 2011; Gomes et al., 2013). Moreover, recently it was also demonstrated that peripheral NMN administration is linked to an amelioration of neuropathology and other phenotypic hallmarks associated with Alzheimer's disease (Long et al., 2015a). This last study suggested that peripherally-injected NMN increases NAD^+ in the central nervous system, although we wondered if this occurred in MJD affected brain regions, such as cerebellum and striatum. Therefore, our next goal was to evaluate NAD^+ levels in the cerebellum and striatum, through a highly sensitive luminescence method in samples from NMN- or PBS-treated MJD mice.

We measured NAD^+ levels in the cerebellum and in the striatum, and we normalized the levels to the protein content of each sample. We observed that NMN-treated animals have a significant higher NAD^+ levels in the cerebellum, as well in the striatum, in comparison to PBS-treated mice (Figures 4.7A-B). Cerebellum is the major affected brain area in the transgenic MJD mouse model that we used, although striatum is not affected. We observed that the increase in the cerebellum was not sufficient to reestablish NAD^+ levels that were robustly compromised (Figure 4.7A). Furthermore, in the striatum we observed that NAD^+ levels were higher than the basal levels in the wild-type mice (Figure 4.7B).

A

B
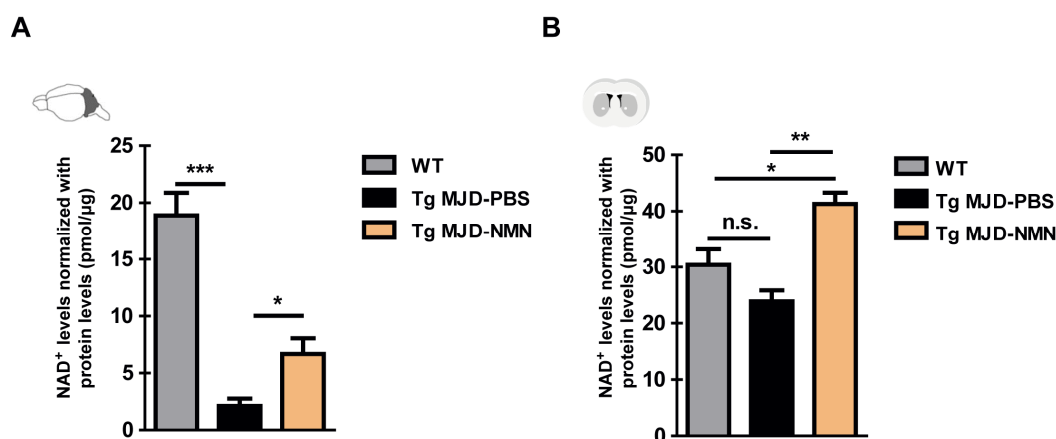
Figure 4.7 <u>NAD⁺ levels are significantly compromised in the cerebellum of MJD mice and peripherally-administered NMN increases NAD⁺ in different brain regions – cerebellum and striatum.</u> **(A-B)** NAD⁺ levels normalized with the protein content in the cerebellum **(A)** and striatum **(B)** of transgenic MJD mice, treated with NMN or PBS, in comparison with littermate wild-type age-matched mice. Results are expressed as pmol of NAD⁺ for μg of protein. <u>NMN</u>: Nicotinamide Mononucleotide; <u>PBS</u>: Phosphate Buffered Saline; <u>Tg MJD-NMN:</u> Transgenic MJD treated with NMN. <u>Tg MJD-PBS:</u> Transgenic MJD treated with vehicle. n.s. $p > 0.05$; * $p < 0.05$; **$p < 0.01$; *** $p < 0.001$. **(A-B)** One-way Analysis of Variance (ANOVA) with Bonferroni's post hoc test. WT: n=6; Tg-PBS: n=4; Tg-NMN: n=5.

All things considered, we observed that peripheral NMN administration is able to increase NAD⁺ levels in the central nervous system, although NMN was not able to reestablish NAD⁺ levels in the cerebellum of transgenic MJD mice.

4.4.7 Nicotinamide mononucleotide alleviates motor incoordination and imbalance of transgenic Machado-Joseph disease mice

As referred before, the MJD transgenic mouse model used in this study exhibits pronounced motor deficits, including motor incoordination, imbalance, and gait problems (Torashima et al., 2008; Nobrega et al., 2013; Nascimento-Ferreira et al., 2013; Simoes et al., 2014; Mendonca et al., 2015; Duarte-Neves et al., 2015; Conceicao et al., 2016). This phenotype is very clear since the third week of age, and aggravates during mouse life. Since we started the NMN administration in five-week-old mice, this study was performed in a post-symptomatic stage of the disease. To determine the motor activity of mice, we performed specific motor behavioral tests, namely rotarod tests (stationary and accelerating protocols), beam walking test, swimming test, and grip strength.

Transgenic MJD mice exhibited striking motor deficits in the rotarod tests. Although, NMN-treated transgenic MJD mice were able to equilibrate in the rotarod apparatus longer than vehicle-treated transgenic MJD mice (Figures 4.8A-B). This result was statistically significant since the second week after the beginning of the treatment in

the accelerating rotarod, and since the fourth week in the stationary rotarod (Figures 4.8A-B). Even though, it seems that at the end of the study (eighth week) the improvement was lower than in the fourth week, mainly in the stationary rotarod, suggesting a time-dependency. A similar result was observed in the beam walking test (Figure 4.8C). In the fourth week after the beginning of the study we see a clear, although not significant improvement in the motor performance of NMN-treated animals, in comparison with the vehicle-treated ones. At the end of the study the performance of NMN-treated animals was slightly better than vehicle-treated mice, achieving significance in the 9 mm diameter round beam (Figure 4.8C).
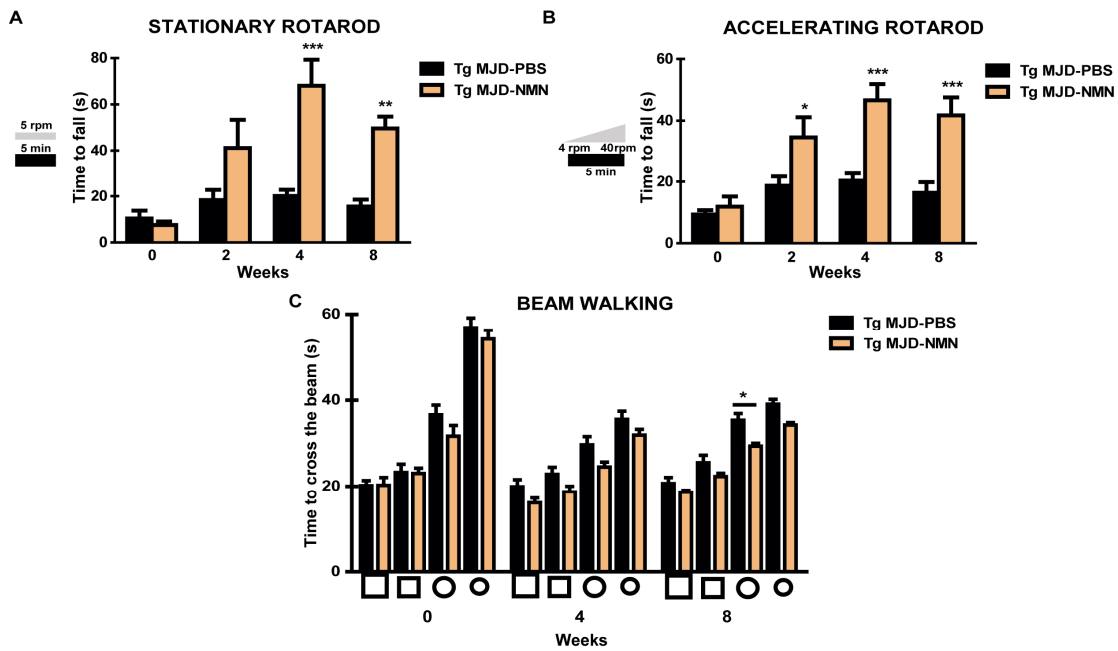
Figure 4.8 Motor performance of transgenic MJD mice intraperitoneally injected with PBS or NMN during eight weeks. **(A-B)** Transgenic MJD mice were placed in the rotarod apparatus at a constant velocity of 5 r.p.m. **(A)** or accelerating velocity (from 4 r.p.m. up to 40 r.p.m. in 5 minutes) **(B)**, and time that mice took to fall off the rotarod was measured. The average time for each group and each time-point is represented. **(C)** Beam walking performance of NMN- or PBS-treated transgenic MJD mice. Two square beams (18 and 9 mm of width) and two round beams (9 and 6 mm of diameter) were used, and time that mice took to cross each beam was recorded. The average values for each group, beam, and time point are represented. NMN: Nicotinamide Mononucleotide; PBS: Phosphate Buffered Saline; Tg MJD-NMN: Transgenic MJD treated with NMN; Tg MJD-PBS: Transgenic MJD treated with vehicle. *p<0.05; **p<0.01; ***p<0.001. **(A-B)** One-way Analysis of Variance (ANOVA) with Bonferroni's post hoc test. **(C)** Two-way Analysis of Variance (ANOVA) with Bonferroni's post hoc test. Tg-PBS: n=8; Tg-NMN: n=9.

We also performed other behavioral tests that evaluate motor coordination and also strength, namely swimming test and grip strength test. In the swimming test we did not observe any difference between the two experimental groups (Figure 4.9A). In the grip strength test, after 8 weeks of NMN treatment, we observed a significant difference

between the two groups, indicating an amelioration of the strength on the NMN-treated animals (Figure 4.9B).
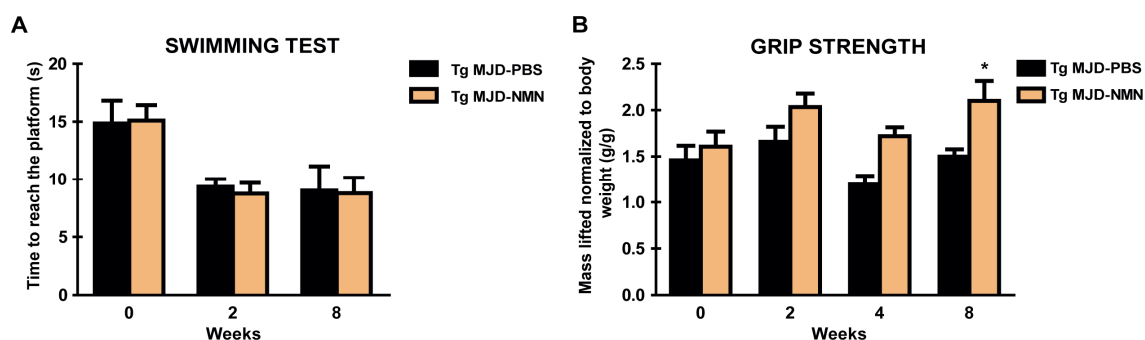
Figure 4.9 Motor performance and muscle strength of transgenic MJD mice injected with PBS or NMN. **(A)** Average time that mice took to reach a safe platform, swimming across one side to the other side of the swimming apparatus, is represented on the graph. **(B)** Grip strength of mice represented as the mass that mouse can lift (in grams), normalized with the specific mouse body weight (in grams). NMN: Nicotinamide Mononucleotide. PBS: Phosphate Buffered Saline. Tg MJD-NMN: Transgenic MJD treated with NMN. Tg MJD-PBS: Transgenic MJD treated with vehicle. *p<0.05. **(A,B)** One-way Analysis of Variance (ANOVA) with Bonferroni's post hoc test. Tg-PBS: n=8; Tg-NMN: n=9.

Altogether, these results suggest that the increase in NAD^+ in the cerebellum can ameliorate the motor impairments in a transgenic mouse model of the disease.

4.4.8 Nicotinamide mononucleotide treatment does not ameliorate cerebellar neuropathology of transgenic Machado-Joseph disease mice

The transgenic MJD mouse model that we used in this study displays a strong cerebellar atrophy, leading to motor incoordination and imbalance (Torashima et al., 2008; Nobrega et al., 2013; Nascimento-Ferreira et al., 2013; Simoes et al., 2014; Duarte-Neves et al., 2015; Conceicao et al., 2016). This cerebellar atrophy is triggered by the specific expression of a mutated ataxin-3 in the Purkinje cells of the cerebellar cortex (Torashima et al., 2008). As demonstrated before, NMN treatment ameliorated motor incoordination and next we wondered if this amelioration correlates with histopathological changes in the cerebellum. To evaluate this we counted the number of the mutant ataxin-3 inclusions that are present in the Purkinje cells, and we evaluated the thickness of the two main cerebellar cortical layers, and the cerebellar volume.

We performed a cresyl violet staining that allows the histological identification of the three cerebellar cortex layers: molecular, Purkinje, and granular layers. We measured the thickness of the molecular and granular layers through a semi-automatic system, and we did not observe differences in both layers (Figures 4.10A-C). Moreover, we evaluated the volume of the entire cerebellum and we did not observe any significant

difference in the total volume between the two groups, suggesting an absence of effects of NMN in the neuropathology (Figure 4.10D). Furthermore, after performing an immunohistochemistry targeting mutant ataxin-3, we counted the number of the inclusions within Purkinje cells. We only observe a small, but not significant reduction of the number of mutant ataxin-3 inclusions, in the transgenic MJD mice treated with NMN, in comparison with animals injected with the vehicle (Figure 4.10E).
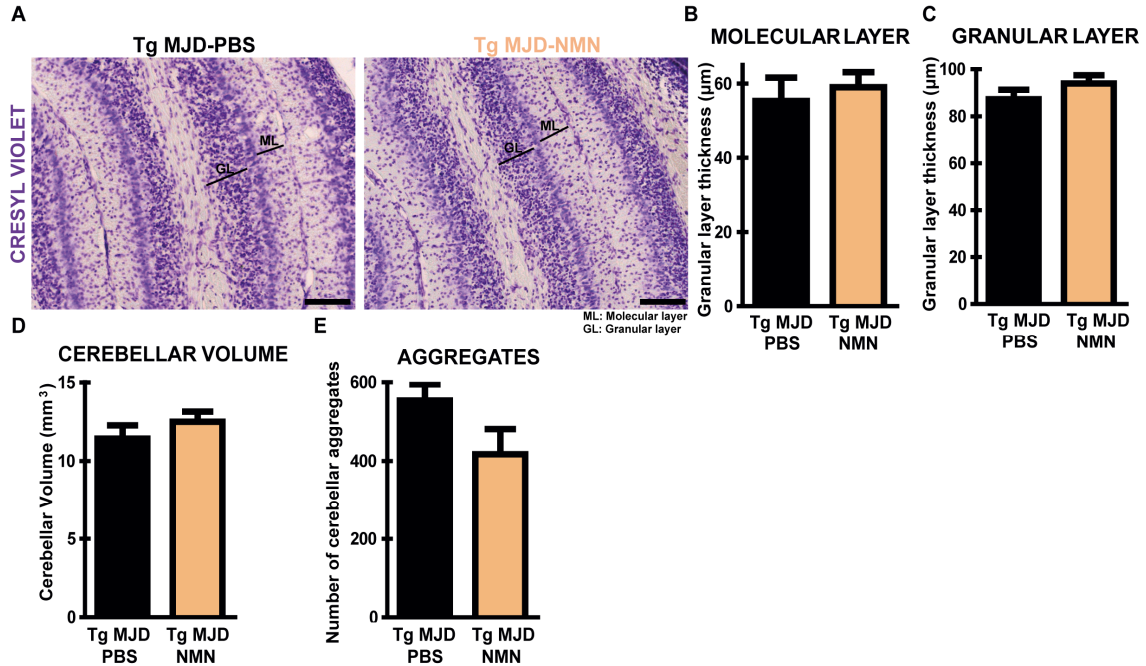
Figure 4.10 NMN treatment does not significantly ameliorate MJD neuropathology in the transgenic MJD mice. **(A)** Cresyl violet staining showing a representative molecular and granular layers thickness in the cerebellar cortex of MJD animals treated with vehicle *vs* NMN during eight weeks. Quantification of molecular and granular layers thickness are represented in **(B)** and **(C)**, respectively. **(D)** Cerebellar volume quantification of MJD animals treated with vehicle *vs* NMN. **(E)** Counting of mutant ataxin-3 inclusions present in the Purkinje cells after an immunohistochemistry targeting the mutated protein. NMN: Nicotinamide Mononucleotide; PBS: Phosphate Buffered Saline; Tg MJD-NMN: Transgenic MJD treated with NMN; Tg MJD-PBS: Transgenic MJD treated with vehicle. Compared to Tg MJD-PBS. **(B-E)** Unpaired Student's t-test. Tg MJD-PBS: n=4; Tg MJD-NMN: n=4. Scale bar: 100 μm).

In sum, these results show that NMN does not contribute to a significant improvement of the neuropathology of MJD on this transgenic MJD mice, although further studies are needed in order to clarify this.

4.5 <u>Discussion</u>

In the present study we provide compelling evidence demonstrating that a therapy based on the pharmacological activation of SIRT1 can be a promising therapy to treat MJD patients.

In the Chapter 2 we demonstrated that CR is able to robustly ameliorate MJD motor deficits and neuropathology, and we provided strong evidence demonstrating that SIRT1 was the central player in the CR effects. Moreover, we used lentiviral vectors to specifically overexpress SIRT1 and we observed again a strong beneficial effect on MJD neuropathology. In order to explore an easier and faster translational approach to activate SIRT1, we performed another study using the transgenic mouse model of MJD. We started the study in five-week-old transgenic MJD mice, at a post-symptomatic stage of the disease. We administered resveratrol, a well-known pharmacological compound that is able to activate SIRT1, through the intraperitoneal route, every day at the same time, and we observed an amelioration of the motor performance of animals. Furthermore, we observed a robust alleviation of the neuropathology, after eight weeks of treatment with resveratrol. These beneficial effects of resveratrol on this severe mouse model of MJD suggest a potential relevant therapeutic role of resveratrol for the disease. The beneficial effects of resveratrol are in agreement with a previous *in vitro* study (HEK293T cell line and a primary neuronal culture), in which the authors demonstrated that resveratrol suppresses cell death induced by mutant ataxin-3 (Li et al., 2007).

In the present study we also showed that resveratrol increases SIRT1 expression, reestablishing cerebellar SIRT1 levels in the transgenic MJD mice. This result is in accordance with a recent paper, that describes an increase in SIRT1 mRNA and protein levels after duodenal infusion of resveratrol, reinstating SIRT1 levels to the levels observed on their controls (Cote et al., 2015). In fact, in the previous chapters we demonstrated that SIRT1 levels were compromised in the disease. On Chapter 2 we observed that CR was able to reestablish the SIRT1 levels. With the results presented in this chapter we provide evidence supporting the hypothesis that activation of SIRT1 pathway induced by resveratrol, lead to a relevant amelioration of MJD phenotype. This is accordance with other studies that demonstrate that resveratrol ameliorates other neurodegenerative diseases, as instance Alzheimer's disease (Porquet et al., 2013; Feng et al., 2013), Parkinson's disease (Albani et al., 2009; Wu et al., 2011), Huntington's disease (Parker et al., 2005; Ho et al., 2010; Naia et al., 2016), and

amyotrophic lateral sclerosis (Wang et al., 2011; Mancuso et al., 2014; Song et al., 2014).

The mechanism of action of resveratrol has been under debate in the last years. In 2010, Pacholec and colleagues, suggested that resveratrol and other STACs are not direct activators of SIRT1, since they apparently failed to activate SIRT1 in the presence of the native peptide or full-length protein substrates, whereas they only do activate SIRT1 with peptide substrate containing a covalently attached fluorophore (Pacholec et al., 2010). This study was controversial in the field, however later, a study from the Sinclair's group demonstrated that a single amino acid in SIRT1, Glu230, was critical for the activation of SIRT1 by resveratrol, suggesting that SIRT1 can be directly activated through an allosteric mechanism (Hubbard et al., 2013). More recently, the structure of SIRT1 in complex with resveratrol was solved providing further insights demonstrating an allosteric activation of SIRT1 by resveratrol (Cao et al., 2015). As indicated before, we also observed a novel effect of resveratrol, corroborating a previous study (Cote et al., 2015). Our results suggest an interference of resveratrol on the transcription of SIRT1, but further studies are needed in order to clarify this.

One important question related to the translational use of resveratrol is its tolerability and safety in a clinical context. Recent results from clinical trials demonstrate that resveratrol is well-tolerated and safe, even in high doses (5 g daily; Turner et al., 2015; Yiu et al., 2015). Our pre-clinical data and the success of the current clinical trials, support the idea of studying resveratrol in a clinical context of MJD.

NAD^+ is the pinnacle of metabolic control, all the way from yeast to humans. SIRT1 senses alterations on intranuclear NAD^+ levels, which reflects energy levels. As showed in Chapter 3, in the cerebellum of transgenic MJD mice, NAD^+ is strongly compromised and this decrease is tissue- and disease-specific due to the absence of alterations in a non-affected brain area of this transgenic mouse model of MJD (striatum). With this result, the most obvious strategy to test whether enhancing NAD^+ levels impacts MJD progression, consisted in boosting NAD^+ regeneration, by supplementation with NAD^+ precursors. One way to increase NAD^+ is with nicotinamide mononucleotide (NMN) supplementation (Long et al., 2015a). This molecule only needs one step to be converted into NAD^+, namely through the action of nicotinamide mononucleotide adenylyltransferase (NMNAT). We administered NMN in transgenic MJD mice, in order to explore its potential beneficial effect for the disease. We showed that peripheral administration of NMN increased NAD^+ in, at least, two brain regions (cerebellum and striatum). These results suggest that NMN is able to increase NAD^+ in the brain. Furthermore, we observed that NMN is able to ameliorate motor incoordination and

imbalance. Although, regarding neuropathology, we did not observe any difference between the two groups, suggesting an absence of effects at this level.

Recent studies show beneficial effects of NMN in neurodegenerative diseases, such as Alzheimer's disease and amyotrophic lateral sclerosis (Wang et al., 2016; Harlan et al., 2016). Another study demonstrated that NMN can reverse age-related arterial dysfunction through the decrease on the oxidative stress (de Picciotto et al., 2016). Although, in MJD the effects of NMN were relatively limited, possibly related with the pathogenesis of MJD. In fact, the results that we obtained with NMN treatment were not as exciting as the results obtained with resveratrol. In the NMN treatment, as demonstrated in Figure 4.8, we observed an amelioration of the motor incoordination and imbalance promoted by NMN on rotarod tests, although from the forth to the eighth week, we observed a small reversion of the amelioration of the phenotype, mainly in the stationary rotarod test. Likewise, the amelioration of the phenotype was not consistent regarding all the behavioral tests, and regarding neuropathology. We observed that cerebellar NAD^+ was increased in the cerebellum of MJD mice after NMN administration, although the levels were too far away from the normal levels. Therefore, we were not able to completely reestablish NAD^+ levels, and this could be contributing to the results that we obtained. One explanation for this result remains in the pathogenesis of MJD that we explored in Chapter 3. In fact, in Chapter 3 we showed that NMNAT1, the enzyme responsible for the conversion of NMN into NAD^+, is significantly compromised in the cerebellum of MJD mice, so potentially NMN is not being efficiently converted into NAD^+. Another explanation for this result remains in the severe CD38 upregulation on the cerebellum of MJD mice that we previously demonstrated in Chapter 3. It is well known that CD38 is a NAD^+-consuming enzyme, so the increase in CD38 could be related with an increase in the consumption of NAD^+, avoiding a higher NAD^+ increase. Furthermore, recently it was demonstrated that *in vivo*, in different tissues, including the brain, CD38 is a NMN-degrading enzyme (Camacho-Pereira et al., 2016), corroborating the results observed *in vitro* before (Grozio et al., 2013). Thus, the increase in CD38 leads to an intensification of NMN degradation, potentially contributing to the non-effective effect of NMN.

Taking all together, our results show that resveratrol have a better potential to treat MJD than NMN. Therefore, these results suggest that a therapy with resveratrol could be a promising therapy to treat MJD, and further studies in the future have to be done.

CHAPTER 5

General Discussion and Conclusion

There is real poetry in the real world. Science is the poetry of reality.

(Richard Dawkins)

5.1 <u>General Discussion</u>

This thesis demonstrates, for the first time, that a therapeutic approach based on SIRT1 activation can be a promising strategy to treat MJD. Moreover, it also unravels a new pathological pathway associated with the mitochondrial dysfunction that is patent in this neurodegenerative disease. This pathway is intrinsically related with cellular NAD$^+$ levels, and consequently with SIRT1 activity.

Neurodegenerative diseases are age-related, progressive, and fatal disorders, in which the underlying mechanisms are not yet fully elucidated, and MJD is not an exception. Consequently, an effective treatment is yet to be developed. The discovery of new therapeutic strategies urges and for that we should deepening our understanding about the pathogenesis underlying the diseases, in order to create potential targets to revert them.

CR is a previously identified approach that can be used as neuroprotective strategy (Park et al., 1990; Bruce-Keller et al., 1999). The potential beneficial effects of CR have been explored for some neurodegenerative diseases, such as AD, PD, and HD (Duan et al., 2003; Maswood et al., 2004; Qin et al., 2006b). In the case of polyQ diseases, particularly in HD, CR has been shown to mitigate neuropathological hallmarks of the disease (Duan et al., 2003; Moreno et al., 2016). Nevertheless, nothing was known about the potential of CR to alleviate other polyQ diseases, such as SBMA, DRPLA, and all the SCA's, including MJD/SCA3. In Chapter 2 we provide compelling evidence, using two different mouse models of MJD – a transgenic mouse model (Torashima et al., 2008), and a striatal lentiviral mouse model of MJD (Simoes et al., 2012) –, demonstrating that CR alleviates phenotypic abnormalities associated with MJD pathogenesis. Moreover, the transgenic MJD mouse model used in this study (Torashima et al., 2008) expresses a truncated form of mutant ataxin-3 that exhibits a small portion of the normal ataxin-3, generating a more general polyQ protein. Taking this into account, we can probably infer these results to other polyQ diseases, spanning the relevance of these evidences to other diseases of the same group, even though further work should be done to clarify this.

In Chapter 2 we also demonstrated that SIRT1 levels are compromised in the cerebellum of MJD-diseased mice, in comparison with age-matched wild-type mice. Interestingly, CR was able to reestablish SIRT1 levels, suggesting a role for SIRT1 in the effects of CR and in the disease. Indeed, in other polyQ diseases, the polyQ-expanded proteins were, by some way, linked to SIRT1. For example, the acetylated

levels of mutant ataxin-7 were related with the turnover of the protein, namely as higher the acetylation levels the lower the turnover of the protein (Mookerjee et al., 2009). In the same year, in HD it was also demonstrated that the turnover of huntingtin is affected by its acetylation levels (Jeong et al., 2009). Therefore, it seems that acetylation levels of polyQ proteins can affect their metabolism and their neuronal toxicity. Thus, SIRT1 can play a major role in these polyQ-associated disorders. Several studies provided evidence of dysregulation of SIRT1 in polyQ disorders. In the case of HD, it was described that huntingtin interacts with SIRT1 and reduces its activity, and as in MJD, in HD SIRT1 is also compromised (Jiang et al., 2012). Another recent study also showed that SIRT1 levels are compromised in HD (Tulino et al., 2016). This study demonstrated that a striatum-specific phosphorylation-dependent regulatory mechanism of SIRT1 induction is impaired in two different HD mouse models (Tulino et al., 2016). In another polyQ disease, SBMA, it was also showed that the polyQ-expanded androgen receptor (AR) is hyperacetylated and the reduction of these acetylation levels decreases mutant AR aggregation (Montie et al., 2011). In the near future it is important to clarify the possible interaction between ataxin-3 and SIRT1, contributing to the understanding of the disease pathogenesis and probably creating new data to support the development of other new therapies for MJD.

As referred before, CR is not an easy translational approach to treat human diseases. CR can lead to an excessive loss of body fat, inducing the decrease in steroid hormones, which leads to several complications in the reproductive, bone, and immune systems (Devlin et al., 2010; Dos Santos et al., 2011; Colman et al., 2012; Williams et al., 2015; Mitchell et al., 2015a; Mitchell et al., 2015b; Mitchell et al., 2015c). Furthermore, the epidemiological studies that aim to evaluate the beneficial effect of CR in humans are few, and the studies involving non-human experiments were conducted in well-controlled, pathogen-free, and environmentally-protected facilities. Additionally, it is difficult for most of people to voluntarily reduce their energy intake by an amount that is likely to activate the subsequent mechanisms related with CR. Therefore, it is not easy to implement CR in humans, and the knowledge of the main mechanisms underlying the effects of CR for the development of a CR mimetic is imperative. In our studies, in Chapter 2 we demonstrated that SIRT1 is, at least, one of the central players of CR beneficial effects in MJD mice, since its knockdown blocked the beneficial effects of CR (Figure 2.12). In fact, other studies also highlighted the relevant role of SIRT1 in the beneficial effects of CR on neurodegenerative diseases, and also on longevity (Cohen et al., 2004; Bordone et al., 2007; Chen et al., 2008a; Chen et al., 2008b; Cohen et al., 2009; Smith et al., 2009; Graff et al., 2013; Ma et al., 2015). Due to the limitations of CR,

it was plausible the study of other strategies to mimic CR based on SIRT1 increase – SIRT1 lentiviral overexpression through gene therapy and resveratrol.

Even though gene therapy has accomplished exhilarating growth in recent years, there are some obstacles regarding its introduction as a therapeutic strategy. Actually, some of the problems related to gene therapy reside in its cost and the difficulty to target specific regions, their immunogenicity and toxicity, and their potential oncogenesis. With all these concerns, the study of a more translational approach to the human care urged. Resveratrol activates SIRT1 and is a translational approach to humans. Moreover, in our studies we showed that resveratrol effects were only slightly weaker than CR, but even so it was a robust therapeutic strategy (see Figure 5.1). These studies support the relevance of a clinical trial for the use of resveratrol on MJD patients. In *clinicaltrials.gov* there are registered 109 clinical trials, mainly in USA and Europe (42 and 40, respectively), using resveratrol, particularly to evaluate its pharmacokinetics and also its efficacy in some diseases, including neurodegenerative diseases, as Alzheimer's disease, Huntington's disease, and Friedrich Ataxia. Our results and the good outcomes from clinical trials support the relevance of a clinical trial with resveratrol in MJD.

As referred before, the activation of SIRT1 was a good strategy to mimic CR beneficial effects. Now regarding the mechanistic underlying SIRT1, it was already described that SIRT1 activates autophagy (Lee et al., 2008; Huang et al., 2015), and reduces neuroinflammation (Yeung et al., 2004). Moreover, in MJD two of the known pathogenic mechanisms involved, include the development of a neuroinflammatory network in the cerebellum and other brain regions (Evert et al., 2001; Evert et al., 2006b), as well as a decrease on autophagy (Menzies et al., 2010; Nascimento-Ferreira et al., 2011; Nascimento-Ferreira et al., 2013). In Chapter 2, we concluded that CR is able to increase SIRT1, contributing through this way to the decrease of neuroinflammation and the activation of autophagy, ameliorating MJD phenotype.

It is known that in MJD a nuclear localization of aggregated mutant ataxin-3 is strongly related with the pathogenesis of the disease (Paulson et al., 1997b; Evert et al., 1999; Bichelmeier et al., 2007). As in other neurodegenerative diseases, in MJD mitochondria are dysfunctional (Laco et al., 2012; Kazachkova et al., 2013; Ramos et al., 2015). We hypothesized that some nuclear changes could be the main responsible for the mitochondrial dysregulation, as previously showed in aged muscle cells (Gomes et al., 2013). In fact, in Chapter 3 we observed that a decrease in the nuclear NAD^+ levels is associated with a nuclear-mitochondrial communication dysregulation. There are some studies demonstrating that NAD^+ levels decline during aging (Braidy et al., 2011; Massudi et al., 2012; Gomes et al., 2013; Scheibye-Knudsen et al., 2014; Zhu et al.,

2015), but it is still lacking the evaluation of NAD$^+$ levels in several neurodegenerative diseases. In our study we described for the first time *in vivo* that in a neurodegenerative disease – MJD – and at a neuronal level, cerebellar NAD$^+$ levels are compromised, affecting nucleus and mitochondria communication, leading to a mitochondrial dysfunction. These results were the basis for the next step – to increase NAD$^+$ levels with a NAD$^+$ booster in the transgenic MJD mice. We injected through intraperitoneal route 500 mg/kg of body weight/day of NMN, as described in the Chapter 4, and in comparison with the other three therapeutic strategies tested (CR, resveratrol, and SIRT1 lentiviral overexpression), we obtained weaker effects regarding the amelioration in the motor phenotype and neuropathology (see Figure 5.1). There are some potential explanations for this result: i) CD38 levels are extremely high in the cerebellum of transgenic MJD mice and NMN treatment did not change CD38 levels, so even if we are increasing NAD$^+$, CD38 is competitively consuming NAD$^+$; ii) NMNAT1 levels are compromised in MJD and consequently not all NMN is being converted into NAD$^+$, being potentially accumulated; iii) previously it was demonstrated that the accumulation of NMN can lead to neurodegeneration (Di Stefano et al., 2015); and iv) CD38 is destroying NMN, as demonstrated in a recent study (Camacho-Pereira et al., 2016). A CD38 increase was also described in AD and during aging (Braidy et al., 2014; Long et al., 2015a; Blacher et al., 2015). In the near future it is important to clarify the veracity of these hypothesis, testing CD38 inhibitors, such as apigenin, quercetin, and GSK 897-78c, in association or not with NMN, to further clarify the relevance for the disease.

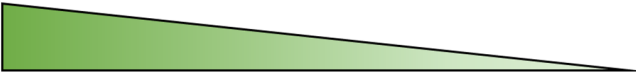|		CR	Resveratrol	SIRT1 overexpression	NMN
BEHAVIORAL OUTCOMES	**Rotarod tests**	++++	++++	n.d.	+++
	Beam walking test	+++	+++	n.d.	+
	Swimming test	++	+/=	n.d.	=
	Grip strength test	n.d.	+/=	n.d.	+
	Footprint analysis	++	n.d.	n.d.	n.d.
	Open-field test	+	n.d.	n.d.	n.d.
NEUROPATHOLOGY	**Number of inclusions**	++	+++	++++	=
	Atx3MUT levels reduction	+	+	++	=
	Cerebellar volume	+	+	n.d.	=
	Cerebellar layers thickness	++	++	n.d.	=
	DARPP-32 volume depletion	++	n.d.	++++	n.d.

Figure 5.1 Summary of the results obtained in MJD mouse models, and described in the Chapters 2, 3, and 4. CR was the therapeutic approach that more robustly ameliorated **Figure 5.1 (cont.)** the behavioral deficits and associated neuropathology of MJD, in two different and complementary mouse models of MJD. Resveratrol was used as a CR

mimetic, and its effects were only slightly weaker than CR, suggesting that it is a relevant and interesting pharmacological approach to treat MJD. The overexpression of SIRT1 through lentiviral vectors is also a good and interesting strategy to robustly ameliorate neuropathological hallmarks of MJD, but still is a challenging translational approach to humans. NMN treatment was the weaker therapeutic strategy, improving only motor incoordination and imbalance, but not thoroughly, and did not ameliorate neuropathology on the transgenic mouse model of MJD. n.d. not determined; ++++ represents an amelioration of more than 75%; +++ represents an amelioration between 50 and 75%; ++ represents an amelioration between 25 and 50%; + represents an amelioration lower than 25%; = represents an absence of changes; and +/= represents an amelioration lower than 25%, although without statistical significance; in every case in comparison with the corresponding controls. Atx3MUT: Mutant ataxin-3. CR: Caloric restriction. DARPP-32: Dopamine- and cAMP-regulated neuronal phosphoprotein. NMN: Nicotinamide mononucleotide. SIRT1: Sirtuin 1.

In Chapter 3 we demonstrated that the decrease in nuclear NAD^+ is linked with MJD pathogenesis. Therefore, the development of NMNAT1 activators to increase nuclear NAD^+ levels is also important. Interestingly, some studies have demonstrated that NMNAT1 overexpression retards significantly the *Wallerian* axonal degeneration after injury (Conforti et al., 2000; Mack et al., 2001; Araki et al., 2004). It was also demonstrated that NAD^+ levels decrease in degenerating axons and the prevention of NAD^+ decline can protect neurons from degeneration (Wang et al., 2005b). Moreover, NMNAT1 overexpression reduced the observed decline in glycolysis and in mitochondrial respiration in the Wallerian degeneration (Godzik and Coleman, 2015). This is in agreement with the results that we obtained (Chapter 3), where we demonstrated that NMNAT1 overexpression was able to reestablish mitochondrial function, and corroborates the importance of a specific and effective strategy to increase NAD^+ levels to prevent neurodegeneration in a broad range of diseases, in which MJD is included.

As referred before, in this thesis we also proposed a new mechanism underlying the mitochondrial dysfunction associated with MJD pathogenesis (see Figure 5.2). The results presented in Chapter 3 suggest that the mitochondrial dysfunction observed in MJD is related with the decrease in NAD^+. At the end of 2013, Sinclair's group demonstrated that the mitochondrial dysfunction in aged muscle cells resulted from a decrease in nuclear NAD^+ levels, resulting in a decrease of SIRT1 activity, and by a PGC1α-independent mechanism, *Tfam* expression was also decreased (Gomes et al., 2013). In fact, we obtained similar results at a neuronal level and associated with a neurodegenerative disease. In the near future we have to explore the alterations induced by the decrease in SIRT1 activity that explain the decrease in *Tfam* expression. There are some possibilities that we have to explore in order to better understand the mechanistic underlying these alterations, namely: i) SIRT1 directly regulates NRF-1 and

NRF-2, that are downstream *Tfam* regulators; ii) the decrease in SIRT1 activity is related to c-Myc expression decrease (Lim et al., 2010), and taking into account that c-Myc regulates *Tfam* expression (Li et al., 2005), the c-Myc decrease can lead to a reduction of *Tfam* expression; and iii) the SIRT1 decrease is influencing PGC-1α activity, and at a neuronal level in MJD, these changes in TFAM expression are due to a decrease in PGC-1α activity, possibly along with NRF-1 and NRF-2.
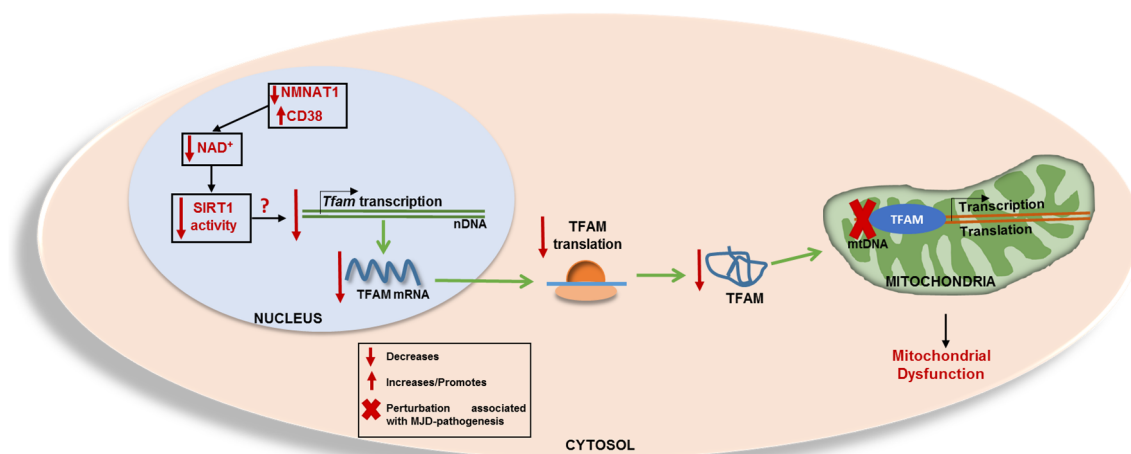
Figure 5.2 <u>Pathological mechanism underlying mitochondrial dysfunction in Machado-Joseph disease.</u> The results presented in Chapter 3 suggest that in mouse models of MJD, NAD$^+$ levels are severely compromised. This is probably related with a decrease in NMNAT1 and an increase in CD38. The decrease in NAD$^+$ levels leads to a decrease in SIRT1 activity and by a mechanism not yet completely elucidated, the *Tfam* expression is compromised leading to a reduction in mtDNA transcription, translation and replication, and consequently to mitochondrial dysfunction. So, in MJD the nuclear-mitochondrial communication is disrupted contributing to the mitochondrial dysfunction. Text and symbols in **red** color are based on results presented in Chapter 3. <u>CD38:</u> Cluster of differentiation 38; <u>mtDNA:</u> Mitochondrial DNA; <u>NAD$^+$:</u> Nicotinamide adenine dinucleotide; <u>nDNA:</u> Nuclear DNA; <u>NMNAT1:</u> Nicotinamide mononucleotide adenylyltransferase 1; <u>TFAM:</u> Mitochondrial transcription factor A.

5.2 <u>Conclusion</u>

Putting all together, the results presented in this thesis suggest different successful therapeutic strategies to treat MJD, namely: i) <u>CR</u> that is the strongest, but not the easiest to translate into human therapy; ii) <u>SIRT1 overexpression</u> through gene therapy that demonstrated beneficial effects, but like CR is not easy to translate into human therapy; and iii) a therapy with <u>resveratrol</u> that is a relevant and promising strategy that opens the possibility to go further into a clinical trial in the future. Moreover, we unraveled a new mechanism related with MJD pathogenesis and particularly with mitochondrial dysfunction. Our results suggest that a decrease in nuclear NAD^+ leads to a decreased expression of nuclear-encoded factors that regulate mtDNA expression and replication, contributing to the mitochondrial dysfunction patent on MJD. Furthermore, the overexpression of NMNAT1 positively contributed to the normalization of mitochondrial function.

Figure 5.3 summarizes the positive changes in the pathogenesis of MJD promoted by the treatments that were explored in this thesis.
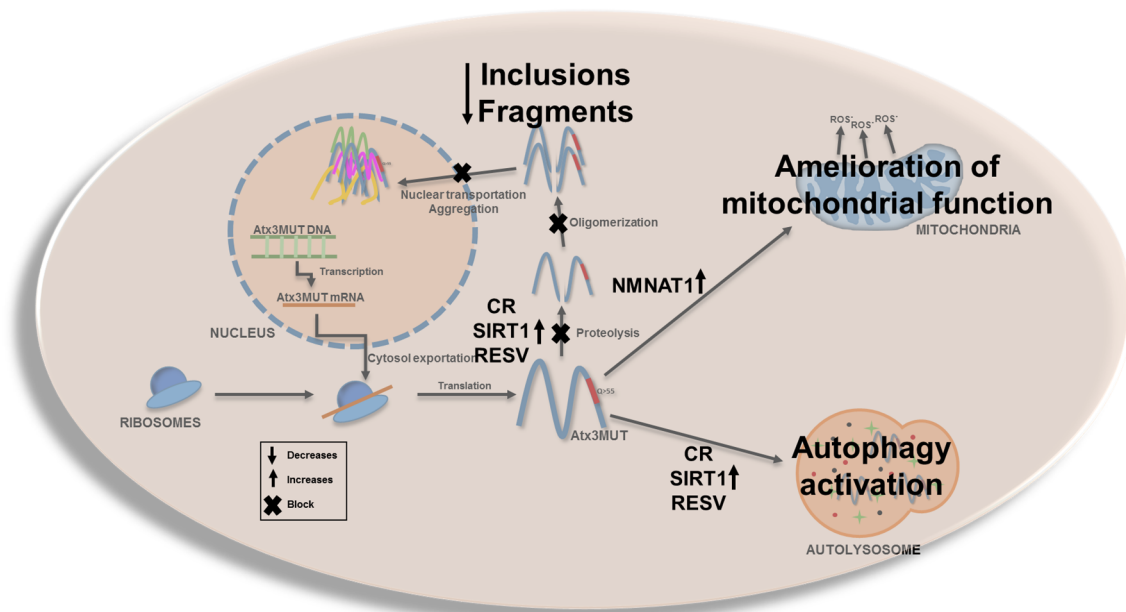
Figure 5.3 <u>Summary of the beneficial effects and outcomes of the therapeutic strategies studied in this thesis, regarding MJD pathogenesis.</u> As summarized in Figure 1.4 of Chapter 1, three of the main mechanisms involved in MJD pathogenesis are: i) proteolysis, oligomerization, and aggregation of mutant ataxin-3, leading to the formation of toxic species of mutant ataxin-3; ii) autophagy disruption generating the accumulation of misfolded and non-functional proteins; and iii) mitochondrial dysfunction. In the Chapters 2, 3, and 4 we presented several therapeutic approaches for MJD, and their involvement in MJD pathogenesis are summarized in this figure. CR and the increase in SIRT1 activity and levels, through the use of lentiviral vectors encoding for SIRT1 or

Figure 5.3 (cont.) through resveratrol administration, led to a decrease of the levels of toxic species of mutant ataxin-3 (fragments and aggregates). This is done, at least in part, by the activation of autophagy that leads to an increase in mutant ataxin-3 clearance. Moreover, the increase of nuclear NAD^+ through NMNAT1 lentiviral overexpression, ameliorated mitochondrial dysfunction. Altogether, these treatments contributed to an amelioration of MJD phenotype in two different MJD mouse models. <u>Atx3MUT:</u> Mutant ataxin-3; <u>CR:</u> Caloric restriction; <u>NMNAT1:</u> Nicotinamide mononucleotide adenylyltransferase; <u>RESV:</u> Resveratrol; <u>ROS:</u> Reactive oxygen species.

In conclusion, this work opens new therapeutic windows and targets to treat and to retard the progression of the fatal and incurable MJD.

REFERENCES

Aksoy, P., C. Escande, T. A. White, et al. Regulation of SIRT 1 mediated NAD dependent deacetylation: a novel role for the multifunctional enzyme CD38. *Biochem Biophys Res Commun* **349**(1): 353-359(2006).

Albani, D., L. Polito, S. Batelli, et al. The SIRT1 activator resveratrol protects SK-N-BE cells from oxidative stress and against toxicity caused by alpha-synuclein or amyloid-beta (1-42) peptide. *J Neurochem* **110**(5): 1445-1456(2009).

Albrecht, M., M. Golatta, U. Wullner, et al. Structural and functional analysis of ataxin-2 and ataxin-3. *Eur J Biochem* **271**(15): 3155-3170(2004).

Alcendor, R. R., S. Gao, P. Zhai, et al. Sirt1 regulates aging and resistance to oxidative stress in the heart. *Circ Res* **100**(10): 1512-1521(2007).

Alirezaei, M., C. C. Kemball, C. T. Flynn, et al. Short-term fasting induces profound neuronal autophagy. *Autophagy* **6**(6): 702-710(2010).

Alirezaei, M., C. C. Kemball and J. L. Whitton. Autophagy, inflammation and neurodegenerative disease. *Eur J Neurosci* **33**(2): 197-204(2011).

Alves, S., I. Nascimento-Ferreira, G. Auregan, et al. Allele-specific RNA silencing of mutant ataxin-3 mediates neuroprotection in a rat model of Machado-Joseph disease. *PLoS One* **3**(10): e3341(2008a).

Alves, S., E. Regulier, I. Nascimento-Ferreira, et al. Striatal and nigral pathology in a lentiviral rat model of Machado-Joseph disease. *Hum Mol Genet* **17**(14): 2071-2083(2008b).

Alves, S., I. Nascimento-Ferreira, N. Dufour, et al. Silencing ataxin-3 mitigates degeneration in a rat model of Machado-Joseph disease: no role for wild-type ataxin-3? *Hum Mol Genet* **19**(12): 2380-2394(2010).

Aly, K. B., J. L. Pipkin, W. G. Hinson, et al. Chronic caloric restriction induces stress proteins in the hypothalamus of rats. *Mech Ageing Dev* **76**(1): 11-23(1994).

Anderson, R. M., K. J. Bitterman, J. G. Wood, et al. Manipulation of a nuclear NAD+ salvage pathway delays aging without altering steady-state NAD+ levels. *J Biol Chem* **277**(21): 18881-18890(2002).

Anderson, R. M., K. J. Bitterman, J. G. Wood, et al. Nicotinamide and PNC1 govern lifespan extension by calorie restriction in Saccharomyces cerevisiae. *Nature* **423**(6936): 181-185(2003).

Anson, R. M., Z. Guo, R. de Cabo, et al. Intermittent fasting dissociates beneficial effects of dietary restriction on glucose metabolism and neuronal resistance to injury from calorie intake. *Proc Natl Acad Sci U S A* **100**(10): 6216-6220(2003).

Araki, T., Y. Sasaki and J. Milbrandt. Increased nuclear NAD biosynthesis and SIRT1 activation prevent axonal degeneration. *Science* **305**(5686): 1010-1013(2004).

Armentero, M. T., G. Levandis, P. Bramanti, et al. Dietary restriction does not prevent nigrostriatal degeneration in the 6-hydroxydopamine model of Parkinson's disease. *Exp Neurol* **212**(2): 548-551(2008).

Aspnes, L. E., C. M. Lee, R. Weindruch, et al. Caloric restriction reduces fiber loss and mitochondrial abnormalities in aged rat muscle. *FASEB J* **11**(7): 573-581(1997).

Avery, M. A., A. E. Sheehan, K. S. Kerr, et al. Wld S requires Nmnat1 enzymatic activity and N16-VCP interactions to suppress Wallerian degeneration. *J Cell Biol* **184**(4): 501-513(2009).

References

Azulay, J. P., O. Blin, D. Mestre, et al. Contrast sensitivity improvement with sulfamethoxazole and trimethoprim in a patient with Machado-Joseph disease without spasticity. *J Neurol Sci* **123**(1-2): 95-99(1994).

Bai, P., C. Canto, A. Brunyanszki, et al. PARP-2 regulates SIRT1 expression and whole-body energy expenditure. *Cell Metab* **13**(4): 450-460(2011a).

Bai, P., C. Canto, H. Oudart, et al. PARP-1 inhibition increases mitochondrial metabolism through SIRT1 activation. *Cell Metab* **13**(4): 461-468(2011b).

Banerjee, K. K., C. Ayyub, S. Z. Ali, et al. dSir2 in the adult fat body, but not in muscles, regulates life span in a diet-dependent manner. *Cell Rep* **2**(6): 1485-1491(2012).

Banerjee, S., T. F. Walseth, K. Borgmann, et al. CD38/cyclic ADP-ribose regulates astrocyte calcium signaling: implications for neuroinflammation and HIV-1-associated dementia. *J Neuroimmune Pharmacol* **3**(3): 154-164(2008).

Barger, J. L., T. Kayo, T. D. Pugh, et al. Short-term consumption of a resveratrol-containing nutraceutical mixture mimics gene expression of long-term caloric restriction in mouse heart. *Exp Gerontol* **43**(9): 859-866(2008a).

Barger, J. L., T. Kayo, J. M. Vann, et al. A low dose of dietary resveratrol partially mimics caloric restriction and retards aging parameters in mice. *PLoS One* **3**(6): e2264(2008b).

Barinaga, M. New Alzheimer's gene found. *Science* **268**(5219): 1845-1846(1995).

Bates, G. P. and E. Hockly. Experimental therapeutics in Huntington's disease: are models useful for therapeutic trials? *Curr Opin Neurol* **16**(4): 465-470(2003).

Bauer, J. H., S. Goupil, G. B. Garber, et al. An accelerated assay for the identification of lifespan-extending interventions in Drosophila melanogaster. *Proc Natl Acad Sci U S A* **101**(35): 12980-12985(2004).

Bauer, J. H., S. N. Morris, C. Chang, et al. dSir2 and Dmp53 interact to mediate aspects of CR-dependent lifespan extension in D. melanogaster. *Aging (Albany NY)* **1**(1): 38-48(2009).

Baur, J. A., K. J. Pearson, N. L. Price, et al. Resveratrol improves health and survival of mice on a high-calorie diet. *Nature* **444**(7117): 337-342(2006).

Baur, J. A. and D. A. Sinclair. Therapeutic potential of resveratrol: the in vivo evidence. *Nat Rev Drug Discov* **5**(6): 493-506(2006).

Baur, J. A., Z. Ungvari, R. K. Minor, et al. Are sirtuins viable targets for improving healthspan and lifespan? *Nat Rev Drug Discov* **11**(6): 443-461(2012).

Beauchemin, A. M., B. Gottlieb, L. K. Beitel, et al. Cytochrome c oxidase subunit Vb interacts with human androgen receptor: a potential mechanism for neurotoxicity in spinobulbar muscular atrophy. *Brain Res Bull* **56**(3-4): 285-297(2001).

Berger, F., C. Lau, M. Dahlmann, et al. Subcellular compartmentation and differential catalytic properties of the three human nicotinamide mononucleotide adenylyltransferase isoforms. *J Biol Chem* **280**(43): 36334-36341(2005).

Berke, S. J., Y. Chai, G. L. Marrs, et al. Defining the role of ubiquitin-interacting motifs in the polyglutamine disease protein, ataxin-3. *J Biol Chem* **280**(36): 32026-32034(2005).

Bettencourt, C., C. Santos, T. Kay, et al. Analysis of segregation patterns in Machado-Joseph disease pedigrees. *J Hum Genet* **53**(10): 920-923(2008).

Bettencourt, C., C. Santos, R. Montiel, et al. Increased transcript diversity: novel splicing variants of Machado-Joseph disease gene (ATXN3). *Neurogenetics* **11**(2): 193-202(2010).

Bettencourt, C. and M. Lima. Machado-Joseph Disease: from first descriptions to new perspectives. *Orphanet J Rare Dis* **6**: 35(2011).

Bettencourt, C., M. Raposo, R. Ros, et al. Transcript diversity of Machado-Joseph disease gene (ATXN3) is not directly determined by SNPs in exonic or flanking intronic regions. *J Mol Neurosci* **49**(3): 539-543(2013).

Bevilacqua, L., J. J. Ramsey, K. Hagopian, et al. Effects of short- and medium-term calorie restriction on muscle mitochondrial proton leak and reactive oxygen species production. *Am J Physiol Endocrinol Metab* **286**(5): E852-861(2004).

Bhattacharya, A., A. Bokov, F. L. Muller, et al. Dietary restriction but not rapamycin extends disease onset and survival of the H46R/H48Q mouse model of ALS. *Neurobiol Aging* **33**(8): 1829-1832(2012).

Biancalana, V., F. Serville, J. Pommier, et al. Moderate instability of the trinucleotide repeat in spino bulbar muscular atrophy. *Hum Mol Genet* **1**(4): 255-258(1992).

Bichelmeier, U., T. Schmidt, J. Hubener, et al. Nuclear localization of ataxin-3 is required for the manifestation of symptoms in SCA3: in vivo evidence. *J Neurosci* **27**(28): 7418-7428(2007).

Bieganowski, P. and C. Brenner. Discoveries of nicotinamide riboside as a nutrient and conserved NRK genes establish a Preiss-Handler independent route to NAD+ in fungi and humans. *Cell* **117**(4): 495-502(2004).

Bingham, P. M., M. O. Scott, S. Wang, et al. Stability of an expanded trinucleotide repeat in the androgen receptor gene in transgenic mice. *Nat Genet* **9**(2): 191-196(1995).

Bitterman, K. J., R. M. Anderson, H. Y. Cohen, et al. Inhibition of silencing and accelerated aging by nicotinamide, a putative negative regulator of yeast sir2 and human SIRT1. *J Biol Chem* **277**(47): 45099-45107(2002).

Bjorkoy, G., T. Lamark, A. Brech, et al. p62/SQSTM1 forms protein aggregates degraded by autophagy and has a protective effect on huntingtin-induced cell death. *J Cell Biol* **171**(4): 603-614(2005).

Blacher, E., T. Dadali, A. Bespalko, et al. Alzheimer's disease pathology is attenuated in a CD38-deficient mouse model. Ann Neurol 78(1): 88-103(2015).

Blesa, J. and S. Przedborski. Parkinson's disease: animal models and dopaminergic cell vulnerability. *Front Neuroanat* **8**: 155(2014).

Bodkin, N. L., T. M. Alexander, H. K. Ortmeyer, et al. Mortality and morbidity in laboratory-maintained Rhesus monkeys and effects of long-term dietary restriction. *J Gerontol A Biol Sci Med Sci* **58**(3): 212-219(2003).

Bogan, K. L. and C. Brenner. Nicotinic acid, nicotinamide, and nicotinamide riboside: a molecular evaluation of NAD+ precursor vitamins in human nutrition. *Annu Rev Nutr* **28**: 115-130(2008).

Boily, G., E. L. Seifert, L. Bevilacqua, et al. SirT1 regulates energy metabolism and response to caloric restriction in mice. *PLoS One* **3**(3): e1759(2008).

Bonini, N. M. A genetic model for human polyglutamine-repeat disease in Drosophila melanogaster. *Philos Trans R Soc Lond B Biol Sci* **354**(1386): 1057-1060(1999).

Bordone, L. and L. Guarente. Calorie restriction, SIRT1 and metabolism: understanding longevity. *Nat Rev Mol Cell Biol* **6**(4): 298-305(2005).

Bordone, L., D. Cohen, A. Robinson, et al. SIRT1 transgenic mice show phenotypes resembling calorie restriction. *Aging Cell* **6**(6): 759-767(2007).

Borra, M. T., B. C. Smith and J. M. Denu. Mechanism of human SIRT1 activation by resveratrol. *J Biol Chem* **280**(17): 17187-17195(2005).

Boy, J., T. Schmidt, H. Wolburg, et al. Reversibility of symptoms in a conditional mouse model of spinocerebellar ataxia type 3. *Hum Mol Genet* **18**(22): 4282-4295(2009).

Boy, J., T. Schmidt, U. Schumann, et al. A transgenic mouse model of spinocerebellar ataxia type 3 resembling late disease onset and gender-specific instability of CAG repeats. *Neurobiol Dis* **37**(2): 284-293(2010).

Bradamante, S., L. Barenghi and A. Villa. Cardiovascular protective effects of resveratrol. *Cardiovasc Drug Rev* **22**(3): 169-188(2004).

Braidy, N., A. Poljak, R. Grant, et al. Mapping NAD(+) metabolism in the brain of ageing Wistar rats: potential targets for influencing brain senescence. Biogerontology 15(2): 177-198(2014).

Braidy, N., G. J. Guillemin, H. Mansour, et al. Age related changes in NAD+ metabolism oxidative stress and Sirt1 activity in wistar rats. *PLoS One* **6**(4): e19194(2011).

Braidy, N., B. E. Jugder, A. Poljak, et al. Resveratrol as a Potential Therapeutic Candidate for the Treatment and Management of Alzheimer's Disease. *Curr Top Med Chem* **16**(17): 1951-1960(2016).

Breese, C. R., R. L. Ingram and W. E. Sonntag. Influence of age and long-term dietary restriction on plasma insulin-like growth factor-1 (IGF-1), IGF-1 gene expression, and IGF-1 binding proteins. *J Gerontol* **46**(5): B180-187(1991).

Browne, S. E., A. C. Bowling, U. MacGarvey, et al. Oxidative damage and metabolic dysfunction in Huntington's disease: selective vulnerability of the basal ganglia. *Ann Neurol* **41**(5): 646-653(1997).

Brownlow, M. L., A. Joly-Amado, S. Azam, et al. Partial rescue of memory deficits induced by calorie restriction in a mouse model of tau deposition. *Behav Brain Res* **271**: 79-88(2014).

Bruce-Keller, A. J., G. Umberger, R. McFall, et al. Food restriction reduces brain damage and improves behavioral outcome following excitotoxic and metabolic insults. *Ann Neurol* **45**(1): 8-15(1999).

Brunet, A., L. B. Sweeney, J. F. Sturgill, et al. Stress-dependent regulation of FOXO transcription factors by the SIRT1 deacetylase. *Science* **303**(5666): 2011-2015(2004).

Burnett, B., F. Li and R. N. Pittman. The polyglutamine neurodegenerative protein ataxin-3 binds polyubiquitylated proteins and has ubiquitin protease activity. *Hum Mol Genet* **12**(23): 3195-3205(2003).

Burnett, C., S. Valentini, F. Cabreiro, et al. Absence of effects of Sir2 overexpression on lifespan in C. elegans and Drosophila. *Nature* **477**(7365): 482-485(2011).

Byles, V., L. K. Chmilewski, J. Wang, et al. Aberrant cytoplasm localization and protein stability of SIRT1 is regulated by PI3K/IGF-1R signaling in human cancer cells. *Int J Biol Sci* **6**(6): 599-612(2010).

Calliari, A., N. Bobba, C. Escande, et al. Resveratrol delays Wallerian degeneration in a NAD(+) and DBC1 dependent manner. *Exp Neurol* **251**: 91-100(2014).

Camacho-Pereira, J., M. G. Tarrago, C. C. Chini, et al. CD38 Dictates Age-Related NAD Decline and Mitochondrial Dysfunction through an SIRT3-Dependent Mechanism. *Cell Metab* **23**(6): 1127-1139(2016).

Camargos, S. T., W. Marques, Jr. and A. C. Santos. Brain stem and cerebellum volumetric analysis of Machado Joseph disease patients. *Arq Neuropsiquiatr* **69**(2B): 292-296(2011).

Campbell, C. T., J. E. Kolesar and B. A. Kaufman. Mitochondrial transcription factor A regulates mitochondrial transcription initiation, DNA packaging, and genome copy number. *Biochim Biophys Acta* **1819**(9-10): 921-929(2012).

Canto, C., Z. Gerhart-Hines, J. N. Feige, et al. AMPK regulates energy expenditure by modulating NAD+ metabolism and SIRT1 activity. *Nature* **458**(7241): 1056-1060(2009).

Canto, C., L. Q. Jiang, A. S. Deshmukh, et al. Interdependence of AMPK and SIRT1 for metabolic adaptation to fasting and exercise in skeletal muscle. *Cell Metab* **11**(3): 213-219(2010).

Cao, D., M. Wang, X. Qiu, et al. Structural basis for allosteric, substrate-dependent stimulation of SIRT1 activity by resveratrol. *Genes Dev* **29**(12): 1316-1325(2015).

Cemal, C. K., C. J. Carroll, L. Lawrence, et al. YAC transgenic mice carrying pathological alleles of the MJD1 locus exhibit a mild and slowly progressive cerebellar deficit. *Hum Mol Genet* **11**(9): 1075-1094(2002).

Chai, Y., S. L. Koppenhafer, S. J. Shoesmith, et al. Evidence for proteasome involvement in polyglutamine disease: localization to nuclear inclusions in SCA3/MJD and suppression of polyglutamine aggregation in vitro. *Hum Mol Genet* **8**(4): 673-682(1999).

Chai, Y., S. S. Berke, R. E. Cohen, et al. Poly-ubiquitin binding by the polyglutamine disease protein ataxin-3 links its normal function to protein surveillance pathways. *J Biol Chem* **279**(5): 3605-3611(2004).

Chapman, T. and L. Partridge. Female fitness in Drosophila melanogaster: an interaction between the effect of nutrition and of encounter rate with males. *Proc Biol Sci* **263**(1371): 755-759(1996).

Chen, D., A. D. Steele, S. Lindquist, et al. Increase in activity during calorie restriction requires Sirt1. *Science* **310**(5754): 1641(2005a).

Chen, D., J. Bruno, E. Easlon, et al. Tissue-specific regulation of SIRT1 by calorie restriction. *Genes Dev* **22**(13): 1753-1757(2008a).

Chen, J., Y. Zhou, S. Mueller-Steiner, et al. SIRT1 protects against microglia-dependent amyloid-beta toxicity through inhibiting NF-kappaB signaling. *J Biol Chem* **280**(48): 40364-40374(2005b).

Chen, S., J. Seiler, M. Santiago-Reichelt, et al. Repression of RNA polymerase I upon stress is caused by inhibition of RNA-dependent deacetylation of PAF53 by SIRT7. *Mol Cell* **52**(3): 303-313(2013).

Chen, S., M. F. Blank, A. Iyer, et al. SIRT7-dependent deacetylation of the U3-55k protein controls pre-rRNA processing. *Nat Commun* **7**: 10734(2016).

Chen, W. Y., D. H. Wang, R. C. Yen, et al. Tumor suppressor HIC1 directly regulates SIRT1 to modulate p53-dependent DNA-damage responses. *Cell* **123**(3): 437-448(2005c).

Chen, X., T. S. Tang, H. Tu, et al. Deranged calcium signaling and neurodegeneration in spinocerebellar ataxia type 3. *J Neurosci* **28**(48): 12713-12724(2008b).

Cheng, H. L., R. Mostoslavsky, S. Saito, et al. Developmental defects and p53 hyperacetylation in Sir2 homolog (SIRT1)-deficient mice. *Proc Natl Acad Sci U S A* **100**(19): 10794-10799(2003).

Choi, S. E., T. Fu, S. Seok, et al. Elevated microRNA-34a in obesity reduces NAD+ levels and SIRT1 activity by directly targeting NAMPT. *Aging Cell* **12**(6): 1062-1072(2013).

Chou, A. H., T. H. Yeh, Y. L. Kuo, et al. Polyglutamine-expanded ataxin-3 activates mitochondrial apoptotic pathway by upregulating Bax and downregulating Bcl-xL. *Neurobiol Dis* **21**(2): 333-345(2006).

Chou, A. H., T. H. Yeh, P. Ouyang, et al. Polyglutamine-expanded ataxin-3 causes cerebellar dysfunction of SCA3 transgenic mice by inducing transcriptional dysregulation. *Neurobiol Dis* **31**(1): 89-101(2008).

Chou, A. H., S. Y. Chen, T. H. Yeh, et al. HDAC inhibitor sodium butyrate reverses transcriptional downregulation and ameliorates ataxic symptoms in a transgenic mouse model of SCA3. *Neurobiol Dis* **41**(2): 481-488(2011a).

Chou, A. H., A. C. Lin, K. Y. Hong, et al. p53 activation mediates polyglutamine-expanded ataxin-3 upregulation of Bax expression in cerebellar and pontine nuclei neurons. *Neurochem Int* **58**(2): 145-152(2011b).

Christie, N. T., A. L. Lee, H. G. Fay, et al. Novel polyglutamine model uncouples proteotoxicity from aging. *PLoS One* **9**(5): e96835(2014).

Chujo, Y., N. Fujii, N. Okita, et al. Caloric restriction-associated remodeling of rat white adipose tissue: effects on the growth hormone/insulin-like growth factor-1 axis, sterol regulatory element binding protein-1, and macrophage infiltration. *Age (Dordr)* **35**(4): 1143-1156(2013).

Civitarese, A. E., S. Carling, L. K. Heilbronn, et al. Calorie restriction increases muscle mitochondrial biogenesis in healthy humans. *PLoS Med* **4**(3): e76(2007).

Cohen, A. and M. N. Hall. An amino acid shuffle activates mTORC1. *Cell* **136**(3): 399-400(2009).

Cohen, H. Y., C. Miller, K. J. Bitterman, et al. Calorie restriction promotes mammalian cell survival by inducing the SIRT1 deacetylase. *Science* **305**(5682): 390-392(2004).

Colman, R. J., R. M. Anderson, S. C. Johnson, et al. Caloric restriction delays disease onset and mortality in rhesus monkeys. *Science* **325**(5937): 201-204(2009).

Colman, R. J., T. M. Beasley, D. B. Allison, et al. Skeletal effects of long-term caloric restriction in rhesus monkeys. *Age (Dordr)* **34**(5): 1133-1143(2012).

Colman, R. J., T. M. Beasley, J. W. Kemnitz, et al. Caloric restriction reduces age-related and all-cause mortality in rhesus monkeys. *Nat Commun* **5**: 3557(2014).

Colomer Gould, V. F., D. Goti, D. Pearce, et al. A mutant ataxin-3 fragment results from processing at a site N-terminal to amino acid 190 in brain of Machado-Joseph disease-like transgenic mice. *Neurobiol Dis* **27**(3): 362-369(2007).

Conceicao, M., L. Mendonca, C. Nobrega, et al. Intravenous administration of brain-targeted stable nucleic acid lipid particles alleviates Machado-Joseph disease neurological phenotype. *Biomaterials* **82**: 124-137(2016).

Conforti, L., A. Tarlton, T. G. Mack, et al. A Ufd2/D4Cole1e chimeric protein and overexpression of Rbp7 in the slow Wallerian degeneration (WldS) mouse. Proc Natl Acad Sci U S A 97(21): 11377-11382(2000).

Conforti, L., A. Wilbrey, G. Morreale, et al. Wld S protein requires Nmnat activity and a short N-terminal sequence to protect axons in mice. *J Cell Biol* **184**(4): 491-500(2009).

Correia, M., P. Coutinho, M. C. Silva, et al. Evaluation of the effect of sulphametoxazole and trimethoprim in patients with Machado-Joseph disease. *Rev Neurol* **23**(121): 632-634(1995).

Cortes, C. J. and A. R. La Spada. Autophagy in polyglutamine disease: Imposing order on disorder or contributing to the chaos? *Mol Cell Neurosci* **66**(Pt A): 53-61(2015).

Costa, M. C., J. Gomes-da-Silva, C. J. Miranda, et al. Genomic structure, promoter activity, and developmental expression of the mouse homologue of the Machado-Joseph disease (MJD) gene. *Genomics* **84**(2): 361-373(2004).

Costa Mdo, C. and H. L. Paulson. Toward understanding Machado-Joseph disease. *Prog Neurobiol* **97**(2): 239-257(2012).

Costa Mdo, C., K. Luna-Cancalon, S. Fischer, et al. Toward RNAi therapy for the polyglutamine disease Machado-Joseph disease. *Mol Ther* **21**(10): 1898-1908(2013).

Cote, C. D., B. A. Rasmussen, F. A. Duca, et al. Resveratrol activates duodenal Sirt1 to reverse insulin resistance in rats through a neuronal network. *Nat Med* **21**(5): 498-505(2015).

Coutinho, P. and C. Andrade. Autosomal dominant system degeneration in Portuguese families of the Azores Islands. A new genetic disorder involving cerebellar, pyramidal, extrapyramidal and spinal cord motor functions. *Neurology* **28**(7): 703-709(1978).

Coutinho, P., A. Guimaraes and F. Scaravilli. The pathology of Machado-Joseph disease. Report of a possible homozygous case. *Acta Neuropathol* **58**(1): 48-54(1982).

Cuervo, A. M. Autophagy: many paths to the same end. *Mol Cell Biochem* **263**(1-2): 55-72(2004).

Cui, J., S. Shi, X. Sun, et al. Mitochondrial autophagy involving renal injury and aging is modulated by caloric intake in aged rat kidneys. *PLoS One* **8**(7): e69720(2013).

D'Abreu, A., M. C. Franca, Jr., H. L. Paulson, et al. Caring for Machado-Joseph disease: current understanding and how to help patients. *Parkinsonism Relat Disord* **16**(1): 2-7(2010).

Dai, H., L. Kustigian, D. Carney, et al. SIRT1 activation by small molecules: kinetic and biophysical evidence for direct interaction of enzyme and activator. *J Biol Chem* **285**(43): 32695-32703(2010).

de Almeida, L. P., D. Zala, P. Aebischer, et al. Neuroprotective effect of a CNTF-expressing lentiviral vector in the quinolinic acid rat model of Huntington's disease. *Neurobiol Dis* **8**(3): 433-446(2001).

de Almeida, L. P., C. A. Ross, D. Zala, et al. Lentiviral-mediated delivery of mutant huntingtin in the striatum of rats induces a selective neuropathology modulated by polyglutamine repeat size, huntingtin expression levels, and protein length. *J Neurosci* **22**(9): 3473-3483(2002).

de Picciotto, N. E., L. B. Gano, L. C. Johnson, et al. Nicotinamide mononucleotide supplementation reverses vascular dysfunction and oxidative stress with aging in mice. *Aging Cell* **15**(3): 522-530(2016).

Deglon, N. and P. Hantraye. Viral vectors as tools to model and treat neurodegenerative disorders. *J Gene Med* **7**(5): 530-539(2005).

Dehay, B., M. Bourdenx, P. Gorry, et al. Targeting alpha-synuclein for treatment of Parkinson's disease: mechanistic and therapeutic considerations. *Lancet Neurol* **14**(8): 855-866(2015).

Delic, V., M. Brownlow, A. Joly-Amado, et al. Calorie restriction does not restore brain mitochondrial function in P301L tau mice, but it does decrease mitochondrial F0F1-ATPase activity. *Mol Cell Neurosci* **67**: 46-54(2015).

Delmas, D., V. Aires, E. Limagne, et al. Transport, stability, and biological activity of resveratrol. *Ann N Y Acad Sci* **1215**: 48-59(2011).

Deriu, M. A., G. Grasso, G. Licandro, et al. Investigation of the Josephin Domain protein-protein interaction by molecular dynamics. *PLoS One* **9**(9): e108677(2014).

Devlin, M. J., A. M. Cloutier, N. A. Thomas, et al. Caloric restriction leads to high marrow adiposity and low bone mass in growing mice. *J Bone Miner Res* **25**(9): 2078-2088(2010).

Dillin, A., A. L. Hsu, N. Arantes-Oliveira, et al. Rates of behavior and aging specified by mitochondrial function during development. *Science* **298**(5602): 2398-2401(2002).

Dilova, I., E. Easlon and S. J. Lin. Calorie restriction and the nutrient sensing signaling pathways. *Cell Mol Life Sci* **64**(6): 752-767(2007).

Di Stefano, M., I. Nascimento-Ferreira, G. Orsomando, et al. A rise in NAD precursor nicotinamide mononucleotide (NMN) after injury promotes axon degeneration. Cell Death Differ 22(5): 731-742(2015).

Dogan, S., A. C. Johannsen, J. P. Grande, et al. Effects of intermittent and chronic calorie restriction on mammalian target of rapamycin (mTOR) and IGF-I signaling pathways in mammary fat pad tissues and mammary tumors. *Nutr Cancer* **63**(3): 389-401(2011).

Donaldson, K. M., W. Li, K. A. Ching, et al. Ubiquitin-mediated sequestration of normal cellular proteins into polyglutamine aggregates. *Proc Natl Acad Sci U S A* **100**(15): 8892-8897(2003).

Dong, W., R. Wang, L. N. Ma, et al. Autophagy involving age-related cognitive behavior and hippocampus injury is modulated by different caloric intake in mice. *Int J Clin Exp Med* **8**(7): 11843-11853(2015).

Dos Santos, Z. A., R. J. Da Silva, R. F. Bacurau, et al. Effect of food restriction and intense physical training on estrous cyclicity and plasma leptin concentrations in rats. *J Nutr Sci Vitaminol (Tokyo)* **57**(1): 1-8(2011).

Du, J., Y. Zhou, X. Su, et al. Sirt5 is a NAD-dependent protein lysine demalonylase and desuccinylase. *Science* **334**(6057): 806-809(2011).

Duan, W. and M. P. Mattson. Dietary restriction and 2-deoxyglucose administration improve behavioral outcome and reduce degeneration of dopaminergic neurons in models of Parkinson's disease. *J Neurosci Res* **57**(2): 195-206(1999).

Duan, W., Z. Guo, H. Jiang, et al. Dietary restriction normalizes glucose metabolism and BDNF levels, slows disease progression, and increases survival in huntingtin mutant mice. *Proc Natl Acad Sci U S A* **100**(5): 2911-2916(2003).

Duarte-Neves, J., N. Goncalves, J. Cunha-Santos, et al. Neuropeptide Y mitigates neuropathology and motor deficits in mouse models of Machado-Joseph disease. *Hum Mol Genet* **24**(19): 5451-5463(2015).

Dubinsky, A. N., S. G. Dastidar, C. L. Hsu, et al. Let-7 coordinately suppresses components of the amino acid sensing pathway to repress mTORC1 and induce autophagy. *Cell Metab* **20**(4): 626-638(2014).

Dunn, S. E., F. W. Kari, J. French, et al. Dietary restriction reduces insulin-like growth factor I levels, which modulates apoptosis, cell proliferation, and tumor progression in p53-deficient mice. *Cancer Res* **57**(21): 4667-4672(1997).

Durr, A., G. Stevanin, G. Cancel, et al. Spinocerebellar ataxia 3 and Machado-Joseph disease: clinical, molecular, and neuropathological features. *Ann Neurol* **39**(4): 490-499(1996).

Ehninger, D., F. Neff and K. Xie. Longevity, aging and rapamycin. *Cell Mol Life Sci* **71**(22): 4325-4346(2014).

Escande, C., C. C. Chini, V. Nin, et al. Deleted in breast cancer-1 regulates SIRT1 activity and contributes to high-fat diet-induced liver steatosis in mice. *J Clin Invest* **120**(2): 545-558(2010).

Escande, C., V. Nin, N. L. Price, et al. Flavonoid apigenin is an inhibitor of the NAD+ ase CD38: implications for cellular NAD+ metabolism, protein acetylation, and treatment of metabolic syndrome. *Diabetes* **62**(4): 1084-1093(2013).

Esteves, S., S. Duarte-Silva, L. Naia, et al. Limited Effect of Chronic Valproic Acid Treatment in a Mouse Model of Machado-Joseph Disease. *PLoS One* **10**(10): e0141610(2015).

Evert, B. O., U. Wullner, J. B. Schulz, et al. High level expression of expanded full-length ataxin-3 in vitro causes cell death and formation of intranuclear inclusions in neuronal cells. *Hum Mol Genet* **8**(7): 1169-1176(1999).

Evert, B. O., I. R. Vogt, C. Kindermann, et al. Inflammatory genes are upregulated in expanded ataxin-3-expressing cell lines and spinocerebellar ataxia type 3 brains. *J Neurosci* **21**(15): 5389-5396(2001).

Evert, B. O., I. R. Vogt, A. M. Vieira-Saecker, et al. Gene expression profiling in ataxin-3 expressing cell lines reveals distinct effects of normal and mutant ataxin-3. *J Neuropathol Exp Neurol* **62**(10): 1006-1018(2003).

Evert, B. O., J. Araujo, A. M. Vieira-Saecker, et al. Ataxin-3 represses transcription via chromatin binding, interaction with histone deacetylase 3, and histone deacetylation. *J Neurosci* **26**(44): 11474-11486(2006a).

Evert, B. O., J. Schelhaas, H. Fleischer, et al. Neuronal intranuclear inclusions, dysregulation of cytokine expression and cell death in spinocerebellar ataxia type 3. *Clin Neuropathol* **25**(6): 272-281(2006b).

Feige, J. N., M. Lagouge, C. Canto, et al. Specific SIRT1 activation mimics low energy levels and protects against diet-induced metabolic disorders by enhancing fat oxidation. *Cell Metab* **8**(5): 347-358(2008).

Feng, X., N. Liang, D. Zhu, et al. Resveratrol inhibits beta-amyloid-induced neuronal apoptosis through regulation of SIRT1-ROCK1 signaling pathway. *PLoS One* **8**(3): e59888(2013).

Fontana, L. and L. Partridge. Promoting health and longevity through diet: from model organisms to humans. *Cell* **161**(1): 106-118(2015).

Frye, R. A. Phylogenetic classification of prokaryotic and eukaryotic Sir2-like proteins. *Biochem Biophys Res Commun* **273**(2): 793-798(2000).

Fujigasaki, H., T. Uchihara, S. Koyano, et al. Ataxin-3 is translocated into the nucleus for the formation of intranuclear inclusions in normal and Machado-Joseph disease brains. *Exp Neurol* **165**(2): 248-256(2000).

Furuyama, T., H. Yamashita, K. Kitayama, et al. Effects of aging and caloric restriction on the gene expression of Foxo1, 3, and 4 (FKHR, FKHRL1, and AFX) in the rat skeletal muscles. *Microsc Res Tech* **59**(4): 331-334(2002).

Gambini, J., M. Ingles, G. Olaso, et al. Properties of Resveratrol: In Vitro and In Vivo Studies about Metabolism, Bioavailability, and Biological Effects in Animal Models and Humans. *Oxid Med Cell Longev* **2015**: 837042(2015).

Gao, J., W. Y. Wang, Y. W. Mao, et al. A novel pathway regulates memory and plasticity via SIRT1 and miR-134. *Nature* **466**(7310): 1105-1109(2010).

Gatchel, J. R. and H. Y. Zoghbi. Diseases of unstable repeat expansion: mechanisms and common principles. *Nat Rev Genet* **6**(10): 743-755(2005).

Genade, T. and D. M. Lang. Resveratrol extends lifespan and preserves glia but not neurons of the Nothobranchius guentheri optic tectum. *Exp Gerontol* **48**(2): 202-212(2013).

Gerhart-Hines, Z., J. T. Rodgers, O. Bare, et al. Metabolic control of muscle mitochondrial function and fatty acid oxidation through SIRT1/PGC-1alpha. *EMBO J* **26**(7): 1913-1923(2007).

Giannakou, M. E., M. Goss and L. Partridge. Role of dFOXO in lifespan extension by dietary restriction in Drosophila melanogaster: not required, but its activity modulates the response. *Aging Cell* **7**(2): 187-198(2008).

Gines, S., I. S. Seong, E. Fossale, et al. Specific progressive cAMP reduction implicates energy deficit in presymptomatic Huntington's disease knock-in mice. *Hum Mol Genet* **12**(5): 497-508(2003).

Glass, C. K., K. Saijo, B. Winner, et al. Mechanisms underlying inflammation in neurodegeneration. *Cell* **140**(6): 918-934(2010).

Goate, A., M. C. Chartier-Harlin, M. Mullan, et al. Segregation of a missense mutation in the amyloid precursor protein gene with familial Alzheimer's disease. *Nature* **349**(6311): 704-706(1991).

Godzik, K. and M. P. Coleman. The axon-protective WLD(S) protein partially rescues mitochondrial respiration and glycolysis after axonal injury. J Mol Neurosci 55(4): 865-871(2015).

Goldberg, D. M., J. Yan and G. J. Soleas. Absorption of three wine-related polyphenols in three different matrices by healthy subjects. *Clin Biochem* **36**(1): 79-87(2003).

Gomes, A. P., F. V. Duarte, P. Nunes, et al. Berberine protects against high fat diet-induced dysfunction in muscle mitochondria by inducing SIRT1-dependent mitochondrial biogenesis. *Biochim Biophys Acta* **1822**(2): 185-195(2012).

Gomes, A. P., N. L. Price, A. J. Ling, et al. Declining NAD(+) induces a pseudohypoxic state disrupting nuclear-mitochondrial communication during aging. *Cell* **155**(7): 1624-1638(2013).

Goncalves, N., A. T. Simoes, R. A. Cunha, et al. Caffeine and adenosine A(2A) receptor inactivation decrease striatal neuropathology in a lentiviral-based model of Machado-Joseph disease. *Ann Neurol* **73**(5): 655-666(2013).

Gong, B., Y. Pan, P. Vempati, et al. Nicotinamide riboside restores cognition through an upregulation of proliferator-activated receptor-gamma coactivator 1alpha

regulated beta-secretase 1 degradation and mitochondrial gene expression in Alzheimer's mouse models. *Neurobiol Aging* **34**(6): 1581-1588(2013).

Goti, D., S. M. Katzen, J. Mez, et al. A mutant ataxin-3 putative-cleavage fragment in brains of Machado-Joseph disease patients and transgenic mice is cytotoxic above a critical concentration. *J Neurosci* **24**(45): 10266-10279(2004).

Goto, J., M. Watanabe, Y. Ichikawa, et al. Machado-Joseph disease gene products carrying different carboxyl termini. *Neurosci Res* **28**(4): 373-377(1997).

Graff, J., M. Kahn, A. Samiei, et al. A dietary regimen of caloric restriction or pharmacological activation of SIRT1 to delay the onset of neurodegeneration. *J Neurosci* **33**(21): 8951-8960(2013).

Gredilla, R., G. Barja and M. Lopez-Torres. Effect of short-term caloric restriction on H2O2 production and oxidative DNA damage in rat liver mitochondria and location of the free radical source. *J Bioenerg Biomembr* **33**(4): 279-287(2001a).

Gredilla, R., A. Sanz, M. Lopez-Torres, et al. Caloric restriction decreases mitochondrial free radical generation at complex I and lowers oxidative damage to mitochondrial DNA in the rat heart. *FASEB J* **15**(9): 1589-1591(2001b).

Green, K. N., J. S. Steffan, H. Martinez-Coria, et al. Nicotinamide restores cognition in Alzheimer's disease transgenic mice via a mechanism involving sirtuin inhibition and selective reduction of Thr231-phosphotau. *J Neurosci* **28**(45): 11500-11510(2008).

Griffioen, K. J., S. M. Rothman, B. Ladenheim, et al. Dietary energy intake modifies brainstem autonomic dysfunction caused by mutant alpha-synuclein. *Neurobiol Aging* **34**(3): 928-935(2013).

Grozio, A., G. Sociali, L. Sturla, et al. CD73 protein as a source of extracellular precursors for sustained NAD+ biosynthesis in FK866-treated tumor cells. *J Biol Chem* **288**(36): 25938-25949(2013).

Guarente, L. Sir2 links chromatin silencing, metabolism, and aging. *Genes Dev* **14**(9): 1021-1026(2000).

Guarente, L. Calorie restriction and sirtuins revisited. *Genes Dev* **27**(19): 2072-2085(2013).

Guo, W., L. Qian, J. Zhang, et al. Sirt1 overexpression in neurons promotes neurite outgrowth and cell survival through inhibition of the mTOR signaling. *J Neurosci Res* **89**(11): 1723-1736(2011).

Guo, X., J. G. Williams, T. T. Schug, et al. DYRK1A and DYRK3 promote cell survival through phosphorylation and activation of SIRT1. *J Biol Chem* **285**(17): 13223-13232(2010).

Guo, Y. J., S. Y. Dong, X. X. Cui, et al. Resveratrol alleviates MPTP-induced motor impairments and pathological changes by autophagic degradation of alpha-synuclein via SIRT1-deacetylated LC3. *Mol Nutr Food Res*(2016).

Haberhausen, G., M. S. Damian, F. Leweke, et al. Spinocerebellar ataxia, type 3 (SCA3) is genetically identical to Machado-Joseph disease (MJD). *J Neurol Sci* **132**(1): 71-75(1995).

Haffner, C. D., J. D. Becherer, E. E. Boros, et al. Discovery, Synthesis, and Biological Evaluation of Thiazoloquin(az)olin(on)es as Potent CD38 Inhibitors. *J Med Chem* **58**(8): 3548-3571(2015).

Haigis, M. C., R. Mostoslavsky, K. M. Haigis, et al. SIRT4 inhibits glutamate dehydrogenase and opposes the effects of calorie restriction in pancreatic beta cells. *Cell* **126**(5): 941-954(2006).

Haigis, M. C. and D. A. Sinclair. Mammalian sirtuins: biological insights and disease relevance. *Annu Rev Pathol* **5**: 253-295(2010).

Halagappa, V. K., Z. Guo, M. Pearson, et al. Intermittent fasting and caloric restriction ameliorate age-related behavioral deficits in the triple-transgenic mouse model of Alzheimer's disease. *Neurobiol Dis* **26**(1): 212-220(2007).

Hallows, W. C., S. Lee and J. M. Denu. Sirtuins deacetylate and activate mammalian acetyl-CoA synthetases. *Proc Natl Acad Sci U S A* **103**(27): 10230-10235(2006).

Hamadeh, M. J., M. C. Rodriguez, J. J. Kaczor, et al. Caloric restriction transiently improves motor performance but hastens clinical onset of disease in the Cu/Zn-superoxide dismutase mutant G93A mouse. *Muscle Nerve* **31**(2): 214-220(2005).

Hamadeh, M. J. and M. A. Tarnopolsky. Transient caloric restriction in early adulthood hastens disease endpoint in male, but not female, Cu/Zn-SOD mutant G93A mice. *Muscle Nerve* **34**(6): 709-719(2006).

Han, L., R. Zhou, J. Niu, et al. SIRT1 is regulated by a PPAR{gamma}-SIRT1 negative feedback loop associated with senescence. *Nucleic Acids Res* **38**(21): 7458-7471(2010).

Harlan, B. A., M. Pehar, D. R. Sharma, et al. Enhancing NAD+ Salvage Pathway Reverts the Toxicity of Primary Astrocytes Expressing Amyotrophic Lateral Sclerosis-linked Mutant Superoxide Dismutase 1 (SOD1). *J Biol Chem* **291**(20): 10836-10846(2016).

Harris, G. M., K. Dodelzon, L. Gong, et al. Splice isoforms of the polyglutamine disease protein ataxin-3 exhibit similar enzymatic yet different aggregation properties. *PLoS One* **5**(10): e13695(2010).

Harrison, D. E., R. Strong, Z. D. Sharp, et al. Rapamycin fed late in life extends lifespan in genetically heterogeneous mice. *Nature* **460**(7253): 392-395(2009).

Harvey, A. E., L. M. Lashinger, G. Otto, et al. Decreased systemic IGF-1 in response to calorie restriction modulates murine tumor cell growth, nuclear factor-kappaB activation, and inflammation-related gene expression. *Mol Carcinog* **52**(12): 997-1006(2013).

Harvey, A. E., L. M. Lashinger, D. Hays, et al. Calorie restriction decreases murine and human pancreatic tumor cell growth, nuclear factor-kappaB activation, and inflammation-related gene expression in an insulin-like growth factor-1-dependent manner. *PLoS One* **9**(5): e94151(2014).

Hayashida, S., A. Arimoto, Y. Kuramoto, et al. Fasting promotes the expression of SIRT1, an NAD+ -dependent protein deacetylase, via activation of PPARalpha in mice. *Mol Cell Biochem* **339**(1-2): 285-292(2010).

Herranz, D., M. Munoz-Martin, M. Canamero, et al. Sirt1 improves healthy ageing and protects from metabolic syndrome-associated cancer. *Nat Commun* **1**: 3(2010).

Herranz, D. and M. Serrano. Impact of Sirt1 on mammalian aging. *Aging (Albany NY)* **2**(6): 315-316(2010).

Herskovits, A. Z. and L. Guarente. SIRT1 in neurodevelopment and brain senescence. *Neuron* **81**(3): 471-483(2014).

Herzig, S., F. Long, U. S. Jhala, et al. CREB regulates hepatic gluconeogenesis through the coactivator PGC-1. *Nature* **413**(6852): 179-183(2001).

Heydari, A. R., S. You, R. Takahashi, et al. Effect of caloric restriction on the expression of heat shock protein 70 and the activation of heat shock transcription factor 1. *Dev Genet* **18**(2): 114-124(1996).

Heyward, F. D., R. G. Walton, M. S. Carle, et al. Adult mice maintained on a high-fat diet exhibit object location memory deficits and reduced hippocampal SIRT1 gene expression. *Neurobiol Learn Mem* **98**(1): 25-32(2012).

Hirschey, M. D., T. Shimazu, E. Goetzman, et al. SIRT3 regulates mitochondrial fatty-acid oxidation by reversible enzyme deacetylation. *Nature* **464**(7285): 121-125(2010).

Hisahara, S., S. Chiba, H. Matsumoto, et al. Histone deacetylase SIRT1 modulates neuronal differentiation by its nuclear translocation. *Proc Natl Acad Sci U S A* **105**(40): 15599-15604(2008).

Ho, D. J., N. Y. Calingasan, E. Wille, et al. Resveratrol protects against peripheral deficits in a mouse model of Huntington's disease. *Exp Neurol* **225**(1): 74-84(2010).

Hochfeld, W. E., S. Lee and D. C. Rubinsztein. Therapeutic induction of autophagy to modulate neurodegenerative disease progression. *Acta Pharmacol Sin* **34**(5): 600-604(2013).

Hoffmann, E., J. Wald, S. Lavu, et al. Pharmacokinetics and tolerability of SRT2104, a first-in-class small molecule activator of SIRT1, after single and repeated oral administration in man. *Br J Clin Pharmacol* **75**(1): 186-196(2013).

Horrillo, D., J. Sierra, C. Arribas, et al. Age-associated development of inflammation in Wistar rats: Effects of caloric restriction. *Arch Physiol Biochem* **117**(3): 140-150(2011).

Houthoofd, K., B. P. Braeckman, T. E. Johnson, et al. Life extension via dietary restriction is independent of the Ins/IGF-1 signalling pathway in Caenorhabditis elegans. *Exp Gerontol* **38**(9): 947-954(2003).

Houtkooper, R. H., C. Canto, R. J. Wanders, et al. The secret life of NAD+: an old metabolite controlling new metabolic signaling pathways. *Endocr Rev* **31**(2): 194-223(2010).

Howitz, K. T., K. J. Bitterman, H. Y. Cohen, et al. Small molecule activators of sirtuins extend Saccharomyces cerevisiae lifespan. *Nature* **425**(6954): 191-196(2003).

Hu, J., D. W. Dodd, R. H. Hudson, et al. Cellular localization and allele-selective inhibition of mutant huntingtin protein by peptide nucleic acid oligomers containing the fluorescent nucleobase [bis-o-(aminoethoxy)phenyl]pyrrolocytosine. *Bioorg Med Chem Lett* **19**(21): 6181-6184(2009).

Hu, J., K. T. Gagnon, J. Liu, et al. Allele-selective inhibition of ataxin-3 (ATX3) expression by antisense oligomers and duplex RNAs. *Biol Chem* **392**(4): 315-325(2011).

Huang, F., L. Zhang, Z. Long, et al. miR-25 alleviates polyQ-mediated cytotoxicity by silencing ATXN3. *FEBS Lett* **588**(24): 4791-4798(2014).

Huang, R., Y. Xu, W. Wan, et al. Deacetylation of nuclear LC3 drives autophagy initiation under starvation. *Mol Cell* **57**(3): 456-466(2015).

Hubbard, B. P., A. P. Gomes, H. Dai, et al. Evidence for a common mechanism of SIRT1 regulation by allosteric activators. *Science* **339**(6124): 1216-1219(2013).

Hubener, J., F. Vauti, C. Funke, et al. N-terminal ataxin-3 causes neurological symptoms with inclusions, endoplasmic reticulum stress and ribosomal dislocation. *Brain* **134**(Pt 7): 1925-1942(2011).

References

Hubener, J., J. J. Weber, C. Richter, et al. Calpain-mediated ataxin-3 cleavage in the molecular pathogenesis of spinocerebellar ataxia type 3 (SCA3). *Hum Mol Genet* **22**(3): 508-518(2013).

Ichikawa, Y., J. Goto, M. Hattori, et al. The genomic structure and expression of MJD, the Machado-Joseph disease gene. *J Hum Genet* **46**(7): 413-422(2001).

Ikeda, H., M. Yamaguchi, S. Sugai, et al. Expanded polyglutamine in the Machado-Joseph disease protein induces cell death in vitro and in vivo. *Nat Genet* **13**(2): 196-202(1996).

Imai, S., C. M. Armstrong, M. Kaeberlein, et al. Transcriptional silencing and longevity protein Sir2 is an NAD-dependent histone deacetylase. *Nature* **403**(6771): 795-800(2000).

Ivy, J. M., J. B. Hicks and A. J. Klar. Map positions of yeast genes SIR1, SIR3 and SIR4. *Genetics* **111**(4): 735-744(1985).

Jang, M., L. Cai, G. O. Udeani, et al. Cancer chemopreventive activity of resveratrol, a natural product derived from grapes. *Science* **275**(5297): 218-220(1997).

Jarolim, S., J. Millen, G. Heeren, et al. A novel assay for replicative lifespan in Saccharomyces cerevisiae. *FEMS Yeast Res* **5**(2): 169-177(2004).

Jeong, H., D. E. Cohen, L. Cui, et al. Sirt1 mediates neuroprotection from mutant huntingtin by activation of the TORC1 and CREB transcriptional pathway. *Nat Med* **18**(1): 159-165(2012).

Jeong, H., F. Then, T. J. Melia, Jr., et al. Acetylation targets mutant huntingtin to autophagosomes for degradation. *Cell* **137**(1): 60-72(2009).

Jia, K., D. Chen and D. L. Riddle. The TOR pathway interacts with the insulin signaling pathway to regulate C. elegans larval development, metabolism and life span. *Development* **131**(16): 3897-3906(2004).

Jiang, J. C., E. Jaruga, M. V. Repnevskaya, et al. An intervention resembling caloric restriction prolongs life span and retards aging in yeast. *FASEB J* **14**(14): 2135-2137(2000).

Jiang, M., J. Wang, J. Fu, et al. Neuroprotective role of Sirt1 in mammalian models of Huntington's disease through activation of multiple Sirt1 targets. *Nat Med* **18**(1): 153-158(2012).

Jin, Q., T. Yan, X. Ge, et al. Cytoplasm-localized SIRT1 enhances apoptosis. *J Cell Physiol* **213**(1): 88-97(2007).

Jing, E., S. Gesta and C. R. Kahn. SIRT2 regulates adipocyte differentiation through FoxO1 acetylation/deacetylation. *Cell Metab* **6**(2): 105-114(2007).

Johnson, J. E. and F. B. Johnson. Methionine restriction activates the retrograde response and confers both stress tolerance and lifespan extension to yeast, mouse and human cells. *PLoS One* **9**(5): e97729(2014).

Jung, J., K. Xu, D. Lessing, et al. Preventing Ataxin-3 protein cleavage mitigates degeneration in a Drosophila model of SCA3. *Hum Mol Genet* **18**(24): 4843-4852(2009).

Kaeberlein, M., M. McVey and L. Guarente. The SIR2/3/4 complex and SIR2 alone promote longevity in Saccharomyces cerevisiae by two different mechanisms. *Genes Dev* **13**(19): 2570-2580(1999).

Kaeberlein, M., T. McDonagh, B. Heltweg, et al. Substrate-specific activation of sirtuins by resveratrol. *J Biol Chem* **280**(17): 17038-17045(2005a).

Kaeberlein, M., R. W. Powers, 3rd, K. K. Steffen, et al. Regulation of yeast replicative life span by TOR and Sch9 in response to nutrients. *Science* **310**(5751): 1193-1196(2005b).

Kaeberlein, M. and R. W. Powers, 3rd. Sir2 and calorie restriction in yeast: a skeptical perspective. *Ageing Res Rev* **6**(2): 128-140(2007).

Kaeberlein, T. L., E. D. Smith, M. Tsuchiya, et al. Lifespan extension in Caenorhabditis elegans by complete removal of food. *Aging Cell* **5**(6): 487-494(2006).

Kagawa, Y. Impact of Westernization on the nutrition of Japanese: changes in physique, cancer, longevity and centenarians. *Prev Med* **7**(2): 205-217(1978).

Kanda, T., E. Isozaki, S. Kato, et al. Type III Machado-Joseph disease in a Japanese family: a clinicopathological study with special reference to the peripheral nervous system. *Clin Neuropathol* **8**(3): 134-141(1989).

Kanfi, Y., S. Naiman, G. Amir, et al. The sirtuin SIRT6 regulates lifespan in male mice. *Nature* **483**(7388): 218-221(2012).

Kapahi, P., B. M. Zid, T. Harper, et al. Regulation of lifespan in Drosophila by modulation of genes in the TOR signaling pathway. *Curr Biol* **14**(10): 885-890(2004).

Kastman, E. K., A. A. Willette, C. L. Coe, et al. A calorie-restricted diet decreases brain iron accumulation and preserves motor performance in old rhesus monkeys. *J Neurosci* **30**(23): 7940-7947(2010).

Kawaguchi, Y., T. Okamoto, M. Taniwaki, et al. CAG expansions in a novel gene for Machado-Joseph disease at chromosome 14q32.1. *Nat Genet* **8**(3): 221-228(1994).

Kayo, T., D. B. Allison, R. Weindruch, et al. Influences of aging and caloric restriction on the transcriptional profile of skeletal muscle from rhesus monkeys. *Proc Natl Acad Sci U S A* **98**(9): 5093-5098(2001).

Kazachkova, N., M. Raposo, R. Montiel, et al. Patterns of mitochondrial DNA damage in blood and brain tissues of a transgenic mouse model of Machado-Joseph disease. *Neurodegener Dis* **11**(4): 206-214(2013).

Keller, J. N., E. Dimayuga, Q. Chen, et al. Autophagy, proteasomes, lipofuscin, and oxidative stress in the aging brain. *Int J Biochem Cell Biol* **36**(12): 2376-2391(2004).

Kemnitz, J. W., R. Weindruch, E. B. Roecker, et al. Dietary restriction of adult male rhesus monkeys: design, methodology, and preliminary findings from the first year of study. *J Gerontol* **48**(1): B17-26(1993).

Kennedy, B. K., N. R. Austriaco, Jr., J. Zhang, et al. Mutation in the silencing gene SIR4 can delay aging in S. cerevisiae. *Cell* **80**(3): 485-496(1995).

Kennedy, B. K., M. Gotta, D. A. Sinclair, et al. Redistribution of silencing proteins from telomeres to the nucleolus is associated with extension of life span in S. cerevisiae. *Cell* **89**(3): 381-391(1997).

Kerr, F., H. Augustin, M. D. Piper, et al. Dietary restriction delays aging, but not neuronal dysfunction, in Drosophila models of Alzheimer's disease. *Neurobiol Aging* **32**(11): 1977-1989(2011).

Khan, L. A., P. O. Bauer, H. Miyazaki, et al. Expanded polyglutamines impair synaptic transmission and ubiquitin-proteasome system in Caenorhabditis elegans. *J Neurochem* **98**(2): 576-587(2006).

Khan, R. S., K. Dine, J. Das Sarma, et al. SIRT1 activating compounds reduce oxidative stress mediated neuronal loss in viral induced CNS demyelinating disease. *Acta Neuropathol Commun* **2**: 3(2014).

Kieling, C., P. R. Prestes, M. L. Saraiva-Pereira, et al. Survival estimates for patients with Machado-Joseph disease (SCA3). *Clin Genet* **72**(6): 543-545(2007).

Kim, D., M. D. Nguyen, M. M. Dobbin, et al. SIRT1 deacetylase protects against neurodegeneration in models for Alzheimer's disease and amyotrophic lateral sclerosis. *EMBO J* **26**(13): 3169-3179(2007a).

Kim, E. J., J. H. Kho, M. R. Kang, et al. Active regulator of SIRT1 cooperates with SIRT1 and facilitates suppression of p53 activity. *Mol Cell* **28**(2): 277-290(2007b).

Kim, H. J., J. H. Kim, S. Noh, et al. Metabolomic analysis of livers and serum from high-fat diet induced obese mice. *J Proteome Res* **10**(2): 722-731(2011).

Kim, J. E., J. Chen and Z. Lou. DBC1 is a negative regulator of SIRT1. *Nature* **451**(7178): 583-586(2008).

Kim, Y. T., S. M. Shin, W. Y. Lee, et al. Expression of expanded polyglutamine protein induces behavioral changes in Drosophila (polyglutamine-induced changes in Drosophila). *Cell Mol Neurobiol* **24**(1): 109-122(2004).

Kimball, S. R., L. M. Shantz, R. L. Horetsky, et al. Leucine regulates translation of specific mRNAs in L6 myoblasts through mTOR-mediated changes in availability of eIF4E and phosphorylation of ribosomal protein S6. *J Biol Chem* **274**(17): 11647-11652(1999).

Kish, S. J., F. Mastrogiacomo, M. Guttman, et al. Decreased brain protein levels of cytochrome oxidase subunits in Alzheimer's disease and in hereditary spinocerebellar ataxia disorders: a nonspecific change? *J Neurochem* **72**(2): 700-707(1999).

Kitada, M., S. Kume, A. Takeda-Watanabe, et al. Calorie restriction in overweight males ameliorates obesity-related metabolic alterations and cellular adaptations through anti-aging effects, possibly including AMPK and SIRT1 activation. *Biochim Biophys Acta* **1830**(10): 4820-4827(2013).

Klebanov, S., S. Diais, W. B. Stavinoha, et al. Hyperadrenocorticism, attenuated inflammation, and the life-prolonging action of food restriction in mice. *J Gerontol A Biol Sci Med Sci* **50**(2): B78-82(1995).

Klockgether, T., M. Skalej, D. Wedekind, et al. Autosomal dominant cerebellar ataxia type I. MRI-based volumetry of posterior fossa structures and basal ganglia in spinocerebellar ataxia types 1, 2 and 3. *Brain* **121 (Pt 9)**: 1687-1693(1998).

Knott, A. B., G. Perkins, R. Schwarzenbacher, et al. Mitochondrial fragmentation in neurodegeneration. *Nat Rev Neurosci* **9**(7): 505-518(2008).

Krehl, W. A., P. S. Sarma and C. A. Elvehjem. The effect of protein on the nicotinic acid and tryptophane requirement of the growing rat. *J Biol Chem* **162**: 403-411(1946).

Kumada, S., M. Hayashi, M. Mizuguchi, et al. Cerebellar degeneration in hereditary dentatorubral-pallidoluysian atrophy and Machado-Joseph disease. *Acta Neuropathol* **99**(1): 48-54(2000).

Kwong, J. Q., M. F. Beal and G. Manfredi. The role of mitochondria in inherited neurodegenerative diseases. *J Neurochem* **97**(6): 1659-1675(2006).

La Spada, A. R., E. M. Wilson, D. B. Lubahn, et al. Androgen receptor gene mutations in X-linked spinal and bulbar muscular atrophy. *Nature* **352**(6330): 77-79(1991).

La Spada, A. R., H. L. Paulson and K. H. Fischbeck. Trinucleotide repeat expansion in neurological disease. *Ann Neurol* **36**(6): 814-822(1994).

La Spada, A. R. and J. P. Taylor. Repeat expansion disease: progress and puzzles in disease pathogenesis. *Nat Rev Genet* **11**(4): 247-258(2010).

Laco, M. N., C. R. Oliveira, H. L. Paulson, et al. Compromised mitochondrial complex II in models of Machado-Joseph disease. *Biochim Biophys Acta* **1822**(2): 139-149(2012).

Lagouge, M., C. Argmann, Z. Gerhart-Hines, et al. Resveratrol improves mitochondrial function and protects against metabolic disease by activating SIRT1 and PGC-1alpha. *Cell* **127**(6): 1109-1122(2006).

Lam, E. W., J. J. Brosens, A. R. Gomes, et al. Forkhead box proteins: tuning forks for transcriptional harmony. *Nat Rev Cancer* **13**(7): 482-495(2013).

Landry, J., A. Sutton, S. T. Tafrov, et al. The silencing protein SIR2 and its homologs are NAD-dependent protein deacetylases. *Proc Natl Acad Sci U S A* **97**(11): 5807-5811(2000).

Lane, M. A., D. K. Ingram and G. S. Roth. Calorie restriction in nonhuman primates: effects on diabetes and cardiovascular disease risk. *Toxicol Sci* **52**(2 Suppl): 41-48(1999).

Langcake, P. and R. J. Pryce. A new class of phytoalexins from grapevines. *Experientia* **33**(2): 151-152(1977).

Lanza, I. R. and K. S. Nair. Mitochondrial function as a determinant of life span. *Pflugers Arch* **459**(2): 277-289(2010).

Leblond, C. S., H. M. Kaneb, P. A. Dion, et al. Dissection of genetic factors associated with amyotrophic lateral sclerosis. *Exp Neurol* **262 Pt B**: 91-101(2014).

Lee, B. C., A. Kaya and V. N. Gladyshev. Methionine restriction and life-span control. *Ann N Y Acad Sci* **1363**: 116-124(2016).

Lee, C. K., R. G. Klopp, R. Weindruch, et al. Gene expression profile of aging and its retardation by caloric restriction. *Science* **285**(5432): 1390-1393(1999).

Lee, C. M., L. E. Aspnes, S. S. Chung, et al. Influences of caloric restriction on age-associated skeletal muscle fiber characteristics and mitochondrial changes in rats and mice. *Ann N Y Acad Sci* **854**: 182-191(1998).

Lee, G. D., M. A. Wilson, M. Zhu, et al. Dietary deprivation extends lifespan in Caenorhabditis elegans. *Aging Cell* **5**(6): 515-524(2006a).

Lee, I. H., L. Cao, R. Mostoslavsky, et al. A role for the NAD-dependent deacetylase Sirt1 in the regulation of autophagy. *Proc Natl Acad Sci U S A* **105**(9): 3374-3379(2008).

Lee, J., W. Duan and M. P. Mattson. Evidence that brain-derived neurotrophic factor is required for basal neurogenesis and mediates, in part, the enhancement of neurogenesis by dietary restriction in the hippocampus of adult mice. *J Neurochem* **82**(6): 1367-1375(2002).

Lee, J., S. J. Kim, T. G. Son, et al. Interferon-gamma is up-regulated in the hippocampus in response to intermittent fasting and protects hippocampal neurons against excitotoxicity. *J Neurosci Res* **83**(8): 1552-1557(2006b).

Lee, J., A. Padhye, A. Sharma, et al. A pathway involving farnesoid X receptor and small heterodimer partner positively regulates hepatic sirtuin 1 levels via microRNA-34a inhibition. *J Biol Chem* **285**(17): 12604-12611(2010).

Lee, S. H. and K. J. Min. Caloric restriction and its mimetics. *BMB Rep* **46**(4): 181-187(2013).

Lee, S. S., S. Kennedy, A. C. Tolonen, et al. DAF-16 target genes that control C. elegans life-span and metabolism. *Science* **300**(5619): 644-647(2003).

Lei, L. F., G. P. Yang, J. L. Wang, et al. Safety and efficacy of valproic acid treatment in SCA3/MJD patients. *Parkinsonism Relat Disord* **26**: 55-61(2016).

Lerin, C., J. T. Rodgers, D. E. Kalume, et al. GCN5 acetyltransferase complex controls glucose metabolism through transcriptional repression of PGC-1alpha. *Cell Metab* **3**(6): 429-438(2006).

Levine, B. and D. J. Klionsky. Development by self-digestion: molecular mechanisms and biological functions of autophagy. *Dev Cell* **6**(4): 463-477(2004).

Li, F., T. Macfarlan, R. N. Pittman, et al. Ataxin-3 is a histone-binding protein with two independent transcriptional corepressor activities. *J Biol Chem* **277**(47): 45004-45012(2002).

Li, F., Y. Wang, K. I. Zeller, et al. Myc stimulates nuclearly encoded mitochondrial genes and mitochondrial biogenesis. Mol Cell Biol 25(14): 6225-6234(2005).

Li, L. B., Z. Yu, X. Teng, et al. RNA toxicity is a component of ataxin-3 degeneration in Drosophila. *Nature* **453**(7198): 1107-1111(2008a).

Li, X., H. Li and X. J. Li. Intracellular degradation of misfolded proteins in polyglutamine neurodegenerative diseases. *Brain Res Rev* **59**(1): 245-252(2008b).

Li, X. H., C. Chen, Y. Tu, et al. Sirt1 promotes axonogenesis by deacetylation of Akt and inactivation of GSK3. *Mol Neurobiol* **48**(3): 490-499(2013).

Li, Y., T. Yokota, V. Gama, et al. Bax-inhibiting peptide protects cells from polyglutamine toxicity caused by Ku70 acetylation. *Cell Death Differ* **14**(12): 2058-2067(2007).

Libert, S. and L. Guarente. Metabolic and neuropsychiatric effects of calorie restriction and sirtuins. *Annu Rev Physiol* **75**: 669-684(2013).

Libri, V., A. P. Brown, G. Gambarota, et al. A pilot randomized, placebo controlled, double blind phase I trial of the novel SIRT1 activator SRT2104 in elderly volunteers. *PLoS One* **7**(12): e51395(2012).

Lim, J. H., Y. M. Lee, Y. S. Chun, et al. Sirtuin 1 modulates cellular responses to hypoxia by deacetylating hypoxia-inducible factor 1alpha. Mol Cell 38(6): 864-878(2010).

Lima, L. and P. Coutinho. Clinical criteria for diagnosis of Machado-Joseph disease: report of a non-Azorena Portuguese family. *Neurology* **30**(3): 319-322(1980).

Lin, A. L., D. Coman, L. Jiang, et al. Caloric restriction impedes age-related decline of mitochondrial function and neuronal activity. *J Cereb Blood Flow Metab* **34**(9): 1440-1443(2014a).

Lin, M. T. and M. F. Beal. Mitochondrial dysfunction and oxidative stress in neurodegenerative diseases. *Nature* **443**(7113): 787-795(2006).

Lin, S. J., P. A. Defossez and L. Guarente. Requirement of NAD and SIR2 for life-span extension by calorie restriction in Saccharomyces cerevisiae. *Science* **289**(5487): 2126-2128(2000).

Lin, S. J., M. Kaeberlein, A. A. Andalis, et al. Calorie restriction extends Saccharomyces cerevisiae lifespan by increasing respiration. *Nature* **418**(6895): 344-348(2002).

Lin, S. J., E. Ford, M. Haigis, et al. Calorie restriction extends yeast life span by lowering the level of NADH. *Genes Dev* **18**(1): 12-16(2004).

Lin, X. P., L. Feng, C. G. Xie, et al. Valproic acid attenuates the suppression of acetyl histone H3 and CREB activity in an inducible cell model of Machado-Joseph disease. *Int J Dev Neurosci* **38**: 17-22(2014b).

Liou, G. G., J. C. Tanny, R. G. Kruger, et al. Assembly of the SIR complex and its regulation by O-acetyl-ADP-ribose, a product of NAD-dependent histone deacetylation. *Cell* **121**(4): 515-527(2005).

Liszt, G., E. Ford, M. Kurtev, et al. Mouse Sir2 homolog SIRT6 is a nuclear ADP-ribosyltransferase. *J Biol Chem* **280**(22): 21313-21320(2005).

Liu, C. S., H. M. Hsu, W. L. Cheng, et al. Clinical and molecular events in patients with Machado-Joseph disease under lamotrigine therapy. *Acta Neurol Scand* **111**(6): 385-390(2005).

Liu, T., H. Qi, L. Ma, et al. Resveratrol Attenuates Oxidative Stress and Extends Life Span in the Annual Fish Nothobranchius guentheri. *Rejuvenation Res* **18**(3): 225-233(2015).

Liu, Y., R. Dentin, D. Chen, et al. A fasting inducible switch modulates gluconeogenesis via activator/coactivator exchange. *Nature* **456**(7219): 269-273(2008).

Liu, Y., Z. Yao, L. Zhang, et al. Insulin induces neurite outgrowth via SIRT1 in SH-SY5Y cells. *Neuroscience* **238**: 371-380(2013).

Liu, Z. Q., M. Kunimatsu, J. P. Yang, et al. Proteolytic processing of nuclear factor kappa B by calpain in vitro. *FEBS Lett* **385**(1-2): 109-113(1996).

Lodi, R., A. H. Schapira, D. Manners, et al. Abnormal in vivo skeletal muscle energy metabolism in Huntington's disease and dentatorubropallidoluysian atrophy. *Ann Neurol* **48**(1): 72-76(2000).

Lombard, D. B., F. W. Alt, H. L. Cheng, et al. Mammalian Sir2 homolog SIRT3 regulates global mitochondrial lysine acetylation. *Mol Cell Biol* **27**(24): 8807-8814(2007).

Long, A. N., K. Owens, A. E. Schlappal, et al. Effect of nicotinamide mononucleotide on brain mitochondrial respiratory deficits in an Alzheimer's disease-relevant murine model. *BMC Neurol* **15**: 19(2015a).

Long, Z., Z. Chen, C. Wang, et al. Two novel SNPs in ATXN3 3' UTR may decrease age at onset of SCA3/MJD in Chinese patients. *PLoS One* **10**(2): e0117488(2015b).

Lopez-Lluch, G., N. Hunt, B. Jones, et al. Calorie restriction induces mitochondrial biogenesis and bioenergetic efficiency. *Proc Natl Acad Sci U S A* **103**(6): 1768-1773(2006).

Lopez-Torres, M., R. Gredilla, A. Sanz, et al. Influence of aging and long-term caloric restriction on oxygen radical generation and oxidative DNA damage in rat liver mitochondria. *Free Radic Biol Med* **32**(9): 882-889(2002).

Lou, S., V. C. Lepak, L. E. Eberly, et al. Oxygen consumption deficit in Huntington disease mouse brain under metabolic stress. *Hum Mol Genet*(2016).

Lowenstein, D. H., P. H. Chan and M. F. Miles. The stress protein response in cultured neurons: characterization and evidence for a protective role in excitotoxicity. *Neuron* **7**(6): 1053-1060(1991).

Luo, J., A. Y. Nikolaev, S. Imai, et al. Negative control of p53 by Sir2alpha promotes cell survival under stress. *Cell* **107**(2): 137-148(2001).

Luoma, P., A. Melberg, J. O. Rinne, et al. Parkinsonism, premature menopause, and mitochondrial DNA polymerase gamma mutations: clinical and molecular genetic study. *Lancet* **364**(9437): 875-882(2004).

Ma, L., W. Dong, R. Wang, et al. Effect of caloric restriction on the SIRT1/mTOR signaling pathways in senile mice. Brain Res Bull 116: 67-72(2015).

MacDonald, L., A. Hazi, A. G. Paolini, et al. Calorie restriction dose-dependently abates lipopolysaccharide-induced fever, sickness behavior, and circulating interleukin-6 while increasing corticosterone. *Brain Behav Immun* **40**: 18-26(2014).

Maciel, P., C. Gaspar, A. L. DeStefano, et al. Correlation between CAG repeat length and clinical features in Machado-Joseph disease. *Am J Hum Genet* **57**(1): 54-61(1995).

Maciel, P., M. C. Costa, A. Ferro, et al. Improvement in the molecular diagnosis of Machado-Joseph disease. *Arch Neurol* **58**(11): 1821-1827(2001).

Mack, T. G., M. Reiner, B. Beirowski, et al. Wallerian degeneration of injured axons and synapses is delayed by a Ube4b/Nmnat chimeric gene. *Nat Neurosci* **4**(12): 1199-1206(2001).

Mamik, M. K., S. Banerjee, T. F. Walseth, et al. HIV-1 and IL-1beta regulate astrocytic CD38 through mitogen-activated protein kinases and nuclear factor-kappaB signaling mechanisms. *J Neuroinflammation* **8**: 145(2011).

Mancuso, R., J. del Valle, L. Modol, et al. Resveratrol improves motoneuron function and extends survival in SOD1(G93A) ALS mice. *Neurotherapeutics* **11**(2): 419-432(2014).

Mao, Y., F. Senic-Matuglia, P. P. Di Fiore, et al. Deubiquitinating function of ataxin-3: insights from the solution structure of the Josephin domain. *Proc Natl Acad Sci U S A* **102**(36): 12700-12705(2005).

Marchal, J., S. Blanc, J. Epelbaum, et al. Effects of chronic calorie restriction or dietary resveratrol supplementation on insulin sensitivity markers in a primate, Microcebus murinus. *PLoS One* **7**(3): e34289(2012).

Martin, B., M. P. Mattson and S. Maudsley. Caloric restriction and intermittent fasting: two potential diets for successful brain aging. *Ageing Res Rev* **5**(3): 332-353(2006).

Maruyama, H., S. Nakamura, Z. Matsuyama, et al. Molecular features of the CAG repeats and clinical manifestation of Machado-Joseph disease. *Hum Mol Genet* **4**(5): 807-812(1995).

Mascarucci, P., D. Taub, S. Saccani, et al. Cytokine responses in young and old rhesus monkeys: effect of caloric restriction. *J Interferon Cytokine Res* **22**(5): 565-571(2002).

Masino, L., V. Musi, R. P. Menon, et al. Domain architecture of the polyglutamine protein ataxin-3: a globular domain followed by a flexible tail. *FEBS Lett* **549**(1-3): 21-25(2003).

Masoro, E. J., K. Iwasaki, C. A. Gleiser, et al. Dietary modulation of the progression of nephropathy in aging rats: an evaluation of the importance of protein. *Am J Clin Nutr* **49**(6): 1217-1227(1989).

Masoro, E. J., R. J. McCarter, M. S. Katz, et al. Dietary restriction alters characteristics of glucose fuel use. *J Gerontol* **47**(6): B202-208(1992).

Massudi, H., R. Grant, N. Braidy, et al. Age-associated changes in oxidative stress and NAD+ metabolism in human tissue. PLoS One 7(7): e42357(2012).

Maswood, N., J. Young, E. Tilmont, et al. Caloric restriction increases neurotrophic factor levels and attenuates neurochemical and behavioral deficits in a primate model of Parkinson's disease. *Proc Natl Acad Sci U S A* **101**(52): 18171-18176(2004).

Matsuishi, T., T. Sakai, E. Naito, et al. Elevated cerebrospinal fluid lactate/pyruvate ratio in Machado-Joseph disease. *Acta Neurol Scand* **93**(1): 72-75(1996).

Matsuura, K., H. Kabuto, H. Makino, et al. Pole test is a useful method for evaluating the mouse movement disorder caused by striatal dopamine depletion. *J Neurosci Methods* **73**(1): 45-48(1997).

Matsuura, T., P. Fang, X. Lin, et al. Somatic and germline instability of the ATTCT repeat in spinocerebellar ataxia type 10. *Am J Hum Genet* **74**(6): 1216-1224(2004).

Mattagajasingh, I., C. S. Kim, A. Naqvi, et al. SIRT1 promotes endothelium-dependent vascular relaxation by activating endothelial nitric oxide synthase. *Proc Natl Acad Sci U S A* **104**(37): 14855-14860(2007).

Mattison, J. A., M. A. Lane, G. S. Roth, et al. Calorie restriction in rhesus monkeys. *Exp Gerontol* **38**(1-2): 35-46(2003).

Mattison, J. A., G. S. Roth, T. M. Beasley, et al. Impact of caloric restriction on health and survival in rhesus monkeys from the NIA study. *Nature* **489**(7415): 318-321(2012).

Mayeux, R. and Y. Stern. Epidemiology of Alzheimer disease. *Cold Spring Harb Perspect Med* **2**(8)(2012).

McBurney, M. W., X. Yang, K. Jardine, et al. The mammalian SIR2alpha protein has a role in embryogenesis and gametogenesis. *Mol Cell Biol* **23**(1): 38-54(2003).

McCampbell, A., J. P. Taylor, A. A. Taye, et al. CREB-binding protein sequestration by expanded polyglutamine. *Hum Mol Genet* **9**(14): 2197-2202(2000).

McCay, C. M., M. F. Crowell and L. A. Maynard. The effect of retarded growth upon the length of life span and upon the ultimate body size. *Nutrition* **5**: 155-171(1935).

McCay, C. M., L. A. Maynard, G. Sperling, et al. Retarded growth, life span, ultimate body size and age changes in the albino rat after feeding diets restricted in calories. *Nutr. Rev.* **33**(8): 241-243(1939).

Mello, K. A. and B. P. Abbott. Effect of sulfamethoxazole and trimethoprim on neurologic dysfunction in a patient with Joseph's disease. *Arch Neurol* **45**(2): 210-213(1988).

Mendonca, L. S., C. Nobrega, H. Hirai, et al. Transplantation of cerebellar neural stem cells improves motor coordination and neuropathology in Machado-Joseph disease mice. *Brain* **138**(Pt 2): 320-335(2015).

Menzies, F. M., J. Huebener, M. Renna, et al. Autophagy induction reduces mutant ataxin-3 levels and toxicity in a mouse model of spinocerebellar ataxia type 3. *Brain* **133**(Pt 1): 93-104(2010).

Michan, S., Y. Li, M. M. Chou, et al. SIRT1 is essential for normal cognitive function and synaptic plasticity. *J Neurosci* **30**(29): 9695-9707(2010).

Michishita, E., J. Y. Park, J. M. Burneskis, et al. Evolutionarily conserved and nonconserved cellular localizations and functions of human SIRT proteins. *Mol Biol Cell* **16**(10): 4623-4635(2005).

Michishita, E., R. A. McCord, E. Berber, et al. SIRT6 is a histone H3 lysine 9 deacetylase that modulates telomeric chromatin. *Nature* **452**(7186): 492-496(2008).

Milne, J. C., P. D. Lambert, S. Schenk, et al. Small molecule activators of SIRT1 as therapeutics for the treatment of type 2 diabetes. *Nature* **450**(7170): 712-716(2007).

Minina, E. A., V. Sanchez-Vera, P. N. Moschou, et al. Autophagy mediates caloric restriction-induced lifespan extension in Arabidopsis. *Aging Cell* **12**(2): 327-329(2013).

Minor, R. K., J. A. Baur, A. P. Gomes, et al. SRT1720 improves survival and healthspan of obese mice. *Sci Rep* **1**: 70(2011).

Mirkin, S. M. DNA structures, repeat expansions and human hereditary disorders. *Curr Opin Struct Biol* **16**(3): 351-358(2006).

Mishra, V., B. Shuai, M. Kodali, et al. Resveratrol Treatment after Status Epilepticus Restrains Neurodegeneration and Abnormal Neurogenesis with Suppression of Oxidative Stress and Inflammation. *Sci Rep* **5**: 17807(2015).

Mitchell, S. E., C. Delville, P. Konstantopedos, et al. The effects of graded levels of calorie restriction: III. Impact of short term calorie and protein restriction on mean daily body temperature and torpor use in the C57BL/6 mouse. *Oncotarget* **6**(21): 18314-18337(2015a).

Mitchell, S. E., C. Delville, P. Konstantopedos, et al. The effects of graded levels of calorie restriction: II. Impact of short term calorie and protein restriction on circulating hormone levels, glucose homeostasis and oxidative stress in male C57BL/6 mice. *Oncotarget* **6**(27): 23213-23237(2015b).

Mitchell, S. E., Z. Tang, C. Kerbois, et al. The effects of graded levels of calorie restriction: I. impact of short term calorie and protein restriction on body composition in the C57BL/6 mouse. *Oncotarget* **6**(18): 15902-15930(2015c).

Mitchell, S. J., A. Martin-Montalvo, E. M. Mercken, et al. The SIRT1 activator SRT1720 extends lifespan and improves health of mice fed a standard diet. *Cell Rep* **6**(5): 836-843(2014).

Mizushima, N., B. Levine, A. M. Cuervo, et al. Autophagy fights disease through cellular self-digestion. *Nature* **451**(7182): 1069-1075(2008).

Monte, T. L., C. R. Rieder, A. B. Tort, et al. Use of fluoxetine for treatment of Machado-Joseph disease: an open-label study. *Acta Neurol Scand* **107**(3): 207-210(2003).

Montie, H. L., R. G. Pestell and D. E. Merry. SIRT1 modulates aggregation and toxicity through deacetylation of the androgen receptor in cell models of SBMA. *J Neurosci* **31**(48): 17425-17436(2011).

Mookerjee, S., T. Papanikolaou, S. J. Guyenet, et al. Posttranslational modification of ataxin-7 at lysine 257 prevents autophagy-mediated turnover of an N-terminal caspase-7 cleavage fragment. *J Neurosci* **29**(48): 15134-15144 (2009).

Moreno, C. L., M. E. Ehrlich and C. V. Mobbs. Protection by dietary restriction in the YAC128 mouse model of Huntington's disease: Relation to genes regulating histone acetylation and HTT. *Neurobiol Dis* **85**: 25-34(2016).

Mori, F., K. Tanji, S. Odagiri, et al. Autophagy-related proteins (p62, NBR1 and LC3) in intranuclear inclusions in neurodegenerative diseases. *Neurosci Lett* **522**(2): 134-138(2012).

Moroz, N., J. J. Carmona, E. Anderson, et al. Dietary restriction involves NAD(+) - dependent mechanisms and a shift toward oxidative metabolism. *Aging Cell* **13**(6): 1075-1085(2014).

Morselli, E., L. Galluzzi, O. Kepp, et al. Autophagy mediates pharmacological lifespan extension by spermidine and resveratrol. *Aging (Albany NY)* **1**(12): 961-970(2009).

Morselli, E., M. C. Maiuri, M. Markaki, et al. Caloric restriction and resveratrol promote longevity through the Sirtuin-1-dependent induction of autophagy. *Cell Death Dis* **1**: e10(2010).

Mostoslavsky, R., K. F. Chua, D. B. Lombard, et al. Genomic instability and aging-like phenotype in the absence of mammalian SIRT6. *Cell* **124**(2): 315-329(2006).

Motta, M. C., N. Divecha, M. Lemieux, et al. Mammalian SIRT1 represses forkhead transcription factors. *Cell* **116**(4): 551-563(2004).

Mouchiroud, L., R. H. Houtkooper and J. Auwerx. NAD(+) metabolism: a therapeutic target for age-related metabolic disease. *Crit Rev Biochem Mol Biol* **48**(4): 397-408(2013a).

Mouchiroud, L., R. H. Houtkooper, N. Moullan, et al. The NAD(+)/Sirtuin pathway modulates longevity through activation of mitochondrial UPR and FOXO signaling. *Cell* **154**(2): 430-44(2013b).

Mouton, P. R., M. E. Chachich, C. Quigley, et al. Caloric restriction attenuates amyloid deposition in middle-aged dtg APP/PS1 mice. *Neurosci Lett* **464**(3): 184-187(2009).

Muhl, H. and J. Pfeilschifter. Anti-inflammatory properties of pro-inflammatory interferon-gamma. *Int Immunopharmacol* **3**(9): 1247-1255(2003).

Mulligan, P., F. Yang, L. Di Stefano, et al. A SIRT1-LSD1 corepressor complex regulates Notch target gene expression and development. *Mol Cell* **42**(5): 689-699(2011).

Mulrooney, T. J., J. Marsh, I. Urits, et al. Influence of caloric restriction on constitutive expression of NF-kappaB in an experimental mouse astrocytoma. *PLoS One* **6**(3): e18085(2011).

Munoz, E., M. J. Rey, M. Mila, et al. Intranuclear inclusions, neuronal loss and CAG mosaicism in two patients with Machado-Joseph disease. *J Neurol Sci* **200**(1-2): 19-25(2002).

Myers, R. H., J. J. Madden, J. L. Teague, et al. Factors related to onset age of Huntington disease. *Am J Hum Genet* **34**(3): 481-488(1982).

Myers, R. H., D. S. Sax, W. J. Koroshetz, et al. Factors associated with slow progression in Huntington's disease. *Arch Neurol* **48**(8): 800-804(1991).

Naia, L, T. R. Rosenstock, A. M. Oliveira, et al. Comparative mitochondrial-based protective effects of resveratrol and nicotinamide in Huntington's disease models. *Mol Neurobiol* (2016).

Nakagawa, T. and L. Guarente. Urea cycle regulation by mitochondrial sirtuin, SIRT5. *Aging (Albany NY)* **1**(6): 578-581(2009).

Nakagawa, T. and L. Guarente. SnapShot: sirtuins, NAD, and aging. *Cell Metab* **20**(1): 192-192 e191(2014).

Nakano, K. K., D. M. Dawson and A. Spence. Machado disease. A hereditary ataxia in Portuguese emigrants to Massachusetts. *Neurology* **22**(1): 49-55(1972).

Nascimento-Ferreira, I., T. Santos-Ferreira, L. Sousa-Ferreira, et al. Overexpression of the autophagic beclin-1 protein clears mutant ataxin-3 and alleviates Machado-Joseph disease. *Brain* **134**(Pt 5): 1400-1415(2011).

Nascimento-Ferreira, I., C. Nobrega, A. Vasconcelos-Ferreira, et al. Beclin 1 mitigates motor and neuropathological deficits in genetic mouse models of Machado-Joseph disease. *Brain* **136**(Pt 7): 2173-2188(2013).

Nasrin, N., V. K. Kaushik, E. Fortier, et al. JNK1 phosphorylates SIRT1 and promotes its enzymatic activity. *PLoS One* **4**(12): e8414(2009).

Nelson, D. L., H. T. Orr and S. T. Warren. The unstable repeats--three evolving faces of neurological disease. *Neuron* **77**(5): 825-843(2013).

Nemoto, S., M. M. Fergusson and T. Finkel. Nutrient availability regulates SIRT1 through a forkhead-dependent pathway. *Science* **306**(5704): 2105-2108(2004).

Nicholls, D. G. Mitochondrial function and dysfunction in the cell: its relevance to aging and aging-related disease. *Int J Biochem Cell Biol* **34**(11): 1372-1381(2002).

Ning, Y. C., G. Y. Cai, L. Zhuo, et al. Short-term calorie restriction protects against renal senescence of aged rats by increasing autophagic activity and reducing oxidative damage. *Mech Ageing Dev* **134**(11-12): 570-579(2013).

Nisoli, E., C. Tonello, A. Cardile, et al. Calorie restriction promotes mitochondrial biogenesis by inducing the expression of eNOS. *Science* **310**(5746): 314-317(2005).

Nobrega, C., I. Nascimento-Ferreira, I. Onofre, et al. Overexpression of mutant ataxin-3 in mouse cerebellum induces ataxia and cerebellar neuropathology. *Cerebellum* **12**(4): 441-455(2013a).

Nobrega, C., I. Nascimento-Ferreira, I. Onofre, et al. Silencing mutant ataxin-3 rescues motor deficits and neuropathology in Machado-Joseph disease transgenic mice. *PLoS One* **8**(1): e52396(2013b).

Nobrega, C., I. Nascimento-Ferreira, I. Onofre, et al. RNA interference mitigates motor and neuropathological deficits in a cerebellar mouse model of Machado-Joseph disease. *PLoS One* **9**(8): e100086(2014).

Nobrega, C., S. Carmo-Silva, D. Albuquerque, et al. Re-establishing ataxin-2 downregulates translation of mutant ataxin-3 and alleviates Machado-Joseph disease. *Brain*(2015).

Noriega, L. G., J. N. Feige, C. Canto, et al. CREB and ChREBP oppositely regulate SIRT1 expression in response to energy availability. *EMBO Rep* **12**(10): 1069-1076(2011).

North, B. J., B. L. Marshall, M. T. Borra, et al. The human Sir2 ortholog, SIRT2, is an NAD+-dependent tubulin deacetylase. *Mol Cell* **11**(2): 437-444(2003).

North, B. J. and E. Verdin. Interphase nucleo-cytoplasmic shuttling and localization of SIRT2 during mitosis. *PLoS One* **2**(8): e784(2007).

Okazaki, M., Y. Iwasaki, M. Nishiyama, et al. PPARbeta/delta regulates the human SIRT1 gene transcription via Sp1. *Endocr J* **57**(5): 403-413(2010).

Onofre, I., N. Mendonca, S. Lopes, et al. Fibroblasts of Machado Joseph Disease patients reveal autophagy impairment. *Sci Rep* **6**: 28220(2016).

Onos, K. D., S. J. Sukoff Rizzo, G. R. Howell, et al. Toward more predictive genetic mouse models of Alzheimer's disease. *Brain Res Bull* **122**: 1-11(2016).

Orr, A. L., S. Li, C. E. Wang, et al. N-terminal mutant huntingtin associates with mitochondria and impairs mitochondrial trafficking. *J Neurosci* **28**(11): 2783-2792(2008).

Osborne, T. B., L. B. Mendel and E. L. Ferry. The Effect of Retardation of Growth Upon the Breeding Period and Duration of Life of Rats. *Science* **45**(1160): 294-295(1917).

Oue, M., K. Mitsumura, T. Torashima, et al. Characterization of mutant mice that express polyglutamine in cerebellar Purkinje cells. *Brain Res* **1255**: 9-17(2009).

Pacholec, M., J. E. Bleasdale, B. Chrunyk, et al. SRT1720, SRT2183, SRT1460, and resveratrol are not direct activators of SIRT1. *J Biol Chem* **285**(11): 8340-8351(2010).

Padiath, Q. S., A. K. Srivastava, S. Roy, et al. Identification of a novel 45 repeat unstable allele associated with a disease phenotype at the MJD1/SCA3 locus. *Am J Med Genet B Neuropsychiatr Genet* **133B**(1): 124-126(2005).

Pandey, U. B., Z. Nie, Y. Batlevi, et al. HDAC6 rescues neurodegeneration and provides an essential link between autophagy and the UPS. *Nature* **447**(7146): 859-863(2007).

Panov, A. V., C. A. Gutekunst, B. R. Leavitt, et al. Early mitochondrial calcium defects in Huntington's disease are a direct effect of polyglutamines. *Nat Neurosci* **5**(8): 731-736(2002).

Parihar, P., I. Solanki, M. L. Mansuri, et al. Mitochondrial sirtuins: emerging roles in metabolic regulations, energy homeostasis and diseases. *Exp Gerontol* **61**: 130-141(2015).

Park, J. C., K. C. Cook and E. A. Verde. Dietary restriction slows the abnormally rapid loss of spiral ganglion neurons in C57BL/6 mice. *Hear Res* **48**(3): 275-279(1990).

Park, S. J., F. Ahmad, A. Philp, et al. Resveratrol ameliorates aging-related metabolic phenotypes by inhibiting cAMP phosphodiesterases. *Cell* **148**(3): 421-433(2012).

Park, S. K., K. Kim, G. P. Page, et al. Gene expression profiling of aging in multiple mouse strains: identification of aging biomarkers and impact of dietary antioxidants. *Aging Cell* **8**(4): 484-495(2009).

Parker, J. A., M. Arango, S. Abderrahmane, et al. Resveratrol rescues mutant polyglutamine cytotoxicity in nematode and mammalian neurons. *Nat Genet* **37**(4): 349-350(2005).

Parsons, X. H., S. N. Garcia, L. Pillus, et al. Histone deacetylation by Sir2 generates a transcriptionally repressed nucleoprotein complex. *Proc Natl Acad Sci U S A* **100**(4): 1609-1614(2003).

Partridge, L., M. D. Piper and W. Mair. Dietary restriction in Drosophila. *Mech Ageing Dev* **126**(9): 938-950(2005).

Patel, B. P., A. Safdar, S. Raha, et al. Caloric restriction shortens lifespan through an increase in lipid peroxidation, inflammation and apoptosis in the G93A mouse, an animal model of ALS. *PLoS One* **5**(2): e9386(2010).

Patel, N. V. and C. E. Finch. The glucocorticoid paradox of caloric restriction in slowing brain aging. *Neurobiol Aging* **23**(5): 707-717(2002).

Patel, N. V., M. N. Gordon, K. E. Connor, et al. Caloric restriction attenuates Abeta-deposition in Alzheimer transgenic models. *Neurobiol Aging* **26**(7): 995-1000(2005).

Paulson, H. (1993). Spinocerebellar Ataxia Type 3. GeneReviews(R). R. A. Pagon, M. P. Adam, H. H. Ardinger et al. Seattle (WA).

Paulson, H. L., S. S. Das, P. B. Crino, et al. Machado-Joseph disease gene product is a cytoplasmic protein widely expressed in brain. *Ann Neurol* **41**(4): 453-462(1997a).

Paulson, H. L., M. K. Perez, Y. Trottier, et al. Intranuclear inclusions of expanded polyglutamine protein in spinocerebellar ataxia type 3. *Neuron* **19**(2): 333-344(1997b).

Pearson, K. J., J. A. Baur, K. N. Lewis, et al. Resveratrol delays age-related deterioration and mimics transcriptional aspects of dietary restriction without extending life span. *Cell Metab* **8**(2): 157-168(2008).

Pedersen, W. A. and M. P. Mattson. No benefit of dietary restriction on disease onset or progression in amyotrophic lateral sclerosis Cu/Zn-superoxide dismutase mutant mice. *Brain Res* **833**(1): 117-120(1999).

Pfluger, P. T., D. Herranz, S. Velasco-Miguel, et al. Sirt1 protects against high-fat diet-induced metabolic damage. *Proc Natl Acad Sci U S A* **105**(28): 9793-9798(2008).

Picard, F., M. Kurtev, N. Chung, et al. Sirt1 promotes fat mobilization in white adipocytes by repressing PPAR-gamma. *Nature* **429**(6993): 771-776(2004).

Porquet, D., G. Casadesus, S. Bayod, et al. Dietary resveratrol prevents Alzheimer's markers and increases life span in SAMP8. *Age (Dordr)* **35**(5): 1851-1865(2013).

Powers, R. W., 3rd, M. Kaeberlein, S. D. Caldwell, et al. Extension of chronological life span in yeast by decreased TOR pathway signaling. *Genes Dev* **20**(2): 174-184(2006).

Pozzi, C., M. Valtorta, G. Tedeschi, et al. Study of subcellular localization and proteolysis of ataxin-3. *Neurobiol Dis* **30**(2): 190-200(2008).

Preiss, J. and P. Handler. Biosynthesis of diphosphopyridine nucleotide. I. Identification of intermediates. *J Biol Chem* **233**(2): 488-492(1958a).

Preiss, J. and P. Handler. Biosynthesis of diphosphopyridine nucleotide. II. Enzymatic aspects. *J Biol Chem* **233**(2): 493-500(1958b).

Price, N. L., A. P. Gomes, A. J. Ling, et al. SIRT1 is required for AMPK activation and the beneficial effects of resveratrol on mitochondrial function. *Cell Metab* **15**(5): 675-690(2012).

Puigserver, P. and B. M. Spiegelman. Peroxisome proliferator-activated receptor-gamma coactivator 1 alpha (PGC-1 alpha): transcriptional coactivator and metabolic regulator. *Endocr Rev* **24**(1): 78-90(2003).

Purushotham, A., T. T. Schug, Q. Xu, et al. Hepatocyte-specific deletion of SIRT1 alters fatty acid metabolism and results in hepatic steatosis and inflammation. *Cell Metab* **9**(4): 327-338(2009).

Qin, W., M. Chachich, M. Lane, et al. Calorie restriction attenuates Alzheimer's disease type brain amyloidosis in Squirrel monkeys (Saimiri sciureus). *J Alzheimers Dis* **10**(4): 417-422(2006a).

Qin, W., T. Yang, L. Ho, et al. Neuronal SIRT1 activation as a novel mechanism underlying the prevention of Alzheimer disease amyloid neuropathology by calorie restriction. *J Biol Chem* **281**(31): 21745-21754(2006b).

Qin, W., W. Zhao, L. Ho, et al. Regulation of forkhead transcription factor FoxO3a contributes to calorie restriction-induced prevention of Alzheimer's disease-type amyloid neuropathology and spatial memory deterioration. *Ann N Y Acad Sci* **1147**: 335-347(2008).

Ramani, B., G. M. Harris, R. Huang, et al. A knockin mouse model of spinocerebellar ataxia type 3 exhibits prominent aggregate pathology and aberrant splicing of the disease gene transcript. *Hum Mol Genet* **24**(5): 1211-1224(2015).

Ramos, A., N. Kazachkova, F. Silva, et al. Differential mtDNA damage patterns in a transgenic mouse model of Machado-Joseph disease (MJD/SCA3). *J Mol Neurosci* **55**(2): 449-453(2015).

Ramsey, K. M., K. F. Mille, A. Satoh, et al. Age-associated loss of Sirt1-mediated enhancement of glucose-stimulated insulin secretion in beta cell-specific Sirt1-overexpressing (BESTO) mice. *Aging Cell* **7**(1): 78-88(2008).

Rane, S., M. He, D. Sayed, et al. Downregulation of miR-199a derepresses hypoxia-inducible factor-1alpha and Sirtuin 1 and recapitulates hypoxia preconditioning in cardiac myocytes. *Circ Res* **104**(7): 879-886(2009).

Ranum, L. P., J. K. Lundgren, L. J. Schut, et al. Spinocerebellar ataxia type 1 and Machado-Joseph disease: incidence of CAG expansions among adult-onset ataxia patients from 311 families with dominant, recessive, or sporadic ataxia. *Am J Hum Genet* **57**(3): 603-608(1995).

Rascon, B., B. P. Hubbard, D. A. Sinclair, et al. The lifespan extension effects of resveratrol are conserved in the honey bee and may be driven by a mechanism related to caloric restriction. *Aging (Albany NY)* **4**(7): 499-508(2012).

Recasens, A., B. Dehay, J. Bove, et al. Lewy body extracts from Parkinson disease brains trigger alpha-synuclein pathology and neurodegeneration in mice and monkeys. *Ann Neurol* **75**(3): 351-362(2014).

Redman, L. M. and E. Ravussin. Endocrine alterations in response to calorie restriction in humans. *Mol Cell Endocrinol* **299**(1): 129-136(2009).

Renaud, S. and M. de Lorgeril. Wine, alcohol, platelets, and the French paradox for coronary heart disease. *Lancet* **339**(8808): 1523-1526(1992).

Renaud, S. C., R. Gueguen, J. Schenker, et al. Alcohol and mortality in middle-aged men from eastern France. *Epidemiology* **9**(2): 184-188(1998).

Reyes-Turcu, F. E., K. H. Ventii and K. D. Wilkinson. Regulation and cellular roles of ubiquitin-specific deubiquitinating enzymes. *Annu Rev Biochem* **78**: 363-397(2009).

Richie, J. P., Jr., Y. Leutzinger, S. Parthasarathy, et al. Methionine restriction increases blood glutathione and longevity in F344 rats. *FASEB J* **8**(15): 1302-1307(1994).

Riess, O., U. Rub, A. Pastore, et al. SCA3: neurological features, pathogenesis and animal models. *Cerebellum* **7**(2): 125-137(2008).

Rine, J. and I. Herskowitz. Four genes responsible for a position effect on expression from HML and HMR in Saccharomyces cerevisiae. *Genetics* **116**(1): 9-22(1987).

Robertson, T. B. and L. A. Ray. Experimental studies on growth: XV. On the growth of relatively long lived compared with that of relatively short lived animals. . *J. Biol. Chem.* **42**: 71-107(1920).

Rodgers, J. T., C. Lerin, W. Haas, et al. Nutrient control of glucose homeostasis through a complex of PGC-1alpha and SIRT1. *Nature* **434**(7029): 113-118(2005).

Rodrigues, A. J., G. Coppola, C. Santos, et al. Functional genomics and biochemical characterization of the C. elegans orthologue of the Machado-Joseph disease protein ataxin-3. *FASEB J* **21**(4): 1126-1136(2007).

Rodriguez-Cabo, T., I. Rodriguez, M. Ramil, et al. Comprehensive evaluation of the photo-transformation routes of trans-resveratrol. *J Chromatogr A* **1410**: 129-139(2015).

Rodriguez-Lebron, E., C. Costa Mdo, K. Luna-Cancalon, et al. Silencing mutant ATXN3 expression resolves molecular phenotypes in SCA3 transgenic mice. *Mol Ther* **21**(10): 1909-1918(2013).

Rodriguez-Oroz, M. C., M. Jahanshahi, P. Krack, et al. Initial clinical manifestations of Parkinson's disease: features and pathophysiological mechanisms. *Lancet Neurol* **8**(12): 1128-1139(2009).

Rogina, B. and S. L. Helfand. Sir2 mediates longevity in the fly through a pathway related to calorie restriction. *Proc Natl Acad Sci U S A* **101**(45): 15998-16003(2004).

Rosenberg, R. N., W. L. Nyhan, C. Bay, et al. Autosomal dominant striatonigral degeneration. A clinical, pathologic, and biochemical study of a new genetic disorder. *Neurology* **26**(8): 703-714(1976).

Rosenberg, R. N. Machado-Joseph disease: an autosomal dominant motor system degeneration. *Mov Disord* **7**(3): 193-203(1992).

Roth, G. S., M. A. Lane, D. K. Ingram, et al. Biomarkers of caloric restriction may predict longevity in humans. *Science* **297**(5582): 811(2002).

Rub, U., E. R. Brunt and T. Deller. New insights into the pathoanatomy of spinocerebellar ataxia type 3 (Machado-Joseph disease). *Curr Opin Neurol* **21**(2): 111-116(2008).

Rubinsztein, D. C., A. Wyttenbach and J. Rankin. Intracellular inclusions, pathological markers in diseases caused by expanded polyglutamine tracts? *J Med Genet* **36**(4): 265-270(1999).

Rubinsztein, D. C. Autophagy induction rescues toxicity mediated by proteasome inhibition. *Neuron* **54**(6): 854-856(2007).

Rusten, T. E. and H. Stenmark. p62, an autophagy hero or culprit? *Nat Cell Biol* **12**(3): 207-209(2010).

Sabatino, F., E. J. Masoro, C. A. McMahan, et al. Assessment of the role of the glucocorticoid system in aging processes and in the action of food restriction. *J Gerontol* **46**(5): B171-179(1991).

Sakai, T., T. Matsuishi, S. Yamada, et al. Sulfamethoxazole-trimethoprim double-blind, placebo-controlled, crossover trial in Machado-Joseph disease: sulfamethoxazole-trimethoprim increases cerebrospinal fluid level of biopterin. *J Neural Transm Gen Sect* **102**(2): 159-172(1995).

Sanz, A., P. Caro, J. Ibanez, et al. Dietary restriction at old age lowers mitochondrial oxygen radical production and leak at complex I and oxidative DNA damage in rat brain. *J Bioenerg Biomembr* **37**(2): 83-90(2005).

Sasaki, T., B. Maier, K. D. Koclega, et al. Phosphorylation regulates SIRT1 function. *PLoS One* **3**(12): e4020(2008).

Sasaki, Y., B. P. Vohra, R. H. Baloh, et al. Transgenic mice expressing the Nmnat1 protein manifest robust delay in axonal degeneration in vivo. *J Neurosci* **29**(20): 6526-6534(2009).

Satoh, A., C. S. Brace, N. Rensing, et al. Sirt1 extends life span and delays aging in mice through the regulation of Nk2 homeobox 1 in the DMH and LH. *Cell Metab* **18**(3): 416-430(2013).

Saute, J. A., R. M. de Castilhos, T. L. Monte, et al. A randomized, phase 2 clinical trial of lithium carbonate in Machado-Joseph disease. *Mov Disord* **29**(4): 568-573(2014).

Saute, J. A., C. R. Rieder, R. M. Castilhos, et al. Planning future clinical trials in Machado Joseph disease: Lessons from a phase 2 trial. *J Neurol Sci* **358**(1-2): 72-76(2015).

Schafer, M. J., M. J. Alldred, S. H. Lee, et al. Reduction of beta-amyloid and gamma-secretase by calorie restriction in female Tg2576 mice. *Neurobiol Aging* **36**(3): 1293-1302(2015).

Scheibye-Knudsen, M., S. J. Mitchell, E. F. Fang, et al. A high-fat diet and NAD(+) activate Sirt1 to rescue premature aging in cockayne syndrome. Cell Metab 20(5): 840-855(2014).

Scher, M. B., A. Vaquero and D. Reinberg. SirT3 is a nuclear NAD+-dependent histone deacetylase that translocates to the mitochondria upon cellular stress. *Genes Dev* **21**(8): 920-928(2007).

Schmidt, M. T., B. C. Smith, M. D. Jackson, et al. Coenzyme specificity of Sir2 protein deacetylases: implications for physiological regulation. *J Biol Chem* **279**(38): 40122-40129(2004).

Schmidt, T., G. B. Landwehrmeyer, I. Schmitt, et al. An isoform of ataxin-3 accumulates in the nucleus of neuronal cells in affected brain regions of SCA3 patients. *Brain Pathol* **8**(4): 669-679(1998).

Schmitt, I., M. Linden, H. Khazneh, et al. Inactivation of the mouse Atxn3 (ataxin-3) gene increases protein ubiquitination. *Biochem Biophys Res Commun* **362**(3): 734-739(2007).

Schols, L., P. Bauer, T. Schmidt, et al. Autosomal dominant cerebellar ataxias: clinical features, genetics, and pathogenesis. *Lancet Neurol* **3**(5): 291-304(2004).

Schulte, T., R. Mattern, K. Berger, et al. Double-blind crossover trial of trimethoprim-sulfamethoxazole in spinocerebellar ataxia type 3/Machado-Joseph disease. *Arch Neurol* **58**(9): 1451-1457(2001).

Schulz, J. B. Update on the pathogenesis of Parkinson's disease. *J Neurol* **255 Suppl 5**: 3-7(2008).

Schulz, J. B., J. Borkert, S. Wolf, et al. Visualization, quantification and correlation of brain atrophy with clinical symptoms in spinocerebellar ataxia types 1, 3 and 6. *Neuroimage* **49**(1): 158-168(2010).

Seidel, K., W. F. den Dunnen, C. Schultz, et al. Axonal inclusions in spinocerebellar ataxia type 3. *Acta Neuropathol* **120**(4): 449-460(2010).

Senut, M. C., S. T. Suhr, B. Kaspar, et al. Intraneuronal aggregate formation and cell death after viral expression of expanded polyglutamine tracts in the adult rat brain. *J Neurosci* **20**(1): 219-229(2000).

Sequeiros, J., I. Silveira, P. Maciel, et al. Genetic linkage studies of Machado-Joseph disease with chromosome 14q STRPs in 16 Portuguese-Azorean kindreds. *Genomics* **21**(3): 645-648(1994).

Serrano-Pozo, A., M. P. Frosch, E. Masliah, et al. Neuropathological alterations in Alzheimer disease. *Cold Spring Harb Perspect Med* **1**(1): a006189(2011).

Shakkottai, V. G., M. do Carmo Costa, J. M. Dell'Orco, et al. Early changes in cerebellar physiology accompany motor dysfunction in the polyglutamine disease spinocerebellar ataxia type 3. *J Neurosci* **31**(36): 13002-13014(2011).

Shankaranarayana, G. D., M. R. Motamedi, D. Moazed, et al. Sir2 regulates histone H3 lysine 9 methylation and heterochromatin assembly in fission yeast. *Curr Biol* **13**(14): 1240-1246(2003).

Shao, J. and M. I. Diamond. Polyglutamine diseases: emerging concepts in pathogenesis and therapy. *Hum Mol Genet* **16 Spec No. 2**: R115-123(2007).

Shimazu, T., M. D. Hirschey, L. Hua, et al. SIRT3 deacetylates mitochondrial 3-hydroxy-3-methylglutaryl CoA synthase 2 and regulates ketone body production. *Cell Metab* **12**(6): 654-661(2010).

Shimokawa, I., T. Komatsu, N. Hayashi, et al. The life-extending effect of dietary restriction requires Foxo3 in mice. *Aging Cell* **14**(4): 707-709(2015).

Shin, B. H., Y. Lim, H. J. Oh, et al. Pharmacological activation of Sirt1 ameliorates polyglutamine-induced toxicity through the regulation of autophagy. *PLoS One* **8**(6): e64953(2013).

Shirasaki, H., C. Ishida, T. Nakajima, et al. [A quantitative evaluation of spinocerebellar degeneration by an acoustic analysis--the effect of taltirelin hydrate on patients with Machado-Joseph disease]. *Rinsho Shinkeigaku* **43**(4): 143-148(2003).

Shore, D., M. Squire and K. A. Nasmyth. Characterization of two genes required for the position-effect control of yeast mating-type genes. *EMBO J* **3**(12): 2817-2823(1984).

Silva-Fernandes, A., C. Costa Mdo, S. Duarte-Silva, et al. Motor uncoordination and neuropathology in a transgenic mouse model of Machado-Joseph disease lacking intranuclear inclusions and ataxin-3 cleavage products. *Neurobiol Dis* **40**(1): 163-176(2010).

Silva-Fernandes, A., S. Duarte-Silva, A. Neves-Carvalho, et al. Chronic treatment with 17-DMAG improves balance and coordination in a new mouse model of Machado-Joseph disease. *Neurotherapeutics* **11**(2): 433-449(2014).

Silveira, I., I. Alonso, L. Guimaraes, et al. High germinal instability of the (CTG)n at the SCA8 locus of both expanded and normal alleles. *Am J Hum Genet* **66**(3): 830-840(2000).

Simoes, A. T., N. Goncalves, A. Koeppen, et al. Calpastatin-mediated inhibition of calpains in the mouse brain prevents mutant ataxin 3 proteolysis, nuclear localization and aggregation, relieving Machado-Joseph disease. *Brain* **135**(Pt 8): 2428-2439(2012).

Simoes, A. T., N. Goncalves, R. J. Nobre, et al. Calpain inhibition reduces ataxin-3 cleavage alleviating neuropathology and motor impairments in mouse models of Machado-Joseph disease. *Hum Mol Genet* **23**(18): 4932-4944(2014).

Sinclair, D. A. and L. Guarente. Extrachromosomal rDNA circles--a cause of aging in yeast. *Cell* **91**(7): 1033-1042(1997).

Sinclair, D. A. Toward a unified theory of caloric restriction and longevity regulation. *Mech Ageing Dev* **126**(9): 987-1002(2005).

Smith, J. J., R. D. Kenney, D. J. Gagne, et al. Small molecule activators of SIRT1 replicate signaling pathways triggered by calorie restriction in vivo. *BMC Syst Biol* **3**: 31(2009).

Smith, J. S., C. B. Brachmann, I. Celic, et al. A phylogenetically conserved NAD+-dependent protein deacetylase activity in the Sir2 protein family. *Proc Natl Acad Sci U S A* **97**(12): 6658-6663(2000).

Smith, M. R., A. Syed, T. Lukacsovich, et al. A potent and selective Sirtuin 1 inhibitor alleviates pathology in multiple animal and cell models of Huntington's disease. *Hum Mol Genet* **23**(11): 2995-3007(2014).

Smith, W. J., L. E. Underwood and D. R. Clemmons. Effects of caloric or protein restriction on insulin-like growth factor-I (IGF-I) and IGF-binding proteins in children and adults. *J Clin Endocrinol Metab* **80**(2): 443-449(1995).

Snell, R. G., J. C. MacMillan, J. P. Cheadle, et al. Relationship between trinucleotide repeat expansion and phenotypic variation in Huntington's disease. *Nat Genet* **4**(4): 393-397(1993).

Sohal, R. S., S. Agarwal, M. Candas, et al. Effect of age and caloric restriction on DNA oxidative damage in different tissues of C57BL/6 mice. *Mech Ageing Dev* **76**(2-3): 215-224(1994a).

Sohal, R. S., H. H. Ku, S. Agarwal, et al. Oxidative damage, mitochondrial oxidant generation and antioxidant defenses during aging and in response to food restriction in the mouse. *Mech Ageing Dev* **74**(1-2): 121-133(1994b).

Song, L., L. Chen, X. Zhang, et al. Resveratrol ameliorates motor neuron degeneration and improves survival in SOD1(G93A) mouse model of amyotrophic lateral sclerosis. *Biomed Res Int* **2014**: 483501(2014).

Sreekumar, R., J. Unnikrishnan, A. Fu, et al. Effects of caloric restriction on mitochondrial function and gene transcripts in rat muscle. *Am J Physiol Endocrinol Metab* **283**(1): E38-43(2002).

Sridharan, A., M. Pehar, M. S. Salamat, et al. Calorie restriction attenuates astrogliosis but not amyloid plaque load in aged rhesus macaques: a preliminary quantitative imaging study. *Brain Res* **1508**: 1-8(2013).

St George-Hyslop, P., D. C. McLachlan, T. Tsuda, et al. Alzheimer's disease and possible gene interaction. *Science* **263**(5146): 537(1994).

Sudarsky, L. and P. Coutinho. Machado-Joseph disease. *Clin Neurosci* **3**(1): 17-22(1995).

Sugino, T., M. Maruyama, M. Tanno, et al. Protein deacetylase SIRT1 in the cytoplasm promotes nerve growth factor-induced neurite outgrowth in PC12 cells. *FEBS Lett* **584**(13): 2821-2826(2010).

Sun, D., A. R. Muthukumar, R. A. Lawrence, et al. Effects of calorie restriction on polymicrobial peritonitis induced by cecum ligation and puncture in young C57BL/6 mice. *Clin Diagn Lab Immunol* **8**(5): 1003-1011(2001).

Sussmuth, S. D., S. Haider, G. B. Landwehrmeyer, et al. An exploratory double-blind, randomized clinical trial with selisistat, a SirT1 inhibitor, in patients with Huntington's disease. *Br J Clin Pharmacol* **79**(3): 465-476(2015).

Swindell, W. R. Dietary restriction in rats and mice: a meta-analysis and review of the evidence for genotype-dependent effects on lifespan. *Ageing Res Rev* **11**(2): 254-270(2012).

Switonski, P. M., W. J. Szlachcic, W. J. Krzyzosiak, et al. A new humanized ataxin-3 knock-in mouse model combines the genetic features, pathogenesis of neurons and glia and late disease onset of SCA3/MJD. *Neurobiol Dis* **73**: 174-188(2015).

Szczepankiewicz, B. G. and P. Y. Ng. Sirtuin modulators: targets for metabolic diseases and beyond. *Curr Top Med Chem* **8**(17): 1533-1544(2008).

Tait, D., M. Riccio, A. Sittler, et al. Ataxin-3 is transported into the nucleus and associates with the nuclear matrix. *Hum Mol Genet* **7**(6): 991-997(1998).

Takahashi, T., S. Katada and O. Onodera. Polyglutamine diseases: where does toxicity come from? what is toxicity? where are we going? *J Mol Cell Biol* **2**(4): 180-191(2010).

Takaoka, M. J. Of the phenolic substances of white hellebore (Veratrum grandiflorum Loes. fil.). *Journal of the Faculty of Science, Hokkaido Imperial University* **3**: 1-16(1940).

Takei, A., T. Fukazawa, T. Hamada, et al. Effects of tandospirone on "5-HT1A receptor-associated symptoms" in patients with Machado-Josephe disease: an open-label study. *Clin Neuropharmacol* **27**(1): 9-13(2004).

Takiyama, Y., M. Nishizawa, H. Tanaka, et al. The gene for Machado-Joseph disease maps to human chromosome 14q. *Nat Genet* **4**(3): 300-304(1993).

Takiyama, Y., S. Igarashi, E. A. Rogaeva, et al. Evidence for inter-generational instability in the CAG repeat in the MJD1 gene and for conserved haplotypes at flanking markers amongst Japanese and Caucasian subjects with Machado-Joseph disease. *Hum Mol Genet* **4**(7): 1137-1146(1995).

Tang, B. L. Sirt1's complex roles in neuroprotection. *Cell Mol Neurobiol* **29**(8): 1093-1103(2009).

Tanida, I., T. Ueno and E. Kominami. LC3 and Autophagy. *Methods Mol Biol* **445**: 77-88(2008).

Taniwaki, T., T. Sakai, T. Kobayashi, et al. Positron emission tomography (PET) in Machado-Joseph disease. *J Neurol Sci* **145**(1): 63-67(1997).

Tanner, K. G., J. Landry, R. Sternglanz, et al. Silent information regulator 2 family of NAD- dependent histone/protein deacetylases generates a unique product, 1-O-acetyl-ADP-ribose. *Proc Natl Acad Sci U S A* **97**(26): 14178-14182(2000).

Tanno, M., J. Sakamoto, T. Miura, et al. Nucleocytoplasmic shuttling of the NAD+-dependent histone deacetylase SIRT1. *J Biol Chem* **282**(9): 6823-6832(2007).

Tao, M., C. P. You, R. R. Zhao, et al. Animal mitochondria: evolution, function, and disease. *Curr Mol Med* **14**(1): 115-124(2014).

Teeuwisse, W. M., R. L. Widya, M. Paulides, et al. Short-term caloric restriction normalizes hypothalamic neuronal responsiveness to glucose ingestion in patients with type 2 diabetes. *Diabetes* **61**(12): 3255-3259(2012).

Teixeira-Castro, A., M. Ailion, A. Jalles, et al. Neuron-specific proteotoxicity of mutant ataxin-3 in C. elegans: rescue by the DAF-16 and HSF-1 pathways. *Hum Mol Genet* **20**(15): 2996-3009(2011).

Teixeira-Castro, A., A. Jalles, S. Esteves, et al. Serotonergic signalling suppresses ataxin 3 aggregation and neurotoxicity in animal models of Machado-Joseph disease. *Brain* **138**(Pt 11): 3221-3237(2015).

Thomas, C. E., A. Ehrhardt and M. A. Kay. Progress and problems with the use of viral vectors for gene therapy. *Nat Rev Genet* **4**(5): 346-358(2003).

Timmers, S., E. Konings, L. Bilet, et al. Calorie restriction-like effects of 30 days of resveratrol supplementation on energy metabolism and metabolic profile in obese humans. *Cell Metab* **14**(5): 612-622(2011).

Tissenbaum, H. A. and L. Guarente. Increased dosage of a sir-2 gene extends lifespan in Caenorhabditis elegans. *Nature* **410**(6825): 227-230(2001).

Todd, T. W. and J. Lim. Aggregation formation in the polyglutamine diseases: protection at a cost? *Mol Cells* **36**(3): 185-194(2013).

Toiber, D., C. Sebastian and R. Mostoslavsky. Characterization of nuclear sirtuins: molecular mechanisms and physiological relevance. *Handb Exp Pharmacol* **206**: 189-224(2011).

Torashima, T., C. Koyama, A. Iizuka, et al. Lentivector-mediated rescue from cerebellar ataxia in a mouse model of spinocerebellar ataxia. *EMBO Rep* **9**(4): 393-399(2008).

Trela, B. C. and A. L. Waterhouse. Resveratrol: isomeric molar absorptivities and stability. . *Journal of Agricultural and Food Chemistry.* **44**(5): 1253-1257(1996).

Trottier, Y., G. Cancel, I. An-Gourfinkel, et al. Heterogeneous intracellular localization and expression of ataxin-3. *Neurobiol Dis* **5**(5): 335-347(1998).

Tsai, H. F., H. J. Tsai and M. Hsieh. Full-length expanded ataxin-3 enhances mitochondrial-mediated cell death and decreases Bcl-2 expression in human neuroblastoma cells. *Biochem Biophys Res Commun* **324**(4): 1274-1282(2004).

Tulino, R., A. C. Benjamin, N. Jolinon, et al. SIRT1 Activity Is Linked to Its Brain Region-Specific Phosphorylation and Is Impaired in Huntington's Disease Mice. *PLoS One* **11**(1): e0145425(2016).

Turner, R. S., R. G. Thomas, S. Craft, et al. A randomized, double-blind, placebo-controlled trial of resveratrol for Alzheimer disease. *Neurology* **85**(16): 1383-1391(2015).

Turturro, A., W. W. Witt, S. Lewis, et al. Growth curves and survival characteristics of the animals used in the Biomarkers of Aging Program. *J Gerontol A Biol Sci Med Sci* **54**(11): B492-501(1999).

Ugochukwu, N. H., J. D. Mukes and C. L. Figgers. Ameliorative effects of dietary caloric restriction on oxidative stress and inflammation in the brain of streptozotocin-induced diabetic rats. *Clin Chim Acta* **370**(1-2): 165-173(2006).

Ugochukwu, N. H. and C. L. Figgers. Caloric restriction inhibits up-regulation of inflammatory cytokines and TNF-alpha, and activates IL-10 and haptoglobin in the plasma of streptozotocin-induced diabetic rats. *J Nutr Biochem* **18**(2): 120-126(2007).

Valenzano, D. R., E. Terzibasi, T. Genade, et al. Resveratrol prolongs lifespan and retards the onset of age-related markers in a short-lived vertebrate. *Curr Biol* **16**(3): 296-300(2006).

Vallejo, E. A. [Hunger diet on alternate days in the nutrition of the aged]. *Prensa Med Argent* **44**(2): 119-120(1957).

van Alfen, N., R. J. Sinke, M. J. Zwarts, et al. Intermediate CAG repeat lengths (53,54) for MJD/SCA3 are associated with an abnormal phenotype. *Ann Neurol* **49**(6): 805-807(2001).

van de Warrenburg, B. P., R. J. Sinke, C. C. Verschuuren-Bemelmans, et al. Spinocerebellar ataxias in the Netherlands: prevalence and age at onset variance analysis. *Neurology* **58**(5): 702-708(2002).

van Ham, T. J., K. L. Thijssen, R. Breitling, et al. C. elegans model identifies genetic modifiers of alpha-synuclein inclusion formation during aging. *PLoS Genet* **4**(3): e1000027(2008).

Vaziri, H., S. K. Dessain, E. Ng Eaton, et al. hSIR2(SIRT1) functions as an NAD-dependent p53 deacetylase. *Cell* **107**(2): 149-159(2001).

Verdery, R. B. and R. L. Walford. Changes in plasma lipids and lipoproteins in humans during a 2-year period of dietary restriction in Biosphere 2. *Arch Intern Med* **158**(8): 900-906(1998).

Verdin, E. NAD(+) in aging, metabolism, and neurodegeneration. *Science* **350**(6265): 1208-1213(2015).

Verghese, P. B., Y. Sasaki, D. Yang, et al. Nicotinamide mononucleotide adenylyl transferase 1 protects against acute neurodegeneration in developing CNS by inhibiting excitotoxic-necrotic cell death. *Proc Natl Acad Sci U S A* **108**(47): 19054-19059(2011).

Vikman, K. S., B. Owe-Larsson, J. Brask, et al. Interferon-gamma-induced changes in synaptic activity and AMPA receptor clustering in hippocampal cultures. *Brain Res* **896**(1-2): 18-29(2001).

Viswanathan, M. and L. Guarente. Regulation of Caenorhabditis elegans lifespan by sir-2.1 transgenes. *Nature* **477**(7365): E1-2(2011).

Walford, R. L., L. Weber and S. Panov. Caloric restriction and aging as viewed from Biosphere 2. *Receptor* **5**(1): 29-33(1995).

Walford, R. L., D. Mock, T. MacCallum, et al. Physiologic changes in humans subjected to severe, selective calorie restriction for two years in biosphere 2: health, aging, and toxicological perspectives. *Toxicol Sci* **52**(2 Suppl): 61-65(1999).

Walford, R. L., D. Mock, R. Verdery, et al. Calorie restriction in biosphere 2: alterations in physiologic, hematologic, hormonal, and biochemical parameters in humans restricted for a 2-year period. *J Gerontol A Biol Sci Med Sci* **57**(6): B211-224(2002).

Walker, A. K., F. Yang, K. Jiang, et al. Conserved role of SIRT1 orthologs in fasting-dependent inhibition of the lipid/cholesterol regulator SREBP. *Genes Dev* **24**(13): 1403-1417(2010).

Wallace, D. C. Mitochondrial DNA mutations in disease and aging. *Environ Mol Mutagen* **51**(5): 440-450(2010).

Walle, T., F. Hsieh, M. H. DeLegge, et al. High absorption but very low bioavailability of oral resveratrol in humans. *Drug Metab Dispos* **32**(12): 1377-1382(2004).

Wang, C., C. T. Wheeler, T. Alberico, et al. The effect of resveratrol on lifespan depends on both gender and dietary nutrient composition in Drosophila melanogaster. *Age (Dordr)* **35**(1): 69-81(2013).

Wang, G., N. Sawai, S. Kotliarova, et al. Ataxin-3, the MJD1 gene product, interacts with the two human homologs of yeast DNA repair protein RAD23, HHR23A and HHR23B. *Hum Mol Genet* **9**(12): 1795-1803(2000).

Wang, G., T. Han, D. Nijhawan, et al. P7C3 neuroprotective chemicals function by activating the rate-limiting enzyme in NAD salvage. *Cell* **158**(6): 1324-1334(2014).

Wang, J., L. Ho, W. Qin, et al. Caloric restriction attenuates beta-amyloid neuropathology in a mouse model of Alzheimer's disease. *FASEB J* **19**(6): 659-661(2005a).

Wang, J., Q. Zhai, Y. Chen, et al. A local mechanism mediates NAD-dependent protection of axon degeneration. *J Cell Biol* **170**(3): 349-355(2005b).

Wang, J., Y. Zhang, L. Tang, et al. Protective effects of resveratrol through the up-regulation of SIRT1 expression in the mutant hSOD1-G93A-bearing motor neuron-like cell culture model of amyotrophic lateral sclerosis. *Neurosci Lett* **503**(3): 250-255(2011).

Wang, L. X., A. Heredia, H. Song, et al. Resveratrol glucuronides as the metabolites of resveratrol in humans: characterization, synthesis, and anti-HIV activity. *J Pharm Sci* **93**(10): 2448-2457(2004).

Wang, S. N., T. Y. Xu, X. Wang, et al. Neuroprotective Efficacy of an Aminopropyl Carbazole Derivative P7C3-A20 in Ischemic Stroke. *CNS Neurosci Ther* **22**(9): 782-788(2016).

Wang, Y. and S. Hekimi. Mitochondrial dysfunction and longevity in animals: Untangling the knot. *Science* **350**(6265): 1204-1207(2015).

Warrick, J. M., H. L. Paulson, G. L. Gray-Board, et al. Expanded polyglutamine protein forms nuclear inclusions and causes neural degeneration in Drosophila. *Cell* **93**(6): 939-949(1998).

Warrick, J. M., H. Y. Chan, G. L. Gray-Board, et al. Suppression of polyglutamine-mediated neurodegeneration in Drosophila by the molecular chaperone HSP70. *Nat Genet* **23**(4): 425-428(1999).

Warrick, J. M., L. M. Morabito, J. Bilen, et al. Ataxin-3 suppresses polyglutamine neurodegeneration in Drosophila by a ubiquitin-associated mechanism. *Mol Cell* **18**(1): 37-48(2005).

Watanabe, S., N. Ageta-Ishihara, S. Nagatsu, et al. SIRT1 overexpression ameliorates a mouse model of SOD1-linked amyotrophic lateral sclerosis via HSF1/HSP70i chaperone system. *Mol Brain* **7**: 62(2014).

Weber, J. J., A. S. Sowa, T. Binder, et al. From pathways to targets: understanding the mechanisms behind polyglutamine disease. *Biomed Res Int* **2014**: 701758(2014).

Weindruch, R., R. L. Walford, S. Fligiel, et al. The retardation of aging in mice by dietary restriction: longevity, cancer, immunity and lifetime energy intake. *J Nutr* **116**(4): 641-654(1986).

Weindruch, R., T. Kayo, C. K. Lee, et al. Microarray profiling of gene expression in aging and its alteration by caloric restriction in mice. *J Nutr* **131**(3): 918S-923S(2001).

Weindruch, R., T. Kayo, C. K. Lee, et al. Gene expression profiling of aging using DNA microarrays. *Mech Ageing Dev* **123**(2-3): 177-193(2002).

Weyer, C., R. L. Walford, I. T. Harper, et al. Energy metabolism after 2 y of energy restriction: the biosphere 2 experiment. *Am J Clin Nutr* **72**(4): 946-953(2000).

Whitaker, R., S. Faulkner, R. Miyokawa, et al. Increased expression of Drosophila Sir2 extends life span in a dose-dependent manner. *Aging (Albany NY)* **5**(9): 682-691(2013).

Willcox, D. C., B. J. Willcox, W. C. Hsueh, et al. Genetic determinants of exceptional human longevity: insights from the Okinawa Centenarian Study. *Age (Dordr)* **28**(4): 313-332(2006).

Willette, A. A., B. B. Bendlin, D. G. McLaren, et al. Age-related changes in neural volume and microstructure associated with interleukin-6 are ameliorated by a calorie-restricted diet in old rhesus monkeys. *Neuroimage* **51**(3): 987-994(2010).

Willette, A. A., B. B. Bendlin, R. J. Colman, et al. Calorie restriction reduces the influence of glucoregulatory dysfunction on regional brain volume in aged rhesus monkeys. *Diabetes* **61**(5): 1036-1042(2012a).

Willette, A. A., C. L. Coe, R. J. Colman, et al. Calorie restriction reduces psychological stress reactivity and its association with brain volume and microstructure in aged rhesus monkeys. *Psychoneuroendocrinology* **37**(7): 903-916(2012b).

Willette, A. A., C. L. Coe, A. C. Birdsill, et al. Interleukin-8 and interleukin-10, brain volume and microstructure, and the influence of calorie restriction in old rhesus macaques. *Age (Dordr)* **35**(6): 2215-2227(2013).

Williams, N. I., H. J. Leidy, B. R. Hill, et al. Magnitude of daily energy deficit predicts frequency but not severity of menstrual disturbances associated with exercise and caloric restriction. *Am J Physiol Endocrinol Metab* **308**(1): E29-39(2015).

Winborn, B. J., S. M. Travis, S. V. Todi, et al. The deubiquitinating enzyme ataxin-3, a polyglutamine disease protein, edits Lys63 linkages in mixed linkage ubiquitin chains. *J Biol Chem* **283**(39): 26436-26443(2008).

Wong, G., Y. Goldshmit and A. M. Turnley. Interferon-gamma but not TNF alpha promotes neuronal differentiation and neurite outgrowth of murine adult neural stem cells. *Exp Neurol* **187**(1): 171-177(2004).

Wood, J. G., B. Rogina, S. Lavu, et al. Sirtuin activators mimic caloric restriction and delay ageing in metazoans. *Nature* **430**(7000): 686-689(2004).

Wu, J., D. Zhang, L. Chen, et al. Discovery and mechanism study of SIRT1 activators that promote the deacetylation of fluorophore-labeled substrate. *J Med Chem* **56**(3): 761-780(2013).

Wu, P., Q. Shen, S. Dong, et al. Calorie restriction ameliorates neurodegenerative phenotypes in forebrain-specific presenilin-1 and presenilin-2 double knockout mice. *Neurobiol Aging* **29**(10): 1502-1511(2008).

Wu, Y., X. Li, J. X. Zhu, et al. Resveratrol-activated AMPK/SIRT1/autophagy in cellular models of Parkinson's disease. *Neurosignals* **19**(3): 163-174(2011).

Wullner, U., M. Reimold, M. Abele, et al. Dopamine transporter positron emission tomography in spinocerebellar ataxias type 1, 2, 3, and 6. *Arch Neurol* **62**(8): 1280-1285(2005).

Yahata, N., S. Yuasa and T. Araki. Nicotinamide mononucleotide adenylyltransferase expression in mitochondrial matrix delays Wallerian degeneration. *J Neurosci* **29**(19): 6276-6284(2009).

Yamada, M., S. Tsuji and H. Takahashi. Pathology of CAG repeat diseases. *Neuropathology* **20**(4): 319-325(2000).

Yamada, M., C. F. Tan, C. Inenaga, et al. Sharing of polyglutamine localization by the neuronal nucleus and cytoplasm in CAG-repeat diseases. *Neuropathol Appl Neurobiol* **30**(6): 665-675(2004).

Yamada, M., T. Sato, S. Tsuji, et al. CAG repeat disorder models and human neuropathology: similarities and differences. *Acta Neuropathol* **115**(1): 71-86(2008).

Yamakuchi, M., M. Ferlito and C. J. Lowenstein. miR-34a repression of SIRT1 regulates apoptosis. *Proc Natl Acad Sci U S A* **105**(36): 13421-13426(2008).

Yang, F., X. Chu, M. Yin, et al. mTOR and autophagy in normal brain aging and caloric restriction ameliorating age-related cognition deficits. *Behav Brain Res* **264**: 82-90(2014).

Yang, H., J. A. Baur, A. Chen, et al. Design and synthesis of compounds that extend yeast replicative lifespan. *Aging Cell* **6**(1): 35-43(2007a).

Yang, Y., W. Fu, J. Chen, et al. SIRT1 sumoylation regulates its deacetylase activity and cellular response to genotoxic stress. *Nat Cell Biol* **9**(11): 1253-1262(2007b).

Yen, T. C., C. S. Lu, K. Y. Tzen, et al. Decreased dopamine transporter binding in Machado-Joseph disease. *J Nucl Med* **41**(6): 994-998(2000).

Yeung, F., J. E. Hoberg, C. S. Ramsey, et al. Modulation of NF-kappaB-dependent transcription and cell survival by the SIRT1 deacetylase. *EMBO J* **23**(12): 2369-2380(2004).

Yi, J., L. Zhang, B. Tang, et al. Sodium valproate alleviates neurodegeneration in SCA3/MJD via suppressing apoptosis and rescuing the hypoacetylation levels of histone H3 and H4. *PLoS One* **8**(1): e54792(2013).

Yiu, E. M., G. Tai, R. E. Peverill, et al. An open-label trial in Friedreich ataxia suggests clinical benefit with high-dose resveratrol, without effect on frataxin levels. *J Neurol* **262**(5): 1344-1353(2015).

Yoshino, J., K. F. Mills, M. J. Yoon, et al. Nicotinamide mononucleotide, a key NAD(+) intermediate, treats the pathophysiology of diet- and age-induced diabetes in mice. *Cell Metab* **14**(4): 528-536(2011).

Yoshizaki, T., J. C. Milne, T. Imamura, et al. SIRT1 exerts anti-inflammatory effects and improves insulin sensitivity in adipocytes. *Mol Cell Biol* **29**(5): 1363-1374(2009).

Yoshizaki, T., S. Schenk, T. Imamura, et al. SIRT1 inhibits inflammatory pathways in macrophages and modulates insulin sensitivity. *Am J Physiol Endocrinol Metab* **298**(3): E419-428(2010).

Yoshizawa, T., H. Yoshida and S. Shoji. Differential susceptibility of cultured cell lines to aggregate formation and cell death produced by the truncated Machado-Joseph disease gene product with an expanded polyglutamine stretch. *Brain Res Bull* **56**(3-4): 349-352(2001).

Young, G. S., E. Choleris, F. E. Lund, et al. Decreased cADPR and increased NAD+ in the Cd38-/- mouse. *Biochem Biophys Res Commun* **346**(1): 188-192(2006).

Yu, B. P., E. J. Masoro, I. Murata, et al. Life span study of SPF Fischer 344 male rats fed ad libitum or restricted diets: longevity, growth, lean body mass and disease. *J Gerontol* **37**(2): 130-141(1982).

Yu, B. P., E. J. Masoro and C. A. McMahan. Nutritional influences on aging of Fischer 344 rats: I. Physical, metabolic, and longevity characteristics. *J Gerontol* **40**(6): 657-670(1985).

Yu, X. and G. Li. Effects of resveratrol on longevity, cognitive ability and aging-related histological markers in the annual fish Nothobranchius guentheri. *Exp Gerontol* **47**(12): 940-949(2012).

Yu, Y. C., C. L. Kuo, W. L. Cheng, et al. Decreased antioxidant enzyme activity and increased mitochondrial DNA damage in cellular models of Machado-Joseph disease. *J Neurosci Res* **87**(8): 1884-1891(2009).

Yu, Z., H. Luo, W. Fu, et al. The endoplasmic reticulum stress-responsive protein GRP78 protects neurons against excitotoxicity and apoptosis: suppression of oxidative stress and stabilization of calcium homeostasis. *Exp Neurol* **155**(2): 302-314(1999).

Yu, Z. F. and M. P. Mattson. Dietary restriction and 2-deoxyglucose administration reduce focal ischemic brain damage and improve behavioral outcome: evidence for a preconditioning mechanism. *J Neurosci Res* **57**(6): 830-839(1999).

Zarse, K., S. Schmeisser, M. Birringer, et al. Differential effects of resveratrol and SRT1720 on lifespan of adult Caenorhabditis elegans. *Horm Metab Res* **42**(12): 837-839(2010).

Zesiewicz, T., P. E. Greenstein, K. L. Sullivan, et al. A randomized trial of varenicline (Chantix) for the treatment of Spinocerebellar ataxia type 3. *Neurology* **78**(8):545-550 (2012).

Zhang, F., S. Wang, L. Gan, et al. Protective effects and mechanisms of sirtuins in the nervous system. *Prog Neurobiol* **95**(3): 373-395(2011).

Zhang, Q., S. Y. Wang, C. Fleuriel, et al. Metabolic regulation of SIRT1 transcription via a HIC1:CtBP corepressor complex. *Proc Natl Acad Sci U S A* **104**(3): 829-833(2007).

Zhang, X., O. V. Kurnasov, S. Karthikeyan, et al. Structural characterization of a human cytosolic NMN/NaMN adenylyltransferase and implication in human NAD biosynthesis. *J Biol Chem* **278**(15): 13503-13511(2003).

Zhao, W., J. P. Kruse, Y. Tang, et al. Negative regulation of the deacetylase SIRT1 by DBC1. *Nature* **451**(7178): 587-590(2008).

Zhou, Y., H. Zhang, B. He, et al. The bicyclic intermediate structure provides insights into the desuccinylation mechanism of human sirtuin 5 (SIRT5). *J Biol Chem* **287**(34): 28307-28314(2012).

Zhu, H., Q. Guo and M. P. Mattson. Dietary restriction protects hippocampal neurons against the death-promoting action of a presenilin-1 mutation. *Brain Res* **842**(1): 224-229(1999).

Zhu, X. H., M. Lu, B. Y. Lee, et al. In vivo NAD assay reveals the intracellular NAD contents and redox state in healthy human brain and their age dependences. Proc Natl Acad Sci U S A 112(9): 2876-2881(2015).

Zhu, Y., L. Zhang, Y. Sasaki, et al. Protection of mouse retinal ganglion cell axons and soma from glaucomatous and ischemic injury by cytoplasmic overexpression of Nmnat1. *Invest Ophthalmol Vis Sci* **54**(1): 25-36(2013).

Zimmerman, J. A., V. Malloy, R. Krajcik, et al. Nutritional control of aging. *Exp Gerontol* **38**(1-2): 47-52(2003).

Zoghbi, H. Y. and H. T. Orr. Glutamine repeats and neurodegeneration. *Annu Rev Neurosci* **23**: 217-247(2000).

Zorn, J. A. and J. A. Wells. Turning enzymes ON with small molecules. *Nat Chem Biol* **6**(3): 179-188(2010).